ROLE OF QUANTUM CORRELATIONS IN QUANTUM COMMUNICATION NETWORKS

By

TAMOGHNA DAS

PHYS08201105007

Harish-Chandra Research Institute, Allahabad

A thesis submitted to the

Board of Studies in Physical Sciences

In partial fulfillment of requirements

for the Degree of

DOCTOR OF PHILOSOPHY

of

HOMI BHABHA NATIONAL INSTITUTE

August, 2017

Homi Bhabha National Institute[1]

Recommendations of the Viva Voce Committee

As members of the Viva Voce Committee, we certify that we have read the dissertation prepared by Tamoghna Das entitled "Role of Quantum Correlations in Quantum Communications Networks" and recommend that it may be accepted as fulfilling the thesis requirement for the award of Degree of Doctor of Philosophy.

Chairman – Prof. Biswarup Mukhopadhyaya	Date: 22.11.17
Guide/Convener– Prof. Aditi Sen (De)	Date: 22.11.2017
Co-Guide - -	Date:
Examiner – Prof. Sai Vinjanampathy	Date: 22/Nov/2017
Member 1- Prof. Ujjwal Sen	Date: 22/11/17
Member 2- Prof. Arun Kumar Pati	Date:
Member 3- Prof. Anshuman Maharana	Date: 22/11/2017

Final approval and acceptance of this thesis is contingent upon the candidate's submission of the final copies of the thesis to HBNI.

I/We hereby certify that I/we have read this thesis prepared under my/our direction and recommend that it may be accepted as fulfilling the thesis requirement.

Date: 22-11-2017

Place: Allahabad

Prof. Aditi Sen (De)
Guide

STATEMENT BY AUTHOR

This dissertation has been submitted in partial fulfillment of requirements for an advanced degree at Homi Bhabha National Institute (HBNI) and is deposited in the Library to be made available to borrowers under rules of the HBNI.

Brief quotations from this dissertation are allowable without special permission, provided that accurate acknowledgement of source is made. Requests for permission for extended quotation from or reproduction of this manuscript in whole or in part may be granted by the Competent Authority of HBNI when in his or her judgment the proposed use of the material is in the interests of scholarship. In all other instances, however, permission must be obtained from the author.

Tamoghna Das

DECLARATION

I, hereby declare that the investigation presented in the thesis has been carried out by me. The work is original and has not been submitted earlier as a whole or in part for a degree / diploma at this or any other Institution / University.

Tamoghna Das

List of Publications arising from the thesis

Journal

1. "Multipartite dense coding versus quantum correlation: Noise inverts relative capability of information transfer", Tamoghna Das, R. Prabhu, Aditi Sen(De), and Ujjwal Sen, *Phys. Rev. A*, **2014**, *Vol. 90*, 022319.

2. "Distributed quantum dense coding with two receivers in noisy environments", Tamoghna Das, R. Prabhu, Aditi Sen(De), and Ujjwal Sen, *Phys. Rev. A*, **2015**, *Vol. 92*, 052330.

3. "Superiority of photon subtraction to addition for entanglement in a multimode squeezed vacuum", Tamoghna Das, R. Prabhu, Aditi Sen(De), and Ujjwal Sen, *Phys. Rev. A*, **2016**, *Vol. 93*, 052313.

Preprint

4. "Deterministic Quantum Dense Coding Networks", Saptarshi Roy, Titas Chanda, Tamoghna Das, Aditi Sen(De), and Ujjwal Sen, arXiv:1707.02449 [quant-ph].

Further Publications of candidate not used substantially in this thesis

Journal

5. "Reducing computational complexity of quantum correlations", Titas Chanda, Tamoghna Das, Debasis Sadhukhan, Amit Kumar Pal, Aditi Sen(De), and Ujjwal Sen, *Phys. Rev. A*, **2015**, *Vol. 92*, 062301.

6. "Statistics of leading digits leads to unification of quan- tum correlations", Titas Chanda, Tamoghna Das, Debasis Sadhukhan, Amit Kumar Pal, Aditi Sen(De), and Ujjwal Sen, *Europhys. Lett.*, **2016**, *Vol. 114*, 30004 (Highlights).

7. "Distribution of Bell-inequality violation versus multiparty-quantum-correlation measures", Kunal Sharma, Tamoghna Das, Aditi Sen(De), and Ujjwal Sen, *Phys. Rev. A*, **2016**, *Vol. 93*, 062344.

8. "Generalized Geometric Measure of Entanglement for Multiparty Mixed States", Tamoghna Das, Sudipto Singha Roy, Shrobona bagchi, Avijit Mishra, Aditi Sen(De), and Ujjwal Sen, *Phys. Rev. A*, **2016**, *Vol. 94*, 022336.

9. "Static and dynamical quantum correlations in phases of an alternating-field XY model", Titas Chanda, Tamoghna Das, Debasis Sadhukhan, Amit Kumar Pal, Aditi Sen(De), and Ujjwal Sen, *Phys. Rev. A*, **2016**, *Vol. 94*, 042310.

10. "Canonical distillation of entanglement", Tamoghna Das, Asutosh Kumar, Amit Kumar Pal, Namrata Shukla, Aditi Sen(De), and Ujjwal Sen, *Phys. Lett.. A*, **2017**, *Vol. 381*, 41.

Accepted

11. "Quantum discord and its allies: a review", Anindita Bera, Tamoghna Das, Debasis Sadhukhan, Sudipto Singha Roy, Aditi Sen(De), and Ujjwal Sen, arXiv:1703.10542 [quant-ph], to be published in Rep. Prog. Phys.

12. "Emergence of entanglement with temperature and time in factorization-surface states", Titas Chanda, Tamoghna Das, Debasis Sadhukhan, Amit Kumar Pal, Aditi Sen(De), and Ujjwal Sen, arXiv:1705.09812 [quant-ph], to be published in Phys. Rev. A.

Preprint

13. "Activation of nonmonogamous multipartite quantum states", Saptarshi Roy, Tamoghna Das, Asutosh Kumar, Aditi Sen(De), and Ujjwal Sen, arXiv:1608.06914 [quant-ph].

14. "Scale-invariant freezing of entanglement", Titas Chanda, Tamoghna Das, Debasis Sadhukhan, Amit Kumar Pal, Aditi Sen(De), and Ujjwal Sen, arXiv:1610.00730 [quant-ph].

15. "Phase boundaries in alternating field quantum XY model with Dzyaloshinskii-Moriya interaction: Sustainable entanglement in dynamics", Saptarshi Roy, Titas Chanda, Tamoghna Das, Debasis Sadhukhan, Aditi Sen(De), and Ujjwal Sen, arXiv:1710.11037 [quant-ph].

Conferences

1. Meeting on Quantum Information Processing and Applications (QIPA-13), 2-8 December 2013, held in Harish-Chandra Research Institute, Allahabad, India.

2. International Program on Quantum Information (IPQI-14), 22 Febuary-02 March 2014, held in Institute of Physics (IOP), Bhubaneshwar, India. Contributed poster entitled "Multiparty Dense Coding vs. Quantum Correlation: Noise Inverts Relative Capability of Information Transfer".

3. One day QIC workshop, 13 November 2014, Harish-Chandra Research Institute, India. Oral presentation on "Canonical Distillation of Entanglement".

4. Young Quantum-2015 (YouQu-15), 23-26 February 2015, Harish-Chandra Research Institute, India. Oral presentation on "Distributed Quantum Dense Coding in Noisy Scenario".

5. International Conference on Quantum Foundations (ICQF-15), 30 November-04 December 2015, held in NIT Patna, India. Contributed poster entitled "Distributed Quantum Dense Coding in Noisy Environments".

6. Meeting on Quantum Information Processing and Applications (QIPA-15), 7-13 December 2015, held in HRI Allahabad, India. Contributed two posters entitled "Regional and global quantum correlations: their interrelation and use", and "Asking quantum correlation about their monogamy score"

7. Joint IAS-ICTP school on Quantum Information, NTU, Singapore, January 2016. Contributed poster entitled "Distributed Quantum Communication".

8. Young Quantum-2017 (YouQu-17), 27 February- 01 March 2017, Harish-Chandra Research Institute, India. Contributed poster entitled "Activation of Nonmonogamous Multipartite Quantum States".

9. Advanced School and Workshop on Quantum Science and Quantum Technologies, ICTP, Trieste, Italy, January 2017. Oral presentation on "Multipartite entanglement measure and its application in quantum communication".

Others

1. Served as a Tutor, Classical Mechanics course, Aug-Dec Semester, 2014.
2. Served as a Tutor, Quantum Information and Computation course, Jan-May Semester, 2016.
3. Members of local organizing committee of Meeting on Quantum Information Processing and Applications (QIPA-2013, QIPA-2015) and Young Quantum Meet (YouQu-15, YouQu-17) at Harish-Chandra Research Institute, 2013, 2015 and 2017.

Tamoghna Das

Tamoghna Das

ACKNOWLEDGEMENTS

Contents

SYNOPSIS

Information transmission between multiple senders and multiple receivers plays an important role in our day-to-day life. The emergence of technologies over the last decades revolutionize the way we communicate. For example, the hand written letters have been replaced by phone-calls, emails, video-chats etc while mass communication also has changed its form from newspaper, mass-gathering to internet version of them. The existing communication systems can broadly be divided into two categories – the communication with security (cryptography) and without securities. In both the cases, it was proven that quantum mechanical laws provide advantages over their classical counterparts [1–4]. Moreover, in a quantum domain, there can be a task which deals with transferring quantum states between two distant locations [5]. During last two decades, it was also found that the common ingredient which makes all these protocols successful is the shared quantum correlation aka entanglement [6] between the sender and the receiver. Apart from the communication schemes, entanglement also plays a crucial role in other technological tasks like error correction [7, 8], and one way quantum computation [9]. In last decade, it has also been established that in physical systems, entanglement as well as other quantum correlations in nearest and next nearest neighbor spins of ground and thermal states can be useful to detect co-operative quantum phenomena like quantum phase transitions, thermal transitions [10, 11].

Let us now concentrate only on classical information transmission (without security) via quantum states and its possible connection with quantum correlation measures. The usual way to transmit classical information is to encode the message in the string of classical bits of 0 and 1, and to send one bit in this manner, one requires two distinguishable objects or two orthogonal states or two dimensional systems. In 1992, Bennett and Wiesner [4] showed that if the sender and the receiver share a maximally entangled state, two bits of classical information can be communicated using only a single quantum bit (qubit), i.e., a two-dimensional quantum system by performing unitary operators on sender's part. It is then sent through a shared quantum channel followed by a measurement on receiver's side. The process is known as quantum dense coding or super dense coding [4]. Note that the sender and the receiver, having no shared entanglement, requires four-dimensional system for sending two classical bits. For an arbitrary shared bipartite quantum state, the capacity of dense coding (DC) can be obtained by performing optimizations over all possible unitary encodings, the probability of encodings, and over all quantum mechanically allowed measurements performed by the receiver. The later optimization over measurements for a given set of states is already obtained by Holevo in 1973 [12]. In particular, it was shown that the information

accessible to the receiver upon measurements, is upper bounded by a quantity, known as a Holevo quantity, which can be achieved assymptotically [13, 14]. Hence, in the two-party scenario, the DC capacity reduces to the maximization of the Holevo quantity over all possible encodings and probabilities. Such optimizations can be performed analytically and hence the capacity of DC is already known in this scenario [15](see also [16–20]). It turns out that for pure bipartite states, the DC capacity increases with the increase of shared bipartite entanglement among the sender and the receiver [6].

The usefulness of communication protocols becomes more prominent, when they involve multiple senders and multiple receivers. On the other hand, the transmission channel in a realistic situation can not be kept completely isolated from the environment, and hence noise almost certainly acts on the encoded parts of the senders' subsystems at the time of sending them through quantum channels. Therefore, extending the DC protocol with several senders and several receivers in the presence of noise is an interesting and important problem in communication theory. The DC capacities involving multiple senders and a single as well as two receivers are obtained for a noiseless case [21, 22], and also recently for a specific noisy channels [23–26] with a single receiver.

In a multiparty domain, the connection of multiparty entanglement or quantum correlation measures with multiparty DC capacity in both noiseless and noisy scenario is still an open question. The challenges behind establishing such connection are as follows: (1) the noisy DC capacity from many senders to more than one receiver is not known; (2) there is no unique measure of multiparty entanglement or quantum correlation, even for pure states. In the proposed thesis, we will overcome both the difficulties. We will find a compact form of DC capacities for multiple senders and two receivers for noisy channels and the second one is settled by considering two computable multiparty measures based on the geometry of the state space of multiparty quantum states [27–29] and the concept of monogamy of quantum correlations [30, 31].

In the finite dimensional case (mainly qubit system), there are some drawbacks in the possible implementation of quantum communication networks in the laboratory [32–35]. However, those drawbacks can be overcome by considering continuous variable (CV) systems. In recent times, the classical information transfer by using a quantum channel has been successfully investigated both theoretically and experimentally, in CV systems, especially in Gaussian states [36–41]. However, it has been discovered that there are several protocols which can not be implemented using Gaussian states with Gaussian operations. Examples include entanglement distillation [42, 43], measurement-based universal quantum computation [44, 45], teleportation [46, 47], and quantum error correction [48]. The increasing importance of non-Gaussian states have led to the discovery of several mechanisms to create such states in the laboratory [49, 50]. An important one is adding and subtracting photons, when the initial state is the

squeezed vacuum state [51–54]. In the proposed thesis, we consider the four-mode squeezed vacuum (FMSV) state as input and deGaussify it by adding and subtracting photons in different modes.

We state below the main results, obtained in the proposed thesis.

- We established a connection between multiparty quantum correlation measures and multiparty DC capacity with arbitrary number of senders and a single receiver [21] in a noiseless scenario [55]. According to the usefulness in DC protocol, we obtained a relative hierarchy among arbitrary multiqubit pure states and the generalized Greenberger-Horne-Zeilinger (gGHZ) [56] states having an equal amount of multipartite entanglement.

- In presence of covariant noise in the senders subsystem, we derived an upper bound on the capacity of classical information transfer between multiple senders and two receivers (distributed DC) [57], where the receivers are situated in distant locations and can only perform local operations and classical communication (LOCC) [6].

- We found that the presence of sufficient amount of noise, in the quantum channels, can invert the relative capability of information transfer for two states (the gGHZ state and the arbitrary multiparty states) with the same multiparty quantum correlation content [55, 57]. The gGHZ state turns out to be more advantageous compared to other three-qubit pure states, having same genuine multiparty entanglement in case of DC scheme with more than one receiver.

- A potential physical system in which quantum communication protocols have successfully been implemented is the class of continuous variable systems. Towards such possible realizations, we have investigated the entanglement patterns of photon-added and -subtracted four-mode squeezed vacuum states [58]. We found that these non-Gaussian states are highly entangled compared to the Gaussian states.

The content of the thesis is divided into seven Chapters.

In Chapter 1 (Introduction), we will discuss about the role of communication network in our day-to-day life and its rapid development over the last few decades. We will also discuss the role of quantum correlations in these revolutionary quantum communication schemes. Chapter 2 (Quantum Correlation Measures), discusses the basic definitions of bipartite entanglement measures and other quantum correlation measures [6], independent of entanglement. Some of the basic measures of multipartite quantum correlations which we will use in the proposed thesis will also be discussed [27, 28, 30, 31] in this chapter. In Chapter 3 (Dense Coding Protocol Involving Multiple Senders and a Single Receiver), we first describe

the dense coding protocol for transferring classical information [15] by using an arbitrary shared bipartite quantum state. We then evaluate the DC capacity for arbitrary bipartite states and extend it to multiple senders and single receiver [21]. Then I will move to a discussion of DC protocol when there is a noise in the transmission channel [23, 24].

A connection between multipartite quantum correlation measures of the shared state and the multiparty DC capacity involving several senders and a single receiver will be reported in Chapter 4 (Multipartite Dense Coding vs. Quantum Correlations) [55]. In particular, we show that for the noiseless channel, if multipartite quantum correlation of an arbitrary multipartite state with arbitrary number of qubits is the same as that of the corresponding generalized Greenberger-Horne-Zeilinger state [56], then the multipartite dense coding capability of former is the same or better than that of the gGHZ state. The result is generic as it holds for the genuine multiparty entangled measure, known as generalized geometric measure [28], as well as for the squared-concurrence [30] and discord monogamy scores [31]. Interestingly, we also analytically prove that the relative capability of classical information transfer between the gGHZ and arbitrary states having the same multiparty quantum correlation content, can be inverted by administering a sufficient amount of noise.

In Chapter 5 (Distributed Quantum Dense Coding), we will first discuss the dense coding protocol between an arbitrary number of senders and two receivers. We will then investigate [57] the effects of noisy channels in this scenario and derive an upper bound on the multipartite DC capacity which is tightened in case of a specific noisy channel, namely the covariant noisy channel [59]. Finally, we also establish a relation between the genuine multiparty entanglement of shared state and the capacity of distributed dense coding using that state, both in the noiseless and the noisy scenarios [57].

Upto now, we have investigated the role of quantum correlation measures in quantum communication schemes in finite dimensional systems. Physical systems that mimic these finite dimensional quantum states include photons with e.g., polarization degrees of freedom, internal levels of ions etc. Such systems have some drawbacks [32–35] which can be overcome by using continuous variable (CV) systems [37, 39, 60]. In CV systems, entanglement are created in the position and momentum variables. Towards creating highly entangled states for possible implementation of quantum communication protocols, in Chapter 6 (Photon Subtracted State is More Entangled than Photon Added State), we report entanglement patterns of four-mode squeezed vacuum states, under addition and subtraction of photons in different modes [58]. We show that entanglement contents of these photon-added and -subtracted states are higher than the initial four mode squeezed vacuum states.

In Chapter 7 (Summary and Future Directions), we will discuss brief summary of all the results

presented in the thesis and some of the future directions which include building of quantum communication network in a deterministic manner [61], which will be easy to realize in experiments.

We believe that the results obtained in the proposed thesis will be step forward to build a quantum communication network in a realistic scenario. It also sheds light on the status of shared multipartite quantum correlations in this network.

List of Figures

List of Tables

Chapter 1

Introduction

At the beginning of the twentieth century, with the development of quantum theory, it has been realized that this theory can show certain features which can not be explained by classical mechanical laws. Quantum correlation shared between two quantum systems is one of such striking properties in quantum mechanics, which have no classical counterparts. In this respect, Einstein Podolosky and Rosen (EPR) argued [62] in 1935 that quantum mechanics is incomplete and the argument was based on the assumptions of locality[1] and reality[2] and by considering two-particle system. In 1964, Bell discarded the EPR argument by constructing a mathematical inequality, based on these two assumptions which can be tested in experiments, and was shown to violate by quantum mechanical states with suitable choices of measurements [63, 64]. It was noticed that the violation of Bell inequality by certain quantum states happens due to the basic postulates of quantum theory, the superposition principle. Moreover, the reason behind the violation is due to the existence of a composite pure quantum system, consisting of two subsystems such that the sum of the information of the individual systems does not add up to the complete information for the whole. Such states are called pure entangled states [6]. For mixed states, the definition of entangled states is much more involved. Specifically, a bipartite mixed quantum state is said to be entangled if it can not be prepared by local quantum mechanically allowed operations and classical communication. Over the last couple of decades, entanglement of bipartite as well as multipartite quantum systems has been shown to be an useful resource [6] due to its vast applicability in quantum computational [9, 65] and communicational tasks [2–5, 66–70]. In all these cases, entangled states turn out to be more advantageous in performing the information processing tasks than the states without entanglement. Most importantly, several of these schemes have been realized in laboratories by using physical systems like photons [71–79], ions [80–87], nuclear magnetic resonances [88–92], and superconducting qubits [93–95]. The usefulness of entanglement enforces us to quantify entanglement content in any arbitrary bipartite and multipartite quantum states. In a bipartite regime, the measure-of-entanglement is well developed subject. In particular, there exists a unique measure of entanglement for any bipartite pure states while for mixed states, there are handful entanglement measures which can be computed efficiently. Notable examples include negativity [96, 97] and logarithmic negativity [97, 98], which are originated from the Peres-

---

[1] The values of the observables of the second particle do not depend on the action of the first one where they are situated in space-like separation.

[2] The measurement results of the particles depend on the direction of the measurement apparatus and some other uncontrollable parameters known as hidden variables [63, 64].

Horodecki entanglement criteria, based on partial transposition [99,100]. The entanglement of formation, defined from the concept of entanglement cost [101–104] is another computable measure for qubit systems. On the other hand, in last decade, several quantum phenomena are reported where entanglement is absent [105–108]. Towards explaining them, quantum correlation measures for two party states, independent of entanglement, were introduced [109,110]. Examples are quantum discord [111–113], and quantum work deficit [114–116] (see also [117–119]), which can capture quantum correlations beyond entanglement.

The situation becomes complicated even for pure states, when the number of parties are increased. However, in recent times significant advances are made to quantify multipartite entanglement for pure quantum states in arbitrary dimensions [6]. They are broadly classified into two catagories - distance-based [27–29] and monogamy-based multipartite quantum correlation measures [2,30,120–122]. In this thesis, some of the bipartite and multipartite quantum correlation measures are introduced (Chapter 2). We will use these measures to obtain the main results of this thesis.

In this thesis, we mainly deal with quantum communication protocol and the role of quantum correlation measures of the shared state in the communication scheme, especially in classical information transmission via quantum states. Specifically, bipartite entanglement of a shared state has been found to be advantageous in the classical information transmission. The classical communication protocol using quantum states can be broadly divided into two major sectors – the communication with security and without security. In the former case, the senders want to share certain information with the receiver secretly, i.e., the information is only known to them, not to any third party. Such a situation has vast applications ranging from internet banking to national security. On the other hand, the latter plays an important role in our day-to-day life. For example, it can be useful for sharing news with our relatives or sharing results of a football match with our friends or sending news to the newspaper office etc. In this thesis, we will consider the classical information transmission without security. The procedure includes three major steps – the encoding of information in quantum states, transmission of a physical system through a transmitor or a channel, and decoding/identifying it by some device. In a classical process, to encode classical information, one uses different distinguishable objects, depending on the number of different information, one intends to send. For example, it can be different colors of balls, or a bit string of 0 or 1. In today's era of electronics, by using computer as encoder, a big sentence or a few words are converted to a bit string, say N bit string of 0 or 1, which corresponds to voltage of some high value as 1, and a low value as 0. It is then transmitted as an electromagnetic wave having high and low voltage pulses. In this situation, to send a message encoded in a bit string of length N, the sender needs to transmit the entire 2^N-dimensional object to the receiver(s) after knowing the information. However, in a quantum domain, the sender can transmit classical information of bit length 2, by sending only a single two dimensional quantum system (a-qubit) to the receiver, provided they apriori share a maximally entangled state (a singlet state), as proposed by Bennett and Wiesner in 1992 [4]. Specifically, the sender performs unitary operations on her part of the shared state, to encode the possible messages, and sends it to the receiver. The unitaries are chosen in such a way that the resulting two party states become mutually orthogonal, which can always be distinguished by a global measurement. The key property behind such advantage is the entanglement content of the shared singlet state, which was quantified as one ebit (entangled bit) [120], used as a unit of entanglement.

For any arbitrary shared quantum states, with non-maximal amount of entanglement, the sender can never be able to transmit 2 bits of classical information, due to the production of non-orthogonal states

after encoding which can only be distinguished probabilistically. Hence, to send the maximal amount of classical information by using these states, the sender as well as the receiver need to optimize the protocol over all possible encoding and the decoding procedures. The capacity of a DC protocol involving a single sender and a single receiver has been obtained in arbitrary dimensions in Refs. [15–20] (see Chapter 3). Moreover, it was observed that for a shared bipartite pure state, the DC capacity is directly related to the entanglement content of the same [6].

In this thesis, we are interested in a communication protocol which involve multiple parties. Such transmission protocol will finally help us to build a communication network, having enormous practical importance. In particular, we will consider a DC protocol with arbitrary number of senders and one or two receivers. Here we call a DC protocol to be a multiparty DC protocol, when all/parts of the senders and the receivers are in distant locations, and a multiparty quantum state is shared among all of them. At the time of encoding the messages, the senders perform local unitary operations and the receivers decode the messages by local quantum operations and classical communication (LOCC). In recent times, the capacity of DC for multiple senders to a single receiver and an upper bound for two receivers are found [21, 22]. However, the similar extension for multiple receivers is not yet known. Let us discuss the reason of not having the extension of DC protocols for arbitrary number of receivers. For the single sender to a single receiver as well as for multiple senders to a single receiver DC scheme the entire ensemble of the encoded states is in possession of the receiver who is allowed to perform any global measurement, and in this situation, the Holevo [12–14] bound provides the maximal information that can be accessed by the receiver upon measurement [21, 22]. In case of two receivers the ensemble is shared between two parties who can perform LOCC. In this scenerio, a local Holevo-like quantity [123, 124] was found and hence the question of capacity for distributed DC protocol or the LOCC-DC capacity can be addressed. In Ref. [21, 22], the upper bound on the capacity of distributed DC was obtained. Note that the Holevo quantity [12] can be achieved asymptotically [13, 14] while for the LOCC-Holevo-like bound, it is still an open question, whether it can be achieved assymptotically or not, resulting only an upper bound on the LOCC-DC [21, 22]. The similar kind of bound on the accessible information for an ensemble, shared among arbitrary number of parties situated far apart is not yet available in the literature and this is the main obstacle for obtaining classical capacities of quantum channels with arbitrary number of receivers.

Upto now, we describe the information transmission protocols in an ideal scenario, showing the advantages of quantum schemes over classical ones. The successful realizations of the DC protocol tell us that the environment, interacting with the system, plays a crucial role in capacities of information transfer. In particular, in the above stated protocols of classical information transmission between multiple senders and a single or two receivers, we have assumed that there is no noise acting on the system. But in reality, the system can never be kept completely isolated from the environment [125], and any environmental interaction, hinders the smooth flow of information, thereby reducing the efficiency of the scheme. In particular, noise can be present either at the time of sharing the multiparty quantum state among all the senders and the receivers, or at the time of sending the encoded part of the state to the receiver(s) in the transmission channel. In the former case, noise acts on the entire system, while for the second kind of noise, only the senders encoded parts are going to be affected. Since the capacities of DC are obtained both for arbitrary pure and mixed states, the first situation is already addressed. On the other hand, the later scenario requires optimization of the Holevo quantity of a noisy ensemble which depends on the noise parameters. Hence, finding the DC capacity is very hard for arbitary noisy environment and there

are only a few noise models for which the capacity is known for a single receiver [23–26]. In Chapter 3, we will discuss the capacities of DC protocol for multiple senders to a single receiver in both noiseless and noisy scenarios.

In Chapter 4, we establish a connection between the multipartite entanglement as well as other QC measures, different than entanglement and the multiport capacity of DC with multiple senders and a single receiver [55]. We report that generalized Greenberger-Horne-Zeilinger (gGHZ) state has a special status in this relation. In particular, we find that among all the multi-qubit pure states having an arbitrary but fixed multiparty DC capacity, the gGHZ states [56] has the highest genuine multiparty entanglement or QC. The above relation is generic as it holds for the multiparty QC measures defined from two different paradigm – the genuine multiparty entanglement measure and the monogamy-based measures. When the transmission channel is sufficiently noisy, we observe that the relative abilities between the gGHZ states and an arbitrary multi-qubit pure states can get inverted. The result holds for both correlated and uncorrelated noise models in the senders' subsystems [55].

Towards developing a dense coding network, i.e., the classical information transfer among arbitrary number of senders and receivers, in Chapter 5, we first discuss an upper bound on the maximal amount of classical information that the two receivers can get by LOCC in a noiseless scenario. When a four-qubit GHZ state is shared among two senders and two receivers, we show by explicitly constructing a LOCC protocol that the upper bound on the LOCC-DC can be achieved. When the senders send their encoded states through a noisy quantum channel, we estimate the LOCC-DC capacity [57]. Moreover, we show that the bound can also be tightened for a specific class of noise model, namely for the covariant noise [59]. When the shared state is four-qubit GHZ state, and the noisy channels are among the amplitude damping, phase damping or the Pauli channels, the upper bounds on the noisy LOCC-DC are analytically evaluated. In this chapter, we also report a relation between the mutiparty entanglement and the LOCC-DC capacity.

We now move to the part of the thesis which is close to the experimental implementation of quantum information processing tasks. The physical system that we consider here is the photonic system. The polarization degrees of freedom in photons mimics the finite-dimensional systems, having some limitations which include no perfect discrimination of Bell states by linear optics [35] etc. If one uses nuclear magnetic resonance (NMR) or ion trap, one can faithfully distinguish Bell states and hence can realize the DC protocol [33, 34], although they can transfer information over a very short distance with currently available technology, compared to the photons. However, all these problems can be overcame by using the continuous variable (CV) systems, i.e., photonic system where instead of considering the polarization degrees of freedom, one uses entanglement between two canonical conjugate coordinates, the position and the momenta of two photonic modes. The communication protocols like teleportation [5] and dense coding [4] have been successfully realized in CV systems, especially by using Gaussian states [36, 38, 39, 41, 60]. However, it was shown that there are quantum technological tasks like entanglement distillation [42], measurement based universal quantum computation [44], teleportation [46] and quantum error correction [48] can not be either implemented or improved by Gaussian states with Gaussian measurements or operations. In recent times, non-Gaussian states are found to be important in several applications and hence several methods are discovered to create them [49, 50]. One of the method to prepare non-Gaussian states is to add and subtract photons from a Gaussian state. In Chapter 6, we choose an entangled multimode squeezed vacuum state, as an initial state and add or subtract photons in(from) its different modes. In particular, we will start with a multimode CV system, namely the four

mode squeezed vacuum state, (FMSV) state, which is a Gaussian entangled state. We briefly discuss about the preparation of two mode and four mode squeezed vacuum (FMSV) states, with the help of a single mode squeezed vacuum states and beam splitters. We investigate the trends of entanglement in different bipartitions of the FMSV state, by adding(subtracting) photons in(from) different modes. To study entanglement systematically, we will introduce two situations – a mode where the number of photons added or subtracted are varying is referred as the "player" modes, while the other modes where no photon or fixed number of photons are added (subtracted), are called the "spectator" modes. We find that the photon-subtracted state can give us higher entanglement [58] than the photon-added state which is in contrast of the two-mode situation [54]. We also study the logarithmic negativity of the two-mode reduced density matrix obtained from the four-mode state which again shows that the state after photon subtraction can possess higher entanglement than that of the photon-added state, and we then compare it to that of the two-mode squeezed vacuum state. Moreover, we examine the non-Gaussianity of the photon-added and -subtracted states to find that the rich features provided by entanglement cannot be captured by the measure of non-classicality.

In the last chapter (Chapter 7), we will summarize our main results and discuss some of the future directions, towards the development of a classical communication network. The classical information transfer considered in this thesis (Chapters 4, 5) via a shared quantum state is in general probabilistic in nature [126–130]. On the other hand, experimental-friendly DC protocol in a single copy level should be deterministic in nature. For a two-party scenario, such scheme was introduced [126]. In particular, if a shared state is not maximally entangled, one has to design the unitary operators in such a way, that the encoded states are mutually orthogonal, thereby distinguishing the output states without any error i.e., deterministically by performing global measurements. Towards building a quantum communication network, one of the future directions is to propose a multiparty deterministic dense coding protocol [61].

In this direction, we present some preliminary results [61] in Chapter 7. Specifically, we describe a multiport deterministic DC protocol and find that three- and four-qubit generalized W states [131] are useful for deterministic DC while generalized GHZ states [56] are not beneficial in this task. However, the extension of this protocol as well as the original DC with higher number of parties, especially, with multiple receivers are still an open question. Another future direction is to build a quantum communication network where the task is to study of quantum state transmission involving multiple parties which are also limited in literature due to mathematical complexities.

Chapter 2

Quantum Correlation Measures

In recent times, characterization and quantification of entanglement in bipartite as well as multipartite quantum systems have created lots of interests [6]. This is due to the fact that correlation, between several parties beyond classical, enables us to realize several quantum information protocols like quantum dense coding [4], quantum teleportation [5], quantum error correction [7, 8], secure quantum cryptography [2], and one way quantum computation [9], in an efficient way compared to their classical counterparts. This increasing interest is further boosted by successful realization of multipartite entangled states in different physical substrates including photons [72–77], ion traps [80–87], nuclear magnetic resonances [88–92], and superconducting qubits [93–95]. On the other hand, many counterintuitive phenomena like nonclassical efficiency of quantum algorithm with vanishingly small entanglement [105, 106] and local indistinguishabality of orthogonal product states [107, 108], are discovered which motivate us to search for quantum correlation (QC) measures, independent of entanglement-separability paradigm. In this chapter, after introducing the definition of entanglement, we will briefly discuss bipartite and multipartite entanglement measures, which we will use in this Thesis. We will also introduce the concept of QC measures, namely quantum discord and quantum work-deficit, which are different than entanglement measures.

2.1   Bipartite entanglement

Let us consider a system consisting of several subsystems. Let $\mathcal{H}^n$ be the Hilbert space of the n-th subsystem. The Hilbert space of the total/joint system, consisting of N different subsystems, can be represented as

$$\mathcal{H} = \bigotimes_{n=1}^{N} \mathcal{H}^n.$$ (2.1)

In a bipartite regime i.e. for $N = 2$, a pure state $|\psi_{AB}\rangle$, shared between A and B, is said to be separable/product, if it is of the form

$$|\psi_{AB}\rangle = |\psi_A\rangle \otimes |\psi_B\rangle.$$ (2.2)

7

The above state can be prepared by local operations only i.e., two parties Alice (A) and Bob (B) can prepare $|\psi_A\rangle$ and $|\psi_B\rangle$, in their own laboratories without any classical communication. Similarly, a mixed state ρ_{AB} is called a product state if

$$\rho_{AB} = \sigma_A \otimes \sigma_B, \tag{2.3}$$

with $\sigma_A(\sigma_B)$ being the respective local subsystem and such state can also be prepared locally by A and B without any classical communication. An arbitrary state that Alice and Bob can prepare by local operations and classical communication (LOCC) is called a separable state. Mathematically,

$$\rho_{AB} = \sum_i p_i \rho_A^i \otimes \rho_B^i, \tag{2.4}$$

where $p_i \geq 0$ and $\sum_i p_1 = 1$. These definitions lead to the definition of an entangled state, which can be stated as follows:

Definition : A bipartite quantum state, ρ_{AB}, is called entangled *iff* it can not be written as a convex combination of the product states of its constituent parties, given in Eq. (2.4), i.e., if ρ_{AB} is entangled,

$$\rho_{AB} \neq \sum_i p_i \rho_A^i \otimes \rho_B^i. \tag{2.5}$$

In case of pure state, $|\psi_{AB}\rangle \neq |\psi_A\rangle \otimes |\psi_B\rangle$, represents an entangled state.

2.2 Measures of bipartite entanglement

Let us now discuss how to quantify entanglement content of a given bipartite state, ρ_{AB}. Before giving definitions of entanglement measures, we briefly discuss certain properties which a valid entanglement measure should follow [101, 120, 132–134]. They are as follows:

1. Entanglement measures, E, of a given state ρ, should be non-negative i.e., $E(\rho) \geq 0$ for all states ρ. E vanishes if and only if ρ is separable.

2. A valid entanglement measure can not increase on average under LOCC. In other words, for any LOCC protocol, described by a trace preserving map Θ, one has $\sum_i p_i E\big(\Theta(\rho_i)\big) \leq E(\rho)$.

3. $E(\rho)$ should be convex. For an ensemble $\{p_i, \rho_i\}$, $E(\sum_i p_i \rho_i) \leq \sum_i p_i E(\rho_i)$.

It was first noted that the singlet state $|\psi^-\rangle = \frac{1}{\sqrt{2}}(|01\rangle - |10\rangle)$ can perform several quantum information processing tasks with maximum efficiency and hence, it was assumed that the singlet state possess maximum amount of entanglement, quantified as one "ebit" [120] (entangled bit). Considering singlet as a resource, two entanglement measures were introduced by using two basic quantum information processes [6] namely entanglement creation and distillation, – entanglement cost and distilable entanglement. For any arbitrary quantum state ρ_{AB}, entanglement cost (E_c) [6] is the minimum number of singlet states needed (per copy level) to prepare ρ_{AB} by performing LOCC in the asymptotic level. On the other hand, distillable entanglement (E_d) [120] is quantified as the maximum number of $|\psi^-\rangle$ states that can be extracted (per copy) by LOCC, from ρ_{AB} when multiple copies ρ_{AB} are available. We are now going to discuss some of the measures of entanglement, which are computable analytically as well as numerically, for a huge class of bipartite states. In case of pure states, we consider entanglement entropy, which turns

out to be an unique measure while for mixed states, we describe entanglement of formation [101–103], concurrence [103, 104], negativity [96, 97] and logarithmic negativity [97, 98]. (See Ref. [6] for other measures.)

2.2.1 Entanglement entropy

For a pure bipartite state $|\psi_{AB}\rangle$, when many copies of the same state are shared between the two parties, say Alice and Bob, and they are only allowed to perform LOCC, it was shown that the amount of singlet state, that can be extracted on average is the von Neumann entropy S of the reduced density matrices ρ_A or ρ_B of $|\psi_{AB}\rangle$ [120]. The von Neumann entropy [135] of any operator σ is defined as

$$S(\sigma) = -\text{tr}(\sigma \log_2 \sigma) = -\sum_i \lambda_i \log_2 \lambda_i, \tag{2.6}$$

where λ_i's are the eigenvalues of σ. And hence, the entanglement entropy E is defined as

$$E(|\psi_{AB}\rangle) = S(\rho_A) = S(\rho_B), \tag{2.7}$$

where

$$\rho_A = \text{tr}_B(|\psi_{AB}\rangle\langle\psi_{AB}|), \tag{2.8}$$

and

$$\rho_B = \text{tr}_A(|\psi_{AB}\rangle\langle\psi_{AB}|). \tag{2.9}$$

A bipartite state $|\psi_{AB}\rangle$ can always be written in the Schimdt decomposition [136] form as

$$|\psi_{AB}\rangle = \sum_i^{\min\{d_A, d_B\}} \sqrt{\mu_i}|i_A\rangle|i_B\rangle, \tag{2.10}$$

with μ_i being the Schmidt coefficient and $\sum_i^{\min\{d_A, d_B\}} \mu_i = 1$. Here d_A and d_B are the dimensions of the Hilbert spaces $\mathcal{H}^A$ and $\mathcal{H}^B$ respectively. Hence, the entanglement entropy reduces to

$$E(|\psi_{AB}\rangle) = -\sum_i \mu_i \log_2 \mu_i, \tag{2.11}$$

which is non-negative as $\mu_i \leq 1$, $\forall i$. It is zero when either all $\mu_i = 0$ or one $\mu_i = 1$, and others vanish, reducing the state to a product state which is clear from Eqs. (2.2) and (2.10). From Eq.(2.7), we also obtain that the entanglement of a pure state is bounded above by the quantity $\min\{\log_2 d_A, \log_2 d_B\}$.

2.2.2 Entanglement of formation and Concurrence

The entanglement of formation (EOF), E_f, and concurrence, $\mathcal{C}$, [102–104] are two interrelated quantities defined from the concept of entanglement cost. EOF of a bipartite state, ρ_{AB}, is the average number of singlet states $|\psi^-\rangle$, that are required to prepare a single copy of the state by LOCC. For the set of pure states, EOF reduces to the entanglement entropy. For any bipartite mixed state ρ_{AB}, the EOF is defined as

$$E_f(\rho_{AB}) = \min_{\{p_i, |\psi^i_{AB}\rangle\}} \sum_i p_i E(|\psi^i_{AB}\rangle). \tag{2.12}$$

The minimization is taken over all possible pure state decompositions of the given state $\rho_{AB} = \sum_i p_i |\psi_{AB}^i\rangle\langle\psi_{AB}^i|$ and $E(|\psi_{AB}^i\rangle)$ is the entanglement entropy, given in Eq. (2.7).

To obtain E_f of any arbitrary state ρ_{AB}, one has to perform the optimization over all pure state decompositions, and it is almost impossible for arbitrary states in any arbitrary dimension, since there exists infinitely many pure state decompositions of ρ_{AB}. However, for two qubit systems (in $2 \otimes 2$)[1], the optimum pure state decomposition has been found in Refs. [102–104] and the compact form of E_f is given by

$$E_f(\rho_{AB}) = h\Big(\frac{1 + \sqrt{1 - \mathcal{C}^2}}{2}\Big), \tag{2.13}$$

where

$$h(x) = -x \log_2 x - (1 - x) \log_2 (1 - x), \tag{2.14}$$

is the binary entropy, and $\mathcal{C}$ is the concurrence of the quantum state ρ_{AB}, given by

$$\mathcal{C}(\rho_{AB}) = \max\{0, \lambda_1 - \lambda_2 - \lambda_3 - \lambda_4\}. \tag{2.15}$$

Here $\{\lambda_i\}_i^4$ are the square roots of the eigenvalues of the non-Hermitian operator, $\rho_{AB}\tilde{\rho}_{AB}$, in descending order. And $\tilde{\rho}_{AB}$ is the spin flipped state of ρ_{AB}, given by

$$\tilde{\rho}_{AB} = \sigma_y \otimes \sigma_y \rho_{AB}^* \sigma_y \otimes \sigma_y, \tag{2.16}$$

where ρ_{AB}^* is the complex conjugation of ρ_{AB} in a fixed basis, namely in the computational basis[2]. For a pure state $|\psi_{AB}\rangle$ in dimension $2 \otimes d$, the concurrence has a compact form [30], given by

$$\mathcal{C}(|\psi_{AB}\rangle) = 2\sqrt{\det(\rho_A)}, \tag{2.17}$$

where ρ_A is the reduced density matrix of $|\psi_{AB}\rangle$, given in Eq. (2.8).

2.2.3 Negativity and Logarithmic Negativity

Negativity [96, 97] and logarithmic negativity [97, 98] of a bipartite quantum state ρ_{AB} in arbitrary dimensions are entanglement measures based on the Peres-Horodecki separability criterion of partial transposition [99, 100]. An arbitrary quantum state ρ_{AB} can always be expressed as

$$\rho_{AB} = \sum_{ik;jl} a_{ij}^{kl} |i_A\rangle\langle k_A| \otimes |j_B\rangle\langle l_B|, \tag{2.18}$$

where $\{|i_A\rangle\}, \{|k_A\rangle\}$ and $\{|j_B\rangle\}, \{|l_B\rangle\}$ are the orthonormal bases in the Hilbert spaces of $\mathcal{H}^A$ and $\mathcal{H}^B$ respectively. Now the partial transposition of ρ_{AB}, with respect to the subsystem A, is given by

$$\rho_{AB}^{T_A} = \sum_{ik;jl} a_{ij}^{kl} |k_A\rangle\langle i_A| \otimes |j_B\rangle\langle l_B|. \tag{2.19}$$

---

[1]The joint Hilbert space comprises of two subsystems $\mathcal{H}^A$ and $\mathcal{H}^B$, with equal dimension two.

[2]The computational basis in a Hilbert space of dimension d is $|0\rangle, |1\rangle, \ldots, |d-1\rangle$, i.e., the eigenbasis of the z-component of spin angular momentum operator of spin $\frac{d-1}{2}$.

Similarly, partial transposition with respect to the other party B can also be achieved by $\rho_{AB}^{T_B} = (\rho_{AB}^{T_A})^T$. For a separable state, given in Eq. (2.4), the partial transposed state, $\rho_{AB}^{T_A}$, is necessarily positive semi-definite[3] [99]. For an arbitrary quantum state ρ_{AB}, the negativity $\mathcal{N}$ is then defined as [96, 97]

$$\mathcal{N}(\rho_{AB}) = \frac{||\rho_{AB}^{T_A}|| - 1}{2}, \tag{2.20}$$

where $||\sigma|| = \sqrt{\sigma^\dagger \sigma}$ is the trace norm or one norm [135] of σ. Note that $\mathcal{N}$ is independent of the parties on which the partial transposition is taken. The above equation reduces to

$$\mathcal{N}(\rho_{AB}) = \sum_i |\lambda_i^n|, \tag{2.21}$$

the absolute sum of the negative eigenvalues $\{\lambda_i^n\}$ of $\rho_{AB}^{T_A}$. By definition, $\mathcal{N}(\rho_{AB})$ vanishes for all the states having positive partial transpose and is non-zero otherwise.

The logarithmic negativity (LN) is obtained in terms of negativity as [97, 98]

$$LN(\rho_{AB}) = \log_2(2\mathcal{N}(\rho_{AB}) + 1) = \log_2 ||\rho_{AB}^{T_A}||. \tag{2.22}$$

Note that for a state of the form $\rho \otimes \sigma$, the LN is additive by construction but negativity is not.

These two entanglement measures, negativity and logarithmic negativity, ensure the non-vanishing entanglement content of all non-positive partial transpose (NPPT) states in all dimensions. However, there exists states [137], which are entangled but remain positive under partial transposition (PPT), known as PPT bound entangled state [138, 139], for which $E_c > 0$ while $E_d = 0$. Hence the above two measures can not quantify the entanglement content for the set of PPT entangled states. However, it was shown in Ref. [100] that in $2 \otimes 2$ and $2 \otimes 3$, a quantum state is separable if and only if it is PPT [139], and hence non-zero values of negativity and logarithmic negativity are necessary and sufficient in these dimensions.

2.3 Information theoretic quantum correlation measures

In this section, we will introduce information theoretic measures of QC [109, 110], which are different than the concept of entanglement measures, discussed in the preceding section. Quantum correlation measures belonging to this category are quantum discord (QD) [111–113], symmetric version of QD [119], geometric QD [117], relative entropy based QD [118], quantum work deficit (WD) [114–116], measurement induced non-locality [140] and many others (see [109, 110]). In this section, we will mainly discuss about QD and quantum WD which we will use in the thesis.

2.3.1 Quantum Discord

Suppose there are two classical random variables X and Y, and the joint probability distribution of getting $X = x$ and $Y = y$ is $p(x, y)$, with their marginal probability distributions $p(x) = \sum_y p(x, y)$ and $p(y) = \sum_x p(x, y)$. The classical mutual information quantifies the interdependence of one random

---

[3] An operator σ is called positive semi-definite if for all arbitrary vector $|\psi\rangle$, $\langle\psi|\sigma|\psi\rangle \geq 0$, i.e., all the eigenvalues of σ are non-negative.

variable on the other [141] and it is given by

$$I(X, Y) = H(X) + H(Y) - H(X, Y), \tag{2.23}$$

where

$$H(X) = -\sum_x p(x) \log_2 p(x), \tag{2.24}$$

is the Shannon entropy, of the probability distribution $p(x)$, quantifying the information content in the distribution and similarly for $H(Y)$. Here $H(X, Y)$ denotes the Shannon entropy of the joint probability distribution of X and Y, i.e., $p(x, y)$. Using Bayes' rule, the conditional probability of getting $X = x$, when $Y = y$ has already occurred, is given by

$$p(x|y) = \frac{p(x, y)}{p(y)}. \tag{2.25}$$

By using the above equation, one can rewrite the classical mutual information as

$$I(X, Y) = H(X) - H(X|Y), \tag{2.26}$$

where

$$H(X|Y) = \sum_y p_y H(X|Y = y) = H(X, Y) - H(Y) \tag{2.27}$$

is the conditional Shannon entropy, which determines the information remained in the joint probability distribution of random variable X and Y, when the outcome of Y is already known.

In the quantum domain, these two classically equivalent definitions of mutual information i.e., Eqs. (2.23) and (2.26), become unequal and their difference has been proposed to be a measure of quantum correlation, known as quantum discord [111–113]. For any composite system, ρ_{AB}, quantizing the first definition of mutual information, one obtains

$$\mathcal{I}(\rho_{AB}) = S(\rho_A) + S(\rho_B) - S(\rho_{AB}), \tag{2.28}$$

where S is the von Neumann entropy defined in Eq. (2.6). This quantity has been argued to be the total correlation in a bipartite state [142]. Quantizing the second definition is not straightforward, since the quantity obtained by replacing the Shannon entropies by the von Neumann ones can be negative for some quantum states [143]. To overcome this drawback, one can make a measurement on one of the subsystems, say subsystem B, of ρ_{AB}, and the measured conditional entropy of ρ_{AB} can be obtained as

$$S(\rho_{A|B}) = \min_{\{B_i\}} \sum_i p_i S(\rho_{A|i}), \tag{2.29}$$

where the rank-1 projective[4] measurement $\{B_i\}$ (one can also use positive operator valued measurement

---

[4] A set of measurement $\{\Pi_i\}$ is called projective valued (PV) measurements or von Neumann measurements if they are positive and satisfying the property $\Pi_i^2 = \Pi_i$. In case of rank-1 PV measurements, $\Pi_i = |\psi_i\rangle\langle\psi_i|$ for some set of mutually orthogonal pure states $\{|\psi_i\rangle\}$. Its action on a quantum state ρ is defined as

$$\rho \to \rho_i = \Pi_i \rho \Pi_i / p_i = |\psi_i\rangle\langle\psi_i|, \text{ with } p_i = \langle\psi|\rho|\psi\rangle. \tag{2.30}$$

The number of measurement operators i.e., i can not be more than the dimension of the Hilbert space of ρ.

(POVM)[5]) is performed on the B-part of the system. Here $\rho_{A|i} = \frac{1}{p_i}\text{tr}_B\big((I_A \otimes B_i)\rho_{AB}(I_A \otimes B_i)\big)$, with $p_i = \text{tr}\big((I_A \otimes B_i)\rho_{AB}(I_A \otimes B_i)\big)$, and I_A being the identity operator on the Hilbert space of subsystem A. Using this quantity, one then quantizes the second definition of mutual information as

$$\mathcal{J}(\rho_{AB}) = S(\rho_A) - S(\rho_{A|B}), \tag{2.32}$$

which has been argued to be a measure of classical correlation of ρ_{AB} [113]. And hence the bipartite states defined in Eqs. (2.2) and (2.3) have no classical correlations according to this measure, although the states in Eq. (2.4) can have non-vanishing value of $\mathcal{J}$ unless all p_i vanishes except one. Finally, quantum discord is defined as

$$\mathcal{D}^{\leftarrow}(\rho_{AB}) = \mathcal{I}(\rho_{AB}) - \mathcal{J}(\rho_{AB}). \tag{2.33}$$

The notation "$\leftarrow$" in the superscript of QD indicates that the measurement has been performed in the subsystem 'B' while $\mathcal{D}^{\rightarrow}$ denotes QD when the measurement is done in the first subsystem, i.e. in subsystem 'A'.

For a pure state $|\psi_{AB}\rangle$, the conditional entropy given in Eq. (2.29) vanishes and hence it reduces to the von Neumann entropy of the reduced density matrix i.e.,

$$\mathcal{D}^{\leftarrow}(|\psi_{AB}\rangle) = S(\rho_B) = S(\rho_A) = \mathcal{D}^{\rightarrow}(|\psi_{AB}\rangle), \tag{2.34}$$

coinciding with the entanglement content in $|\psi_{AB}\rangle$.

2.3.2 Quantum work deficit

Like quantum discord, quantum work deficit of a bipartite state ρ_{AB} is the difference between two quantities, the extractable work from a quantum state under "closed operations" (CO) and "closed local operations and classical communication" (CLOCC) [114–116]. The operations in CO include

1. global unitary operations,

2. dephasing of ρ_{AB} by projective operators defined in the Hilbert space of ρ_{AB},

while CLOCC involves

1. local unitary operations,

2. dephasing by local measurements on the subsystem A or B,

3. communicating the dephased subsystem to the complementary subsystem B or A, over a noiseless quantum channel.

Under CO, the amount of extractable work from ρ_{AB} is

$$I_{CO}(\rho_{AB}) = \log(\dim\mathcal{H}^{AB}) - S(\rho_{AB}), \tag{2.35}$$

---

[5] A positive operator valued measurement (POVM) [135] is a set of generalized measurement operators $\{\mathcal{A}_i\}$, which are positive semidefinite, and acts on a quantum state ρ in the following way:

$$\rho \rightarrow \rho_i = \mathcal{A}_i\rho\mathcal{A}_i^\dagger/p_i, \text{ with } p_i = \text{tr}(\mathcal{A}_i\rho\mathcal{A}_i^\dagger), \tag{2.31}$$

where $\sum_i \mathcal{A}_i^\dagger\mathcal{A}_i = \mathbb{I}$, and p_i is the probability of obtaining the post-measurement state ρ_i.

with $\dim \mathcal{H}^{AB}$ being the dimension of the Hilbert space of ρ_{AB}, while under CLOCC, it is given by

$$I_{CLOCC}(\rho_{AB}) = \log(\dim \mathcal{H}^{AB}) - \min_{\{B_i\}} S(\rho_{AB}^{'}), \qquad (2.36)$$

where $\rho_{AB}^{'} = \sum_i (I_A \otimes B_i)\rho_{AB}(I_A \otimes B_i)$. Quantum work deficit is then defined as

$$WD^{\leftarrow}(\rho_{AB}) = I_{CO}(\rho_{AB}) - I_{CLOCC}(\rho_{AB}). \qquad (2.37)$$

Similarly, one can have $WD^{\rightarrow}(\rho_{AB})$, when the measurement is performed on subsystem A. The quantum WD also reduces to the von Neumann entropy of local density matrix in case of pure bipartite states.

For a general quantum state, evaluation of QD and quantum WD involves an optimization over measurements, which in general, is not easy and hence obtaining a closed analytical expression for arbitrary states is not always possible. In particular, for calculating $S(\rho_{A|B})$ in Eq. (2.29), and I_{CLOCC} in Eq. (2.36), the minimum has to be taken over a set of projective measurements on subsystem B (or A) which requires optimization over certain parameters. It was shown in Ref. [144] that the time required for numerical computation of QD grows exponentially with the increase of the dimension of the Hilbert space, implying that computation of QD is NP-complete. To reduce such complexity, one can constrain their computations by restricting the set of measurements on which optimization has to be performed. Such restrictions are imposed in such a way that a very small amount of error occurs from their actual values. In this way, we obtain a closed analytical form of QD and quantum WD in Ref. [145] for a wide range of mixed bipartite quantum states in two and higher dimensions, including some classes of PPT bound entangled states.

2.4 Multipartite measures of entanglement

It has been established that entanglement is the key resource in building several quantum information technologies [6]. Although most of the studies are limited to the situation involving only two parties [4,5,9], advantages of quantum protocols over classical will be prominent only when they involve multiple parties. Hence quantification of entanglement or QC for a multipartite state is important. Moreover, few party quantum correlated states are now possible to prepare in laboratories by photons [72–77], ions [80–86], superconducting qubits [93–95], and in many others [146, 147].

In last two decades, two-party QC measures and their computations have extensively been studied both for pure and mixed states and they are now well understood. However, this is not the case even for pure multipartite state. There are only a few computable multipartite quantum correlation measures, existing in the literature [6]. One can broadly classify these measures into two categories –

(1) distance based measures and

(2) monogamy based measures.

The measures lying in the first category include geometric measure of entanglement (GM) [27], generalized geometric measure (GGM) [28], multiparty relative entropy of entanglement (MREE) [132, 133, 148], global quantum discord (GQD) [119] and dissonance [149]. On the other hand n-tangle [121], discord monogamy score [110, 150–153], work deficit monogamy score [153, 154], etc belong to the second category.

2.4.1 Distance-based measure

Given a multipartite quantum state, the distance based measures of multiparty entanglement or QC are based on the geometry of the quantum state space. They are defined as the minimum distance of a given state from a set of states that are either non-genuinely multiparty entangled (for GGM and MREE), or completely product (for GM) or classically correlated[6] (for GQD, dissonance) states. Different distance measures like Fubini-Study metric [155], relative entropy distance [135] have been used to define these measures. In the thesis, I mainly discuss about GGM which I will use extensively.

Generalized geometric measure

A multiparty pure state is genuinely multiparty entangled if it is not product across any bipartition. Otherwise it is not genuine multiparty entangled pure state. The genuine multiparty entanglement measure, GGM, is defined as the minimum distance of a given state from a set of multiparty states which are not genuinely multiparty entangled, i.e., which is product at least across one bipartition. For an arbitrary N-party pure quantum state, $|\psi_{12...N}\rangle$, GGM is defined as

$$\mathcal{E}(|\psi_{12...N}\rangle) = 1 - \max_{|\chi\rangle \in \mathcal{S}} |\langle\chi|\psi_{12...N}\rangle|^2, \tag{2.39}$$

where the maximization is taken over the set $\mathcal{S}$, of all N-party pure states $|\chi\rangle$, which are not genuinely multiparty entangled. The distance measure used in this case is the Fubini study metric [155]. Since $|\chi\rangle$ is product in at least one bipartition, we can always write

$$|\chi\rangle = |\chi_{12...N}\rangle = |\chi_{\mathcal{A}}\rangle \otimes |\chi_{\mathcal{B}}\rangle, \tag{2.40}$$

where $\mathcal{A} \cup \mathcal{B} = 1, 2, \ldots, N$ and $\mathcal{A} \cap \mathcal{B} = \emptyset$. We can write the given state $|\psi_{12...N}\rangle$, by using the Schmidt decomposition in the same $\mathcal{A} : \mathcal{B}$ bipartition, as

$$|\psi_{12...N}\rangle = \sum_i \sqrt{\lambda_i}|\mu_{\mathcal{A}}^i\rangle \otimes |\nu_{\mathcal{B}}^i\rangle, \tag{2.41}$$

where $\{\lambda_i\}$ are the set of Schmidt coefficients which are always positive and $\sum_i \lambda_i = 1$. Here $\{|\mu_{\mathcal{A}}^i\rangle\} \in \mathcal{H}^{\mathcal{A}}$ and $\{|\nu_{\mathcal{B}}^i\rangle\} \in \mathcal{H}^{\mathcal{B}}$ are the Schmidt basis (also form a basis[7] in the Hilbert spaces of $\mathcal{A}$ and $\mathcal{B}$) and i runs upto $\min\{\dim\mathcal{H}^{\mathcal{A}}, \dim\mathcal{H}^{\mathcal{B}}\}$. One can also expand $|\chi_{\mathcal{A}}\rangle$ and $|\chi_{\mathcal{B}}\rangle$ in terms of the corresponding Schmidt basis, given by

$$|\chi_{\mathcal{A}}\rangle = \sum_i a_i|\mu_{\mathcal{A}}^i\rangle, \tag{2.42}$$

and

$$|\chi_{\mathcal{B}}\rangle = \sum_i b_i|\nu_{\mathcal{B}}^i\rangle, \tag{2.43}$$

---

[6]A multiparty state is said to be classically correlated if

$$\rho = \sum_i p_i|i_1\rangle\langle i_1| \otimes |i_2\rangle\langle i_2| \otimes \cdots \otimes |i_N\rangle\langle i_N|, \tag{2.38}$$

where $\{|i_k\rangle\}$, $k = 1, 2, \ldots, N$, form a basis in the respective Hilbert spaces.

[7]If the Schmidt basis does not span the entire space i.e., it forms a basis in their respective Hilbert space, one can include more mutually orthonormal states, so that it spans the entire space, thereby form a basis.

where $\sum_i |a_i|^2 = 1$ and $\sum_i |b_i|^2 = 1$. Using Eqs. (2.41) – (2.43), we can rewrite the second term in the right hand side of Eq. (2.39) as

$$
\begin{aligned}
\max_{|\chi\rangle \in \mathcal{S}} |\langle\chi|\psi_{12\ldots N}\rangle| &= \max_{\{a_i\},\{b_j\}} |\sum_i \sum_j a_i^* b_j^* \langle\mu_\mathcal{A}^i| \otimes \langle\nu_\mathcal{B}^j| \sum_k \sqrt{\lambda_k}|\mu_\mathcal{A}^k\rangle \otimes |\nu_\mathcal{B}^k\rangle| \\
&= \max_{\{a_i\},\{b_j\}} |\sum_k a_k^* b_k^* \sqrt{\lambda_k}| \quad (2.44) \\
&\leq \max_{\{a_i\},\{b_j\}} \sum_k |a_k||b_k|\sqrt{\lambda_k} \,. \quad (2.45)
\end{aligned}
$$

To obtain the inequality (2.45), we use the triangle inequality[8]. The optimization over all non genuinely multiparty entangled states $|\chi\rangle$ now reduces to the optimization over the state parameters $\{a_i\}$ and $\{b_j\}$. If we assume that the Schmidt coefficients $\{\lambda_i\}$'s are arranged in the descending order, we have

$$
\begin{aligned}
\max_{|\chi\rangle \in \mathcal{S}} |\langle\chi|\psi_{12\ldots N}\rangle| &\leq \sqrt{\lambda_1} \max_{\{a_i\},\{b_j\}} \sum_k |a_k||b_k| \\
&\leq \sqrt{\lambda_1} \max_{\{a_i\},\{b_j\}} \sqrt{\sum_i |a_i|^2 \sum_j |b_j|^2} \quad (2.46) \\
&\leq \sqrt{\lambda_1}. \quad (2.47)
\end{aligned}
$$

The second inequality (2.46) is obtained by using the well known Cauchy-Schwarz inequality, and the inequality (2.47) is due to the normalization conditions in terms of a_i and b_j. By choosing $|a_1| = |b_1| = 1$ and the rest of the coefficients to be 0 in Eq. (2.44), the above bound can be achieved, and hence the GGM of $|\psi_{12\ldots N}\rangle$ reduces to [28, 29]

$$
\mathcal{E}(|\psi_{12\ldots N}\rangle) = 1 - \max\{\lambda_{\mathcal{A}:\mathcal{B}}|\mathcal{A} \cup \mathcal{B} = \{1, 2, \ldots, N\}, \mathcal{A} \cap \mathcal{B} = \emptyset\}, \quad (2.48)
$$

where $\lambda_{\mathcal{A}:\mathcal{B}}$ is the maximal Schmidt coefficient in the $\mathcal{A} : \mathcal{B}$ bipartite split of $|\psi_{12\ldots N}\rangle$.

2.4.2 Monogamy-based measure

Monogamy of quantum correlations in a shared multipartite quantum state quantifies the sharability of QC in its constituent parties [30]. Monogamy of QC states that in a multipartite state, if QC between two parties is maximum, then these two parties can not share any QC with the third party. Quantitatively, it can be defined as follows: The state $\rho_{12\ldots N}$ is said to be monogamous with respect to a bipartite quantum correlation measure, $\mathcal{Q}$, if [30]

$$
\sum_{i=2}^N \mathcal{Q}_{1i} \leq \mathcal{Q}_{1:rest}, \quad (2.49)
$$

where $\mathcal{Q}_{1i}$ $(i = 2, \ldots, N)$ denotes the amount of quantum correlation shared between its reduced density matrix ρ_{1i} $(i = 2, \ldots, N)$, of $\rho_{12\ldots N}$, and $\mathcal{Q}_{1:rest}$ represents the same between the party 1 and rest of the parties. Here party 1 acts as a "nodal" observer. Eventually, the above inequality restricts the sharability of the bipartite QC measure $\mathcal{Q}$ arbitrarily among its possible partners of the given multipartite state. In quantum information theory, there are many physical quantities which satisfy the monogamy relation. Example include the squared concurrence [30, 121], squared entanglement of formation [156, 157], squared

---

[8]$|a + b| \leq |a| + |b|$.

negativity [158–160], squared quantum discord [161], global quantum discord [162, 163], violation of Bell inequality [164–166], EPR steering [167, 168], contextual inequalities [169, 170] etc.

One should stress here that this restriction of limited sharability of correlation is completely quantum in nature, since in a multiparty state, classical correlations can be shared between its constituent parties arbitrarily. For example, consider a system of three spin-$\frac{1}{2}$ particles, shared between Alice (A), Bob (B) and Charu (C) in a state which is the equal mixture of all spin-up and all spin-down, in the z-direction i.e., the joint state is given by

$$\frac{1}{2}\left(|\uparrow_z\uparrow_z\uparrow_z\rangle\langle\uparrow_z\uparrow_z\uparrow_z| + |\downarrow_z\downarrow_z\downarrow_z\rangle\langle\downarrow_z\downarrow_z\downarrow_z|\right)_{ABC}. \tag{2.50}$$

All two-particle reduced states are then

$$\frac{1}{2}\left(|\uparrow_z\uparrow_z\rangle\langle\uparrow_z\uparrow_z| + |\downarrow_z\downarrow_z\rangle\langle\downarrow_z\downarrow_z|\right), \tag{2.51}$$

which is certainly maximally classically correlated according to the measure given in Eq. (2.32). Therefore, if Alice and Bob share maximal classical correlation, at the same time, they can also share maximum classical correlation with the third party. However, the situation is completely different in the quantum domain as stated before. In this sense, the monogamy of quantum correlations plays an important role in quantum cryptographic protocols [2, 3].

Based on the monogamy inequality (2.49), one can define a measure of multiparty QC, known as a the monogamy score [30, 150–152] of a bipartite QC, $\mathcal{Q}$, as

$$\delta_{\mathcal{Q}} = \mathcal{Q}_{1:rest} - \sum_{i=2}^{N} \mathcal{Q}_{1i}, \tag{2.52}$$

with 1 being the nodal observer. Similarly, one can choose any other party as a nodal observer. Therefore, $\mathcal{Q}$ is said to be monogamous if $\delta_{\mathcal{Q}}$ is positive for all states. The advantage of such a multiparty QC measure is that it can be computed in terms of bipartite quantum correlation measures which are well-understood and several bipartite computable QC measures exists in the literature.

In Eq. (2.52), if $\mathcal{Q}$ is chosen to be squared concurrence (see Eq. (2.15)), then we obtain the tangle or N-tangle [30], given by

$$\tau(\rho_{12...N}) = \delta_{\mathcal{C}^2} = \mathcal{C}_{1:rest}^2 - \sum_{i=2}^{N} \mathcal{C}_{1i}^2, \tag{2.53}$$

which is known to be non-negative for all multiqubit states [30, 121]. Choosing $\mathcal{Q}$ to be QD and quantum WD, we obtain the discord [152] and WD monogamy scores [154] respectively, given by

$$\delta_{\mathcal{D}}(\rho_{12...N}) = \mathcal{D}_{1:rest} - \sum_{i=2}^{N} \mathcal{D}_{1i}, \tag{2.54}$$

$$\delta_{\text{WD}}(\rho_{12...N}) = \text{WD}_{1:rest} - \sum_{i=2}^{N} \text{WD}_{1i}. \tag{2.55}$$

They can be negative even for some three qubit pure states [31, 110, 153, 171].

Dense Coding Protocol Involving Multiple Senders and a Single Receiver

In this chapter, we consider a quantum communication protocol whose task is to transfer classical information, involving several senders and a single receiver, with the help of a quantum state shared among all the parties well in advance [4, 15–24]. Any communication protocol involves three major steps which are as follows:

1. Encoding of information in a physical system,

2. Sending the physical system through a physical channel, and

3. Decoding of information.

In this thesis, we mainly concentrate on encoding of classical information in a quantum state. The advantage of classical information transfer by using entangled state, namely the singlet state, was first shown by Bennett and Wiesner in 1992 [4] (see also [15–24]). The protocol is known as "quantum dense coding" or the "superdense coding". In 1996, the quantum dense coding (DC) scheme has been experimentally demonstrated with photons [71] and later on with nuclear magnetic resonance (NMR) [88, 89], trapped ions [87], and also in continuous variable systems [172, 173]. In last ten years or so, the capacities of DC protocol for arbitrary bipartite and multipartite states, having arbitrary number of senders and a single receiver are obtained [15–24].

In this chapter, we first introduce the original DC protocol of Bennett and Wiesner by the singlet state, shared between a single sender and a single receiver. Then we will elaborate the DC protocol for an arbitrary shared bipartite quantum state. We also extend the scheme for multiple senders and a single receiver where a multiparty quantum state is shared between them. We first present all the protocols for the noiseless channel. We will finally discuss the DC protocol in a noisy scenario which we will use in later chapters. We will also describe some of the exemplary noisy channels which we will use later.

3.1 Dense Coding protocol in a noiseless scenario

In this section, we consider classical information transfer from multiple senders to a single receiver when they share a multipartite quantum state and there is no noise acting on the system as well as on the

	Alice's answer	Unitary encoding	Output state	
	Rainy and Win	I	$\lvert\psi^-_{AB}\rangle = \frac{1}{\sqrt{2}}(\lvert01\rangle - \lvert10\rangle)$	
	Rainy and Loss	σ_z	$\lvert\psi^+_{AB}\rangle = \frac{1}{\sqrt{2}}(\lvert01\rangle + \lvert10\rangle)$	
	Sunny and Win	σ_x	$\lvert\phi^-_{AB}\rangle = \frac{1}{\sqrt{2}}(\lvert00\rangle - \lvert11\rangle)$	
	Sunny and Loss	σ_y	$\lvert\phi^+_{AB}\rangle = \frac{1}{\sqrt{2}}(\lvert00\rangle + \lvert11\rangle)$	

Table 3.1: Table of the DC protocol proposed by Bennett and Wiesner. The columns correspond to the four possible answers of two binary questions, Alice's encoding operations and the states shared between Alice and Bob after encoding.

transmission channel. First, we discuss the phenomenal paper of dense coding in details.

3.1.1 Dense coding protocol for singlet

The "dense coding" protocol, proposed by Bennett and Wiesner [4], between a single sender (Alice) and a single receiver (Bob), can transmit upto two bits[1] of classical information, by encoding information using only one quantum bit (qubit)[2]. Before presenting the protocol, let us first discuss the scheme of sending 2 bits from Alice to Bob without using any shared entangled state. Suppose, Alice needs to inform Bob the answers of the following two questions:

1. The weather condition of Alice's hometown which can be either "Rainy" or "Sunny",

2. The result of the football match of Alice's favorite team, either "Win" or "Loss".

To send this 2 bits of classical information, Alice requires *four* distinguishable objects, like four color of balls, four kinds of waves. In other words, Alice requires four orthogonal states or four dimensional object to encode 2 bits of classical information.

Let us now see if Alice and Bob share a maximally entangled two-qubit state, the singlet state $\lvert\psi^-_{AB}\rangle = \frac{1}{\sqrt{2}}(\lvert01\rangle - \lvert10\rangle)_{AB}$, they can get some advantage over classical protocol. Alice's aim is to send two bits or one of the four messages to Bob. It can be done in following steps:

Step 1: Depending on the message, Alice performs unitary operations on her part of the quantum state, i.e., she chooses an operation from the set consisting of the three Pauli matrices[3] and identity, $\{\sigma_x, \sigma_y, \sigma_z, I\}$ which correspond to the four possible answers of the above two binary questions (see Table 3.1). It is assumed that Bob knew the possible unitary encoding corresponding to the answers, before starting the protocol.

---

[1]Any kind of binary information is quantified as a "bit" in information theory. In classical regime bit can be any one of $\{0, 1\}$.
[2]Qubit is an arbitrary two-dimensional quantum state [174].
[3]The three Pauli matrices are given by

$$\sigma_x = \begin{pmatrix} 0 & 1 \\ 1 & 0 \end{pmatrix}, \qquad \sigma_y = \begin{pmatrix} 0 & -i \\ i & 0 \end{pmatrix}, \qquad \sigma_z = \begin{pmatrix} 1 & 0 \\ 0 & -1 \end{pmatrix}.$$

	Alice's answer	Unitary encoding	Output state	
	Rainy and Win	I	$\|\phi_{AB}^1\rangle = a\|01\rangle + b\|10\rangle$	
	Rainy and Loss	σ_z	$\|\phi_{AB}^2\rangle = a\|01\rangle - b\|10\rangle$	
	Sunny and Win	σ_x	$\|\phi_{AB}^3\rangle = a\|11\rangle + b\|00\rangle$	
	Sunny and Loss	σ_y	$\|\phi_{AB}^4\rangle = a\|11\rangle - b\|00\rangle$	

Table 3.2: Table of the Alice's unitary encodings and the corresponding output states for a arbitrary shared bipartite pure quantum state, $|\phi_{AB}\rangle = a|01\rangle + b|10\rangle$.

Step 2. Alice sends her part of the quantum state to Bob, by using a noiseless transmission channel and Bob now possess the entire two-qubit state.

Step 3. Performing a joint Bell basis measurement, $\{|\psi^{\pm}\rangle, |\phi^{\pm}\rangle\}$, Bob can identify the message that Alice has sent to him.

In this process, by sending only her part of the quantum state (a single qubit or a two dimensional object), Alice is able to communicate two bits of classical information to Bob, and hence the capacity of dense coding is considered to be two in this case. Note that, in the entire process, all the answers are considered to be equally probable.

Suppose now that Alice and Bob share an arbitrary two-qubit pure quantum state, $|\phi_{AB}\rangle = a|01\rangle + b|10\rangle$, with $|a|^2 + |b|^2 = 1$, instead of a singlet. After performing the same unitary encoding as given in Table 3.2, we note that the encoded states no longer remain mutually orthogonal. Hence Bob will not be able to distinguish the four non-orthogonal states with certainty by using the unitary operations as before[4] To distinguish them with a non-zero probability, he can perform positive operator valued measurement (POVM) [135], resulting to a probabilistic DC protocol. Protocols unlike the previous deterministic one, we can infer that the capacity decreases when a shared state is nonmaximally entangled which we discuss. We will also discuss how to perform dense coding deterministically with the nonmaximally entangled state, in the last chapter.

3.1.2 DC for arbitrary shared state

We now consider the dense coding scheme when the sender (Alice) and the receiver (Bob) share an arbitrary quantum state ρ_{AB}, defined on $\mathcal{H}^A \otimes \mathcal{H}^B$. Here we assume that both the Hilbert spaces $\mathcal{H}^A$ and $\mathcal{H}^B$ are finite dimensional complex Hilbert spaces, with dimensions d_A and d_B respectively. Suppose, Alice needs to send Bob some messages $\{x\}$, which occur with probabilities p_x. As discussed in the preceding section, she applies unitary operator U_A^x, with probability p_x on her part of the quantum state,

---

[4]It is interesting to ask at this point whether there exists other unitary operations which can be performed on non-maximally entangled states, leading to deterministic transfer of 2 bits. In case of two qubits, it was shown that this is not possible [126]. (see also Chapter 7)

resulting an ensemble of states $\mathcal{E} = \{p_x, \rho_{AB}^x\}$, where

$$\rho_{AB}^x = \left(U_A^x \otimes I_B\right)\rho_{AB}\left(U_A^{x\dagger} \otimes I_B\right). \tag{3.1}$$

Now Alice's task is to send her part of the ensemble $\mathcal{E}$ to Bob by using a noiseless quantum transmission channel. Upon receiving the Alice's part, Bob possess the entire ensemble $\mathcal{E} = \{p_x, \rho_{AB}^x\}$. To gather maximal information about the message x, Bob has to optimize over a set of measurements $\{M_y\}$. If the measurement outcome turns out to be y, occurring with probability p_y, then the maximal amount of information that Bob can extract about $\mathcal{E}$, is called the accessible information I_{acc}, and it is bounded by the *Holevo* quantunity [12], given by

$$I_{acc} \leq \underbrace{S\left(\sum_x p_x \rho_{AB}^x\right) - \sum_x p_x S\left(\rho_{AB}^x\right)}_{\chi(p_x, \rho_{AB}^x)}. \tag{3.2}$$

For an arbitrary quantum state shared between Alice and Bob, the maximal amount of information that Alice is able to send by unitary encoding is called the capacity of dense coding, denoted by C. To obtain the capacity of DC, one has to perform optimizations over all possible unitary encodings, the probabilities of encoding, and over all quantum mechanically allowed measurements performed by the receiver. The optimization over measurements for a given set of states is already obtained via the Holevo quantity which can be achieved assymptotically [13, 14], i.e., when many copy of the same ensemble is provided. Therefore, the DC capacity, C, reduces to the maximization of the Holevo quantity, over all possible encodings and probabilities, i.e.,

$$C(\rho_{AB}) = \max_{\{p_x, U_A^x\}} \chi(p_x, \rho_{AB}^x). \tag{3.3}$$

If we focus on the second term of the Holevo quantity in (3.2), we get

$$\sum_x p_x S\left(\rho_{AB}^x\right) = \left(\sum_x p_x\right)S\left(\rho_{AB}\right) = S\left(\rho_{AB}\right). \tag{3.4}$$

This is due to the fact that the unitary operations do not change the spectrum of a density matrix and $\sum_x p_x = 1$. Moreover, if we apply the subadditivity of the von Neumann entropy, the first term in (3.2) reduces to

$$\begin{aligned}
S\left(\sum_x p_x \rho_{AB}^x\right) &\leq S\left(\sum_x p_x \rho_A^x\right) + S\left(\sum_x p_x \rho_B^x\right) \\
&\leq \log_2 d_A + S(\rho_B).
\end{aligned} \tag{3.5}$$

To obtain the first term in the second line, we use that the von Neumann entropy of ρ is bounded above by the dimension of the state i.e., $S(\rho_A) \leq \log d_A$. On the other hand, the second term involves the von Neumann entropy of the marginal density matrix of Bob, which does not change under the action of unitary on Alice's side i.e.,

$$\rho_B^x = \text{tr}_A\left(\left(U_A^x \otimes I_B\right)\rho_{AB}\left(U_A^{x\dagger} \otimes I_B\right)\right) = \rho_B. \tag{3.6}$$

Hence the capacity [15–20] in Eq. (3.3) reduces to

$$C(\rho_{AB}) \leq \log_2 d_A + S(\rho_B) - S(\rho_{AB}). \tag{3.7}$$

It was shown in Ref. [15] that this bound can be achieved by choosing the encoding operations $\{U_A^x\}$ chosen from a complete set of unitary operators $\{W_x\}_{x=0}^{d_A^2-1} \in \mathcal{H}^A$, satisfying the following conditions

$$\frac{1}{d_A}\text{tr}(W_x W_y^\dagger) = \delta_{xy}, \tag{3.8}$$

$$\frac{1}{d_A}\sum_x W_x \Xi W_x^\dagger = \text{tr}(\Xi)I_A, \tag{3.9}$$

with equal probability $p_x = \frac{1}{d_A^2}$. Therefore, the DC capacity takes the form

$$C(\rho_{AB}) = \log_2 d_A + S(\rho_B) - S(\rho_{AB}). \tag{3.10}$$

Note that the first term in Eq. (3.10) is the capacity of classical information transmission without sharing of an entangled state, since only d distinct massages can be communicated by transmitting a d dimensional object (classical protocol of information transfer). The negation of quantum conditional entropy $-S(A|B) = S(\rho_B) - S(\rho_{AB})$ is known as the quantum advantage of the DC protocol [175], or the coherent information [143]. Therefore, positivity of coherent information guarantees the dense codeability of the shared state ρ_{AB}, which is always the case for a pure entangled states. Note that the quantity $S(A|B)$ becomes sometime positive, which is the situation for all classically correlated (CC) state [5] and hence $C(\rho_{AB}) \leq \log_2 d_A$, for all CC states. In such a situation, one needs to use the classical protocol for information transmission, which always saturates the bound $\log_2 d_A$. On the other hand, we know

$$S(\rho_B) - S(\rho_{AB}) \leq S(\rho_B) \leq \log_2 d_B, \tag{3.11}$$

and hence the upper bound on $C(\rho_{AB})$ is $\log_2 d_{AB}$. Therefore, we define the capacity of DC in the following way:

$$C(\rho_{AB}) = \frac{1}{\log d_{AB}} \max\{\log_2 d_A, \log_2 d_A + S(\rho_B) - S(\rho_{AB})\}. \tag{3.12}$$

If the shared state is a pure one $|\psi_{AB}\rangle$, then the DC capacity reduces to

$$C(|\psi_{AB}\rangle) = \frac{1}{\log d_{AB}} \max\{\log_2 d_A, \log_2 d_A + S(\rho_B)\}, \tag{3.13}$$

since $S(|\psi_{AB}\rangle) = 0$. We can compare the DC capacity given in Eq. (3.13), with the protocol described in Sec 3.1.1. For a shared $|\psi_{AB}^-\rangle$, the reduced density matrix in the receiver's subsystem is $\rho_B = \frac{1}{2}\mathbb{I}_2$, and hence $C(|\psi_{AB}^-\rangle) = \log_2 2 + 1 = 2$, as $d_A = 2$. In $d \otimes d$ system, the DC capacity reaches its maximum value for maximally entangled states, given by

$$|\psi_{AB}\rangle = \frac{1}{\sqrt{d}}\sum_i |ii\rangle, \tag{3.14}$$

---

[5]A classically correlated state is $\rho_{AB} = \sum_{ij} p_{ij}|i_A\rangle\langle i_A| \otimes |j_B\rangle\langle j_B|$, where $\{|i_A\rangle\}$ and $\{|j_B\rangle\}$ are orthogonal set of states in the Hilbert spaces of A and B, with $\sum_{ij} p_{ij} = 1$.

where $\{|i\rangle\}$ forms a basis in d dimensional Hilbert space. Moreover, from Sec. 2.2.1, we have seen that for a pure bipartite state $|\psi_{AB}\rangle$, $E(|\psi_{AB}\rangle) = S(\rho_B)$, and hence we get

$$C(|\psi_{AB}\rangle) = \frac{1}{\log d_{AB}} \max\{\log_2 d_A, \log_2 d_A + E(|\psi_{AB}\rangle)\}. \tag{3.15}$$

This implies the capacity of classical information transfer for a bipartite shared pure state is directly related to the entanglement of the shared state and the state is always useful for DC *iff* it is not product. We will come back to this one-to-one connection between the capacity and entanglement in the next chapter for multipartite states which is one of the results presented in this thesis.

3.1.3   Dense coding protocol involving multiple senders and a single receiver

In the multiparty quantum DC protocol, an arbitrary multipartite quantum state, $\rho_{S_1 \ldots S_N R}$, is shared between N senders, $S_1, \ldots, S_N$ and a single receiver R. Here we assume that the senders are situated in distant locations. Suppose that the jth sender encodes her message x_j, by performing unitary operators $U_j^{x_j}$ on her part of the shared state with probability p_{x_j}, and sends it to the only receiver present in the protocol, with the help of a noiseless quantum channel. Similarly, other senders also perform unitary operations on their part, depending on their message. After obtaining the entire ensemble $\{p_x, \rho_{S_1 \ldots S_N R}^x\}$, where $p_x = p_{x_1} p_{x_2} \ldots p_{x_N}$, and $\rho_{S_1 \ldots S_N R}^x = (U_1^{x_1} \otimes U_2^{x_2} \otimes \ldots \otimes U_N^{x_N} \otimes I_R) \rho_{S_1 \ldots S_N R} (U_1^{x_1 \dagger} \otimes U_2^{x_2 \dagger} \otimes \ldots \otimes U_N^{x_N \dagger} \otimes I_R)$, the receiver now performs measurement on the entire state, to gather as much information as possible about the message x. In this case also, the information accessible to the receiver is bounded above by the Holevo quantity [12] of the given ensemble

$$I_{acc} \leq S\Big(\sum_x p_x \rho_{S_1 \ldots S_N R}^x\Big) - \sum_x p_x S\big(\rho_{S_1 \ldots S_N R}^x\big). \tag{3.16}$$

Since it can be achieved in the asymptotic level, the multiparty DC capacity is obtained by performing the optimization over all unitaries and probabilities i.e.,

$$C(\rho_{S_1 \ldots S_N R}) = \max_{\{p_{x_j}\},\{U_j^{x_j}\}} \Big[S\Big(\sum_x p_x \rho_{S_1 \ldots S_N R}^x\Big) - \sum_x p_x S\big(\rho_{S_1 \ldots S_N R}^x\big) \Big]. \tag{3.17}$$

The optimization has been carried out in Ref. [21] in a similar fashion as discussed in Sec. 3.1.2, and the multiparty DC capacity is given by

$$C(\rho_{S_1 \ldots S_N R}) = \log_2 d_{S_1 \ldots S_N} + S(\rho_R) - S(\rho_{S_1 \ldots S_N R}), \tag{3.18}$$

where $d_{S_1 \ldots S_N} = d_{S_1} \ldots d_{S_N}$, with d_{S_j} $(j = 1, 2, \ldots, N)$ being the dimensions of the Hilbert spaces of the individuals sender, S_j and the DC advantage is $S(\rho_R) - S(\rho_{S_1 \ldots S_N R}) \leq \log_2 d_R$, which can be both positive and negative, with d_R being the dimension of the Hilbert space of the receiver's subsystem. In my thesis, I will therefore use the multiparty DC capacity of an arbitrary $N + 1$ party shared state $\rho_{S_1 \ldots S_N R}$, as

$$C^{multi}(\rho_{S_1 \ldots S_N R}) = \frac{1}{\log d_{S_1 \ldots S_N R}} \max\{\log d_{S_1 \ldots S_N}, \log d_{S_1 \ldots S_N} + S(\rho_R) - S(\rho_{S_1 \ldots S_N R})\}. \tag{3.19}$$

The state will be useful for multiparty DC if $S(\rho_R) - S(\rho_{S_1 \ldots S_N R}) > 0$.

3.2 Dense coding capacity in presence of noise

In this section, we discuss the capacity of classical information transfer in presence of noise. In particular, since the system can not be kept completely isolated from the environment, the noise is unavoidable and is inevitably present in the system [125, 135]. Noise can in general decrease the quantum correlation present in the system and hence decreases its ability in performing many quantum technological tasks, including quantum communicational capacity.

The noise in a quantum channel of the DC protocol can be considered at several levels of complexity. We consider mainly following two scenarios:

1. We consider the case where the noise is present before the encoding of classical information, i.e., noise interacts in the quantum system when it is shared between the senders and the receiver. In this case, we assume that the quantum channel that transmits the encoded state is noiseless.

2. We consider another situation where after the encoding is performed on the sender's part of the shared state, noise acts at the time of sending the encoded part of the senders through a quantum channel. It includes the previous situation as well.

Before presenting the effects of noise on the capacity of DC, let us discuss different types of noise and their formalism that we will use in my thesis.

3.2.1 Mathematical description of noise

Mathematically, noise can be described [125, 135] as a completely positive trace preserving (CPTP) map, Λ and a quantum state ρ after passing through a noisy channel, Λ transforms as

$$\rho :\rightarrow \Lambda(\rho), \tag{3.20}$$

with the following properties

1. Linearity: $\Lambda(\alpha\rho_1 + \beta\rho_2) = \alpha\Lambda(\rho_1) + \beta\lambda(\rho_2)$.

2. Hermiticity: $\rho = \rho^\dagger \Rightarrow \Lambda(\rho) = \Lambda(\rho^\dagger)$.

3. Trace preserving: $\text{tr}(\rho) = \text{tr}\big(\Lambda(\rho)\big) = 1, \ \forall\rho$.

4. Positive: $\Lambda(\rho) \geq 0, \forall \ \rho \geq 0$.

5. Completely positive: For a bipartite state ρ_{AB}, if noise Λ_A acts only on the subsystem A, $\Lambda_A(\rho_{AB}) \geq 0, \forall \ \rho_{AB}$.

The last property is not true for all maps, which are satisfying the properties $1. - 4$. For example, one can consider the partial transposition (PT) map [99], which acts on a composite state ρ_{AB}, as $PT(\rho_{AB}) = \rho_{AB}^{T_A}$, (see Eq. (2.19)), resulting an operator which is not always positive as shown in Refs. [96–100]. Hence PT map is positive but not completely positive.

The noise model can be considered as an interaction of the system ρ_S with the environment, which we consider to be in a state $|0\rangle_E$. Now the joint state is $\rho_S \otimes |0\rangle\langle 0|_E$, and any quantum interaction between

the system S and the environment E, can be described by a joint unitary operator U_{SE}, acting on the entire system-environment duo. Therefore, the system transforms as

$$
\begin{aligned}
\Lambda(\rho_S) &= \mathrm{tr}_E\big(U_{SE}(\rho_S \otimes |0\rangle\langle 0|_E)U_{SE}^\dagger\big) \\
&= \sum_\alpha {}_E\langle\alpha|U_{SE}(\rho_S \otimes |0\rangle\langle 0|_E)U_{SE}^\dagger|\alpha\rangle_E \\
&= \sum_\alpha {}_E\langle\alpha|U_{SE}|0\rangle_E \rho_S \langle 0|U_{SE}^\dagger|\alpha\rangle_E \\
&= \sum_\alpha K_\alpha \rho_S K_\alpha^\dagger,
\end{aligned}
\tag{3.21}
$$

where $\{|\alpha\rangle_E\}$ is a set of orthogonal basis in the Hilbert space of the environment and $K_\alpha = {}_E\langle\alpha|U_{SE}|0\rangle_E$. Therefore, the noise model, i.e., the linear map Λ, can be expressed as the operator sum representation [176] given in Eq. (3.21) by using operators $\{K_\alpha\}$, known as Kraus operators [125, 135, 176], with $\sum_\alpha K_\alpha^\dagger K_\alpha = \mathbb{I}$, belonging to the same Hilbert space in which the quantum state systems ρ is defined and over which it acts and Λ is called quantum channels, represented by

$$
\Lambda(\rho) = \sum_\alpha K_\alpha \rho K_\alpha^\dagger.
\tag{3.22}
$$

3.2.2 Examples of noisy quantum channels

In the realm of quantum information and computation, the noise can either interact with the entire system or some parts of the system or locally in each parts of the system. The noise model can be divided into two broad categories. For an N-party quantum state, $\rho_{1\ldots N}$, they are

1. global noise, and

2. local noise.

Global noise

A noise model, Λ^G, acting on a system of N parties, $\rho_{1\ldots N}$, is said to be global if it acts as

$$
\Lambda^G(\rho_{1\ldots N}) = \sum_\alpha K_\alpha \rho_{1\ldots N} K_\alpha^\dagger,
\tag{3.23}
$$

where $\{K_\alpha\}$, is the set of Kraus operator defined in the joint Hilbert space of all the parties, satisfying $\sum_\alpha K_\alpha^\dagger K_\alpha = I_{1\ldots N}$. If the action of the $\{\tilde{K}_\alpha^j\}_{j=1}^N$ on each subsystem reads as

$$
\Lambda^G(\rho_{1\ldots N}) = \sum_\alpha \tilde{K}_\alpha^1 \otimes \ldots \otimes \tilde{K}_\alpha^N \rho_{1\ldots N} \tilde{K}_\alpha^{1\dagger} \otimes \ldots \otimes \tilde{K}_\alpha^{N\dagger},
\tag{3.24}
$$

the noise can be called completely correlated noise model and can also be considered as a global noise model. If $\{\tilde{K}_\alpha^j\}_{j=1}^N$ are chosen from the Pauli matrices, it is then known as fully correlated Pauli channel, as will be discussed later.

Local Noise

In contrast to the global noise, the local noise acts locally on the subsystems of the entire state, $\rho_{1...N}$, as

$$\Lambda^L(\rho_{1...N}) = \sum_{\{\alpha\}} K_{\alpha_1}^{\mathcal{A}_1} \otimes \ldots \otimes K_{\alpha_r}^{\mathcal{A}_r} \rho_{1...N} K_{\alpha_1}^{\mathcal{A}_1\dagger} \otimes \ldots \otimes K_{\alpha_r}^{\mathcal{A}_r\dagger}, \tag{3.25}$$

where $\mathcal{A}_1 \cup \mathcal{A}_2 \ldots \cup \mathcal{A}_r = N$, and $\mathcal{A}_1 \cap \mathcal{A}_2 \ldots \cap \mathcal{A}_r = \emptyset$, with $\emptyset$ being the null set and $K_{\alpha_j}^{\mathcal{A}_j}$ is some Kraus operator in the Hilbert space of the system $\mathcal{A}_j$, which can comprise of few subsystems of the entire system or a single system. It is called completely uncorrelated or completely local if

$$\Lambda^L(\rho_{1...N}) = \sum_{\{\alpha\}} K_{\alpha_1}^1 \otimes \ldots \otimes K_{\alpha_N}^N \rho_{1...N} K_{\alpha_1}^{1\dagger} \otimes \ldots \otimes K_{\alpha_N}^{N\dagger}, \tag{3.26}$$

where $K_{\alpha_j}^j$ represents the Kraus operator on the jth system which is a subclass of the model, given in Eq. (3.25).

For the qubit system, there are many examples of noisy channels [125, 135], for which Kraus operators can be found. The examples of channels that we will use in this thesis are

    (a) amplitude damping channel.

    (b) phase damping channel.

    (c) Pauli channel.

These channels play important roles in the problem of decoherence [125]. The amplitude damping channel has been used to model the spontaneous decay of a photon from an excited atomic state to its ground state, while the phase damping one can correspond to scattering events. Pauli channels include a reasonably large class of quantum channels like the bit flip, and depolarizing channels, and also play an important role in the problem of decoherence. Pauli channels have been used to study the Pauli cloning machine [177], and they comprise a huge class of noisy channels. We will now discuss them individually and will write down the Kraus operators.

Amplitude damping channel

A single qubit ρ, after passing through the amplitude damping channel, transforms as

$$\rho \longrightarrow \Lambda_\gamma^{AD}(\rho) = M_0 \rho M_0^\dagger + M_1 \rho M_1^\dagger, \tag{3.27}$$

where the Kraus operators, M_i $(i = 0, 1)$, are given by

$$M_0 = \begin{pmatrix} 1 & 0 \\ 0 & \sqrt{1-\gamma} \end{pmatrix}, \quad M_1 = \begin{pmatrix} 0 & \sqrt{\gamma} \\ 0 & 0 \end{pmatrix}, \tag{3.28}$$

satisfying the condition

$$M_0^\dagger M_0 + M_1^\dagger M_1 = 1, \tag{3.29}$$

with $0 \leq \gamma \leq 1$ being the noise parameter.

Phase damping channel

Phase damping channel or dephasing channel, Λ^{PD}, acts on a single qubit state ρ, in the following way:

$$\Lambda^{PD}(\rho) = M_0 \rho M_0^\dagger + M_1 \rho M_1^\dagger + M_2 \rho M_2^\dagger, \tag{3.30}$$

where the M_i's are

$$M_0 = \begin{pmatrix} \sqrt{1-p} & 0 \\ 0 & \sqrt{1-p} \end{pmatrix}, \quad M_1 = \begin{pmatrix} \sqrt{p} & 0 \\ 0 & 0 \end{pmatrix}, \quad M_2 = \begin{pmatrix} 0 & 0 \\ 0 & \sqrt{p} \end{pmatrix}, \tag{3.31}$$

with $0 \leq p \leq 1$ being the noise parameter.

Pauli channel

In case of Pauli channel, the Kraus operators are chosen from the Pauli matrices, given by

$$\sigma_x = \begin{pmatrix} 0 & 1 \\ 1 & 0 \end{pmatrix}, \quad \sigma_y = \begin{pmatrix} 0 & -i \\ i & 0 \end{pmatrix}, \quad \sigma_z = \begin{pmatrix} 1 & 0 \\ 0 & -1 \end{pmatrix}. \tag{3.32}$$

When an arbitrary qubit state, ρ, is passed through the Pauli channel [59, 178, 179], the resulting state is given by

$$\Lambda^P(\rho) = \sum_{m=0}^{3} q_m \sigma^m \rho \sigma^m \tag{3.33}$$

where $\sigma^1 = \sigma_x$, $\sigma^2 = \sigma_y$, $\sigma^3 = \sigma_z$ and $\sigma_0 = \begin{pmatrix} 1 & 0 \\ 0 & 1 \end{pmatrix}$ is the identity operator in the Hilbert space of two dimension. Here $\{q_m\}_{m=0}^{3}$, are the probability in which different Pauli matrices are acting on the system and $\sum_m q_m = 1$. Depending on the probabilities, the Pauli channel can be divided into several subcategories [125, 135]. Here we list some of them which we will use later in the thesis.

(i) Bit flip channel: $q_2 = q_3 = 0$.

(ii) Phase flip channel: $q_1 = q_2 = 0$.

(iii) Bit phase flip channel: $q_1 = q_3 = 0$.

(iv) Depolarizing channel: $q_1 = q_2 = q_3 = \frac{q}{3}$, where $0 \leq q \leq 1$.

For a two-qubit quantum state ρ_{AB}, if both the parties are going through Pauli channels, the output state reads as

$$\Lambda^P(\rho_{AB}) = \sum_{mn=0}^{3} q_{mn} \sigma^m \otimes \sigma^n \rho_{AB} \sigma^m \otimes \sigma^n, \tag{3.34}$$

where $\{q_{mn}\}$ is the set of probability by which the Pauli matrices are acting on the system. Two different kinds of noise models emerge from Eq. (3.34), which are given below.

Case 1: Fully correlated Pauli channel with $q_{mn} = q_m \delta_{mn}$, or a global Pauli channel:

$$\Lambda_c^P(\rho_{AB}) = \sum_{m=0}^{3} q_m \sigma^m \otimes \sigma^m \rho_{AB} \sigma^m \otimes \sigma^m, \tag{3.35}$$

Case 2: Completely uncorrelated Pauli channel with $q_{mn} = q_m q_n$, or local Pauli channel:

$$\Lambda_{uc}^P(\rho_{AB}) = \sum_{mn=0}^{3} q_m q_n \sigma^m \otimes \sigma^n \rho_{AB} \sigma^m \otimes \sigma^n, \qquad (3.36)$$

These two channels can also be extended to higher number of parties like in Eq. (3.26).

3.2.3 Capacity of DC for covariant noise

As we have already mentioned, there are two ways in which capacity of DC can be affected under noise. In the first case, the shared quantum state ρ gets affected by the noise model Λ at the time of sharing of the state between all the senders and the receiver. As a result, $\rho \to \Lambda(\rho)$, and since the output state is also a valid quantum state, one can use Eq. (3.19) to obtain $C(\Lambda(\rho))$, which is valid for arbitrary multiparty quantum state. It is clear from Eq. (3.22), that any pure state, $|\psi\rangle$, is likely to transform into a mixed state, under noisy channel and hence the DC capacity for pure states under noisy environment decreases with noise parameter.

In the second situation, we consider that the noise, Λ, acts only on the senders' part of the encoded state, at the time of sending it to the receiver. Hence, the ensemble that the senders are intended to transfer, is distorted like

$$\{p_x, \rho_{S_1 \ldots S_N R}^x\} \to \{p_x, \Lambda(\rho_{S_1 \ldots S_N R}^x)\}, \qquad (3.37)$$

where

$$\Lambda(\rho_{S_1 \ldots S_N R}^x) = \sum_\mu \left(\mathcal{K}_\mu \otimes I_R\right) \rho_{S_1 \ldots S_N R}^x \left(\mathcal{K}_\mu^\dagger \otimes I_R\right), \qquad (3.38)$$

with $\{\mathcal{K}_\mu\}$ being the set of Kraus operators in the Hilbert space of all the senders. It surely results decrease of accessible information that the receiver is supposed to get from the senders. Note that this situation is completely different from the previous one, and one can not apply Eq. (3.19) in this case[6]. However, the Holevo quantity is still valid and the amount of information that the receiver can extract is again bounded by [12]

$$I_{acc}^{noise} \leq S\left(\sum_x p_x \Lambda(\rho_{S_1 \ldots S_N R}^x)\right) - \sum_x p_x S\left(\Lambda(\rho_{S_1 \ldots S_N R}^x)\right), \qquad (3.39)$$

which can be achieved asymptotically, in this situation also [13, 14]. Therefore, the noisy DC capacity is defined as

$$C_n(\rho_{S_1 \ldots S_N R}) = \max_{\{p_{x_j}\}, \{U_j^{x_j}\}} \left[S\left(\sum_x p_x \Lambda(\rho_{S_1 \ldots S_N R}^x)\right) - \sum_x p_x S\left(\Lambda(\rho_{S_1 \ldots S_N R}^x)\right) \right]. \qquad (3.40)$$

For any arbitrary noise model, finding the optimized unitary encodings and the probabilities is complicated and is still an open question. But for a certain class of noise model like the "covariant noise" [59], the optimization has been carried out and the noisy capacity of DC is obtained in Refs. [23–26]. The covariant noise, Λ^c, is a CPTP map which commutes with a particular set of orthogonal unitaries $\{W_i\}$, satisfying

---

[6] It also includes the previous situation. Since $\rho_{S_1 \ldots S_N R}$ can be generated from noisy initial state.

the properties listed in Eqs. (3.8) and (3.9), and is given by

$$\Lambda^C(W_i \rho W_i^\dagger) = W_i \Lambda^c(\rho) W_i^\dagger, \ \forall i. \tag{3.41}$$

For example, the Pauli channel, introduced in Eq. (3.33) of Sec. 3.2.2, is a covariant channel which commutes with a particular set of orthogonal unitary operators, the Pauli spin matrices itself [59,178,179]. If we assume that the noise is present only in the transmission channel, through which the senders send their encoded part to the receiver, Λ^c then acts only on the senders system, and as it is a CPTP map, the output state is also a valid quantum state. Moreover, the marginal density matrix in the receiver's subsystem, ρ_R, remains unperturbed.

Therefore, the capacity of DC under covariant channel reads as

$$C_n(\rho_{S_1...S_N R}) = \log_2 d_{S_1...S_N} + S(\rho_R) - S(\tilde{\rho}), \tag{3.42}$$

where

$$\tilde{\rho} = \Lambda^c \left((U_{S_1 S_2...S_N}^{min} \otimes I_R) \rho_{S_1...S_N R} (U_{S_1 S_2...S_N}^{min\dagger} \otimes I_R) \right).$$

Here, $U_{S_1 S_2...S_N}^{min}$ denotes the unitary operator on the senders' side, which minimizes the von Neumann entropy of $(U_{S_1...S_N} \otimes I_R) \rho_{S_1...S_N R} (U_{S_1...S_N}^\dagger \otimes I_R)$ over the set of unitaries $\{U_{S_1 S_2...S_N}\}$, that can be global as well as local, depending on the type of encoding. It is reasonable from a practical point of view to assume that the senders perform local encoding. Then $U_{S_1 S_2...S_N}^{min}$ takes the form given by

$$U_{S_1 S_2...S_N}^{min} = U_{S_1}^{min} \otimes U_{S_2}^{min} \otimes ... \otimes U_{S_N}^{min}. \tag{3.43}$$

Like in the previous cases, the upper bound of C_n is $\log_2 d_{S_1...S_N R}$, and the classical limit is $\log_2 d_{S_1...S_N}$. Finally, the noisy DC capacity for N senders and a single receiver is given by

$$C^{noisy}(\rho_{S_1...S_N R}) = \frac{1}{\log_2 d_{S_1...S_N R}} \max\{\log_2 d_{S_1...S_N}, \log_2 d_{S_1...S_N} + S(\rho_R) - S(\tilde{\rho})\}. \tag{3.44}$$

Depending on the structure of Λ^c, the channel can be either correlated (global) or uncorrelated (local), as defined earlier.

Chapter 4

Multipartite Dense Coding vs. Quantum Correlations

In the realm of quantum information and computation, it was a well-established fact both theoretically as well as experimentally, that bipartite entanglement is an essential ingredient for a vast majority of known quantum communication schemes, involving two parties [2–8]. Specifically, it has been established that in case of pure bipartite states, $|\psi_{AB}\rangle$, the capacity of classical information transmission by a shared quantum state (for dense coding capacity see Eq. (3.13)) increases with the increase (see Eq. (3.15)) of quantum correlations quantified according to any measure (see Sec. 2.2.1). Unlike point-to-point communication, involving two parties, a sender and a receiver, communication protocols with multiple parties can have various complexities. One possible scenario involves several senders and a single receiver, and in this chapter we will restrict ourselves to this situation only. Suitable examples of such multipartite communication protocols include several news reporters from different locations, sending various news articles to the editorial office of the newspaper or several weather observers from different places communicating their respective weather reports to the regional meteorological office.

In this chapter, our main goal is to connect multipartite communication protocols with multiparty quantum correlation measures. In particular, we establish a relation between the capacity of multipartite DC and multipartite quantum correlation measures of arbitrary multiqubit states. Such a relation exists for bipartite states and is particularly simple for bipartite pure states. Applications of quantum channels are most likely to be commercially important only in the multiparty domain. However, very little is known about the qualitative structure and the exact values of capacities of multiparty quantum channels except the case with multiple senders and a single or two receivers. In recent times, a lot of interests has been created to characterize and quantify quantum communication schemes in multiparty regime [21, 22]. But a sheer connection between the DC capacity in the multiparty domain and the multiparty quantum correlation measures is still missing. This may be due to the fact that there is no unique measure of multiparty quantum correlation even for multiparty pure states, as derived in Eq. (3.13). In this chapter, we will establish relations between multiparty DC capacity with a single receiver and multiparty quantum correlation measures defined from two different paradigms. The correspondence that we establish is illustrated in the cases of both noiseless and noisy channels for arbitrary shared states.

4.1 Connection of QC measures with capacity DC in a noiseless scenario

In this section, we establish a generic relation between the multiparty DC capacity and various multiparty QC measures, defined in Chapter. 2. The multiparty measures with which we establish the connections are the genuine multiparty entanglement measure [28, 29], defined in Sec. 2.4.1, the monogamy based measures the tangle and discord monogamy score (see Sec. 2.4.2). Throughout this section, we consider the case when the additional quantum channel, that is used post-encoding, is noiseless.

4.1.1 Connection with genuine multiparty entanglement measure

In a bipartite scenario, all the pure states having same amount of entanglement have equal capacity of dense coding. The entanglement in this case is uniquely quantified by the von Neumann entropy of the local density matrices and the capacity is maximal for the maximally entangled states [4].

We will see that this simple situation is no more true in the multiparty regime. However, it is still possible to obtain a generic relation between capacity and entanglement. In a multipartite scenario, quantification of quantum correlations is not unique even for pure states and hence each measure, in principle, identifies its own distinct state with maximal quantum correlation. Nevertheless, the Greenberger-Horne-Zeilinger (GHZ) state [56] has been found to possess a high amount of multipartite quantum correlation, according to violation of certain Bell inequalities [180–182], as well as according to several multipartite entanglement measures [27–29]. In view of these results, we compare the properties of an arbitrary $(N+1)$-qubit[1] pure state with that of the $(N+1)$-qubit generalized GHZ state (gGHZ), which is given by

$$|gGHZ\rangle_{S_1 S_2 \ldots S_N R} \;=\; \sqrt{\alpha}|0_{S_1} \ldots 0_{S_N}\rangle|0_R\rangle + \sqrt{1-\alpha}e^{i\phi}|1_{S_1} \ldots 1_{S_N}\rangle|1_R\rangle, \tag{4.1}$$

where α is the real number in $(0,1)$[2] and $\phi \in [0, 2\pi)$. We find that if the capacity of dense coding with N senders and a single receivers, of an arbitrary $(N+1)$-party state, $|\psi\rangle_{N+1}$, and the gGHZ state are the same, then the genuine multiparty entanglement measure in terms of the generalized geometric measure (GGM), defined in (Eq. (2.39), of these two states may not be the same. However, they follow an ordering, which we establish in the following theorem. Here on, we skip all the subscripts in the notation of the states, for simplicity.

Theorem 1: *Of all the multiqubit pure states with an arbitrary but fixed multiparty dense coding capacity, the generalized GHZ state has the highest GGM.*

`Proof.` Scanning over α in Eq. (4.1), one can obtain an arbitrary value of the GGM. Therefore, to prove the theorem, one needs to show that if the multiparty dense coding capacity of an arbitrary $(N+1)$-qubit pure state is the same as that of an $(N+1)$-party gGHZ state, then the genuine multipartite entanglement, as quantified by the GGM, of that arbitrary pure state is bounded above by that of the gGHZ state, i.e.,

$$\mathcal{E}(|\psi\rangle) \leq \mathcal{E}(|gGHZ\rangle), \tag{4.2}$$

provided

$$C^{multi}(|\psi\rangle) = C^{multi}(|gGHZ\rangle). \tag{4.3}$$

---

[1] $(N+1)$-qubit system comprises tensor product Hilbert spaces of $(N+1)$ two level systems of dimension 2^{N+1}.

[2] We exclude two points, $\alpha = 0$ and $\alpha = 1$, from the definition of gGHZ state as in those points the states no longer remain an entangled state and they are $|1_{S_1} \ldots 1_{S_N}\rangle|1_R\rangle$ and $|0_{S_1} \ldots 0_{S_N}\rangle|0_R\rangle$ respectively.

The multipartite dense coding capacities, C^{multi}, of the $(N+1)$-party gGHZ state and the arbitrary pure state, $|\psi\rangle$, can be obtained by using Eq. (3.19), and are given respectively by

$$C^{multi}(|gGHZ\rangle) = \frac{N}{N+1} - \frac{\alpha \log_2 \alpha + (1-\alpha)\log_2(1-\alpha)}{N+1}$$

and

$$C^{multi}(|\psi\rangle) = \frac{N}{N+1} - \frac{\lambda_R \log_2 \lambda_R + (1-\lambda_R)\log_2(1-\lambda_R)}{N+1},$$

where λ_R is the maximum eigenvalue of the marginal density matrix, ρ_R, of the receiver's part of the state $|\psi\rangle$. The GGMs for the gGHZ state and the $|\psi\rangle$ are obtained respectively by

$$\mathcal{E}(|gGHZ\rangle) = 1 - \alpha, \tag{4.4}$$

and

$$\mathcal{E}(|\psi\rangle) = 1 - \max[\{l_A\}], \tag{4.5}$$

where we assume that $\alpha \geq \frac{1}{2}$ and use the reduced form of GGM given in Eq. (2.48). Here the set $\{l_A\}$ contains the maximum eigenvalues of the reduced density matrices of all possible bipartitions of $|\psi\rangle$. Equating the multiparty dense coding capacities for these two states, we obtain

$$\alpha = \lambda_R. \tag{4.6}$$

Note that $\lambda_R \in \{l_A\}$. Let us now consider the two following cases: (1) the maximum in GGM is attained by λ_R, and (2) the maximum is attained by an eigenvalue which is different from λ_R.

Case 1: Suppose $\lambda_R = \max[\{l_A\}]$. Then

$$\mathcal{E}(|\psi\rangle) = 1 - \lambda_R = 1 - \alpha = \mathcal{E}(|gGHZ\rangle), \tag{4.7}$$

by using Eq. (4.6).

Case 2: Suppose $\lambda_R \neq \max[\{l_A\}]$, so we must have $\lambda_R \leq \lambda_0 = \max[\{l_A\}]$. Therefore, we obtain

$$\mathcal{E}(|\psi\rangle) = 1 - \lambda_0 \leq 1 - \lambda_R = 1 - \alpha = \mathcal{E}(|gGHZ\rangle)$$

Hence the proof. ∎

To visualize the above theorem we randomly generate 10^5 arbitrary three-qubit pure states by using the uniform Haar measure on this space and plot the behavior of the GGM versus the DC capacity for these states. As proven in Theorem 1, the scatter diagram populates only a region outside the parabolic curve of the gGHZ states. See Fig. 4.1. Interestingly, therefore, in the plane of the dense coding capacity and the GGM, there exists a forbidden region which cannot be accessed by any three-qubit pure state. With respect to dense coding in the noiseless case, therefore, the gGHZ state is the least useful state among all states having an equal amount of multiparty entanglement.

The feature we establish here, is generic in the sense that it holds for drastically different choices of quantum correlation measures, namely the monogamy based measures of multiparty quantum correlations.
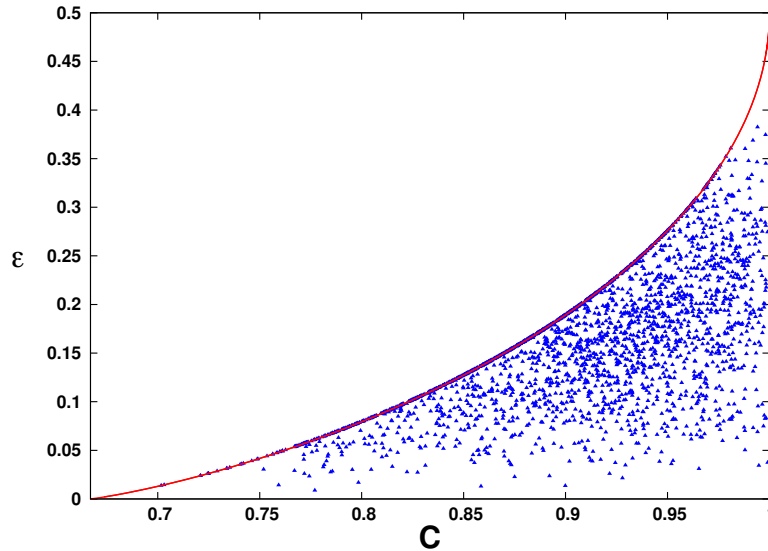
Figure 4.1: GGM vs. multipartite DC capacity. GGM is plotted as the ordinate while multipartite DC capacity is plotted as the abscissa for 10^5 randomly chosen three-qubit pure states, according to the uniform Haar measure over the corresponding space (blue triangles). The red line represents the generalized GHZ states. There is a set of states for which, if the capacity matches with a gGHZ state, then their GGMs are also equal. For the remaining states, if the capacity is equal to a gGHZ state, its GGM is bounded above by that of the gGHZ state. Note that the range of the horizontal axis is considered only when the states are dense codeable. The quantities represented on both the axes are dimensionless. We are considering the case where the post-encoded states are sent through noiseless channels.

4.1.2 Connection with monogamy based measures

In this section, we will show that the relation between the multiparty DC capacity and the genuinely multiparty entanglement measure, obtained in the previous section for multiparty pure state also holds for the QC measures defined from a completely different perspective. The QC measure which will be considered here is the monogamy based measure, defined in Sec. 2.4.2. Specifically, we establish a connections for the squared concurrence monogamy score, tangle τ or δ_{C^2} [30,121] and discord monogamy score, $\delta_{\mathcal{D}}$ [152], and show that the similar hierarchy between the arbitrary multiparty pure states and the gGHZ states also prevails here. In particular, the multiqubit gGHZ state is worst among all arbitrary multiqubit pure states in terms of its ability towards classical information transmission when they all have the same amount of multiparty quantum correlation.

Note: The tangle and discord monogamy score are defined here using receiver of the multiparty DC protocol as the nodal observer.

Connection with squared concurrence monogamy score

We now show that the result stated in Theorem 1, reviews potentially invariant when one takes the squared concurrence monogamy score, the tangle, given in Eq. (2.53) as a QC measure, in the following theorem.

Theorem 2: *Of all the multiqubit pure states with an arbitrary but fixed multiparty dense coding capacity, the generalized GHZ state has the highest concurrence squared monogamy score.*

`Proof.` To prove the above theorem, we first recall the definition of tangle from Eq. (2.53), for an

$(N + 1)$-qubit pure state $|\psi\rangle$, with the receiver as a nodal observer.

$$\tau(|\psi\rangle) = \mathcal{C}^2_{S_1...S_N:R}(|\psi\rangle) - \sum_i \mathcal{C}^2(\rho_{S_i R}), \tag{4.8}$$

where $\rho_{S_i R}$ is the reduced density matrix of the ith sender and the receiver. The first term in the above equation quantifies the squared concurrence of the pure state $|\psi\rangle$, in the bipartition of all the senders and the receiver, and it is given by

$$\mathcal{C}^2_{S_1...S_N:R}(|\psi\rangle) = 4 \det(\rho_R) = 4\lambda_R(1 - \lambda_R), \tag{4.9}$$

where we use the form of concurrence for the pure state given in Eq. (2.17). Now the tangle for the gGHZ state given in Eq. (4.1) is

$$\tau(|gGHZ\rangle) = 4\alpha(1 - \alpha), \tag{4.10}$$

since all the reduced density matrices of the gGHZ state,

$$\rho^{gGHZ}_{S_i R} = \big(\alpha|00\rangle\langle 00| + (1 - \alpha)|11\rangle\langle 11|\big)_{S_i R}, \tag{4.11}$$

are separable, and hence $\mathcal{C}(\rho^{gGHZ}_{S_i R}) = 0$. Now, the equality of the multipartite DC capacities of these two states provide $\alpha = \lambda_R \geq \frac{1}{2}$. Therefore, we have

$$\begin{aligned}
\tau(|\psi\rangle) &= 4\det(\rho_R) - \sum_i \mathcal{C}^2(\rho_{S_i R}) \tag{4.12} \\
&\leq 4\lambda_R(1 - \lambda_R) = 4\alpha(1 - \alpha) = \tau(|gGHZ\rangle). \tag{4.13}
\end{aligned}$$

Hence proved. ∎

Connection with discord monogamy score

We also have a similar relation between the multiparty DC capacity with N senders and a single receiver and discord monogamy score for the qubit system as stated in the following

Theorem 3: *Of all the multiqubit pure states with an arbitrary but fixed multiparty dense coding capacity, the generalized GHZ state has the highest discord monogamy score.*

`Proof.` For an $(N + 1)$-qubit arbitrary $|\psi\rangle$, the discord monogamy score is given by

$$\begin{aligned}
\delta_{\mathcal{D}}(|\psi\rangle) &= S(\rho_R) - \sum_i \mathcal{D}(\rho_{S_i R}) \tag{4.14} \\
&\leq S(\rho_R) = h(\lambda_R) = h(\alpha) = \delta_{\mathcal{D}}(|gGHZ\rangle), \tag{4.15}
\end{aligned}$$

where $S(\rho_R)$ is the von-Neumann entropy (see Eq. (2.6)) of the reduced density matrix in the receivers subsystem and $h(x)$ is the binary Shannon entropy as given in Eq. (2.14). Here we use the facts that discord is a non-negative quantity, which reduces to $S(\rho_R)$ for a multiparty pure state in the senders : receiver bipartition, and

$$\delta_{\mathcal{D}}(|gGHZ\rangle) = h(\alpha), \tag{4.16}$$
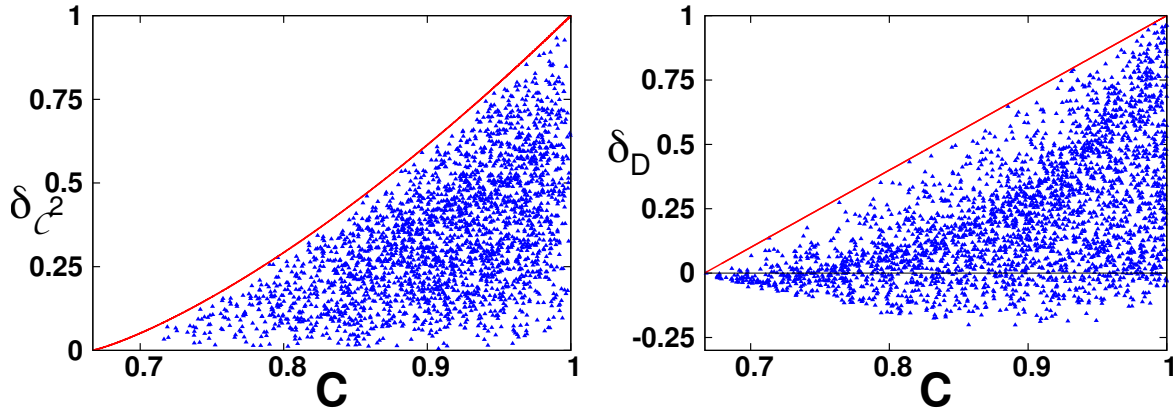
Figure 4.2:   Left: Tangle (vertical axis) vs. multiparty DC capacity (horizontal axis) for randomly generated three-qubit pure states (blue triangles). Right: Discord monogamy score (vertical axis) vs. DC capacity (horizontal axis) for the same states. In both the cases, the gGHZ states give the boundary (red line). The capacity is dimensionless, while the tangle and discord monogamy score are measured in ebits and bits, respectively. All other considerations are the same as in Fig. 4.1.

since $\mathcal{D}(\rho_{S_i R}^{gGHZ}) = 0$.[3] due to the separable states as in Eq. (4.11). Hence the proof. ∎

Note that Theorem 3 holds irrespective of the party on which the measurement is performed for the evaluation of quantum discord according to Eq. (2.33).

To visualize the above theorems, we again randomly generate 10^5 pure three-qubit states, by using the uniform Haar measure in the corresponding space, and prepare scatter diagrams for tangle versus the multiparty DC capacity (Fig. 4.2 (left)) and for the discord monogamy score against the same capacity (Fig. 4.2 (right)). The simulations are clearly in agreement with Theorem 2 and 3. In particular, and just like for GGM with the DC capacity, the planes of $(C, \delta_{\mathcal{C}^2})$ and $(C, \delta_{\mathcal{D}})$ can not be fully accessed by the three-qubit pure states. The discords in Fig. 4.2 (right), have been calculated by performing the measurement in the nodal party R. However, note that measurements in the first party also leads to the similar results.

4.2   Multiparty DC vs. QC for multiparty mixed state

We now investigate the relation between DC capacity and multipartite quantum correlation measures, when the shared quantum state is an arbitrary $(N + 1)$-party mixed state. This relation can be considered as a connection of QC with one kind noisy DC capacity, where the noise is acting on the quantum state at the time of sharing it among all the senders and the receiver. In this case, to establish such connection, the main difficulty is that there are only a few quantum correlation measures available which can be computed. Therefore, we consider the discord monogamy score as the multipartite quantum correlation measure, since quantum discord can be numerically calculated for arbitrary bipartite systems, and investigate its connection with the DC capacity.

In Fig. 4.3, we randomly generate 10^5 mixed states of rank-2 in the space of three-qubit states and plot the discord monogamy score with respect to the DC capacity. The random generation is with respect to the uniform Haar measure induced from that in the appropriate higher-dimensional pure state

---

[3]The reduced density matrix of the gGHZ state, given in Eq. (4.1), is an example of a classically correlated state, defined in Eq. (2.38)

space. The numerical simulation reveals that Theorem 2 does not hold for rank-2 (mixed) three-qubit states. In particular, we find that if a gGHZ state and a rank-2 three-qubit mixed state have the same discord monogamy score, then sharing the gGHZ state is usually more beneficial than the mixed state, for performing the multiparty DC protocol. More precisely, among randomly generated 10^5 rank-2 states, there are only 1.85% states which satisfy Theorem 2. We will later show that a similar picture is true when one considers noise in the transmission channel of the DC protocol. This implies that in the presence of noisy environments, irrespective of whether the noise is afflicted before or after encoding, it is typically better to share a gGHZ state among states with a given discord monogamy score, from the perspective of DC capacity. Before presenting the results obtained by using numerical simulations for higher-rank mixed states, let us discuss the behavior of the DC capacity, as enunciated in the following proposition. We will find that it can be used to intuitively understand the numerical results for higher-rank states presented below.

Proposition 1: *An arbitrary $(N + 1)$-qubit (pure or mixed) state is dense codeable if the maximum eigenvalue of the $(N + 1)$-party state is strictly greater than the maximum eigenvalue of its reduced state at the receiver's side.*

`Proof:` An $(N + 1)$-qubit (pure or mixed) state, $\rho_{S_1 S_2 \ldots S_N R}$, is multiparty dense codeable with N senders, $S_1, S_2, \ldots, S_N$, and a single receiver, R, if and only if the von Neumann entropy of the reduced state at the receiver's side is greater than that of the state $\rho_{S_1 S_2 \ldots S_N R}$, i.e.,

$$S(\rho_R) > S(\rho_{S_1 S_2 \ldots S_N R}). \tag{4.17}$$

Let the eigenvalues, in descending order, of the state ρ_R, be given by $\lambda_R = \{\lambda^1 \geq \frac{1}{2}, 1 - \lambda^1\}$. Let the eigenvalues of the state $\rho_{S_1 S_2 \ldots S_N R}$ be $\lambda_{S_1 S_2 \ldots S_N R} = \{\mu^i\}_{i=1}^r$, where r is the rank of the matrix, and where the μ^i's are arranged in descending order. Specifically, μ^1 gives the largest eigenvalue of $\rho_{S_1 S_2 \ldots S_N R}$. Now, the ordering between the highest eigenvalues of ρ_R and $\rho_{S_1 S_2 \ldots S_N R}$, i.e., between λ^1 and μ^1, can have three possibilities, i.e., $\lambda^1 > \mu^1$, or they are equal, or $\lambda^1 < \mu^1$.

Let us assume that $\lambda^1 \geq \mu^1$. Then, invoking the condition of majorization [183], we have

$$\lambda_R \succ \lambda_{S_1 S_2 \ldots S_N R},$$

which implies

$$S(\rho_R) \leq S(\rho_{S_1 S_2 \ldots S_N R}). \tag{4.18}$$

It immediately implies that the state is not dense codeable. Therefore, to obtain dense codeability of $\rho_{S_1 S_2 \ldots S_N R}$, we must have $\lambda^1 < \mu^1$.
Hence the proof. ∎

Although the above proposition has been presented for qubit systems, it is also valid for an arbitrary (pure or mixed) $(N + 1)$-party quantum state in arbitrary dimensions, provided ρ_R is of rank 2.

Let us now move to mixed states with higher-rank. Numerically, to obtain high-rank three-qubit mixed states, one possibility is to generate pure states with more than three parties. For example, to obtain arbitrary rank-4 states of three qubits, 5-qubit pure states can be created randomly, and then two parties traced out. However, numerical searches become inefficient with the increase of number of parties [184].
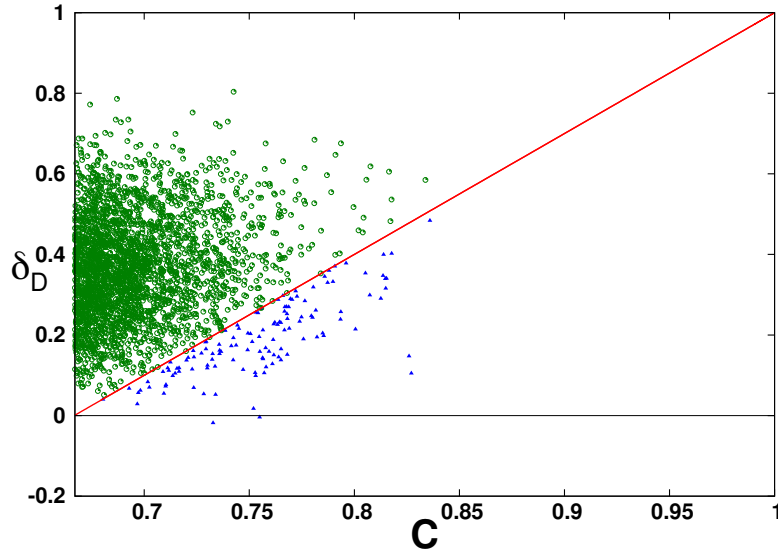
Figure 4.3: Discord monogamy score vs. multipartite DC capacity for Haar uniformly generated rank-2 three-qubit states. The red line represents the gGHZ states. About 1.85% of the randomly generated states lie below the red line, and are represented by blue triangles. The remaining, represented by green "three o'clock" circles, lie above the red line. The horizontal axis is dimensionless while the vertical one is measured in bits.

To overcome this problem, we create mixed states, ρ_8, of full rank, given by

$$\rho_8 = (1-p)\rho + \frac{p}{8}I_8, \tag{4.19}$$

by choosing ρ as arbitrary rank-2 three qubit states, generated randomly from the four-qubit pure states, and where I_8 is the identity matrix on the three-qubit Hilbert space. Moreover, we consider those set of states, ρ, which are dense codeable. In that case, we find that its DC capacity remains nonclassical only for very small values of the mixing parameter p. In Fig. 4.4, we specifically consider the full rank state, ρ_8, with ρ given by

$$\rho = q|GHZ\rangle\langle GHZ| + (1-q)|GHZ'\rangle\langle GHZ'|, \tag{4.20}$$

where $|GHZ'\rangle = \frac{1}{\sqrt{2}}(|000\rangle - |111\rangle)$. We now plot, in Fig. 4.4, the discord monogamy score and the raw[4] DC capacity with respect to the mixing parameter p. For $q = 1$ or $q = 0$, and $p = 0$, the capacity is maximum and δ_D also gives a maximum. Fig. 4.4 shows that there is a small region in which the state remains dense codeable, only when δ_D is very high. It is plausible that the capacity of dense coding for mixed states decreases with the increase of rank of the state. This is intuitively understandable from the condition in Proposition 1, since the typical high-rank state can have eigenvalues more distributed than the typical low-rank state. Therefore, the maximal eigenvalue of a shared state typically gives a lower value than that of the receiver's side, and the condition in Proposition 1 is thereby satisfied for a very small set of states.

---

[4]In Eqs. (3.19) (3.19) and (3.44), we call second terms within the maximum in the numerators, divided by the denominators, as the corresponding "raw" DC capacities.
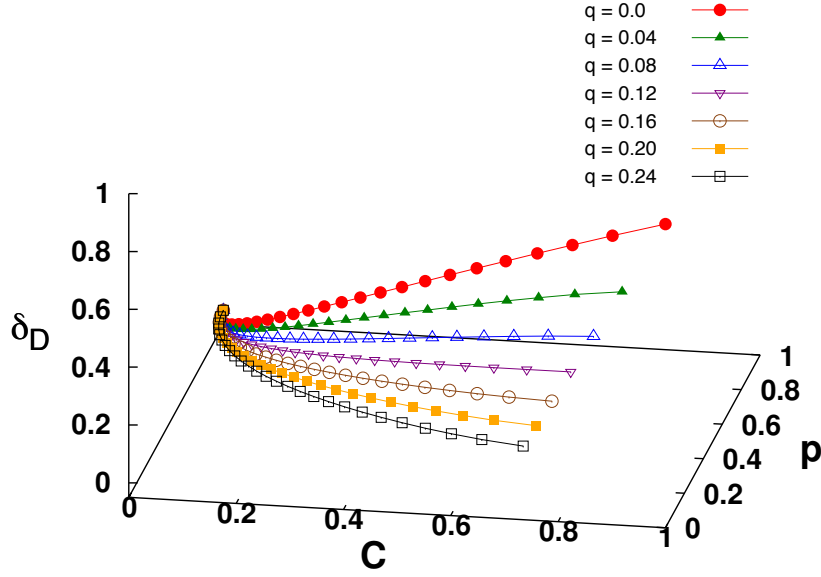
Figure 4.4: Discord monogamy score and the raw DC capacity are plotted against the mixing parameter p, for the rank-8 state, $\rho_8 = (1-p)\rho + \frac{p}{8}I$. Here $\rho = q|GHZ\rangle\langle GHZ| + (1-q)|GHZ'\rangle\langle GHZ'|$. Each value of q provides a curve, and we present several exemplary curves in the figure. All the quantities plotted are dimensionless, except δ_D, which is measured in bits.

4.3 Relation of multiparty QC measures with capacity of DC in presence of noise

In this section, we establish a connection between the multiparty QC measures and the DC capacity of noisy channels, for both correlated and uncorrelated noise, for the $(N+1)$-party state, $\rho_{S_1 S_2 \ldots S_N R}$, shared between N senders and a single receiver. Here we assume that the N senders individually apply local unitary operations on their parts of the shared state and send their encoded parts through a covariant noisy channel (see Sec. 3.2.3). As the encoding has been carried out over the quantum state upon which no noise is acted, so we use here the QC measures of the initial states. We now address the extent to which the relation, established in Sec. 4.1, between multiparty DC capacity for the noiseless channel and multipartite QC measures, in the case of pure shared quantum states, still remains valid for the noisy channel scenario. To this end, we consider two extreme scenarios, one in which the noise between the different sender qubits are fully correlated, and another in which the same are uncorrelated.

4.3.1 Fully correlated Pauli channel

An $(N+1)$-qubit state, $\rho_{S_1 S_2 \ldots S_N R}$, after being acted on by the fully correlated Pauli channel, presented in Eq. (3.35), is given by

$$\Lambda^P(\rho_{S_1 S_2 \ldots S_N R}) = \sum_{i=0}^{3} q_m(\sigma_{S_1}^m \otimes \cdots \otimes \sigma_{S_N}^m \otimes I_R)\rho_{S_1 S_2 \ldots S_N R}(\sigma_{S_1}^m \otimes \cdots \otimes \sigma_{S_N}^m \otimes I_R), \quad (4.21)$$

where $\sum_{m=0}^{3} q_m = 1$, and $q_m \geq 0$, and where we denote, for simplicity, $\sigma_x = \sigma^1, \sigma_y = \sigma^2, \sigma_z = \sigma^3$, and the identity matrix as σ^0 for the sender qubits. The receiver qubit is acted on only by the identity operator,

which we denote by I_R.

Connect noisy DC capacity with GGM

We now establish the parallel of the ordering in Theorem 1 for the fully correlated Pauli channel.

Theorem 4: *If the multiparty dense coding capacity of an arbitrary three-qubit pure state, $|\psi\rangle$, is the same as that of the gGHZ state in the presence of the fully correlated Pauli channel, then the genuine multipartite entanglement, GGM, of that arbitrary pure state is bounded below by that of the gGHZ state, i.e.,*

$$\mathcal{E}(|\psi\rangle) \geq \mathcal{E}(|gGHZ\rangle), \tag{4.22}$$

provided the following two conditions hold: (i) the largest eigenvalue of the noisy $|\psi\rangle$ state is bounded above by $max\{q_1 + q_2, 1 - q_1 - q_2\}$, and (ii) the receiver's side gives the maximum eigenvalue for the GGM of $|\psi\rangle$.

`Proof:` The capacities of multiparty dense coding of the gGHZ state and the three-qubit pure state, $|\psi\rangle$, after being acted on by the correlated noisy channel, can be obtained from Eq. (3.44), and are given respectively by

$$C_c^{noisy}(|gGHZ\rangle) = \frac{2}{3} + \frac{h(\alpha) - S(\tilde{\rho}_{gGHZ})}{3} \tag{4.23}$$

and

$$C_c^{noisy}(|\psi\rangle) = \frac{2}{3} + \frac{h(\lambda_R) - S(\tilde{\rho}_{\psi})}{3} \tag{4.24}$$

where $\tilde{\rho}_{gGHZ} = \Lambda^P((U_{S_1 S_2}^{min} \otimes I_R)|gGHZ\rangle\langle gGHZ| (U_{S_1 S_2}^{min\dagger} \otimes I_R))$ with $U_{S_1 S_2}^{min}$ being the unitary operator at the senders' part that minimizes the relevant von Neumann entropy (see Sec. 3.2.3), and $h(x)$ is the binary entropy given in Eq. (2.14). Here, we are considering only those cases for which the (noisy) capacities of both the gGHZ state as well as of the $|\psi\rangle$ are non-classical, i.e., the corresponding noisy states are dense codeable (in this case, $C_c^{noisy} > 2$). Replacing $|gGHZ\rangle$ by $|\psi\rangle$ in $\tilde{\rho}_{gGHZ}$, one obtains $\tilde{\rho}_{\psi}$ and the corresponding $U_{S_1 S_2}^{min}$ which is of course a function of the input state. For the gGHZ state, the von Neumann entropy of the resulting state after sending through the fully correlated Pauli channel is $S(\tilde{\rho}_{gGHZ}) = h(q_1 + q_2)$, which is independent of the choice of the local unitary operators.

Equating Eqs. (4.23) and (4.24), we have

$$\begin{aligned}
h(\alpha) &= h(\lambda_R) + [h(q_1 + q_2) - S(\tilde{\rho}_{\psi})] \\
&= h(\lambda_R) + [h(q_1 + q_2) - h(\{\lambda_i\})], \tag{4.25}
\end{aligned}$$

where $\{\lambda_i\}_{i=1}^{8}$ are the eigenvalues of $\tilde{\rho}_{\psi}$ in descending order. Here $H(\{\lambda_i\}) = -\sum_i \lambda_i \log_2 \lambda_i$. If we assume that $\lambda_1 \leq \max\{q_1 + q_2, 1 - q_1 - q_2\}$, we have $\{\lambda_i\} \prec \{q_1 + q_2, 1 - q_1 - q_2\}$. The relation between majorization and Shannon entropy [183] then implies that $h(q_1 + q_2) \leq h(\{\lambda_i\})$. Therefore, from Eq. (4.25), we have

$$h(\alpha) \leq h(\lambda_R) \Rightarrow \alpha \geq \lambda_R, \tag{4.26}$$

where we assume $\alpha \geq \frac{1}{2}$.

The GGM for the gGHZ state and the three-qubit state, $|\psi\rangle$, are respectively given by $\mathcal{E}(|gGHZ\rangle) = 1 - \alpha$ and $\mathcal{E}(|\psi\rangle) = 1 - \lambda_{max}$, where λ_{max} is the maximum eigenvalue among the eigenvalues of all
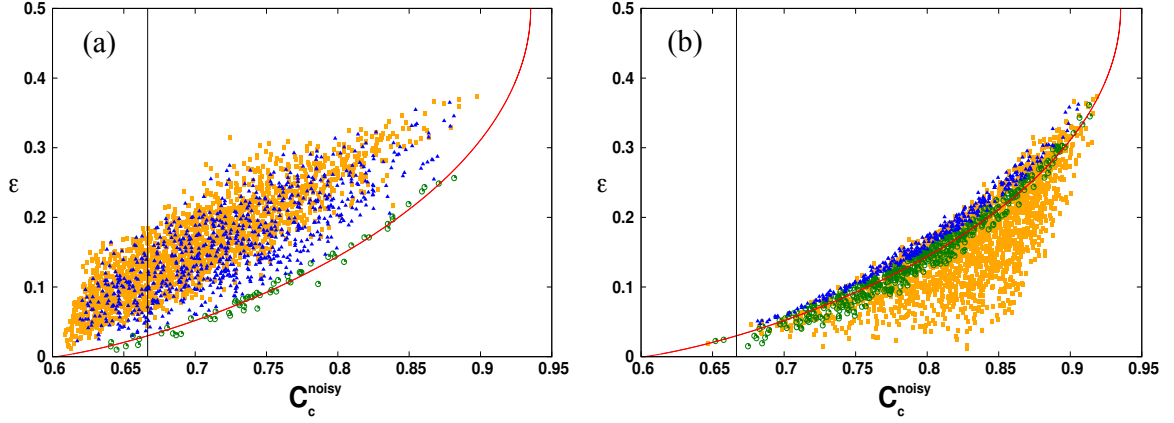
Figure 4.5: GGM (vertical axis) vs. the raw DC capacity (horizontal axis) under the fully correlated Pauli channel, when the shared state is an arbitrary three-qubit pure state (orange squares, green circles, and blue triangles) or the gGHZ state (red line). For figure (a), we choose $q_0 = q_3 = 0.485$, and $q_1 = q_2 = 0.015$ as noise parameters for the arbitrary as well as the gGHZ state, this corresponds to the Case 1. And for figure (b), we choose $\{q_i\}$ as $q_0 = 0.93, q_1 = 0.01, q_2 = 0.02, q_3 = 0.04$, corresponds to the Case 2 in the discussion. We randomly (Haar uniformly) generate 10^5 three-qubit pure states. Both the axes are dimensionless. The vertical line at the $C_c^{noisy} = 2/3$ helps to readily read out the actual capacity from the raw capacity.

the local density matrices of $|\psi\rangle$. If we assume that the eigenvalue from the receiver's side attains the maximum, i.e., if $\lambda_R = \lambda_{max}$, using Eq. (4.26), we obtain

$$\mathcal{E}(|gGHZ\rangle) = 1 - \alpha \leq 1 - \lambda_R = \mathcal{E}(|\psi\rangle). \tag{4.27}$$

Hence the proof. ∎

The above theorem ekes out a subset of the pure three-qubit state space, for which the gGHZ state is more robust with respect to multiparty DC capacity, against fully correlated Pauli noise, as compared to any member of the said subset, provided the gGHZ and the said member have equal amount of genuine multiparty entanglement, as quantified by their GGMs. This specific subset of states are those which satisfy both the conditions (i) and (ii). The situation, at least for this specific subset, has therefore exactly reversed with respect to the noiseless scenario, as enunciated in Theorem 1. For a given amount of multiparty entanglement content, as quantified by the GGM, the gGHZ state can now be better than other pure states, with respect to the multiport classical capacity. The noisy quantum channel can therefore reverse the relative capabilities of classical information transfer of different states in multiparty quantum systems. The above phenomenon of reversal of information carrying capacity with the addition of noise actually holds for a much larger class of states, that do not satisfy the conditions (i) and (ii) in Theorem 4, but holds the relation (4.22). We resort to numerical searches by generating Haar uniform three-qubit pure states for this purpose. The following picture is therefore emerging. Given a three-qubit pure state, $|\psi\rangle$, and a gGHZ state with the same multiparty quantum correlation content, the multiparty DC capacity of the gGHZ state is much less affected by noise than a large class of $|\psi\rangle$, and in many cases, the ordering of the capacities can get reversed in the noisy case as compared to the order in the noiseless case.

To perform the numerical searches, we first observe that the $C_c^{noisy}(|gGHZ\rangle)$ depends on the sum of the two parameters q_1 and q_2 (or $q_0 + q_3$). By fixing $q_1 + q_2 = c$ (or $q_0 + q_3 = 1 - c$), one can set the noise parameter for the gGHZ state. However, the situation for an arbitrary state, $|\psi\rangle$, is more involved,

for which the capacity of dense coding, $C_c^{noisy}(|\psi\rangle)$, depends individually on all the $\{q_i\}$. To quantify the randomness of $\{q_i\}$, and indeed the noise in the channel, we consider the Shannon entropy, $H(\{q_i\})$, given in Eq. (2.24). We now consider two extreme cases: one for which $H(\{q_i\})$ is maximum and the other in which the same is a minimum, both subject to the constraint $q_1 + q_2 = c$, where $0 \leq c \leq 1$. The maximum of $H(\{q_i\})$ is attained when $q_1 = q_2 = c/2$ and $q_0 = q_3 = (1-c)/2$, while the minimum is obtained when any one of the q_1 and q_2 and any one of q_0 and q_3 are zero. It is also evident from Eq. (4.23), that one should deal with a very low or very high values of c, for the state to remain dense codeable.

We now randomly generate 10^5 three-qubit pure states with a uniform Haar measure over that space, and investigate the two extreme cases mentioned above, for fixed $H(q_1 + q_2) = 0.19$. We choose the two sets of values for the q_i's as follows –

Case 1: $q_0 = q_3 = 0.485$, and $q_1 = q_2 = 0.015$ (see Fig. 4.5 (a)), and

Case 2: $q_0 = 0.93, q_1 = 0.01, q_2 = 0.02, q_3 = 0.04$ (see Fig. 4.5 (b)).

For fixed $H(q_1 + q_2) = 0.19$, Case 1 is an example for high noise, and corresponds to the case when $H(\{q_i\})$ is maximum subject to the constraint $H(q_1 + q_2) = 0.19$, which is the same as the constraint $q_1 + q_2 = 0.03$. Case 2 is an example of low noise, and corresponds to a situation that is close to the case when $H(\{q_i\})$ is a minimum subject to the constraint $H(q_1 + q_2) = 0.19$. We present the low noise case, when the configuration is slightly away from the analytical minimum to provide a more non-trivial example.

<u>Case 1</u> (Fig. 4.5 (a)): In presence of high noise, we observe that almost all the randomly generated states have shifted to above the gGHZ state (red line) in the plane of GGM and the raw capacity, C_c^{noisy}. As expected, one-third of the randomly generated states satisfy condition (ii) of Theorem 4. A significantly large fraction (98.6%) of them further satisfies condition (i). They are represented by blue triangles in Fig. 4.5 and lie above the gGHZ line. The remaining 1.4% are represented by green "three o'clock" circles, and may lie below or above the gGHZ curve. The further states are represented by orange squares.

<u>Case 2</u> (Fig. 4.5 (b)): For low noise, the randomly generated states may fall below or above the red line of the gGHZ states. Again, one-third of the generated states satisfy condition (ii). 45.6% of them satisfy condition (i), represented by blue triangles, and fall above the red line. The remaining 54.4% of them are represented by green "three o'clock" circles, and can be below or above the gGHZ line. The other two-thirds are represented by orange squares, and can again be either below or above the gGHZ line.

The occurrence of the randomly generated states both below and above the curve for the gGHZ states on the plane of the GGM and the capacity is expected from continuity arguments, for low noise. However, if one makes a comparison between Figs. 4.1 and 4.5, it is revealed that arbitrary three-qubit pure states require higher amount of multipartite entanglement than the gGHZ states to keep themselves dense codeable in the presence of moderate noise.

Connection with monogamy based measures

For noisy channels, the connection of noisy DC capacity with the monogamy based measures of QC has also been established, for three-qubit pure states as input states. We find that the result obtained in Theorem 4, holds even if we replace the GGM by the squared concurrence monogamy score, the tangle, and the discord monogamy score, provided we consider the set of three-qubit pure states for which the two-party concurrences or quantum discords vanish, and the receiver is used as the nodal observer. Comparing now with Theorems 2 and 3, we see that the phenomenon of the inversion of the relative
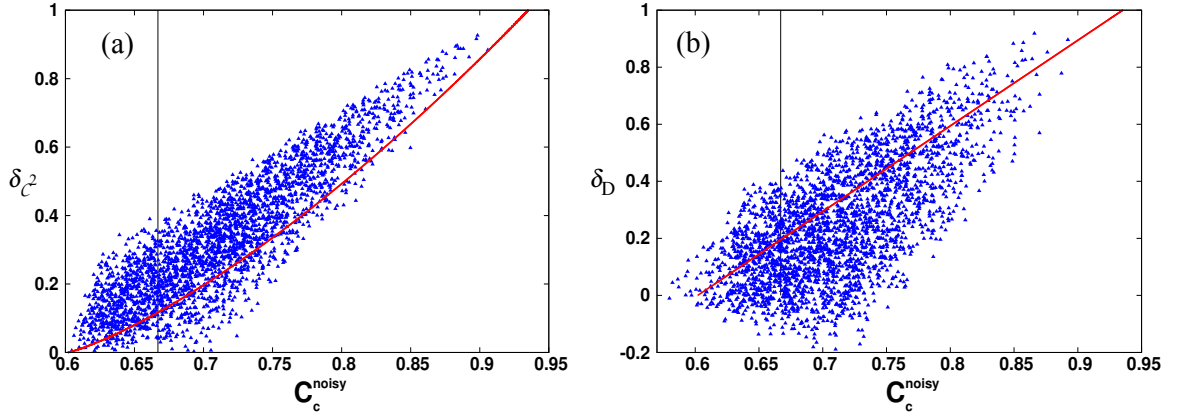
Figure 4.6: Figure (a), Tangle (vertical axis) vs. the raw DC capacity (horizontal axis) under the fully correlated Pauli channel, for randomly (Haar uniformly) generated three-qubit pure states (blue triangles) and the gGHZ states (red line). Figure (b) Discord monogamy score (vertical axis) vs. noisy DC capacity (horizontal axis) for the same set of states. We choose $q_0 = q_3 = 0.485$, and $q_1 = q_2 = 0.015$ as noise parameters for the arbitrary as well as for the gGHZ state, this corresponds to the Case 1. The noisy DC capacity is dimensionless, while the tangle and discord monogamy score are measured in ebits and bits, respectively. The vertical line at the $C_c^{noisy} = 2/3$ is to identify the classical domain of capacity.

capabilities for classical information transfer is generic in this sense: some of the states which were useful for multiparty DC compared to the gGHZ state, having equal amount of monogamy based measure of QC, is now becoming useless as compared to the gGHZ state, when noise is introduced in the transmission channel.

We have also numerically analyzed the randomly generated states by replacing the GGM with the tangle and with the discord monogamy score. We find that the behavior of the DC capacity with these multiparty quantum correlation measures is similar to that between the DC capacity and the GGM. However, the GGM is more sensitive to noise than tangle or discord monogamy score, in the sense that in the presence of small values of noise parameters, the percentages of states which are below the gGHZ line is much higher in the case of the monogamy based measures than for the GGM. The numerical results have been depicted In Fig. 4.6, where we calculate the noisy DC capacity, C_c^{noisy}, under fully correlated Pauli noise with the noise parameters given in Case 1, with the tangle (in Fig. 4.6 (a)) and also with the discord monogamy score (in Fig. 4.6 (b)).

Therefore, Theorem 4 and the numerical simulations strongly suggest that in the presence of fully correlated Pauli noise, the ratio of multipartite entanglement to the DC capacity of the gGHZ state increases at a slower rate than that of the arbitrary three-qubit pure states, where both of them possess same amount of QC, irrespective of the choice of the multiparty quantum correlation measure.

4.3.2 Local depolarizing channel

Consider now a Pauli channel in which the Kraus operators acting on different subsystems are not correlated to each other. More specifically, we suppose that each encoded qubit is sent through a depolarizing channel with noise parameter p. Before analyzing the relation between the multiparty DC capacity and quantum correlation measures, we compare the multiport dense coding capacities for the correlated channels with those of the uncorrelated ones. A three-qubit state, $\rho_{S_1 S_2 R}$, after the post-encoded qubits pass through
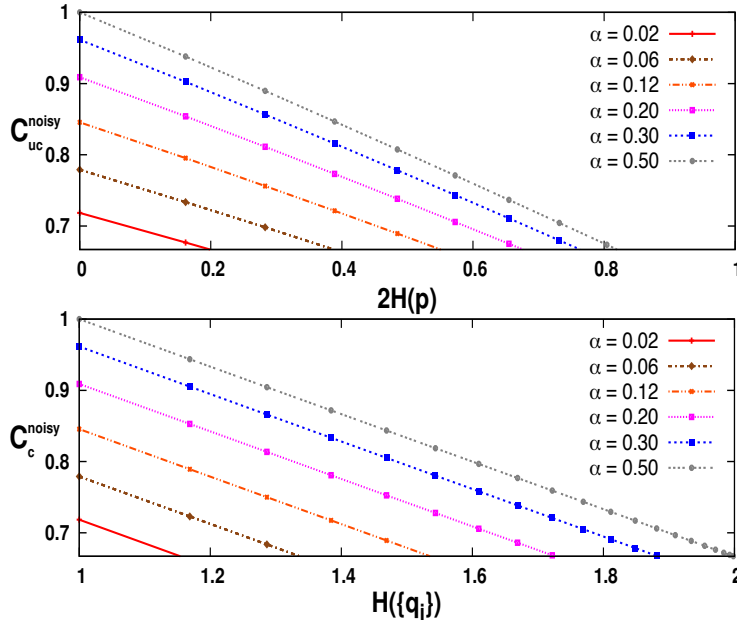
Figure 4.7: DC capacity vs. noise for various choices of α in the gGHZ state. In the top panel, the capacity of DC is plotted against the noise of the depolarizing channel, while in the bottom one, the DC capacity is plotted with respect to the noise in the fully correlated Pauli channel, for the gGHZ state. Different curves correspond to different values of α. The vertical axis starts from 2/3, below which the states are not dense codeable. The states remain dense codeable in the presence of moderate to high Pauli noise while this is not the case for the uncorrelated depolarizing channel. The horizontal axes are measured in bits. All other quantities are dimensionless.

independent (uncorrelated) depolarizing channels, of equal strength, p, takes the form

$$\mathscr{D}(\rho_{S_1S_2R}) = (1-p)^2\rho_{S_1S_2R} \quad + \quad \frac{(1-p)p}{3}\sum_{i=1}^{3}(I_{S_1}\otimes\sigma_{S_2}^i\otimes I_R)\rho_{S_1S_2R}(I_{S_1}\otimes\sigma_{S_2}^i\otimes I_R)$$

$$+ \quad \frac{(1-p)p}{3}\sum_{i=1}^{3}(\sigma_{S_1}^i\otimes I_{S_2}\otimes I_R)\rho_{S_1S_2R}(\sigma_{S_1}^i\otimes I_{S_2}\otimes I_R)$$

$$+ \quad \frac{p^2}{9}\sum_{i=j=1}^{3}(\sigma_{S_1}^i\otimes\sigma_{S_2}^j\otimes I_R)\rho_{S_1S_2R}(\sigma_{S_1}^i\otimes\sigma_{S_2}^j\otimes I_R).$$

In the top panel of Fig. 4.7, the capacity of DC is plotted against the total noise, $2H(p)$, of the uncorrelated channel, for various choices of α in the gGHZ state. The bottom panel represents the DC capacity in the case of the fully correlated Pauli channel with respect to the noise, $H(\{q_i\})$, in this case, for the same gGHZ states. The figure indicates that the amount of correlated Pauli noise, that can keep the gGHZ state dense codeable, is therefore higher than that of the uncorrelated noise.

To analyze the relation between the DC capacity and quantum correlation, we plot, in Fig. 4.8, the GGM against C_{uc}^{noisy}, the DC capacity for two senders and a single receiver, with the post-encoded quantum systems being sent to the receiver via uncorrelated depolarizing channels, for arbitrary pure three-qubit states, which are numerically generated by choosing 10^5 random states. We choose the noise parameter, p, as 0.04 for the purpose of the figures in (Fig. 4.8). Fig. 4.7 shows that for small values of p, the gGHZ state remains dense codeable even for small values of α. In Fig. 4.8, the blue triangles are the
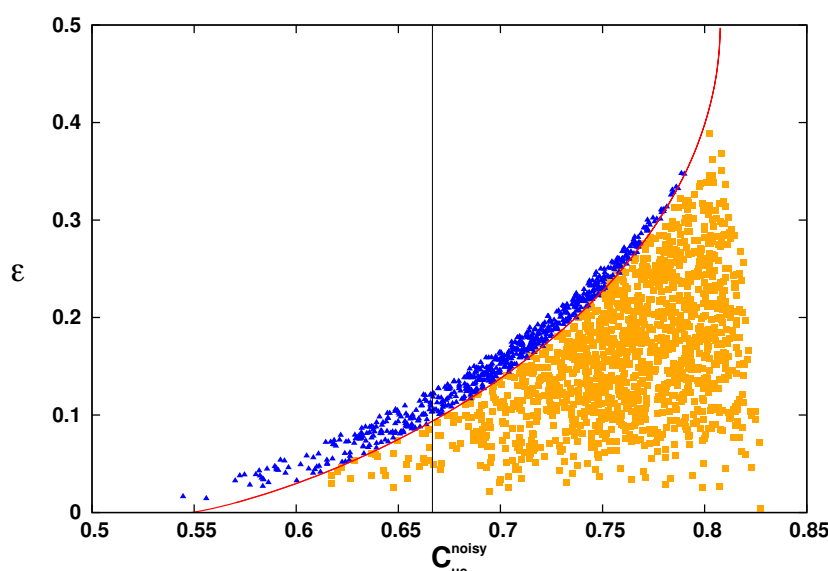
Figure 4.8: (Color online.) GGM vs. the raw DC capacity, C_{uc}^{noisy}, in the presence of the uncorrelated noise. See text for further details. Both axes represent dimensionless quantities. The vertical line at $C_{uc}^{noisy} = 2/3$ again helps to read the actual capacity from the raw capacity.

ones which satisfy condition (ii) of Theorem 4 and we observe that most of them lie above the red curve of the gGHZ states. Note that condition (i) is not well-defined in the current (uncorrelated) scenario. The remaining states are represented by orange squares. The similar behavior has also been noticed for the other multiparty QC measures, the tangle and the discord monogamy score.

4.4 In closing

For transmission of classical information over noiseless and memory-less quantum channels, the capacity in the case of a single sender to a single receiver is well-studied. However, point-to-point communication is of limited commercial use and the exploration of quantum networks with multiple senders and receivers is therefore of far greater interest. Moreover, creation of multipartite systems with quantum correlations, the essential ingredient for several quantum communication as well as computational tasks, is currently being actively pursued in laboratories around the globe. Establishment of connections between multipartite quantum correlation measures and capacities are usually hindered by the unavailability of a unique multiparty quantum correlation measure even for pure states, and the plethora of possibilities for multiparty communication protocols.

For a communication scenario involving several senders and a single receiver, we establish a relation between the capacities of classical information transmission and multipartite computable quantum correlation measures, for both noiseless as well as noisy channels. Specifically, we show that there are hierarchies among multipartite states according to the capacities of the dense coding protocol and hence obtain a tool to classify quantum states according to their usefulness in quantum dense coding.

But when one introduces some amount of noise in the transmission channel of the DC protocol our results strongly indicate that the relative hierarchies among quantum states, get inverted. The results found in this chapter are generic in a sense that they seem to be independent of the choices of the multipartite QC measures as well as for different kinds of noises. A schematic diagram elucidating this phenomena
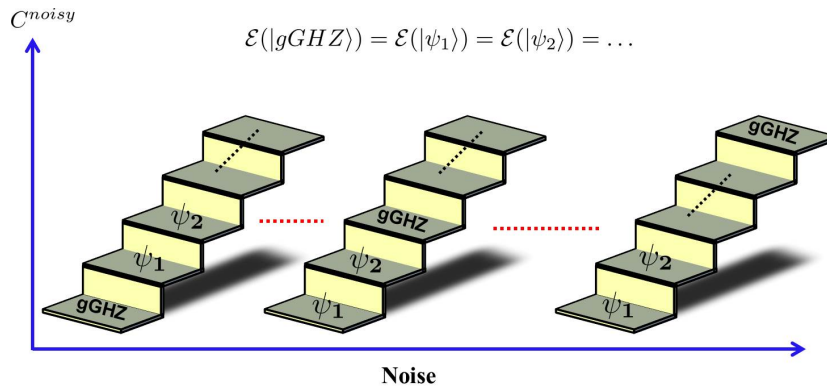
Figure 4.9: Schematic diagram of the change of status of the gGHZ state in comparison to other multipartite states with respect to multipartite DC capacity in the presence of noise. The comparison has been made with the states which posses same amount of multipartite quantum correlations as the gGHZ state. The results obtained in this paper shows that the gGHZ state is more robust against noise as compared to arbitrary states for the dense coding protocol. This is independent of the fact whether the noise in the system is from the source or in the channel after the encoding.

is presented in Fig. 4.9. The results can be an important step forward in building up communication networks using multipartite quantum correlated states in realizable systems.

The results of this Chapter are based on the following paper:

1. *Multipartite Dense Coding vs. Quantum Correlation: Noise Inverts Relative Capability of Information Transfer*, **Tamoghna Das**, R. Prabhu, Aditi Sen De, Ujjwal Sen, Phys. Rev. A **92**, 022319 (2014).

Chapter 5

Distributed Quantum Dense coding

In this chapter, we will discuss about the quantum communication network i.e., the protocol of classical information transmission from many senders to two receivers, by using a shared multiparty quantum state. In this protocol, we have assumed that the two receivers are at distant locations and to get the information or decode the message, they can only perform local quantum operations and classical communication and hence we term this protocol as LOCC-DC protocol. As the ensemble of the encoded states, containing the information, are distributed among the two receivers, it is also named as the "distributed quantum dense coding" [21, 22]. If the two receivers are allowed to come closer and can perform a global quantum measurement in the entire state space, then the situation reduces to the DC protocol for a single receiver which we have already discussed in Chapter 3. The situation of two receivers connected to multiple senders can be seen in many places in our day to day life – for example, in a big country like India, a newspaper company may have several head offices, in particular two major offices situated in two different cities that collect news from the field reporters and to print or telecast the news in a coherent manner, the two editorial offices must know the entire information, by LOCC.

For an arbitrary multiparty quantum state shared between several senders and two receivers, an upper bound on the capacity of distributed DC has been obtained in Ref. [21, 22] in the noiseless scenario. Moreover, it was also shown by giving an explicit LOCC protocol, that the upper bound can be achieved for a shared four-qubit Greenberger-Horne-Zeilinger (GHZ) state, involving two senders and two receivers. In this chapter, we derive an upper bound on the LOCC-DC, in presence of noise in the transmission channel through which the encoded parts are sent to the receivers, for any arbitrary noisy channel. It can be further tightened for a particular noise model, namely, the covariant noise [57]. But before going to this LOCC-DC, we first discuss about how much information, the two party can get, by LOCC when an ensemble of states are shared between them (locally accessible information) [123, 124]. We start our discussion with the chain rule of mutual information in both classical and quantum domain.

5.1   Chain rule of Mutual information

We first derive the chain rule of mutual information derived in Eq. (2.23) in a classical domain. Suppose, that there is a set of $N + 1$ random variables $X, Y_1, Y_2, \ldots, Y_N$. And their joint probability distribution,

$p(x, y_1, \ldots, y_N)$, of getting $X = x$ and $Y_1 = y_1, \ldots, Y_N = y_N$, can be written as

$$
\begin{align}
p(x, y_1, \ldots, y_N) &= p(x)p(y_1, \ldots, y_N | x) \tag{5.1} \\
&= p(x)\frac{p(x, y_1, \ldots, y_N)}{p(x, y_1, \ldots, y_{N-1})}\frac{p(x, y_1, \ldots, y_{N-1})}{p(x, y_1, \ldots, y_{N-2})} \cdots \frac{p(x, y_1)}{p(x)} \tag{5.2} \\
&= \prod_{j=1}^{N} p(y_j | x, y_1, \ldots, y_{j-1})p(x), \tag{5.3}
\end{align}
$$

using Bayes rule of probability distribution [141]. Here, $p(y_j | x, y_1, \ldots, y_{j-1})$ is the conditional probability of getting $Y_j = y_j$, when $X = x$ and $Y_i = y_i$, $\forall i < j$ has already been occurred. Now the conditional entropy, $H(Y_1, \ldots, Y_N | X)$, generalization of Eq. (2.27), for $N + 1$ random variables tells us the remaining uncertainty of the random variables $Y_1, \ldots, Y_N$, when one already knows about X and reads as

$$
\begin{align}
H(Y_1, \ldots, Y_N | X) &= - \sum_{x, y_1, \ldots, y_N} p(x, y_1, \ldots, y_N) \log_2 p(y_1, \ldots, y_N | x) \tag{5.4} \\
&= - \sum_{x, y_1, \ldots, y_N} \sum_{j=1}^{N} p(x, y_1, \ldots, y_N) \log_2 p(y_j | x, y_1, \ldots, y_{j-1}) \tag{5.5} \\
&= \sum_{j=1}^{N} H(Y_j | X, Y_1, \ldots, Y_{j-1}). \tag{5.6}
\end{align}
$$

Similarly, one can also show that the joint Shannon entropy of random variables $Y_1, \ldots, Y_N$ is

$$
H(Y_1, \ldots, Y_N) = \sum_{j=1}^{N} H(Y_j | Y_1, \ldots, Y_{j-1}). \tag{5.7}
$$

The mutual information between X and the set of random variables $Y_1, \ldots, Y_N$, denoted by $I(X : Y_1, \ldots, Y_N)$ quantifies the information which is common between them, and is given by

$$
\begin{align}
I(X : Y_1, \ldots, Y_N) &= H(Y_1, \ldots, Y_N) - H(Y_1, \ldots, Y_N | X) \tag{5.8} \\
&= \sum_{j=1}^{N} H(Y_j | Y_1, \ldots, Y_{j-1}) - H(Y_j | X, Y_1, \ldots, Y_{j-1}) \tag{5.9} \\
&= \sum_{j=1}^{N} I(X : Y_j | Y_1, \ldots, Y_{j-1}). \tag{5.10}
\end{align}
$$

Eq. (5.10) is known as the chain rule of mutual information in classical information theory [141]. In a quantum domain, we assume that the same chain rule of mutual information also holds, where the Shannon entropies are replaced by the von-Neumann entropies.

5.2 Locally accessible information

Suppose that an ensemble $\mathcal{E} = \{p_x, \rho^x_{AB}\}$ is shared between two parties Alice (A) and Bob (B). Alice possess the part of the ensemble $\mathcal{E}^A = \{p_x, \rho^x_A\}$ and Bob $\mathcal{E}^B = \{p_x, \rho^x_B\}$. To know the information
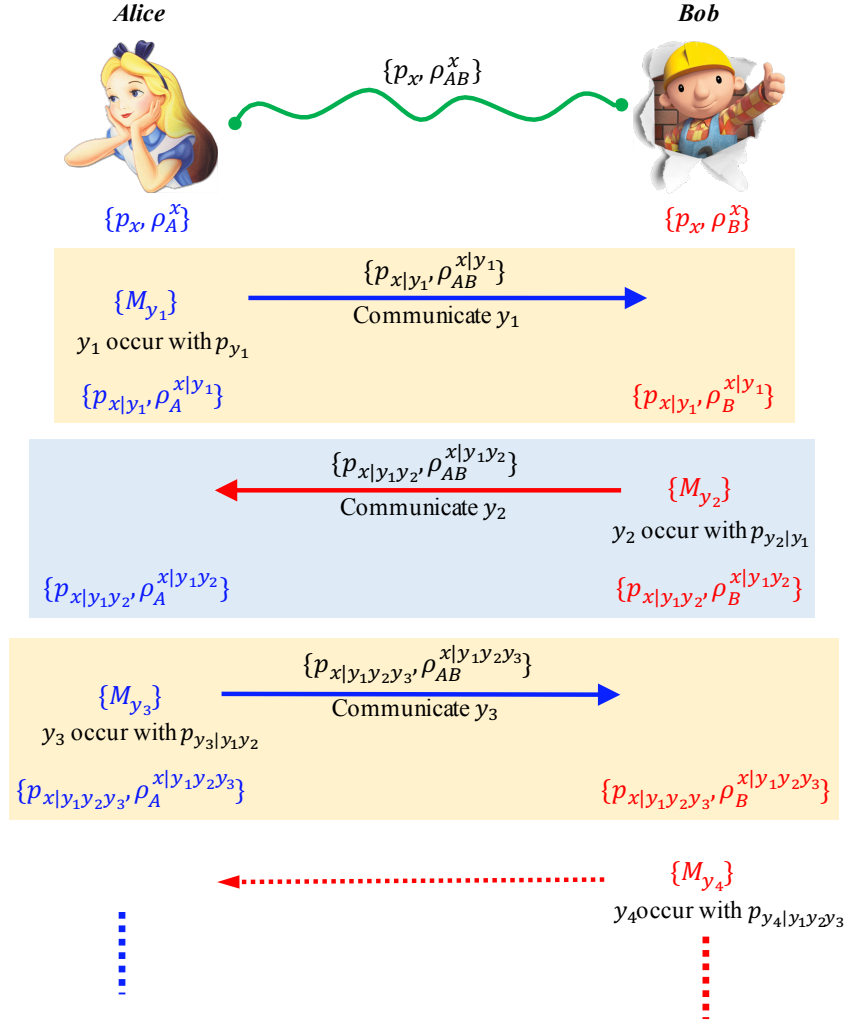
Figure 5.1:   The LOCC protocol of obtaining information about the message x, which occurs with probability p_x, when Alice and Bob share an ensemble $\{p_x, \rho_{AB}^x\}$. First Alice initiates the measurement on her part of the ensemble and communicates the result to Bob. Depending on the Alice's outcome, Bob chooses and performs another measurement on the shared post measurement ensemble and communicates his outcome. The process goes on until they gather maximal information about the ensemble.

about x, Alice and Bob can only perform measurements (PV as well as POVM (see Eqs. (2.30) and (2.31))) in their respective parts of the ensemble, namely on $\mathcal{E}^A$ and $\mathcal{E}^B$, and communicate their outcome to the other. Suppose Alice starts the protocol. Alice performs measurement and obtains the result. She communicates her measurement outcome to Bob by classical channel, say by phone call. Depending on the measurement outcome of Alice, Bob chooses his measurement and again communicates to Alice. The process goes on until the two party gather as much information as possible about the shared ensemble.

Suppose, Alice first performs measurement, $\{M_{y_1}\}$, on her part of the quantum state, obtains the outcome y_1 with the probability p_{y_1}, creates the post measurement ensemble (PME) $\{p_{x|y_1}, \rho_{AB}^{x|y_1}\}$, shared between Alice and Bob. After Alice's measurement, and her communication to Bob, the part of the ensemble in Bob's possession also changes as depicted in Fig. 5.1. Bob next performs measurement, $\{M_{y_2}\}$, in his part of the PME, and obtains the result, say, y_2 which occurs with probability $p_{y_2|y_1}$, resulting PME $\{p_{x|y_1y_2}, \rho_{AB}^{x|y_1y_2}\}$. The outcome has again been communicated to Alice and she performs

another measurement and then communicates her result to Bob and so on, as depicted in Fig. 5.1.

Let us now ask the question. How much information these two parties can gather after this LOCC protocol ? To find the answer of this question, we will use the chain rule of mutual information, as given in Eq. (5.10), where the random variable X will be replaced by the initial ensemble and $Y_1, Y_2, \ldots$ are the measurement outcomes of the Alice's and Bob's measurements denoted by $\{M_{y_i}\}$.

5.2.1 Information gain in a single measurement

Before discussing the information gain by a general LOCC protocol, let us discuss the maximal information obtained by two parties, when one of them performs a measurement on a given ensemble. For a shared ensemble $\{p_x, \rho^x_{AB}\}$, the ensemble which Alice can manipulate is $\mathcal{E}^A$. Suppose, she performs measurement $\{M_{y_1}\}$ on her part of the ensemble. The question is how much information Alice can gain after this single measurement. In this section, we will address this question and derive the information accessible after a measurement [123, 185]. For the sake of simplicity, the subscript A has been omitted from the ensemble of state in the rest of the subsection.

Any ensemble of states $\{p_x, \rho^x\}$ can be considered as a part of a larger system, ρ_{XSY}, given by

$$\rho_{XSY} = \sum_x p_x |x\rangle\langle x|_X \otimes \rho^x_S \otimes |0\rangle\langle 0|_Y, \tag{5.11}$$

where S represents our system of interest, $\{|x\rangle\}$ is a set of orthogonal basis in the system X, which exhausts all the possible preparation of ρ^x and can be considered as a register of ρ^x. Here, $|0\rangle$ is the intial state of an ancillary system Y. Now any measurement $\{M_y\}$[1] on the system S can be considered as a composite operation on the joint Hilbert space of SY [135], i.e.,

$$\rho'_{XSY} = \sum_x p_x |x\rangle\langle x|_X \otimes \sum_y M_y \rho^x_S M_y^\dagger \otimes |y\rangle\langle y|_Y, \tag{5.12}$$

with $\sum_y M_y^\dagger M_y = I_Y$ and $|y\rangle$ is a orthogonal basis in the ancillary system Y, with the same number of elements as $\{M_y\}$. Here, $M_y \rho^x_S M_y^\dagger$, is not a trace preserving operation, and

$$p_{y|x} = \text{tr}\big(M_y \rho^x_S M_y^\dagger\big) \tag{5.13}$$

is the probability of getting the outcome $Y = y$, when the given state is ρ^x, and hence the post measurement state is given by

$$\rho^{x|y} = M_y \rho^x_S M_y^\dagger / p_{y|x}. \tag{5.14}$$

The state in Eq. (5.12), can be rewritten as

$$\rho'_{XSY} = \sum_{xy} p_x p_{y|x} |x\rangle\langle x|_X \otimes \rho^{x|y}_S \otimes |y\rangle\langle y|_Y, \tag{5.15}$$

$$= \sum_y p_y \sum_x p_{x|y} |x\rangle\langle x|_X \otimes \rho^{x|y}_S \otimes |y\rangle\langle y|_Y. \tag{5.16}$$

Here we use the Bayes rule [141] of probability theory. The above equation is the averaged total state, when no one has bothered about the outcome of the measurement. But if the outcome is known, then the

---

[1]We also skip the subscript 1 in $\{M_y\}$ in Alice's measurement.

initial ensemble reduces to an ensemble $\{p_{x|y}, \rho^{x|y}\}$ occurring with probability p_y.

The amount of information gained, in this measurement, is the quantum mutual information of the state ρ'_{XY}. Since, the information of the initial ensemble is registered in the basis $\{|x\rangle_X\}$ and the measurement outcome in the basis $\{|y\rangle_Y\}$. From the chain rule of mutual information of ρ'_{XSY}, in the $X : SY$ bipartition, given in Eq. (5.10), we have

$$I(\rho'_{X:SY}) = I(\rho'_{X:Y}) + I(\rho'_{X:S|Y}). \tag{5.17}$$

But the mutual information is non-increasing under local operations [135], so we get

$$I(\rho'_{X:SY}) \leq I(\rho_{X:SY}) = I(\rho_{X:S}). \tag{5.18}$$

The last equality holds due to the fact that the system Y is in a product form with XS, in ρ_{XSY}, as shown in Eq. (5.11). Therefore,

$$I(\rho_{X:S}) = S(\rho_X) + S(\rho_S) - S(\rho_{XS}), \tag{5.19}$$
$$= H(X) + S\left(\sum_x p_x \rho^x\right) - S(\rho_{XS}), \tag{5.20}$$

where $H(X) = -\sum_x p_x \log_2 p_x$, is the Shannon entropy of $\{p_x\}$. To calculate $S(\rho_{XS})$, we diagonalise each $\rho^x = \sum_\mu \lambda_\mu^x |\mu^x\rangle\langle\mu^x|$, with the mutually orthogonal eigenvector $|\mu^x\rangle$ corresponding to the eigenvalue λ_μ^x, and hence

$$\rho_{XS} = \sum_x p_x |x\rangle\langle x|_X \otimes \sum_\mu \lambda_\mu^x |\mu^x\rangle\langle\mu^x|_S. \tag{5.21}$$

The von-Neumann entropy then reduces to

$$\begin{aligned} S(\rho_{XS}) &= -\sum_{x\mu} p_x \lambda_\mu^x \log_2(p_x \lambda_\mu^x) \\ &= -\sum_{x\mu} \lambda_\mu^x \, p_x \log_2 p_x - \sum_x p_x \sum_\mu \lambda_\mu^x \log_2 \lambda_\mu^x \\ &= H(X) + \sum_x p_x S(\rho^x). \tag{5.22} \end{aligned}$$

The mutual information is then given by

$$I(\rho_{X:S}) = S\left(\sum_x p_x \rho^x\right) - \sum_x p_x S(\rho^x) = \chi^S, \tag{5.23}$$

the Holevo quantity of a given ensemble $\{p_x, \rho^x\}$, as given in Eq. (3.2). The second term in Eq. (5.17) is defined as

$$I(\rho'_{X:S|Y}) = \sum_y p_y I(\rho'_{X:S|Y=y}), \tag{5.24}$$

where

$$\rho'_{X:S|Y=y} = \sum_x p_{x|y} |x\rangle\langle x|_X \otimes \rho_S^{x|y} \otimes |y\rangle\langle y|_Y. \tag{5.25}$$

So we have

$$I(\rho'_{X:S|Y}) = \sum_y p_y \left[S\left(\sum_x p_{x|y} \rho^{x|y} \right) - \sum_x p_{x|y} S(\rho^{x|y}) \right] = \bar{\chi}^S. \tag{5.26}$$

Combining the results in Eqs. (5.17), (5.18), (5.23) and (5.26), the information accessible to Alice, after her first measurement on the shared ensemble $\{p_x, \rho^x_{AB}\}$[2], is given by

$$I(\rho'_{X:Y}) \equiv I^A_1 \leq \chi^A - \bar{\chi}^A, \tag{5.27}$$

where

$$\chi^A = S\left(\sum_x p_x \rho^x_A \right) - \sum_x p_x S(\rho^x_A), \tag{5.28}$$

$$\bar{\chi}^A = \sum_y p_y \left[S\left(\sum_x p_{x|y} \rho^{x|y}_A \right) - \sum_x p_{x|y} S(\rho^{x|y}_A) \right]. \tag{5.29}$$

5.2.2 Information gain in successive measurements

Suppose now that Alice and Bob have performed total N number of local measurements $Y_1, Y_2, \ldots, Y_N$ successively, where all the odd number of measurements are done by Alice and all the even number of measurements are by Bob. Moreover, it is assumed that after each measurement, both of them successfully communicated their results, to the other one and except the first one, all the measurement are chosen depending on the previous measurements results. The information gain in this scenario can be quantified from the joint mutual information as

$$I(\rho_{X:Y_1,Y_2,\ldots,Y_N}) = \sum_{j=1}^{N} I(\rho_{X:Y_j|Y_1,\ldots,Y_{j-1}}) \tag{5.30}$$

$$= I(\rho_{X:Y_1}) + I(\rho_{X:Y_2|Y_1}) + \cdots + I(\rho_{X:Y_N|Y_1,\ldots,Y_{N-1}}), \tag{5.31}$$

where we use Eq. (5.10). Here we assume that Alice initiates the first measurement $\{M_{y_1}\}$, as shown in Fig. 5.1, and the information she obtained, according to Eq. (5.27), is given by

$$I(\rho_{X:Y_1}) \leq \chi^A_1 - \bar{\chi}^A_1, \tag{5.32}$$

where '1' in the subscript indicates the first measurement $\{M_{y_1}\}$. On the other hand, the accessible information by Bob after his measurement $\{M_{y_2}\}$ is given by

$$I(\rho_{X:Y_2|Y_1}) \leq \sum_{y_1} p_{y_1} \left[\chi^B_2 - \bar{\chi}^B_2 \right]. \tag{5.33}$$

where p_{y_1} is the probability of obtaining the outcome y_1 by Alice in the measurement $\{M_{y_1}\}$. Similarly, after Alice's second measurement $\{M_{y_3}\}$, we get

$$I(\rho_{X:Y_3|Y_1,Y_2}) \leq \sum_{y_1 y_2} p_{y_1 y_2} \left[\chi^A_3 - \bar{\chi}^A_3 \right]. \tag{5.34}$$

---

[2] This is the information gain by Alice and Bob after a single measurement performed by Alice and without any classical communication to Bob. Of course, similar result can be obtained if Bob starts the protocol, replacing superscript "A" by "B" in Eq. (5.27)

and so on. Here χ_1^A and $\bar{\chi}_1^A$ is given in Eqs. (5.28) and (5.29), and

$$\chi_2^B = S\Big(\sum_x p_{x|y_1}\rho_B^{x|y_1}\Big) - \sum_x p_{x|y_1}S\big(\rho_B^{x|y_1}\big) \tag{5.35}$$

$$\bar{\chi}_2^B = \sum_{y_2} p_{y_2|y_1}\Big[S\Big(\sum_x p_{x|y_1y_2}\rho_B^{x|y_1y_2}\Big) - \sum_x p_{x|y_1y_2}S\big(\rho_B^{x|y_1y_2}\big)\Big] \tag{5.36}$$

$$\chi_3^A = S\Big(\sum_x p_{x|y_1y_2}\rho_A^{x|y_1y_2}\Big) - \sum_x p_{x|y_1y_2}S\big(\rho_A^{x|y_1y_2}\big) \tag{5.37}$$

$$\bar{\chi}_3^A = \sum_{y_3} p_{y_3|y_1y_2}\Big[S\Big(\sum_x p_{x|y_1y_2y_3}\rho_A^{x|y_1y_2y_3}\Big) - \sum_x p_{x|y_1y_2y_3}S\big(\rho_A^{x|y_1y_2y_3}\big)\Big]. \tag{5.38}$$

Notice that any measurement in Alice's subsystem does not change the average density matrix in the Bob's part, or vice-versa. Mathematically, we have

$$\sum_{y_1} p_{y_1}\sum_x p_{x|y_1}\rho_B^{x|y_1} = \sum_x p_x \text{tr}_A\Big(\sum_{y_1|x} p_{y_1|x}M_{y_1}\otimes I_B\rho_{AB}^x M_{y_1}^\dagger\otimes I_B\Big)\frac{1}{p_{y_1|x}}, \tag{5.39}$$

$$= \sum_x p_x\rho_B^x. \tag{5.40}$$

Similarly, we also have

$$\sum_{y_2} p_{y_2|y_1}\sum_x p_{x|y_1y_2}\rho_A^{x|y_1y_2} = \sum_x p_{x|y_1}\rho_A^{x|y_1}, \tag{5.41}$$

$$\sum_{y_3} p_{y_3|y_1y_2}\sum_x p_{x|y_1y_2y_3}\rho_B^{x|y_1y_2y_3} = \sum_x p_{x|y_1y_2}\rho_B^{x|y_1y_2}, \tag{5.42}$$

$$\sum_{y_4} p_{y_4|y_1y_2y_3}\sum_x p_{x|y_1y_2y_3y_4}\rho_A^{x|y_1y_2y_3y_4} = \sum_x p_{x|y_1y_2y_3}\rho_A^{x|y_1y_2y_3}. \tag{5.43}$$

Now define

$$\bar{\rho}_A = \sum_x p_x\rho_A^x, \tag{5.44}$$

$$\bar{S}_A^x = \sum_x p_x S(\rho_A^x), \tag{5.45}$$

$$\bar{S}_A^{x|1} = \sum_{xy_1} p_{xy_1}S(\rho_A^{x|y_1}), \tag{5.46}$$

and

$$\bar{S}_A^{x|n} = \sum_{xy_1\ldots y_n} p_{xy_1\ldots y_n}S(\rho_A^{x|y_1\ldots y_n}). \tag{5.47}$$

Similarly, one can write, replacing A by B. Putting all the terms in Eq. (5.30), we obtain the accessible information under LOCC performed by both Alice and Bob as

$$I_{acc}^{LOCC} \leq \Big[S(\bar{\rho}_A) - \bar{S}_A^x - \sum_{y_1} p_{y_1}S\Big(\sum_x p_{x|y_1}\rho_A^{x|y_1}\Big) + \bar{S}_A^{x|1}\Big]$$

$$+ \Big[S(\bar{\rho}_B) - \bar{S}_B^{x|1} - \sum_{y_1y_2} p_{y_1y_2}S\Big(\sum_x p_{x|y_1y_2}\rho_B^{x|y_1y_2}\Big) + \bar{S}_B^{x|2}\Big]$$

$$+ \quad \Big[\sum_{y_1 y_2} p_{y_1 y_2} S\Big(\sum_x p_{x|y_1 y_2} \rho_A^{x|y_1 y_2} \Big) - \bar{S}_A^{x|2} - \sum_{y_1 y_2 y_3} p_{y_1 y_2 y_3} S\Big(\sum_x p_{x|y_1 y_2 y_3} \rho_A^{x|y_1 y_2 y_3} \Big) + \bar{S}_A^{x|3} \Big]$$

$$+ \quad \Big[\sum_{y_1 y_2 y_3} p_{y_1 y_2 y_3} S\Big(\sum_x p_{x|y_1 y_2 y_3} \rho_B^{x|y_1 y_2 y_3} \Big) + \cdots \tag{5.48}$$

$$\leq \quad S(\bar{\rho}_A) - \bar{S}_A^x + \bar{S}_A^{x|1} + S(\bar{\rho}_B) - \bar{S}_B^{x|1} + \bar{S}_B^{x|2} - \bar{S}_A^{x|2} + \bar{S}_A^{x|3} - \bar{S}_B^{x|3} + \bar{S}_B^{x|4} + \cdots \tag{5.49}$$

$$= \quad S(\bar{\rho}_A) + S(\bar{\rho}_B) - \bar{S}_B^x - \big\{ \bar{S}_A^x - \bar{S}_A^{x|1} - \big(\bar{S}_B^x - \bar{S}_B^{x|1} \big) \big\} + \big\{ \bar{S}_A^{x|2} - \bar{S}_A^{x|3} - \big(\bar{S}_B^{x|2} - \bar{S}_B^{x|3} \big) \big\}$$

$$+ \cdots . \tag{5.50}$$

Here we use the concavity and the positivity of von-Neumann entropy, in the following terms :

$$\sum_{y_1} p_{y_1} S\Big(\sum_x p_{x|y_1} \rho_B^{x|y_1} \Big) \quad \leq \quad S\Big(\sum_{x y_1} p_{y_1} p_{x|y_1} \rho_B^{x|y_1} \Big) \tag{5.51}$$

$$\sum_{y_1 y_2} p_{y_1 y_2} S\Big(\sum_x p_{x|y_1 y_2} \rho_B^{x|y_1 y_2} \Big) \quad \leq \quad \sum_{y_1} p_{y_1} S\Big(\sum_{y_2} p_{y_2|y_1} \sum_x p_{x|y_1 y_2} \rho_B^{x|y_1 y_2} \Big) \tag{5.52}$$

$$\sum_{y_1 y_2 y_3} p_{y_1 y_2 y_3} S\Big(\sum_x p_{x|y_1 y_2 y_3} \rho_B^{x|y_1 y_2 y_3} \Big) \quad \leq \quad \sum_{y_1 y_2} p_{y_1 y_2} S\Big(\sum_{y_3} p_{y_3|y_1 y_2} \sum_x p_{x|y_1 y_2 y_3} \rho_B^{x|y_1 y_2 y_3} \Big) \tag{5.53}$$

and use Eqs. (5.41), (5.42) and (5.43) to get the form of Eq. (5.49). Let us now use another fact that the average entropic change in the measured party is always bounded above by average entropic change in the unmeasured party. Mathematically,

$$\bar{S}_A^x - \bar{S}_A^{x|1} \quad \geq \quad \bar{S}_B^x - \bar{S}_B^{x|1}, \tag{5.54}$$

$$\bar{S}_A^{x|2} - \bar{S}_A^{x|3} \quad \geq \quad \bar{S}_B^{x|2} - \bar{S}_B^{x|3}. \tag{5.55}$$

The above bound can be proved if one considers the purification of the initial ensemble $\{p_x, \rho_{AB}^x\}$, as $\{p_x, |\psi_{ABC}^x\rangle\}$, where

$$\rho_{AB}^x = \text{tr}_C |\psi_{ABC}^x\rangle \langle \psi_{ABC}^x|, \tag{5.56}$$

by adding an ancilla C in the unmeasured part. Now any measurement $\{M_y\}$ by Alice, with outcome y, occurring with p_y, on the pure state ensemble leaves the PME as $\{p_{x|y}, |\psi_{ABC}^{x|y}\rangle\}$,

$$|\psi_{ABC}^x\rangle \longrightarrow M_y \otimes I_{BC} |\psi_{ABC}^x\rangle / p_{y|x} = |\psi_{ABC}^{x|y}\rangle, \tag{5.57}$$

with $p_{y|x} = \langle \psi_{ABC}^x | M_y^\dagger M_y \otimes I_{BC} | \psi_{ABC}^x \rangle$. Finally, we have

$$\sum_x p_x S(\rho_A^x) - \sum_{x y_1} p_{x y_1} S(\rho_A^{x|y_1}) \quad = \quad \sum_x p_x S(\rho_{BC}^x) - \sum_{x y_1} p_{x y_1} S(\rho_{BC}^{x|y_1})$$

$$\geq \quad \sum_x p_x S(\rho_B^x) - \sum_{x y_1} p_{x y_1} S(\rho_B^{x|y_1}). \tag{5.58}$$

The last inequality comes from the fact that Holevo quantity is non-increasing under discarding the subsystem.

Hence, all the terms in the parentheses of Eq. (5.50) are non-positive, and therefore, we obtain

$$I_{acc}^{LOCC} \leq S(\bar{\rho}_A) + S(\bar{\rho}_B) - \bar{S}_B^x. \tag{5.59}$$
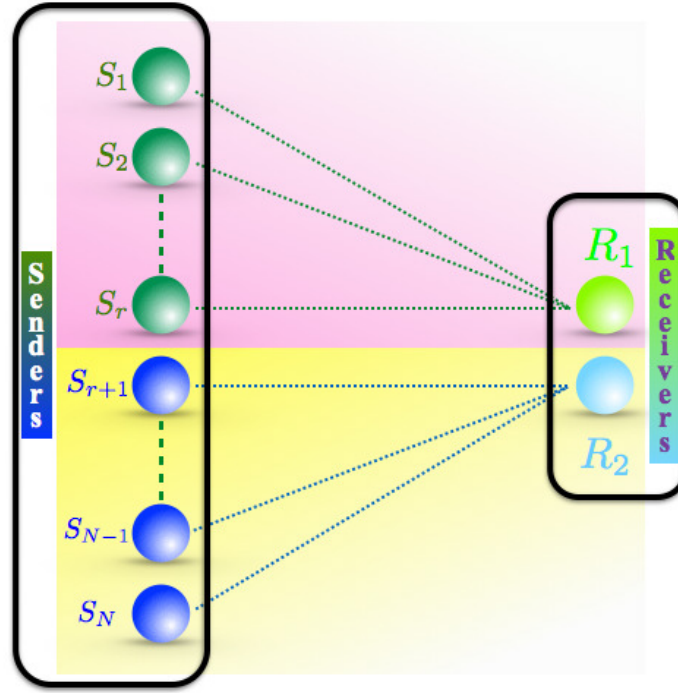
Figure 5.2: A schematic diagram of the DC protocol of two receivers. An $(N+2)$-party quantum state, $\rho_{S_1 S_2 \ldots S_N R_1 R_2}$, is shared between N senders, $S_1, S_2, \ldots, S_N$, and two receivers, R_1 and R_2. We assume that after unitary encoding, the senders, $S_1, S_2, \ldots, S_r$, send their part to the receiver R_1 while the rest send their parts to the receiver, R_2. To decode, R_1 and R_2 are only allowed to perform LOCC.

The term $\bar{S}_B^x$ comes due to the fact that Alice has started the measurement in the LOCC protocol. If it was initiated by Bob, it will be $\bar{S}_A^x$. Therefore the information gained by both the parties via LOCC is given by

$$I_{acc}^{LOCC} \leq S(\bar{\rho}_A) + S(\bar{\rho}_B) - \max_{\alpha \in A, B} \sum_x p_x S(\rho_\alpha^x). \tag{5.60}$$

The above upper bound on locally accessible information can be interpreted as the local version of Holevo quantity, also known as LOCC-Holevo bound [123, 124]. In the DC protocol with single receiver, Holevo bound plays an important role to obtain the capacity of DC. Similarly, LOCC-Holevo bound will be used to get the capacity of DC involving two-receivers, situated in two distant places.

5.3 Distributed quantum dense coding

In this section, we will talk about the capacity of distributed dense coding involving arbitrary number of senders, say N and two receivers, in the noiseless scenario, as shown in Fig. 5.2. The protocol goes as follows:

1. An $N + 2$ party quantum state $\rho_{S_1 \ldots, S_N R_1 R_2}$, is shared between the N senders and 2 receivers.

2. Depending on the messages, that the senders want to communicate, they perform unitary operations

in their respective part of the quantum state, resulting an ensemble of states

$$\{p_{x_1} p_{x_2} \ldots p_{x_N}, (\underbrace{U_{S_1}^{x_1} \otimes U_{S_2}^{x_2} \otimes \ldots \otimes U_{S_N}^{x_N}}_{U_{S_1 \ldots S_N}^{\{x\}}} \otimes I_{R_1 R_2}) \rho_{S_1 \ldots, S_N R_1 R_2} (U_{S_1}^{x_1 \dagger} \otimes U_{S_2}^{x_2 \dagger} \otimes \ldots \otimes U_{S_N}^{x_N \dagger} \otimes I_{R_1 R_2})\},$$

(5.61)

where we have assumed that the jth sender encodes her message x_j, occurring with probability p_{x_j} by performing unitary operator $U_j^{x_j}$ on her part of the shared state.

3. Some of the senders, say, S_1 to $S_{r<N}$, send their encoded parts to the receiver R_1 while the rest send their parts to the receiver R_2, by using a noiseless quantum transmission channel. Hence the ensemble is distributed among the two receivers i.e., $\mathcal{E}^d = \{p_{\{x\}}, \rho_{\mathcal{A}:\mathcal{B}}^{\{x\}}\}$, in the $\mathcal{A} : \mathcal{B}$ bipartition, where $\mathcal{A} = S_1 \ldots S_r R_1$ and $\mathcal{B} = S_{r+1} \ldots S_N R_2$ and $p_{\{x\}} = p_{x_1} p_{x_2} \ldots p_{x_N}$. Notice here that the unitary operations may not be local from all the senders' part, i.e., some of the senders may come together and can, in principal, perform a global unitary encoding, although they must be local in the $A : B$ bipartition, (see Fig. 5.2) i.e.,

$$U_{S_1 \ldots S_N}^{\{x\}} = U_{S_1 \ldots S_r}^{x_1 \ldots x_r} \otimes U_{S_{r+1} \ldots S_N}^{x_{r+1} \ldots x_N}$$

(5.62)

4. After getting the ensemble, given in Eq. (5.61), the receivers, R_1 and R_2, gather maximal information by LOCC about $\{x\}$.

The information accessible to them by LOCC is bounded above by the quantity given in Eq. (5.60), and therefore, in this case, it is given by

$$I_{acc}^{LOCC} \le S\left(\sum_{\{x\}} p_{\{x\}} \rho_{\mathcal{A}}^{\{x\}}\right) + S\left(\sum_{\{x\}} p_{\{x\}} \rho_{\mathcal{B}}^{\{x\}}\right) - \max_{\alpha \in \mathcal{A}, \mathcal{B}} \sum_{\{x\}} p_{\{x\}} S\left(\rho_{\alpha}^{\{x\}}\right).$$

(5.63)

The noiseless distributed DC or LOCC-DC capacity can be obtained by optimizing I_{acc}^{LOCC}, in the $\mathcal{A} : \mathcal{B}$ bipartition, over all possible unitary encodings and the corresponding probabilities of encodings, i.e.

$$C^{LOCC} \le \underbrace{\max_{\{x\}, \{U^{x_j}\}} \left[S\left(\sum_{\{x\}} p_{\{x\}} \rho_{\mathcal{A}}^{\{x\}}\right) + S\left(\sum_{\{x\}} p_{\{x\}} \rho_{\mathcal{B}}^{\{x\}}\right) - \max_{\alpha \in \mathcal{A}, \mathcal{B}} \sum_{\{x\}} p_{\{x\}} S\left(\rho_{\alpha}^{\{x\}}\right) \right]}_{\mathcal{B}^{LOCC}}.$$

(5.64)

In the single receiver case, the Holevo bound [12] on the accessible information, given in Eq. (3.2), is asymptotically achievable [13, 14], but in the two receiver scenario [123, 124], it has not yet been proven whether the local Holevo bound i.e., the right hand side in Eq. (5.63) can be achieved in an asymptotic level or not. Hence, throughout the thesis, we consider the quantity $\mathcal{B}^{LOCC}$ [21, 22], which is an upper bound on the capacity of LOCC-DC and will show that for a certain shared state, it can be saturated (see Subsec. 5.3.2).

5.3.1 Distributed dense coding capacity

To find out the optimized unitaries and the probabilities in $\mathcal{B}^{LOCC}$, let us first consider the upper bound on $\mathcal{B}^{LOCC}$. Since we have assumed that the encoding operation is local in the first set of senders : second

set of senders bipartition we have

$$
\begin{aligned}
S(\rho_{\mathcal{A}}^{\{x\}}) &= S\big(U_{S_1\ldots S_r}^{x_1\ldots x_r} \otimes I_{R_1}\, \rho_{\mathcal{A}}^{\{x\}}\, U_{S_1\ldots S_r}^{x_1\ldots x_r\dagger} \otimes I_{R_1}\big) = S(\rho_{\mathcal{A}}), \quad (5.65)\\
S(\rho_{\mathcal{B}}^{\{x\}}) &= S\big(U_{S_{r+1}\ldots S_N}^{x_{r+1}\ldots x_N} \otimes I_{R_2}\, \rho_{\mathcal{B}}^{\{x\}}\, U_{S_{r+1}\ldots S_N}^{x_{r+1}\ldots x_N\dagger} \otimes I_{R_2}\big) = S(\rho_{\mathcal{B}}), \quad (5.66)
\end{aligned}
$$

and hence the last term of Eq. (5.63) reduces to

$$
\max_{\alpha\in\mathcal{A},\mathcal{B}} \sum_{\{x\}} p_{\{x\}} S\big(\rho_{\alpha}^{\{x\}}\big) = \max_{\alpha\in\mathcal{A},\mathcal{B}} S(\rho_\alpha). \quad (5.67)
$$

If we now apply the subadditivity of von-Neumann entropy in the first term of Eq. (5.63) in the $S_1 \ldots S_r : R_1$, bipartition, we get

$$
\begin{aligned}
S\Big(\sum_{\{x\}} p_{\{x\}}\rho_{\mathcal{A}}^{\{x\}}\Big) &\leq S\Big(\sum_{\{x\}} p_{\{x\}}\rho_{S_1\ldots S_r}^{\{x\}}\Big) + S\Big(\sum_{\{x\}} p_{\{x\}}\rho_{R_1}^{\{x\}}\Big)\\
&\leq \log_2 d_{S_1\ldots S_r} + S(\rho_{R_1}). \quad (5.68)
\end{aligned}
$$

In the last inequality we use that the von-Neumann entropy of the quantum state of the first set of senders is bounded above of the logarithm of the dimension of the sender's system with $d_{S_1\ldots S_r} = d_{S_1} \cdot d_{S_2} \cdots d_{S_r}$ being the dimensions of the first set of senders and $\rho_{R_1}^{\{x\}} = \rho_{R_1}$, $\forall\{x\}$ since as there is no unitary acting on the receivers system. Similarly, we obtain

$$
S\Big(\sum_{\{x\}} p_{\{x\}}\rho_{\mathcal{B}}^{\{x\}}\Big) \leq \log_2 d_{S_{r+1}\ldots S_N} + S(\rho_{R_2}). \quad (5.69)
$$

Hence we have

$$
\mathcal{B}^{LOCC} \leq \log_2 d_{S_1\ldots S_r} + \log_2 d_{S_{r+1}\ldots S_N} + S(\rho_{R_1}) + S(\rho_{R_2}) - \max_{\alpha\in\mathcal{A},\mathcal{B}} S(\rho_\alpha). \quad (5.70)
$$

It can be shown [21] that this upper bound can be achieved by choosing a complete set of orthogonal unitaries $\{W_{S_j}^{i_j}\}_{i=0}^{d_{S_j}^2-1}$ (see Eqs. (3.8) and (3.9)) where the encoding operation on the jth sender occurs with equal probability $p_{i_j} = \frac{1}{d_{S_j}^2}$. For all the senders, we have

$$
U_{S_1,\ldots,S_N}^{\{x\}} = \bigotimes_{j=1}^{N} W_{S_j}^{i_j}, \quad p_{\{x\}} = \frac{1}{\prod_{j=1}^{N} d_{S_j}^2}. \quad (5.71)
$$

Hence, the upper bound on the LOCC-DC capacity reduces to

$$
\mathcal{B}^{LOCC} = \log_2 d_{S_1\ldots S_N} + S(\rho_{R_1}) + S(\rho_{R_2}) - \max_{\alpha\in\mathcal{A},\mathcal{B}} S(\rho_\alpha). \quad (5.72)
$$

5.3.2 Distributed DC with four-qubit GHZ state

In this subsection, the upper bound on the capacity of distributed quantum DC or LOCC-DC, $\mathcal{B}^{LOCC}$, can be achieved for a particular example of shared state. Let us consider a four-qubit GHZ [56] state, given by

$$
|GHZ\rangle_{S_1 S_2 R_1 R_2} = \frac{1}{\sqrt{2}}(|00\rangle_{S_1 S_2}|00\rangle_{R_1 R_2} + |11\rangle_{S_1 S_2}|11\rangle_{R_1 R_2}), \quad (5.73)
$$

Answers by S_1	Encoding	Answers by S_2	Encoding	Output state
Day and Yes	I	Tea	I	$\frac{1}{\sqrt{2}}(|0000\rangle + |1111\rangle)$
Day and No	σ_z	Tea	I	$\frac{1}{\sqrt{2}}(|0000\rangle - |1111\rangle)$
Night and Yes	σ_x	Tea	I	$\frac{1}{\sqrt{2}}(|1000\rangle + |0111\rangle)$
Night and No	σ_y	Tea	I	$\frac{1}{\sqrt{2}}(|1000\rangle - |0111\rangle)$
Day and Yes	I	Coffee	σ_x	$\frac{1}{\sqrt{2}}(|0100\rangle + |1011\rangle)$
Day and No	σ_z	Coffee	σ_x	$\frac{1}{\sqrt{2}}(|0100\rangle - |1011\rangle)$
Night and Yes	σ_x	Coffee	σ_x	$\frac{1}{\sqrt{2}}(|1100\rangle + |0011\rangle)$
Night and No	σ_y	Coffee	σ_x	$\frac{1}{\sqrt{2}}(|1100\rangle - |0011\rangle)$

Table 5.1: Table of encodings for sharing 3 bits of classical information between two senders and two receivers by using distributed dense coding [21]. The senders and receivers share a GHZ state, given in Eq. (5.73). The first and second columns represent the four possible answers of the first sender (S_1) and her encoding procedure, while the third and fourth columns are for the two answers and encodings for the second sender (S_2) . The fifth column shows the output state after encoding.

shared between two senders, S_1, S_2 and two receivers, R_1 and R_2. The upper bound on LOCC-DC for this state is

$$\mathcal{B}^{LOCC}(|GHZ\rangle) = \log_2 d_{S_1 S_2} + S(\rho_{S_1}) + S(\rho_{S_2}) - \max_{\alpha = S_1 R_1, S_2 R_2} S(\rho^\alpha) = 3, \qquad (5.74)$$

since

$$S(\rho_{S_1}) = S(\rho_{S_2}) = S\left(\frac{1}{2}(|0\rangle\langle 0| + |1\rangle\langle 1|)\right) = 1, \qquad (5.75)$$

$$S(\rho_{S_1 R_1}) = S(\rho_{S_2 R_2}) = S\left(\frac{1}{2}(|00\rangle\langle 00| + |11\rangle\langle 11|)\right) = 1. \qquad (5.76)$$

We will now show that there exists a LOCC decoding protocol by which the two receivers can decode 3 bits of classical information which are in distant locations. To show that let us start with the encoding process which will help to describe the local measurement strategy.

Suppose, the first sender S_1 needs to inform the receivers, R_1 and R_2, the answers of the following two questions

1. Whether she prefers "Night" shift or "Day" shift for a job,

2. and whether she needs any vehicle support from the company to come to the job, "Yes" or "No".

The second sender S_2 needs to send only a single information whether she prefers "Tea" or "Cofee" after lunch. Depending on the answers, they perform local unitary operations in their respective parts of the

Outcome by R_1	Reduced state	Another form
P_1 Clicks	$\frac{1}{\sqrt{2}}(\lvert 0000\rangle + \lvert 1111\rangle)_{S_1 S_2 R_1 R_2}$	$\frac{1}{\sqrt{2}}\left(\lvert\phi^+\rangle\lvert\phi^+\rangle + \lvert\phi^-\rangle\lvert\phi^-\rangle\right)_{S_1 R_1 S_2 R_2}$
	$\frac{1}{\sqrt{2}}(\lvert 0000\rangle - \lvert 1111\rangle)_{S_1 S_2 R_1 R_2}$	$\frac{1}{\sqrt{2}}\left(\lvert\phi^+\rangle\lvert\phi^-\rangle + \lvert\phi^-\rangle\lvert\phi^+\rangle\right)_{S_1 R_1 S_2 R_2}$
	$\frac{1}{\sqrt{2}}(\lvert 0100\rangle + \lvert 1011\rangle)_{S_1 S_2 R_1 R_2}$	$\frac{1}{\sqrt{2}}\left(\lvert\phi^+\rangle\lvert\psi^+\rangle - \lvert\phi^-\rangle\lvert\psi^-\rangle\right)_{S_1 R_1 S_2 R_2}$
	$\frac{1}{\sqrt{2}}(\lvert 0100\rangle - \lvert 1011\rangle)_{S_1 S_2 R_1 R_2}$	$\frac{1}{\sqrt{2}}\left(\lvert\phi^-\rangle\lvert\psi^+\rangle - \lvert\phi^+\rangle\lvert\psi^-\rangle\right)_{S_1 R_1 S_2 R_2}$
P_2 Clicks	$\frac{1}{\sqrt{2}}(\lvert 1000\rangle + \lvert 0111\rangle)_{S_1 S_2 R_1 R_2}$	$\frac{1}{\sqrt{2}}\left(\lvert\psi^+\rangle\lvert\phi^+\rangle - \lvert\psi^-\rangle\lvert\phi^-\rangle\right)_{S_1 R_1 S_2 R_2}$
	$\frac{1}{\sqrt{2}}(\lvert 1000\rangle - \lvert 0111\rangle)_{S_1 S_2 R_1 R_2}$	$\frac{1}{\sqrt{2}}\left(\lvert\psi^+\rangle\lvert\phi^-\rangle - \lvert\psi^-\rangle\lvert\phi^+\rangle\right)_{S_1 R_1 S_2 R_2}$
	$\frac{1}{\sqrt{2}}(\lvert 1100\rangle + \lvert 0011\rangle)_{S_1 S_2 R_1 R_2}$	$\frac{1}{\sqrt{2}}\left(\lvert\psi^+\rangle\lvert\psi^+\rangle + \lvert\psi^-\rangle\lvert\psi^-\rangle\right)_{S_1 R_1 S_2 R_2}$
	$\frac{1}{\sqrt{2}}(\lvert 1100\rangle - \lvert 0011\rangle)_{S_1 S_2 R_1 R_2}$	$\frac{-1}{\sqrt{2}}\left(\lvert\psi^+\rangle\lvert\psi^-\rangle + \lvert\psi^-\rangle\lvert\psi^+\rangle\right)_{S_1 R_1 S_2 R_2}$

Table 5.2: List of eight orthonormal states, divided into two subgroups, after the first receiver, R_1, performs a measurement in his part of the shared state by using two rank two projectors P_1 and P_2, given in Eq. (5.78).

shared $\lvert GHZ\rangle$ state. The unitary operators used in this situation and the encoded states are given in Table 5.1. After performing the encoding operations, the senders send their parts of the shared state to the receivers. In this case, suppose S_1 sends her part to the receiver R_1 and S_2 to R_2 by using a noiseless quantum channel. And hence the receivers R_1 and R_2 share the entire four-qubit state. Their task is now to identify particular encoded state sent to them, from all possible encoded states, i.e., from eight mutually orthogonal states, by performing local measurements and classical communication.

Suppose the receiver, R_1, starts the LOCC protocol measurement. The measurement operators, he will use, are the rank-two projective operators, given by

$$P_1 = \lvert 00\rangle\langle 00\rvert + \lvert 11\rangle\langle 11\rvert, \tag{5.77}$$
$$P_2 = \lvert 01\rangle\langle 01\rvert + \lvert 10\rangle\langle 10\rvert. \tag{5.78}$$

Depending on the measurement outcome, the eight mutually orthogonal states can be divided into two blocks, which is depicted in the Table 5.2, and R_1 communicates his measurement outcome to the other receiver R_2. R_2 then performs rank-one Bell basis measurement $\{\lvert\psi^\pm\rangle, \lvert\phi^\pm\rangle\}$ in his part of the quantum states. The measurement outcome is then communicated to R_1. The state has been identified by R_1 by performing another Bell basis measurement. The three consecutive measurements lead to the identification of the eight orthogonal states by LOCC and hence the messages sent by S_1 and S_2 (see Table. 5.3).

Therefore, we show that by using a four-qubit $\lvert GHZ\rangle$ state, shared between two senders and two receivers, the senders are able to communicate 3 bits of classical information to the receivers, located into distant locations, by sending only two qubits via noiseless channel, thereby saturating the upper bound

Outcome of 1st measurement by R_1	Outcome of 2nd measurement by R_2	Outcome of 3rd measurement by R_1	Conclusion
P_1 Clicks	$|\phi^+\rangle$	$|\phi^+\rangle$	$\frac{1}{\sqrt{2}}(|0000\rangle + |1111\rangle)$
	$|\phi^-\rangle$	$|\phi^-\rangle$	
	$|\phi^-\rangle$	$|\phi^+\rangle$	$\frac{1}{\sqrt{2}}(|0000\rangle - |1111\rangle)$
	$|\phi^+\rangle$	$|\phi^-\rangle$	
	$|\psi^+\rangle$	$|\phi^+\rangle$	$\frac{1}{\sqrt{2}}(|0100\rangle + |1011\rangle)$
	$|\psi^-\rangle$	$|\phi^-\rangle$	
	$|\psi^+\rangle$	$|\phi^-\rangle$	$\frac{1}{\sqrt{2}}(|0100\rangle - |1011\rangle)$
	$|\psi^-\rangle$	$|\phi^+\rangle$	
P_2 Clicks	$|\phi^+\rangle$	$|\psi^+\rangle$	$\frac{1}{\sqrt{2}}(|1000\rangle + |0111\rangle)$
	$|\phi^-\rangle$	$|\psi^-\rangle$	
	$|\phi^-\rangle$	$|\psi^+\rangle$	$\frac{1}{\sqrt{2}}(|1000\rangle - |0111\rangle)$
	$|\phi^+\rangle$	$|\psi^-\rangle$	
	$|\psi^+\rangle$	$|\psi^+\rangle$	$\frac{1}{\sqrt{2}}(|1100\rangle + |0011\rangle)$
	$|\psi^-\rangle$	$|\psi^-\rangle$	
	$|\psi^-\rangle$	$|\psi^+\rangle$	$\frac{1}{\sqrt{2}}(|1100\rangle - |0011\rangle)$
	$|\psi^+\rangle$	$|\psi^-\rangle$	

Table 5.3: Table of the LOCC decoding protocol by the two receivers R_1 and R_2. The first column represents the outcome of the 1st measurement by R_1. The second column represents the measurement outcomes of the receiver R_2 , depending on the measurement outcome of R_1. The third column is the third measurement which is performed by R_1 after knowing the outcomes of R_2. The second and third measurements performed by R_2 and R_1 respectively are the Bell basis measurements, $\{|\psi^\pm\rangle, |\phi^\pm\rangle\}$. After all the measurements, the receivers can finally distinguish all the eight orthonormal states as mentioned in the fourth column.

$\mathcal{B}^{LOCC}$, given in Eq. (5.74). We note that the classical limit in this case is $\log_2 4 = 2$, where 4 is the dimension of the senders' subsystem and hence by the GHZ state, we obtain quantum advantage in LOCC protocol.

For the same shared state, i.e., the $|GHZ\rangle$, if the receivers are not allowed to communicate between each other, the protocol can be considered as two distinct dense coding protocols involving a bipartite mixed state $\rho_{S_1 R_1}$ and $\rho_{S_2 R_2}$ shared between the respective senders and the receivers. It can be shown that the DC capacity in this case is not more than 2, which coincides with the classical limit. And hence for that shared state, the LOCC-DC protocol is more advantageous than the individual dense coding protocols on the DC protocol by LO.

This is also evident from the expression of the multiparty DC capacity. If the two receivers do not communicate between each other, then it can be considered as two distinct DC protocols between two blocks of senders and receivers, (pink and yellow blocks as shown in Fig. (5.2)), and their collective DC

capacity is

$$C^{collective} = \left(\log_2 d_{S_1...S_r} + S(\rho_{R_1}) - S(\rho_\mathcal{A}) \right) + \left(\log_2 d_{S_{r+1}...S_N} + S(\rho_{R_2}) - S(\rho_\mathcal{B}) \right). \quad (5.79)$$

The collective DC capacity is smaller than the LOCC-DC capacity, given in Eq. (5.72) since $\min_{\alpha \in \mathcal{A}, \mathcal{B}} S(\rho_\alpha) \geq 0$, assuming that the upper bound can be reached as it is the case for the shared $|GHZ\rangle$ state. The same ordering remains, if the shared state $\rho_{S_1...S_N R_1 R_2}$ is a product of the form $\rho_\mathcal{A} \otimes \rho_\mathcal{B}$, expect when it is a pure product, for which $C^{collective} = \mathcal{B}^{LOCC}$.

5.4 Distributed DC in presence of noisy quantum channels

In this section, our aim is to estimate the capacity of distributed quantum DC, for the shared $N+2$ party quantum state, $\rho_{S_1,...,S_N,R_1,R_2}$, when the senders send their encoded parts of the shared quantum state to the respective receivers by using a general noisy quantum channel. In particular, a system can not be kept completely isolated from the environment and hence noise will inevitably interact with the system, thereby changing the form of the encoded state. As we have already discussed in Sec. 3.2.1, noise in the transmission channel can be characterized by a CPTP map, Λ, acting on the state space of the senders' part of the transmitted state. Therefore, the receivers, R_1 and R_2, after the transmission, possess the distorted ensemble,

$$\mathcal{E}^d_{noisy} = \{p_{\{x\}}, \Lambda_{S_1...S_N}(\rho^{\{x\}}_{S_1...S_N R_1 R_2})\}, \quad (5.80)$$

in the same $S_1 \ldots S_r R_1 : S_{r+1} \ldots S_N R_2 = \mathcal{A} : \mathcal{B}$ bipartition, where

$$\Lambda_{S_1...S_N}\left(\rho^{\{x\}}_{S_1...S_N R_1 R_2}\right) = \Lambda_{S_1...S_N}\left((U^{x_1...x_r}_{S_1...S_r} \otimes U^{x_{r+1}...x_N}_{S_{r+1}...S_N} \otimes I_{R_1 R_2}) \rho_{S_1...S_N R_1 R_2}\right.$$
$$\left. (U^{x_1...x_r\dagger}_{S_1...S_r} \otimes U^{x_{r+1}...x_N\dagger}_{S_{r+1}...S_N} \otimes I_{R_1 R_2})\right) \quad (5.81)$$

Now we will try to find out the upper bound on the noisy $\mathcal{B}^{LOCC}$, for any arbitrary noisy quantum channel Λ, which is also an upper bound on distributed DC capacity.

5.4.1 Upper bound on LOCC-DC for arbitrary noisy channel

To estimate the capacity, let us consider the $(N+2)$-party quantum state, $\rho_{S_1...S_N R_1 R_2}$, which can be expanded as

$$\rho_{S_1...S_N R_1 R_2} = \sum_{\{i,j\}} \lambda_{\{i,j\}} |i_1\rangle\langle j_1|_{S_1...S_N} \otimes |i_2\rangle\langle j_2|_{R_1} \otimes |i_3\rangle\langle j_3|_{R_2}, \quad (5.82)$$

where $\{|i_1\rangle\}_{i_1=0}^{d_{S_1...S_N}-1}$, $\{|i_2\rangle\}_{i_2=0}^{d_{R_1}-1}$, and $\{|i_3\rangle\}_{i_3=0}^{d_{R_2}-1}$ are respectively bases in the Hilbert space $\mathcal{H}^{S_1...S_N}$, of all the senders, and $\mathcal{H}^{R_1}$ $(\mathcal{H}^{R_2})$ of the receiver R_1 (R_2).

After the action of the CPTP map, Λ, on the encoded state, we get

$$\Lambda_{S_1...S_N}(\rho^{\{x\}}_{S_1...S_N R_1 R_2}) = \sum_{\{i,j\}} \lambda_{\{i,j\}} \Lambda_{S_1...S_N}\left((U^{x_1...x_r}_{S_1...S_r} \otimes U^{x_{r+1}...x_N}_{S_{r+1}...S_N}) |i_1\rangle\langle j_1|_{S_1...S_N}(U^{x_1...x_r\dagger}_{S_1...S_r} \otimes U^{x_{r+1}...x_N\dagger}_{S_{r+1}...S_N})\right)$$
$$\otimes |i_2\rangle\langle j_2|_{R_1} \otimes |i_3\rangle\langle j_3|_{R_2}, \quad (5.83)$$

where $\Lambda_{S_1...S_N}$ is collectively or individually acting only on the senders' subsystems. From Eq. (5.60), we know that the amount of classical information that can be extracted from the ensemble, $\{p_{\{x\}}, \Lambda_{S_1...S_N}(\rho_{S_1...S_N R_1 R_2}^{\{x\}})\}$, by LOCC, is given by

$$I_{acc}^{LOCC} \leq S\Big(\sum_{\{x\}} p_{\{x\}} \xi_{\mathcal{A}}^{\{x\}}\Big) + S\Big(\sum_{\{x\}} p_{\{x\}} \xi_{\mathcal{B}}^{\{x\}}\Big) - \max_{\alpha \in \mathcal{A}:\mathcal{B}} \sum_{\{x\}} p_{\{x\}} S(\xi_{\alpha}^{\{x\}}), \qquad (5.84)$$

where $\xi_{\mathcal{A}}^{\{x\}} = \mathrm{tr}_{\mathcal{B}}\Big(\Lambda\big(\rho_{S_1...S_N R_1 R_2}^{\{x\}}\big)\Big)$ and $\xi_{\mathcal{B}}^{\{x\}} = \mathrm{tr}_{\mathcal{A}}\Big(\Lambda\big(\rho_{S_1...S_N R_1 R_2}^{\{x\}}\big)\Big)$. Like in the noiseless case, to obtain the capacity of LOCC-DC in a noisy scenario, one has to maximize the R.H.S. of (5.84) over unitaries and probabilities. The ensemble, in the noisy scenario, involves the CPTP map Λ.

$$C_{noisy}^{LOCC} \leq \underbrace{\max_{\{x\},\{U^{x_j}\}} \Big[S\Big(\sum_{\{x\}} p_{\{x\}} \xi_{\mathcal{A}}^{\{x\}}\Big) + S\Big(\sum_{\{x\}} p_{\{x\}} \xi_{\mathcal{B}}^{\{x\}}\Big) - \max_{\alpha \in \mathcal{A}:\mathcal{B}} \sum_{\{x\}} p_{\{x\}} S(\xi_{\alpha}^{\{x\}})\Big]}_{\chi_{noisy}^{LOCC}} \qquad (5.85)$$

If we apply the subadditivity of von Neumann entropy in the $S_1 \ldots S_r : R_1$ and $S_{r+1} \ldots S_N : R_2$ bipartitions for the first two terms of χ_{noisy}^{LOCC}, we have

$$\begin{aligned} S\Big(\sum_{\{x\}} p_{\{x\}} \xi_{\alpha}^{\{x\}}\Big) &\leq S\Big(\sum_{\{x\}} p_{\{x\}} \xi_{\bar{R}_k}^{\{x\}}\Big) + S\Big(\sum_{\{x\}} p_{\{x\}} \xi_{R_k}^{\{x\}}\Big) \\ &\leq \log_2 d_{\bar{R}_k} + S(\rho_{R_k}), \ k = 1, 2. \end{aligned} \qquad (5.86)$$

where $\alpha \in \mathcal{A}, \mathcal{B}$ and $\bar{R}_1 = S_1 \ldots S_r$, $\bar{R}_2 = S_{r+1} \ldots S_N$. The second inequality is due to the fact that the maximum von Neumann entropy of a d-dimensional quantum state is $\log d$ and no noise is acting on the receivers' subsystems. To deal with the third term in the R.H.S. of (5.85), let us assume that $U_{S_1...S_r}^{min}$ and $U_{S_{r+1}...S_N}^{min}$ are two unitary operators acting on subsystems $S_1 \ldots S_r$ and $S^{r+1} \ldots S_N$ of $\rho^{S_1...S_N R_1 R_2}$ respectively. Let us suppose that after passing through the noisy transmission channel $\Lambda_{S_1...S_N}$, those unitaries give the minimum von Neumann entropy among all the von Neumann entropies of $\xi_{\alpha}^{\{x\}}$, $\alpha \in \mathcal{A}, \mathcal{B}$, of the ensemble. Consider

$$\tilde{\rho}_{S_1...S_N R_1 R_2} = (U_{S_1...S_r}^{min} \otimes U_{S_{r+1}...S_N}^{min} \otimes I_{R_1 R_2}) \, \rho_{S_1...S_N R_1 R_2} \, (U_{S_1...S_r}^{min\dagger} \otimes U_{S_{r+1}...S_N}^{min\dagger} \otimes I_{R_1 R_2}), \quad (5.87)$$

and the corresponding reduced density matrices are given by

$$\begin{aligned} \zeta_{\mathcal{A}} &= \mathrm{tr}_{\mathcal{B}}\Big(\Lambda_{S_1...S_N}\big(\tilde{\rho}_{S_1...S_N R_1 R_2}\big)\Big), & (5.88) \\ \zeta_{\mathcal{B}} &= \mathrm{tr}_{\mathcal{A}}\Big(\Lambda_{S_1...S_N}\big(\tilde{\rho}_{S_1...S_N R_1 R_2}\big)\Big). & (5.89) \end{aligned}$$

Since entropy is concave, one should expect that the set, $\{S(\xi_{\alpha}^{\{x\}})\}$, of real numbers, which depend on the unitary operators $U_{S_1...S_r}^{x_1...x_r}$ or $U_{S_{r+1}...S_N}^{x_{r+1}...x_N}$ must have a minimum value, denoted by $S(\zeta_\alpha)$, which can be achieved by the unitary operators $U_{S_1...S_r}^{min}$ and $U_{S_{r+1}...S_N}^{min}$. Hence we have

$$S(\xi_{\alpha}^{\{x\}}) \geq S(\zeta_\alpha) \ \forall \ \alpha \qquad (5.90)$$

which implies

$$\sum_{\{x\}} p_{\{x\}} S(\xi_\alpha^{\{x\}}) \geq \sum_{\{x\}} p_{\{x\}} S(\zeta_\alpha) = S(\zeta_\alpha). \tag{5.91}$$

One should note here that $U_{S_1\dots S_r}^{min}$ and $U_{S_{r+1}\dots S_N}^{min}$ independently minimize $S(\zeta_\alpha)$ and $S(\zeta_\alpha)$ respectively. For example, to minimize the von Neumann entropy, of $\xi_\mathcal{A}^{\{x\}}$, we already traced out the other partition of $\rho^{S_1\dots S_N R_1 R_2}$ and $U_{S_{r+1}\dots S_N}^{min}$ and hence the minimization procedure in $\sum_{\{x\}} p_{\{x\}} \xi_\mathcal{A}^{\{x\}}$ depends only on $U_{S_1\dots S_r}^{min}$. Similar argument holds for $\sum_{\{x\}} p_{\{x\}} \xi_\mathcal{B}^{\{x\}}$ also. Thus we have the following theorem.

Theorem 1: *For arbitrary noisy channels between multiple senders and the two receivers, the LOCC dense coding capacity, involving two receivers, is bounded above by the quantity*

$$\mathcal{B}_{noisy}^{\text{LOCC}} \equiv \log d_{S_1\dots S_N} + S(\rho_{R_1}) + S(\rho_{R_2}) - \max_{\alpha \in \mathcal{A}, \mathcal{B}} S(\zeta_\alpha). \tag{5.92}$$

Here $\zeta_\mathcal{A}$ and $\zeta_\mathcal{B}$ are respectively given in Eqs. (5.88) and (5.89). The question remains whether there exists any noisy channel for which the upper bound can saturate the one given in Eq. (5.92). We will address the question in the next section.

5.4.2 LOCC-DC capacity under covariant noise

We will now deal with a class of noisy channels called the covariant channels, a CPTP map defined in Sec. 3.2.3. After encoding at the senders' side, we assume that the senders' parts are sent through the noisy covariant channel, $\Lambda_{S_1\dots S_N}^C$. After passing through the channel, the resulting state is given by

$$\Lambda_{S_1\dots S_N}^C(\rho_{S_1\dots S_N R_1 R_2}^{\{x\}}) = \sum_{\{i,j\}} \lambda_{\{i,j\}} \Lambda_{S_1\dots S_N}^C \left(\left(U_{S_1\dots S_r}^{x_1\dots x_r} \otimes U_{S_{r+1}\dots S_N}^{x_{r+1}\dots x_N}\right) |i_1\rangle\langle j_1|_{S_1\dots S_N} \left(U_{S_1\dots S_r}^{x_1\dots x_r\dagger} \otimes U_{S_{r+1}\dots S_N}^{x_{r+1}\dots x_N\dagger}\right) \right)$$
$$\otimes |i_2\rangle\langle j_2|_{R_1} \otimes |i_3\rangle\langle j_3|_{R_2}, \tag{5.93}$$

where we use the form of an arbitrary $(N+2)$-party quantum state given in Eq. (5.82), and, $\Lambda_{S_1\dots S_N}^C$ is a covariant noise acting on the state space of $S_1 \dots S_N$, satisfying Eq. (3.41), with the complete set of orthogonal unitary operators belonging to the linear operator space $\mathcal{L}(\mathcal{H}^{S_1\dots S_N})$. We are going to show that in this case, the maximization involved in the upper bound on the capacity depends on the fixed unitary operator and the Kraus operator of the channel $\Lambda_{S_1\dots S_N}^C$.

Let $\{V_{S_1\dots S_r}^j\}_{j=0}^{d_{S_1\dots S_r}^2-1} \in \mathcal{H}^{S_1\dots S_r}$, with probabilities $p_j = \frac{1}{d_{S_1\dots S_r}^2}$, and $\{V_{S_{r+1}\dots S_N}^{j'}\}_{j'=0}^{d_{S_{r+1}\dots S_N}^2-1} \in \mathcal{H}^{S_{r+1}\dots S_N}$, with probabilities $p_{j'} = \frac{1}{d_{S_{r+1}\dots S_N}^2}$, be two complete sets of orthogonal unitary operators satisfying Eqs. (3.8) and (3.9) which are the encoding operators of the senders $S_1 \dots S_r$, and $S_{r+1} \dots S_N$ respectively in their parts of the shared state. Without loss of generality, we assume that the first bunch of senders send their encoded parts to the receiver R_1, while the rest sends to the receiver R_2. Let

$$\rho_{S_1\dots S_N R_1 R_2}^{j,j'} = (V_{S_1\dots S_r}^j \otimes V_{S_{r+1}\dots S_N}^{j'} \otimes I_{R_1 R_2}) \rho_{S_1\dots S_N R_1 R_2} (V_{S_1\dots S_r}^{j\dagger} \otimes V_{S_{r+1}\dots S_N}^{j'\dagger} \otimes I_{R_1 R_2}). \tag{5.94}$$

One can always write $V_{S_1\dots S_r}^j = W_{S_1\dots S_r}^j U_{S_1\dots S_r}^1$ and $V_{S_{r+1}\dots S_N}^{j'} = W_{S_{r+1}\dots S_N}^{j'} U_{S_{r+1}\dots S_N}^2$, where $W_{S_1\dots S_r}^j \otimes W_{j'}^{S_{r+1}\dots S_N}$ acting on the senders state space, satisfying Eqs. (3.8) and (3.9), commutes with the covariant map, $\Lambda_{S_1\dots S_N}^C$, while $U_1^{S_1\dots S_r}$ and $U_2^{S_{r+1}\dots S_N}$ are fixed unitary operators. Therefore, after the encodings

and passing through the covariant channels, the ensemble states of the DC protocol are

$$\Lambda^C_{S_1...S_N}(\rho^{j,j'}_{S_1...S_N R_1 R_2}) = W^j_{S_1...S_r} \otimes W^{j'}_{S_{r+1}...S_N} \otimes \mathrm{I}_{R_1 R_2} \Lambda^C_{S_1...S_N} \left(U^1 \otimes U^2 \otimes \mathrm{I}^{R_1 R_2}\, \rho_{S_1...S_N R_1 R_2} \right.$$
$$\left. U^{1\dagger} \otimes U^{2\dagger} \otimes \mathrm{I}_{R_1 R_2} \right) W^{j\dagger}_{S_1...S_r} \otimes W^{j'\dagger}_{S_{r+1}...S_N} \otimes \mathrm{I}_{R_1 R_2} \quad (5.95)$$

where we have used the covariant condition, given in Eq. (3.41), on $\Lambda^C_{S_1...S_N}$. Let us denote $\Lambda^C_{S_1...S_N} \left(U^1 \otimes U^2 \otimes \mathrm{I}_{R_1 R_2}\, \rho^{S_1...S_N R_1 R_2}\, U^{1\dagger} \otimes U^{2\dagger} \otimes \mathrm{I}_{R_1 R_2} \right)$ as ρ^C. The reduced density matrix shared between $S_1 \ldots S_r$ and R_1 is given by

$$
\begin{aligned}
\xi^j_{\mathcal{A}} &= \mathrm{tr}_{\mathcal{B}} \left(\Lambda^C_{S_1...S_N R_1 R_2} \left(\rho^{j,j'}_{S_1...S_N R_1 R_2} \right) \right) \\
&= (W^j_{S_1...S_r} \otimes \mathrm{I}_{R_1}) \, \mathrm{tr}_{\mathcal{B}}(\rho^C) \, (W^{j\dagger}_{S_1...S_r} \otimes \mathrm{I}_{R_1}) \quad (5.96)
\end{aligned}
$$

where we have used the fact that any bipartite state, ρ_{AB}, satisfy

$$\mathrm{tr}_A \left((U_A \otimes U_B) \rho_{AB} (U^\dagger_A \otimes U^\dagger_B) \right) = U_B \mathrm{tr}_A(\rho_{AB}) U^\dagger_B. \quad (5.97)$$

The Hilbert-Schmidt decomposition of $\rho^1 = \mathrm{tr}_{\mathcal{B}}(\rho^C)$ on $\mathcal{H}^{\mathcal{A}}$ in the $S_1 \ldots S_r : R_1$ bipartition is given by

$$\rho^1 = \frac{\mathrm{I}_{S_1...S_r}}{d_{S_1...S_r}} \otimes \rho^1_{R_1} + \sum_{k=0}^{d^2_{S_1...S_r}-1} r_k\, \mu^k_{S_1...S_r} \otimes \mathrm{I}_{R_1} + \sum_{k=0}^{d^2_{S_1...S_r}-1} \sum_{l=0}^{d^2_{R_1}-1} t_{kl}\, \mu^k_{S_1...S_r} \otimes \eta^l_{R_1}, \quad (5.98)$$

where $\mathrm{tr}_{S_1...S_r} \rho^1 = \rho^1_{R_1}$, μ^k and η^l respectively are the generators of $SU(d_{S_1...S_r})$ and $SU(d_{R_1})$, and where $\mathrm{tr}\, \mu^k = \mathrm{tr}\, \eta^l = 0$ and r_k, t_{kl} are real numbers. Using this form, the reduced density matrix of the output state is given by

$$\sum_j p_j \xi^j_{\mathcal{A}} = \frac{1}{d^2_{S_1...S_r}} \sum_j \xi^j_{\mathcal{A}} = \frac{\mathrm{I}_{S_1...S_r}}{d_{S_1...S_r}} \otimes \rho^1_{R_1}, \quad (5.99)$$

where the second equality comes from the fact that $\sum_j W^j \mu^k_{S_1...S_r} W^{j\dagger} = d_{S_1...S_r} \mathrm{tr}\left(\mu^k_{S_1...S_r} \right) \mathrm{I} = 0$. Since neither the CPTP map nor the unitary operators are acting on the part of the shared state in the receiver's side, R_1, we have $\rho^1_{R_1} = \rho_{R_1}$. Finally, we have

$$S\left(\sum_j p_j \xi^j_{\mathcal{A}} \right) = \log d_{S_1...S_r} + S(\rho_{R_1}), \quad (5.100)$$

and similarly

$$S\left(\sum_{j'} p_{j'} \xi^{j'}_{\mathcal{B}} \right) = \log d_{S_{r+1}...S_N} + S(\rho_{R_2}). \quad (5.101)$$

Note that in the case of arbitrary noise, the above equalities were inequalities as given in (5.86).

Let us now consider the third term in the R.H.S. of (5.85). For example, if $\alpha = \mathcal{A}$, we have

$$\sum_j p_j S(\xi^j_{\mathcal{A}}) = S(\rho^1), \quad (5.102)$$

where we use Eq. (5.96) and the fact that unitary operations do not change the spectrum of any density matrix.

Interestingly, $S(\rho^1)$ does not depend on $W^j_{S_1...S_r}$ and $W^{j'}_{S_{r+1}...S_N}$. It only depends on the fixed unitary operators $U^1_{S_1...S_r}$ and the covariant channel, $\Lambda^C_{S_1...S_N}$. The remaining task is to minimize $S(\rho^1)$, by varying the $U^1_{S_1...S_r}$'s. Note that we have already shown that the first two terms in the R.H.S. of (5.85) are independent of maximizations. We now suppose that the minimum value of $S(\rho^1)$ is $S(\zeta_\mathcal{A})$ which will be achieved by setting $U^1_{min} = U^{min}_{S_1...S_r}$. Similarly, for $\alpha = \mathcal{B}$, we have that the optimal $\sum_{j'} p_{j'} S(\xi^{j'}_\mathcal{B})$ is $S(\zeta_\mathcal{B})$, for the optimal unitary $U^2_{min} = U^{min}_{S_{r+1}...S_N}$. Both the above inequalities can be achieved by using orthogonal unitary operators applied with equal probabilities. We have therefore proved the following proposition.

Proposition 1: *For any covariant noisy channel between an arbitrary number of senders and two receivers in a multiparty DC protocol, the capacity of LOCC-DC is bounded above by*

$$\chi^{\text{LOCC}}_{noisy} = \log d_{S_1...S_N} + S(\rho_{R_1}) + S(\rho_{R_2}) - \max_{\alpha \in \mathcal{A}:\mathcal{B}} S(\zeta_\alpha), \tag{5.103}$$

where ζ_α are given by

$$\zeta_\mathcal{A} = \text{tr}_\mathcal{B}\Big(\Lambda_{S_1...S_N}\big(\rho^C_{min}\big)\Big), \tag{5.104}$$

and

$$\zeta_\mathcal{B} = \text{tr}_\mathcal{A}\Big(\Lambda_{S_1...S_N}\big(\rho^C_{min}\big)\Big). \tag{5.105}$$

Here

$$\rho^C_{min} = \Lambda^C_{S_1...S_N}\big(U^1_{min} \otimes U^2_{min} \otimes \mathrm{I}_{R_1 R_2} \rho_{S_1...S_N R_1 R_2} U^{1\dagger}_{min} \otimes U^{2\dagger}_{min} \otimes \mathrm{I}_{R_1 R_2}\big). \tag{5.106}$$

Depending on the specific covariant channels, the minimum unitaries, U^1_{min} and U^2_{min} can be obtained. We find minimum unitaries for certain specific channels in the next section, where both covariant as well as non-covariant channels will be considered. In Theorem 1, we proved that for an arbitrary noisy channel, the upper bound on the LOCC-DC capacity as given in inequality (5.85) is further bounded above by the expression given in Eq. (5.92). Proposition 1 shows that for covariant noisy channels, the two upper bounds are equal.

5.5 Examples of noisy quantum channels

In Sec. 5.3.2, we have seen that the upper bound on the LOCC-DC capacity can be reached for a shared four-qubit GHZ state. Now in this section, we consider the effect of noise on the LOCC-DC capacity of the same state, in presence of different types of noisy channels. Undoubtedly, the GHZ state is one of the most important multiparty states, having maximal genuine multiparty entanglement [27, 28] as well as maximal violations of certain Bell inequalities [180]. Moreover, it has been successfully realized in laboratories by using several physical systems, including photons and ions [73, 81, 85]. Our aim is to find the minimum unitary operators U_{min} involved in $\zeta_\mathcal{A}$ and $\zeta_\mathcal{B}$ for different channels for this state, when the latter is used for LOCC-DC.

For a four-qubit GHZ state, given in Eq. (5.73), we are now going to find out the $U^{S_1}_{min} \otimes U^{S_2}_{min}$ that

minimizes $\max_{\alpha \in \mathcal{A}, \mathcal{B}} S(\zeta_\alpha)$, where

$$\zeta_\mathcal{A} = \text{tr}_{S_2 R_2}\Big(\Lambda_{S_1 S_2}\big(\tilde{\rho}_{S_1 S_2 R_1 R_2}\big)\Big), \tag{5.107}$$

$$\zeta_\mathcal{B} = \text{tr}_{S_1 R_1}\Big(\Lambda_{S_1 S_2}\big(\tilde{\rho}_{S_1 S_2 R_1 R_2}\big)\Big). \tag{5.108}$$

where $\tilde{\rho}_{S_1 S_2 R_1 R_2} = U_{min}^{S_1} \otimes U_{min}^{S_2} \otimes \text{I}_{R_1 R_2} |GHZ\rangle\langle GHZ|_{S_1 S_2 R_1 R_2} U_{min}^{S_1\dagger} \otimes U_{min}^{S_2\dagger} \otimes \text{I}^{R_1 R_2}$. Note that $\Lambda_{S_1 S_2}$ acts only on the senders' subsystems. We also denote $|GHZ\rangle\langle GHZ|$ as ρ_{GHZ}.

To find the form of $U_{min}^{S_1}$ and $U_{min}^{S_2}$, let us consider an arbitrary 2×2 unitary matrix, acting on a sender's subsystem, given by

$$U_{S_i} = \begin{pmatrix} a_i e^{i\theta_i^1} & \sqrt{1-a_i^2}\, e^{-i\theta_i^2} \\ -\sqrt{1-a_i^2}\, e^{i\theta_i^2} & a_i e^{-i\theta_i^1} \end{pmatrix}, \tag{5.109}$$

for $i = 1, 2$, where $0 \le a_i \le 1$ and $0 \le \theta_i^1, \theta_i^2 \le \frac{\pi}{2}$. To find $\zeta_\mathcal{A}$, we require only to manipulate the U_{S_1}, since U_{S_2} is not involved in $\zeta_\mathcal{A}$. A similar statement is true for $\zeta_\mathcal{B}$.

Let us now consider three classes of noisy channels, viz.

1. amplitude damping,

2. phase damping, and

3. pauli channels.

Note that only the Pauli channel is a covariant one. In all the examples considered in this section, we consider that there are local channels which act on the individual channels running from the two senders to the two receivers. Note that from the perspective of the actual realizations, this is the more reasonable scenario.

The fully correlated Pauli channel was considered in [23–26, 55], for calculating the DC capacity in case of a single receiver. A quantitative study for the general Pauli channel is given in Sec. 5.5.3 and 4.3.1.

5.5.1 Amplitude Damping Channel

The effect of amplitude damping channel on a single qubit system, is already explained in Eqs. (3.27) and (3.28) of Sec. (3.2.1). In the dense coding scenario, the senders, S_1 and S_2, send their parts of the four-qubit GHZ state through local amplitude damping channels, after encoding, and the corresponding output state is given by

$$\Lambda^{ADC}(\rho_{GHZ}^{S_1 S_2 R_1 R_2}) = \frac{1}{2}\Big\{ A_{\gamma_1}(|0\rangle\langle 0|) \otimes A_{\gamma_2}(|0\rangle\langle 0|) \otimes |00\rangle\langle 00| + A_{\gamma_1}(|0\rangle\langle 1|) \otimes A_{\gamma_2}(|0\rangle\langle 1|) \otimes |00\rangle\langle 11|$$
$$+ A_{\gamma_1}(|1\rangle\langle 0|) \otimes A_{\gamma_2}(|1\rangle\langle 0|) \otimes |11\rangle\langle 00| + A_{\gamma_1}(|1\rangle\langle 1|) \otimes A_{\gamma_2}(|1\rangle\langle 1|) \otimes |11\rangle\langle 11| \Big\}. \tag{5.110}$$

Here, we consider γ_1 and γ_2 are the damping parameters of the Kraus operators, as in Eq. (3.28), for the two independent amplitude damping channels corresponding to the two channels from the senders to their corresponding receivers. Due to the symmetry of the GHZ state, it can be seen that $S(\zeta_\mathcal{A})$, $\mathcal{A} = S_1 R_1$ takes the same functional form like $S(\zeta_\mathcal{B})$, $\mathcal{B} = S_2 R_2$, when γ_1 and γ_2 are interchanged.
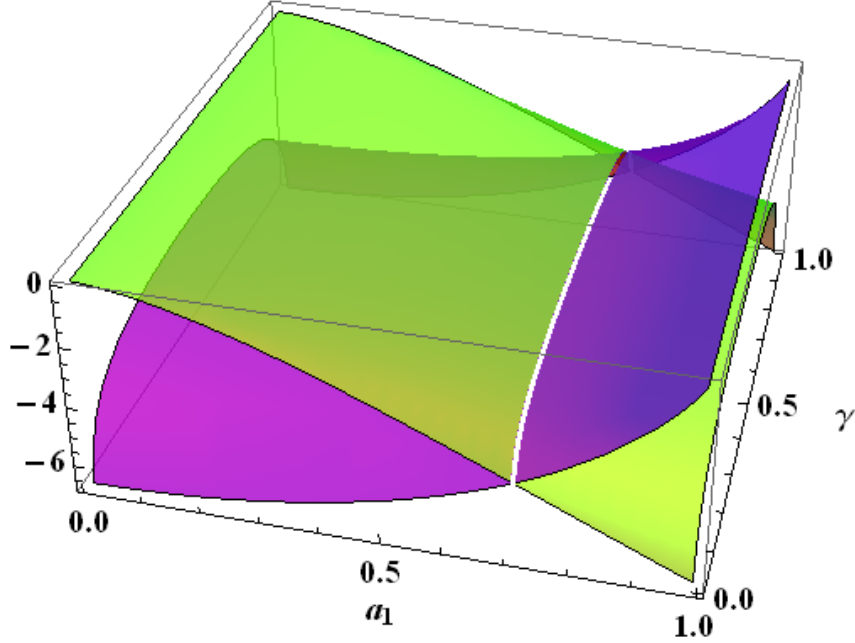
Figure 5.3: Plots of the quantities $\frac{a_1^2}{\sqrt{f(a_1)}} \log \frac{1-\sqrt{f(a_1)}}{1+\sqrt{f(a_1)}}$ and $\frac{1-a_1^2}{\sqrt{g(a_1)}} \log \frac{1-\sqrt{g(a_1)}}{1+\sqrt{g(a_1)}}$, which are respectively the left-hand- and right-hand-sides of Eq. (5.116), against a_1 and γ. The green (gray in print) surface represents the first while the purple (dark in print) one is for the second expression. The intersection line (white line) is $a_1 = \frac{1}{\sqrt{2}}$, for all γ. The base axes are dimensionless, while the vertical axis is in bits.

By using the unitary operator given in Eq. (5.109), one can find that the eigenvalues of ζ_A are

$$\lambda_1 = \frac{1}{4}\left(1 - \sqrt{f(a_1)}\right), \tag{5.111}$$

$$\lambda_2 = \frac{1}{4}\left(1 + \sqrt{f(a_1)}\right), \tag{5.112}$$

$$\lambda_3 = \frac{1}{4}\left(1 - \sqrt{g(a_1)}\right), \tag{5.113}$$

$$\lambda_4 = \frac{1}{4}\left(1 + \sqrt{g(a_1)}\right), \tag{5.114}$$

where $f(a) = 1 - 4\gamma_1(1-\gamma_1)a^4$ and $g(a) = 1 - 4\gamma_1(1-\gamma_1)(1-a^2)^2$. Note that the λ_i's are independent of the θ_1^j.

The minimization of $S(\zeta_A) = -\sum_i \lambda_i \log \lambda_i \equiv F(a_1)$, say, is obtained by calculating

$$\frac{dF(a_1)}{da_1} = 0, \tag{5.115}$$

which lead to the relation given by

$$\frac{a_1^2}{\sqrt{f(a_1)}} \log \frac{1-\sqrt{f(a_1)}}{1+\sqrt{f(a_1)}} = \frac{1-a_1^2}{\sqrt{g(a_1)}} \log \frac{1-\sqrt{g(a_1)}}{1+\sqrt{g(a_1)}}, \tag{5.116}$$

Solutions of the above equation give the extrema. In Fig. 5.3, we plot the L.H.S (left-hand-side, green surface) and R.H.S (purple surface) of Eq. (5.116). The intersection line, $a_1 = \frac{1}{\sqrt{2}}$, of these two surfaces

gives the solution of Eq. (5.116).To check whether it is minimum or not, we find

$$\frac{d^2 F(a_1)}{da_1^2}\Bigg|_{a_1=\frac{1}{\sqrt{2}}} = -\frac{\gamma(1-\gamma)}{\sqrt{(1-\gamma+\gamma^2)^3}}\left[\log\left(\frac{1-\sqrt{1-\gamma+\gamma^2}}{1+\sqrt{1-\gamma+\gamma^2}}\right) \times 4 + 8\sqrt{1-\gamma+\gamma^2}\right], \quad (5.117)$$

which is non-negative for all γ, at $a_1 = \frac{1}{\sqrt{2}}$, confirming the minimum. Therefore, the minimum of $S(\zeta_{\mathcal{A}})$ is obtained at $a_1 = \frac{1}{\sqrt{2}}$ and is given by $1 + H(\frac{1}{2}(1 - \sqrt{1 - \gamma_1 + \gamma_1^2}))$, where $h(x) = -x\log x - (1-x)\log(1-x)$ is the Shannon binary entropy given in Eq. (2.14). Similarly, one can obtain the minimum of $S(\zeta_{\mathcal{B}})$. Note that there is a single extremal point obtained and the corresponding function is continuous, which implies that the local minimum obtained here is actually the global minimum. Therefore, for the amplitude damping channel, if the input state is the GHZ state, then the upper bound on the LOCC-DC capacity is given by

$$\mathcal{B}_{ADC}^{LOCC} = 3 - \max_{x \in 1,2} h\left(\frac{1}{2}(1 - \sqrt{1 - \gamma_x + \gamma_x^2})\right). \quad (5.118)$$

Note that in a noiseless scenario, $C^{LOCC} = 3 = \mathcal{B}^{LOCC}$ for the shared GHZ state.

5.5.2 Phase Damping Channel

Phase damping channel, Λ^{PD}, transformed the state ρ, as

$$\Lambda^{PD}(\rho) = M_0 \rho M_0^\dagger + M_1 \rho M_1^\dagger + M_2 \rho M_2^\dagger, \quad (5.119)$$

where the M_i's are the Kraus operators given in Eq. (3.31), Here we again assume that the noise is local on the senders' parts. In this case, the eigenvalues of $\zeta_{\mathcal{A}}$ are given by

$$\lambda_1 = \lambda_2 = \frac{1}{4}\left(1 - \sqrt{f_P(a_1)}\right), \quad (5.120)$$

$$\lambda_3 = \lambda_4 = \frac{1}{4}\left(1 + \sqrt{f_P(a_1)}\right), \quad (5.121)$$

where $f_P(a) = 1 - 4a^2(1 - a^2)p(2 - p)$. Like in the case of the amplitude damping channel, the minimization does not depend on the θ_i's. It is also clear from the concavity of the von Neumann entropy that maximizing $f_P(a_1)$ is enough to minimize $S(\zeta^1)$. Note that when $f_P(a_1)$ increases, λ_1 and λ_2 go close to zero while λ_3 and λ_4 tend to 0.5, which in turn minimize $S(\zeta_{\mathcal{A}})$. The second term in $f_P(a_1)$ is a positive quantity, the maximum value of $f_P(a_1)$ is 1, when $a = 0$ or 1, and hence we have $S(\zeta^1) = 1$. Therefore, for the phase damping channel, we get

$$\mathcal{B}_{PD}^{\text{LOCC}} = 3, \quad (5.122)$$

which is independent of the parameters of the channel.

5.5.3 Pauli Noise: A Covariant Channel

Pauli noise is an example of a covariant noise, which satisfies the covariant condition, given in Eq. (3.41). When an arbitrary qubit state, is passed through the channel with Pauli noise [59, 178], the state is

transformed as

$$\Lambda^P(\rho) = \sum_{m=0}^{3} q_m \sigma_m \rho \sigma_m \tag{5.123}$$

where $\{\sigma_m\}$ are the well-known Pauli spin matrices along with the identity operators, i.e,

$$\sigma_1 = \sigma_x = \begin{pmatrix} 0 & 1 \\ 1 & 0 \end{pmatrix}, \quad \sigma_2 = \sigma_y = \begin{pmatrix} 0 & -i \\ i & 0 \end{pmatrix},$$

$$\sigma_3 = \sigma_z = \begin{pmatrix} 1 & 0 \\ 0 & -1 \end{pmatrix}, \quad \sigma_0 = I = \begin{pmatrix} 1 & 0 \\ 0 & 1 \end{pmatrix}.$$

Consider a four-qubit state, $\rho_{S_1 S_2 R_1 R_2}$, shared between two senders and two receivers. After passing through the Pauli channel, it transforms as

$$\Lambda^P_{S_1 S_2 R_1 R_2}(\rho_{S_1 S_2 R_1 R_2}) = \sum_{m,n=0}^{3} q_{mn} \left(\sigma_m^{S_1} \otimes \sigma_n^{S_2} \otimes I_{R_1 R_2}\right) \rho_{S_1 S_2 R_1 R_2} \left(\sigma_m^{S_1} \otimes \sigma_n^{S_2} \otimes I_{R_1 R_2}\right), \tag{5.124}$$

where $\sum_{mn} q_{mn} = 1$. Depending on the choice of q_{mn}, the channel can be correlated (see Sec. 4.3.1) or uncorrelated (see Sec. 4.3.2) . We deal with the fully-correlated Pauli channel, i.e, when $q_{mn} = q_m \delta_{mn}$. Eq. (5.124) in this case reduces to

$$\Lambda^{fP}_{S_1 S_2 R_1 R_2}(\rho_{S_1 S_2 R_1 R_2}) = \sum_{m=0}^{3} q_m \left(\sigma_m^{S_1} \otimes \sigma_m^{S_2} \otimes I_{R_1 R_2}\right) \rho_{S_1 S_2 R_1 R_2} \left(\sigma_m^{S_1} \otimes \sigma_m^{S_2} \otimes I_{R_1 R_2}\right). \tag{5.125}$$

Let us find out the U_{min} for the four-qubit GHZ state shared between two senders and two receivers, in the presence of the fully-correlated Pauli noise as in Eq. (5.125). From the symmetry of the GHZ state, we have $S(\zeta_\mathcal{A}) = S(\zeta_\mathcal{B})$. The eigenvalues of $\zeta_\mathcal{A}$ are given by

$$\lambda_1 = \lambda_2 = \frac{1}{4}\left(1 - \sqrt{g(a_1, \theta_1^1, \theta_1^2)}\right), \tag{5.126}$$

$$\lambda_3 = \lambda_4 = \frac{1}{4}\left(1 + \sqrt{g(a_1, \theta_1^1, \theta_1^2)}\right), \tag{5.127}$$

where

$$\tilde{g}(a, \theta) \equiv g(a, \theta_1, \theta_2) = (q_0 - q_1 - q_2 + q_3)^2 + f_1(a)[8q_1 q_2 + 8q_0 q_3 - 4(q_0 + q_3)(q_1 + q_2)$$
$$-4(q_1 - q_2)(q_0 - q_3)\cos(2(\theta_1 + \theta_2))] \tag{5.128}$$

and $f_1(a) = 2a^2(-1 + a^2)$. Arguing in the same way as in other cases, it is enough to maximize $\tilde{g}(a, \theta)$, with $\theta = \theta_1 + \theta_2$, in order to minimize $S(\zeta_\mathcal{A})$. To find the extremum of $\tilde{g}(a, \theta)$, we have to solve

$$\frac{\partial \tilde{g}(a, \theta)}{\partial a} = 0, \tag{5.129}$$

and

$$\frac{\partial \tilde{g}(a, \theta)}{\partial \theta} = 0, \tag{5.130}$$

which give the extremum value at $a = a_0 \equiv 0$ or $\frac{1}{\sqrt{2}}$, and $\theta = \theta_0 \equiv \frac{n\pi}{2}$, where $n \in \mathbb{Z}$. $\tilde{g}(a, \theta)$ is a function of the noise parameters $\{q_m\}$, and to find the extremum, without loss of generality, we assume an ordering of those parameters, i.e., we assume

$$q_0 \geq q_2 \geq q_1 \geq q_3. \tag{5.131}$$

And $\tilde{g}(a, \theta)$ is maximum, when

$$\left. \frac{\partial^2 \tilde{g}(a, \theta)}{\partial a^2} \right|_{a_0, \theta_0}, \ \left. \frac{\partial^2 \tilde{g}(a, \theta)}{\partial \theta^2} \right|_{a_0, \theta_0} < 0, \tag{5.132}$$

$$\left. \left(\frac{\partial^2 \tilde{g}}{\partial a \partial \theta} \right)^2 \right|_{a_0, \theta_0} < \left. \frac{\partial^2 \tilde{g}}{\partial a^2} \frac{\partial^2 \tilde{g}}{\partial \theta^2} \right|_{a_0, \theta_0}, \tag{5.133}$$

are satisfied simultaneously. For the above choice of q_m, the maximum value of $\sqrt{\tilde{g}(a, \theta)}$ is $|q_0 - q_1 + q_2 - q_3|$, which will be achieved, when $a = \frac{1}{\sqrt{2}}$ and θ is odd multiple of $\frac{\pi}{2}$, $S(\zeta_{\mathcal{A}}) = q(q_0 + q_2) + 1$, and $U_{min}^{S_1}$ is given by

$$U_{min}^{S_1} = \frac{1}{\sqrt{2}} \begin{pmatrix} e^{i\theta_1^1} & -ie^{i\theta_1^1} \\ -ie^{-i\theta_1^1} & e^{-i\theta_1^1} \end{pmatrix}.$$

If we take another ordering of $\{q_m\}$, for e.g., $q_1 \geq q_2 \geq q_0 \geq q_3$, we have $S(\zeta^1) = H(q_1 + q_2) + 1$, and the unitary operator, in this case, is given by

$$U_{min}^{S_1} = \begin{pmatrix} 0 & e^{i\theta_1^1} \\ e^{-i\theta_1^1} & 0 \end{pmatrix}.$$

The above two cases indicate that the minimum entropy depends on the ordering of q_m, involved in the channel with Pauli noise. In general, when the shared state is the GHZ state, the capacity χ_{Pauli}^{LOCC} is bounded above by $3 - h(b_1 + b_2)$, where $\{b_m\}_{m=1}^4$, is an arrangement of $\{q_m\}$ in descending order.

Instead of fully correlated Pauli noise, if we now assume that the q_{mn} is arbitrary, the strategy of fully correlated Pauli noise can also be applied in this case. Suppose, $p_m = \sum_n q_{mn}$ and $r_n = \sum_m q_{mn}$. Then the capacity is bounded above as

$$\chi_{Pauli}^{LOCC} = 3 - \max\{h(b_1 + b_2), h(c_1 + c_2)\}, \tag{5.134}$$

where $\{b_m\}_{m=1}^4$ and $\{c_n\}_{n=1}^4$ are the sets $\{p_m\}$ and $\{r_n\}$ in descending order.

5.6   Connecting Multipartite Entanglement with LOCC-DC

In this section, we establish a relation between the capacities of LOCC-DC of four-qubit pure states with two senders and two receivers and their genuine multiparty entanglement content in terms of GGM ($\mathcal{E}$). The protocol considered here is due to collective involvement/contribution of all the parties involved, i.e., senders and receivers. This led us to establish a connection between the capacity of such dense coding protocol to a genuine multiparty entanglement present in the system. Specifically, we will estimate the ordering of the GGMs between the generalized GHZ state and an arbitrary four-qubit pure state, when both

of them have equal LOCC dense coding capacities. Such estimation will shed light on the bridge between multiparty entanglement as quantified by the generalized geometric measure and multiport capacity as quantified by the LOCC-DC capacity.

Note that although the exact capacity of dense coding by LOCC for arbitrary multiparty pure state is not known, it was shown [21, 22] that the exact capacity is 3 for the four-qubit GHZ state, given in Eq. (5.73). In case of the gGHZ state, shared between two senders and two receivers, given in Eq. (4.1), is

$$|gGHZ\rangle_{S_1S_2R_1R_2} = (\sqrt{\alpha}|0000\rangle + \sqrt{1-\alpha^2}e^{i\phi}|1111\rangle)_{S_1S_2R_1R_2}, \tag{5.135}$$

the capacity of LOCC-DC is bounded above by

$$\mathcal{B}^{LOCC}(|gGHZ\rangle) = 2 + h(\alpha). \tag{5.136}$$

From the intuition obtained from bipartite non-maximally entangled states, we conjecture here that the capacity of LOCC-DC for the gGHZ state saturates the upper bound, $\mathcal{B}^{LOCC}$. With this assumption, we have the following result.

Result: *Consider a multiparty DC protocol where there are two senders and two receivers, and where the channels from the senders to the receivers are noiseless. In this case if a four-qubit gGHZ state and an arbitrary four-qubit pure state have equal capacities of LOCC-DC, then the gGHZ state possesses less genuine multiparty entanglement than that of the arbitrary state i.e, we have*

$$\mathcal{E}(|\psi\rangle) \geq \mathcal{E}(|gGHZ\rangle), \tag{5.137}$$

if (i) $S(\rho^{R_1}) \leq S(\rho^{S_1R_1})$, i.e., the reduced state, $\rho^{S_1R_1}$, has more disorder than its local subsystem, ρ^{R_1}, and (ii) the maximum eigenvalue required for GGM is obtained from the density matrix, ρ^{R_2}. Similar conditions can be obtained by interchanging S_1 and R_1 with S_2 and R_2 respectively.

`Proof:` As argued above, it is plausible that for the $gGHZ$ state,

$$C_{gGHZ}^{LOCC} = 2 + h(\alpha). \tag{5.138}$$

For an arbitrary four-qubit pure state, $|\psi\rangle$, shared between the senders S_1, S_2 and receivers R_1, R_2, the upper bound of the capacity of LOCC-DC is given by

$$C_\psi^{LOCC} \leq \mathcal{B}^{LOCC}(|\psi\rangle) = 2 + S(\rho_{R_1}) + S(\rho_{R_2}) - S(\rho_{S_1R_1}), \tag{5.139}$$

where $S(\rho_{R_i}), i = 1, 2$, and $S(\rho_{S_1R_1})$ are the reduced density matrices of $|\psi\rangle$.

Note that for pure state $S(\rho_{S_1R_1}) = S(\rho_{S_2R_2})$. Let us now assume that the LOCC-DC capacities for $|\psi\rangle$ and the gGHZ state are equal, so that

$$\begin{aligned} C_{gGHZ}^{LOCC} &= 2 + h(\alpha) = C_\psi^{LOCC} \\ &\leq 2 + S(\rho_{R_1}) + S(\rho_{R_2}) - S(\rho_{S_1R_1}), \end{aligned} \tag{5.140}$$

which implies $h(\alpha) \leq S(\rho_{R_2})$, provided $S(\rho_{R_1}) \leq S(\rho_{S_1R_1})$. This implies that

$$\alpha \geq \lambda_{R_2}, \tag{5.141}$$

where λ_{R_2} is the maximum eigenvalue of ρ_{R_2}.

The GGMs of the gGHZ and the arbitrary four-qubit pure state are respectively given by

$$\mathcal{E}(|gGHZ\rangle) = 1 - \alpha, \tag{5.142}$$

$$\mathcal{E}(|\psi\rangle) = 1 - \lambda_{R_2}, \tag{5.143}$$

provided that λ_{R_2} is the maximum eigenvalue among all the eigenvalues of its single site and two site density matrices. Then, by using (5.141), we get

$$\mathcal{E}(|\psi\rangle) \geq \mathcal{E}(|gGHZ\rangle).$$

Hence the results. ∎

While the above Result has been stated for two senders and two receivers, simple changes in the premises render its validity for the case of multiple senders and two receivers.

One should stress here that if the DC protocol involves several senders and a single receiver, it has recently been shown that the gGHZ state requires to be more multiparty entangled than an arbitrary four-qubit state if they both want to have equal DC capacities in a noiseless scenario [55] (see Sec. 4.1). For both uncorrelated and correlated noise models, the relative abilities of the general quantum state and the generalized GHZ state to transfer classical information in a dense coding protocol can get inverted by administering a sufficient amount of noise. These results led us to believe that the generalized GHZ state may have a special status also in the case of more than one receiver. Here we show that changing the number of receivers from one to two can alter the hierarchy with respect to the multiparty entanglement and the multiparty DC capacity among four-qubit states and the gGHZ state under the assumption that the LOCC-DC capacity saturates the bound, $\mathcal{B}^{LOCC}$, given in Eq. (5.136).

To visualize the above Result, and to check the relevance of the imposed conditions, we randomly generate 10^5 arbitrary four-qubit pure states, Haar-uniformly on that space. In Fig. 5.4, the GGM ($\mathcal{E}$) is plotted against the upper bound, $\mathcal{B}^{\text{LOCC}}$, of the LOCC-DC capacity for the generated states. The red curved line represents the gGHZ states. Among the randomly generated states, 47.6% states (blue triangles) satisfy both the conditions (i) and (ii) of Result. Interestingly however, 49% states (orange squares) violate at least one of the above conditions, and yet reside above the gGHZ line i.e., satisfy the conclusion of Result. And only 3.4% of the total violate the conclusion of Result (green circles). Numerical simulations show that there exists states which satisfy Eq. (5.137), even after violating one of the assumptions in Result, indicating that Result is probably true even when one relaxes the two proposed conditions.

The topology of the quantum communication protocol with two receivers may hint us to consider two natural bipartitions of the N+2 parties. See Fig. 5.2. Let us call them the horizontal and vertical partitions. The horizontal partition has the parties $\mathcal{A}$ on one side and $\mathcal{B}$ on the other. On the other hand, the vertical partition has the senders on one side and the receivers on another side. We then define a multiparty entanglement measure for an arbitrary pure (N+2)-party quantum state, $|\psi\rangle$, as

$$\mathcal{E}^{HV}(|\psi\rangle) = 1 - \max |\langle \chi | \psi \rangle|^2, \tag{5.144}$$
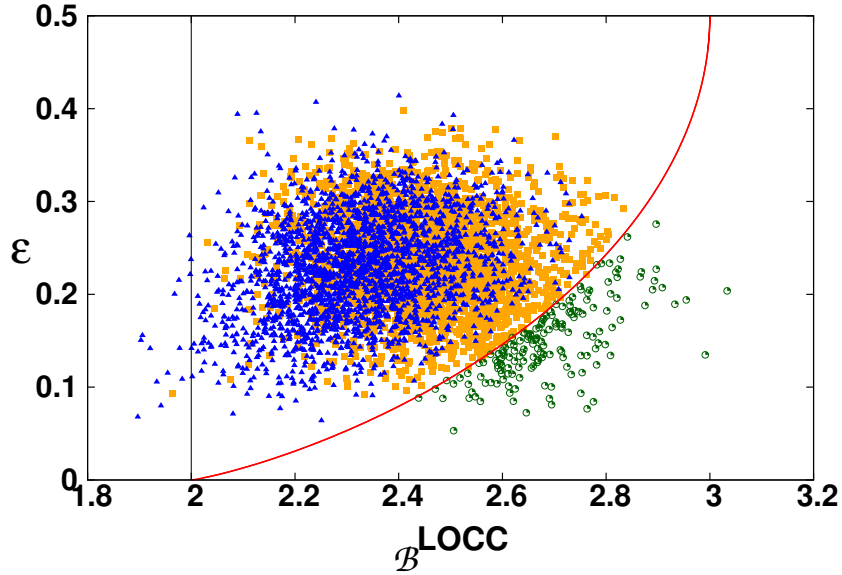
Figure 5.4: Noiseless case: How does a general four-qubit pure state compare with the gGHZ states? We randomly generate 10^5 four-qubit pure states uniformly with respect to the corresponding Haar measure, and their GGM is plotted as the abscissa while $\mathcal{B}^{\text{LOCC}}$ is plotted as the ordinate. The red curved line represents the gGHZ states. Among the states generated randomly, 47.6% (blue triangles) satisfy both the conditions in Result, 49% (orange squares) violate either of the conditions, but still falls above the gGHZ line. Green circles represent 3.4% states which violate the conclusion of Result. The line at abscissa equals to 2 corresponds to the capacity achievable without prior shared entanglement. The vertical axis is dimensionless, while the horizontal one is in bits.

where the maximization is over all $|\chi\rangle$ that are product across either the horizontal or the vertical partition. Compare this definition with that in Eq. (2.39). This quantity can be expressed in terms of Schmidt coefficients, just like Eq. (2.39) and can be reduced to Eq. (2.48). In particular, for four-party pure states (N=2), the reduced form is given by

$$\mathcal{E}^{HV}(|\psi_{1234}\rangle) = 1 - \max[e_1, e_2], \tag{5.145}$$

where e_1 and e_2 respectively denote the maximal Schmidt coefficients in the $S_1 R_1 : S_2 R_2$ and the $S_1 S_2 : R_1 R_2$ splits. It may be noted that just like the GGM, the quantity $\mathcal{E}^{HV}$ is an LOCC monotone, that is, it is monotonically non-increasing under local quantum operations at the N+2 sites and classical communication between them. It is therefore a valid multiparty entanglement measure. However, unlike the GGM, it is not a measure of genuine multiparty entanglement. From the topology of the quantum communication protocol under study, it may seem that $\mathcal{E}^{HV}$ will be of relevance in quantifying and understanding the capacity of the information transfer here. Evidently, $\mathcal{E} \leq \mathcal{E}^{HV}$. We have created a scatter diagram as in Fig. 5.4, but with the $\mathcal{E}$ axis replaced by $\mathcal{E}^{HV}$ (see Fig. 5.5). The new measure varies in [0,3/4] for generic states, while its value for the gGHZ states varies in [0,1/2]. We find that among randomly generated 4-qubit states, 1.2% states (orange squares) have $\mathcal{E}^{HV} > 0.5$ and 0.7% of states (green circles) fall below the gGHZ line. The result indicates that even if one modifies the entanglement measure motivated by the DC protocol, we can again find that the gGHZ state has a special status in the sense that a large majority of the points in the scatter diagram falls above the gGHZ line. Note here that with this modification, we are able to reduce the percentage of states that are below the gGHZ line.
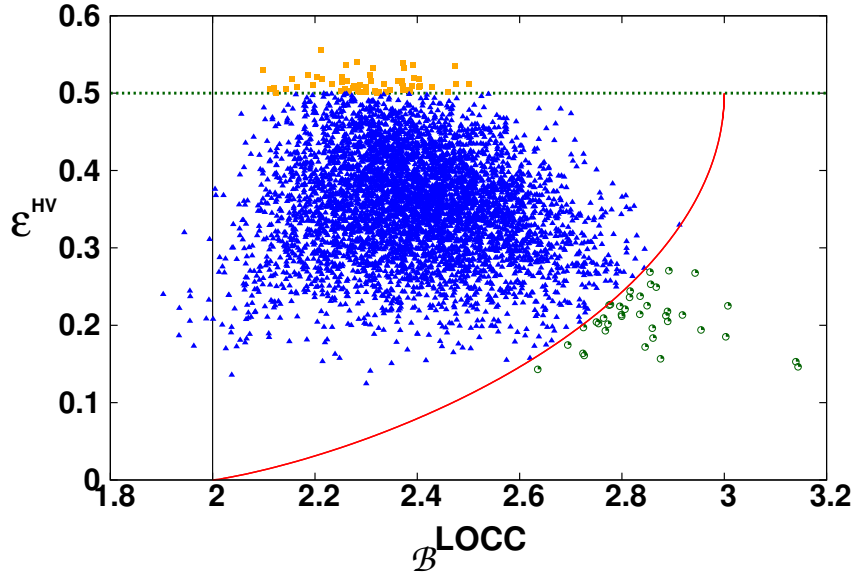
Figure 5.5: Noiseless case: Comparison between arbitrary four-qubit pure states and the gGHZ states, with constrained GGM. We randomly generate 10^5 four-qubit pure states uniformly with respect to the corresponding Haar measure, and their HV-GGM ($\mathcal{E}^{HV}$) is plotted as the abscissa while $\mathcal{B}^{LOCC}$ is plotted as the ordinate. The red curved line represents the gGHZ states. Among the states generated randomly, 0.7% (green circles) states fall below the gGHZ line. Orange squares represent those state whose $\mathcal{E}^{HV}$ is greater than 0.5 (above the horizontal line) – they are very few in number, and constitute only 1.2% of total generated random states. The line at abscissa equals to 2 corresponds to the capacity achievable without prior shared entanglement. The vertical axis is dimensionless, while the horizontal one is in bits.

5.6.1 Connection of multiparty entanglement with noisy LOCC-DC

We now try to find a relation between the GGM and the maximal classical information transfer by LOCC, as quantified by χ_{noisy}^{LOCC} given in Eq. (5.103), under fully correlated Pauli noisy channel. We randomly generate 10^5 four-qubit pure states Haar-uniformly on the state space, and calculate the χ_{noisy}^{LOCC}, for the states under Pauli noise. We do the same for the generalized GHZ states. We choose two sets of noise parameters: (i) parameters that lead to a state which is close to the state of the noiseless case, and we refer it as the low noise case, and (ii) parameters which take the state close to the maximally mixed state, and we refer to it as the high noise case. Our aim is to connect the LOCC-DC capacity in the presence of Pauli noise, and multiparty entanglement, as quantified by the GGM, of the initially shared state.

For the low noise case, we choose the noise parameters as $q_0 = 0.93$, $q_1 = 0.01$, $q_2 = 0.02$, and $q_3 = 0.04$, and plot the GGM against χ_{noisy}^{LOCC}. For the high noise case, we choose $q_0 = 0.485$, $q_1 = 0.015$, $q_2 = 0.015$, $q_3 = 0.485$. The plots are presented in Fig. 5.6. In the high-noise case, the upper bound on the LOCC-DC capacity, as expected, suggests that most of the states have capacities which are lower than the capacity achieved by the classical protocol. In the noiseless as well as the low noise scenarios, we see that there exists a set of states which is not bounded by the gGHZ line, while such states are almost absent in the presence of higher amounts of noise (see Fig. 5.6). It suggests that the gGHZ state is more robust to noise among four-qubit pure states.

For the case of multiple senders and a single receiver, the gGHZ state changes its role as one increases noise in the channel that carries the encoded quantum systems from the senders to the receiver [55]. Precisely, the gGHZ state requires less multiparty entanglement (as quantified by GGM) than a generic
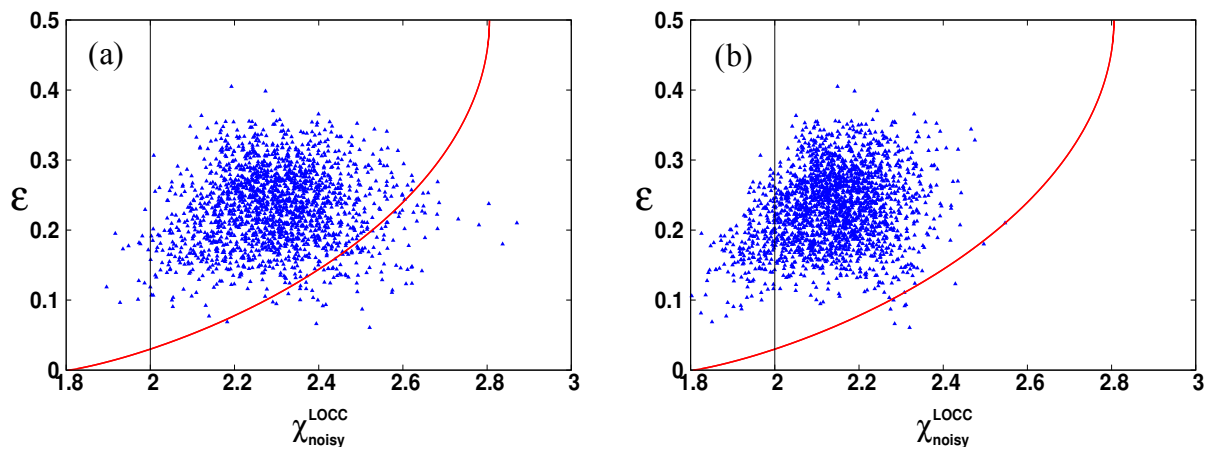
Figure 5.6: Fully correlated Pauli noise: The gGHZ states are again better than a significant fraction of states. We plot the GGM as the ordinate and χ_{noisy}^{LOCC} as the abscissa for 10^5 randomly generated four-qubit pure states uniformly with respect to the corresponding Haar measure for low (figure (a)) and high (figure (b)) full correlated Pauli noise. In figure (a), $q_0 = 0.93, q_1 = 0.01, q_2 = 0.02, q_3 = 0.04$, while in figure (b), we choose $q_0 = 0.485, q_1 = 0.015, q_2 = 0.015, q_3 = 0.485$. In the presence of high noise, almost all states are bounded by the four-qubit gGHZ states (red curved line). A significant fraction of the generated states lie above the gGHZ line even for low noise. It indicates that the gGHZ state is more robust against noise as compared to an arbitrary four-qubit pure state. The lines at abscissa equals to 2 correspond to the capacity achievable without prior shared entanglement. The vertical axis is dimensionless, while the horizontal one is in bits.

state to be equal in dense coding capacity with the generic state, if the channels are noisy. The opposite is true when the channels are noiseless. Here we see that if there are two receivers in the protocol, there is no such role reversal. The gGHZ state requires less multiparty entanglement than a generic state to have the same LOCC dense coding capacity as the generic state. Note that this statement in under the assumption that the upper bounds on the LOCC-DC capacities faithfully mirror the qualitative features of the actual capacities.

5.7 In closing

The dense coding protocol is a quantum communication scheme which demonstrates that the classical information can be transferred via quantum states more efficiently than any classical protocol. The "Holevo bound" is applied to obtain the capacities, when there is a single sender and a single receiver as well as when there are multiple senders and a single receiver. Capacities are known for both noiseless and for certain noisy channels. However, realistic scenarios of a communication protocol should involve multiple senders and multiple receivers, when the receivers can not make any global quantum operations. The difficulty in such generalization is due to the nonexistence, hitherto, of a Holevo-like bound in the multipartite decoding process in the many-receivers scenario in the case of noisy channels. In this chapter, we discuss the problem in getting the distributed dense coding capacity or LOCC-DC capacity involving multiple senders and two receivers, and observe that there is an upper bound on the LOCC-DC which is achievable for four-qubit GHZ state. We address the problem of estimating the dense coding capacity, in the same situation when the transmission channel used by the senders to send their encoded part to the receivers is noisy. In particular, we find an upper bound on the classical capacity of the multipartite

quantum channel, when the senders and receivers share a multiparty quantum state and noisy channels, and the receivers are allowed to perform only local quantum operations and classical communication. A compact form of the upper bound on the capacity is obtained when the noisy channels are covariant. When the four-party shared state is the GHZ state, several paradigmatic noisy channels are considered and the upper bounds on the capacities are determined. Finally, we connect the capacity of dense coding with a multiparty entanglement measure, both in the noiseless and noisy scenarios.

The results of this Chapter are based on the following paper:

1. *Distributed quantum dense coding with two receivers in noisy environments*, **Tamoghna Das**, R. Prabhu, Aditi Sen De, Ujjwal Sen, Phys. Rev. A **92**, 052330 (2015).

Photon Subtracted State is More Entangled than Photon Added State

In the earlier chapters, we have talked about the quantum communication protocol involving several senders and single as well as two receivers in both noiseless and noisy scenarios with the help of shared quantum state. We connect the multiparty entanglement of the shared state with multiparty DC capacity and LOCC-DC capacity for noiseless and noisy scenarios and found that entanglement content of the shared state plays an important role in realizing those protocols. But to realize this quantum communication protocol in the laboratory for finite dimensional system, for example, in the qubit systems, there exists some difficulties [32–35].

One of the physical systems in which quantum information tasks have been realized in the laboratory is the class of continuous variable (CV) systems. Historically, the notion of the quantum correlated state of two particles in CV systems first arrived in the seminal paper of Einstein, Podolosky, and Rosen in 1935 [62]. In recent years, several communications schemes like teleportation [5] and classical information transfer by quantum channels [4], have extensively been investigated both theoretically and experimentally, in CV systems, especially in Gaussian states [36, 38, 39, 41, 60]. However, it has been discovered that there are several protocols which can not be implemented using Gaussian states with Gaussian operations. Examples include entanglement distillation [42], measurement-based universal quantum computation [44], teleportation [46], and quantum error correction [48]. Non-Gaussian states are increasingly being found to be important in several applications. They have also been realized in the laboratory [49, 50].

An important method to make such states is by adding and subtracting photons, from the Gaussian states. The multimode squeezed vacuum state [51–54] is good example of entangled Gaussian state as its quasiprobability distribution, the Wigner function [186], is a Gaussian function of its quadrature variables [187, 188]. Starting from an entangled two-mode squeezed vacuum (TMSV) state, whose Wigner function [186] is always positive, it was shown that photon addition can generate a negative dip of the Wigner function in the phase space [189] and hence can deviate from being a Gaussian state. In case of the two-mode squeezed vacuum (TMSV) state as input state, both the entanglement and fidelity of teleportation can be increased by adding and subtracting photons to (from) one or two modes [51–54]. For such experiments, see [190–192]. Moreover, the entanglement content of the photon-added state obtained

from the TMSV state was shown to be always higher than that of the photon-subtracted state [51–54].

Investigations of the squeezed vacuum state with respect to photon addition and subtraction are usually restricted to the two-mode case, even though the importance of multimode CV system is unquestionable [193–203]. Moreover, it is believed that multimode entangled states can be a resource to build quantum communication network, both for transferring classical as well as quantum information between several senders and several receivers [202]. In this paper, we consider the four-mode squeezed vacuum (FMSV) state as input, and deGaussify it by adding and subtracting photons in different modes.

We evaluate entanglement between different modes in all possible bipartitions and compare the results of the photon-added state with the subtracted ones. We call a mode as "player" mode when we analyse the effect on entanglement, by varying the number of photons added or subtracted in that mode. There could be several such player modes. The remaining modes, in which either no photons or a fixed number of photons are added or subtracted, are referred to as the "spectator" modes. At last, we will also analyze the bipartite entanglement of the output two party state which can be obtained by discarding either two player modes or two spectator modes, and study the distance-based measure of non-Gaussianity of the output four-mode state under the effect of photon addition and subtraction.

6.1 N-mode squeezed vacuum state

In this section, we discuss the N-mode squeezed vacuum state (NMSV), specifically the two-mode and four-mode squeezed vacuum states, and a state obtained after adding (subtracting) an arbitrary number of photons at the ith mode. These states are examples of entangled states in continuous variables which can be used in various quantum information tasks. To define such states, let us first denote the bosonic creation and annihilation operators at the mode i, as $\hat{a}_i^\dagger$ and $\hat{a}_i$ respectively, which satisfy the bosonic commutation relations, $[\hat{a}_i, \hat{a}_j^\dagger] = \delta_{ij}$, and $[\hat{a}_i, \hat{a}_j] = 0$, $[\hat{a}_i^\dagger, \hat{a}_j^\dagger] = 0$. By using bosonic operators, an N-mode squeezed vacuum state is given by

$$|\psi_N\rangle = \mathcal{S}(\epsilon)|0_1 0_2 \ldots 0_N\rangle, \tag{6.1}$$

where $|0_1 0_2 \ldots 0_N\rangle$ is the N-mode vacuum state and $\mathcal{S}(\epsilon)$ is squeezing operator, which is defined as

$$\mathcal{S}(\epsilon) = \exp\left(\frac{1}{2}\sum_{i=1}^{N}\left(\epsilon^* \hat{a}_i \hat{a}_{i+1} - \epsilon \hat{a}_i^\dagger \hat{a}_{i+1}^\dagger\right)\right), \tag{6.2}$$

where $\hat{a}_{N+1} = \hat{a}_1$ and $\epsilon = re^{i\theta}$ is the squeezing parameter. The above state in Eq. (6.1) is called a squeezed state. To show that, let us consider the variances of N-mode quadrature operators ΔX_1, and ΔX_2, given by

$$\Delta X_1 = \sqrt{\langle X_1^2\rangle - \langle X_1\rangle^2}, \tag{6.3}$$

$$\Delta X_2 = \sqrt{\langle X_1^2\rangle - \langle X_2\rangle^2}, \tag{6.4}$$

where

$$X_1 = \sum_j \hat{q}_j = \frac{1}{2\sqrt{N}}\sum_{j=1}^{N}(\hat{a}_j^\dagger + \hat{a}_j), \tag{6.5}$$

$$X_2 = \sum_j \hat{p}_j = \frac{1}{2\sqrt{N}} \sum_{j=1}^{N} -i(\hat{a}_j^\dagger - \hat{a}_j), \tag{6.6}$$

with the position and momentum operators for each mode being

$$\hat{q}_j = (\hat{a}_j^\dagger + \hat{a}_j), \tag{6.7}$$

$$\hat{p}_j = -i(\hat{a}_j^\dagger - \hat{a}_j). \tag{6.8}$$

Here the average is taken over the NMSV state. To obtain the variances of ΔX_1 and ΔX_2, we need to obtain the following relations:

$$
\begin{aligned}
\mathcal{S}(\epsilon)^\dagger \sum_j \hat{a}_j \mathcal{S}(\epsilon) &= e^{\left(-\frac{1}{2}\sum_{i=1}^{N}\left(\epsilon^* \hat{a}_i \hat{a}_{i+1} - \epsilon \hat{a}_i^\dagger \hat{a}_{i+1}^\dagger\right)\right)} \sum_{j=1}^{N} \hat{a}_j e^{\left(\frac{1}{2}\sum_{i=1}^{N}\left(\epsilon^* \hat{a}_i \hat{a}_{i+1} - \epsilon \hat{a}_i^\dagger \hat{a}_{i+1}^\dagger\right)\right)} \\
&= \sum_{j=1}^{N} \hat{a}_j - \epsilon \hat{a}_j^\dagger + \frac{|\epsilon|^2}{2!} \hat{a}_j - \frac{\epsilon |\epsilon|^2}{3!} \hat{a}_j^\dagger + \cdots \\
&= \sum_{j=1}^{N} \hat{a}_j \cosh r - e^{i\theta} \hat{a}_j^\dagger \sinh r, \tag{6.9}
\end{aligned}
$$

where we use the Baker-Campbell-Hausdorff formula of any two operators $\hat{A}$ and $\hat{B}$, given by

$$e^{-\hat{A}} \hat{B} e^{\hat{A}} = \hat{B} - [\hat{A}, \hat{B}] + \frac{1}{2!}[\hat{A}, [\hat{A}, \hat{B}]] - \frac{1}{3!}[\hat{A}, [\hat{A}, [\hat{A}, \hat{B}]]] + \cdots . \tag{6.10}$$

Similarly, we have

$$\mathcal{S}(\epsilon)^\dagger \sum_{j=1}^{N} \hat{a}_j^\dagger \mathcal{S}(\epsilon) = \sum_{j=1}^{N} \hat{a}_j^\dagger \cosh r - e^{-i\theta} \hat{a}_j \sinh r. \tag{6.11}$$

Now putting these expressions in the expectation values of X_1^2 and X_1, we have,

$$
\begin{aligned}
\langle X_1^2 \rangle &= \frac{1}{4N} \langle 0_1 0_2 \ldots 0_N | \mathcal{S}(\epsilon)^\dagger \left(\sum_{j=1}^{N} (\hat{a}_j^\dagger + \hat{a}_j) \right)^2 \mathcal{S}(\epsilon) | 0_1 0_2 \ldots 0_N \rangle, \\
&= \frac{1}{4N} \langle 0_1 0_2 \ldots 0_N | \sum_{jk}^{N} \left(\hat{a}_j \hat{a}_k^\dagger + \hat{a}_k^\dagger \hat{a}_j \right) | 0_1 0_2 \ldots 0_N \rangle | \cosh r - e^{i\theta} \sinh r |^2, \\
&= \frac{1}{4} \left(e^{2r} \sin^2 \frac{\theta}{2} + e^{-2r} \cos^2 \frac{\theta}{2} \right), \tag{6.12}
\end{aligned}
$$

and

$$\langle X_1 \rangle = \frac{1}{2\sqrt{N}} \langle 0_1 0_2 \ldots 0_N | \mathcal{S}(\epsilon)^\dagger \sum_{j=1}^{N} (\hat{a}_j^\dagger + \hat{a}_j) \mathcal{S}(\epsilon) | 0_1 0_2 \ldots 0_N \rangle = 0. \tag{6.13}$$

We finally get

$$\Delta X_1^2 = \frac{1}{4} \left(e^{2r} \sin^2 \frac{\theta}{2} + e^{-2r} \cos^2 \frac{\theta}{2} \right). \tag{6.14}$$

Similarly, we have

$$\Delta X_2^2 = \frac{1}{4}\left(e^{-2r}\sin^2\frac{\theta}{2} + e^{2r}\cos^2\frac{\theta}{2}\right). \tag{6.15}$$

Thus for $\theta = 0$ or π, we have $\Delta X_1 \Delta X_2 = \frac{1}{4}$. However, for any one of the $i = 1, 2$, $\Delta X_1 = \frac{1}{2}e^{-r} \leq \frac{1}{2}$, while $\Delta X_2 = \frac{1}{2}e^r \geq \frac{1}{2}$ and vice-versa. This guarantees that the state, given in Eq. (6.1) is a squeezed state. We assume $\theta = 0$ throughout this chapter.

6.1.1   Another form of NMSV state

In this section, we will try to find out another form of the NMSV state, so that we can express the NMSV state in terms of the photon number states or in the Fock number basis $|n_j\rangle$ of the jth mode, where

$$\hat{a}_j|n_j\rangle = \sqrt{n_j}|n_j - 1\rangle, \tag{6.16}$$
$$\hat{a}_j^\dagger|n_j\rangle = \sqrt{n_j + 1}|n_j + 1\rangle. \tag{6.17}$$

To do this, we need some tools. Let us first calculate

$$
\begin{aligned}
\mathcal{S}(r)^\dagger \hat{a}_j \mathcal{S}(r) &= \hat{a}_j - \Big[\underbrace{\frac{1}{2}\sum_{i=1}^{N}\left(r\hat{a}_i\hat{a}_{i+1} - r\hat{a}_i^\dagger\hat{a}_{i+1}^\dagger\right)}_{\hat{A}}, \hat{a}_j\Big] + \frac{1}{2!}[\hat{A},[\hat{A},\hat{a}_j]] - \frac{1}{3!}[\hat{A},[\hat{A},[\hat{A},\hat{a}_j]]] + \cdots \\
&= \hat{a}_j - r\sum_{k=1}^{N}Q_{jk}\hat{a}_k^\dagger + \frac{1}{2!}r^2\sum_{k=1}^{N}Q_{jk}^2\hat{a}_k - \frac{1}{3!}r^3\sum_{k=1}^{N}Q_{jk}^3\hat{a}_k^\dagger + \cdots, \tag{6.18} \\
&= \left(I + \frac{1}{2!}r^2Q^2 + \frac{1}{4!}r^4Q^4 + \cdots\right)_{jk}\hat{a}_k - \left(rQ + \frac{1}{3!}r^3Q^3 + \cdots\right)_{jk}\hat{a}_k^\dagger \tag{6.19} \\
&= \sum_{k=1}^{N}\cosh(rQ)_{jk}\hat{a}_k - \sinh(rQ)_{jk}\hat{a}_k^\dagger, \tag{6.20}
\end{aligned}
$$

where the matrix Q can be obtained from the commutation relations

$$\left[\hat{A},\hat{a}_j\right] = r\frac{1}{2}\left(\hat{a}_{j+1}^\dagger + \hat{a}_{j-1}^\dagger\right) = r\sum_{k=1}^{N}Q_{jk}\hat{a}_k^\dagger, \ \forall j, \tag{6.21}$$

$$[\hat{A},[\hat{A},\hat{a}_j]] = r\sum_{k=1}^{N}Q_{jk}[\hat{A},\hat{a}_k^\dagger] = r^2\sum_{k,l=1}^{N}Q_{jk}Q_{kl}\hat{a}_l = r^2\sum_{k=1}^{N}Q_{jk}^2\hat{a}_k, \tag{6.22}$$

which is given by $Q_{jk} = \frac{1}{2}(\delta_{j+1,k} + \delta_{j-1,k})$. Similar relations, like Eq. (6.20), can also be obtained which are given by

$$\mathcal{S}(r)^\dagger\hat{a}_j^\dagger\mathcal{S}(r) = \sum_{k=1}^{N}\cosh(rQ)_{jk}\hat{a}_k^\dagger - \sinh(rQ)_{jk}\hat{a}_k, \tag{6.23}$$

$$\mathcal{S}(r)\hat{a}_j\mathcal{S}(r)^\dagger = \sum_{k=1}^{N}\cosh(rQ)_{jk}\hat{a}_k + \sinh(rQ)_{jk}\hat{a}_k^\dagger, \tag{6.24}$$

$$\mathcal{S}(r)\hat{a}_j^\dagger \mathcal{S}(r)^\dagger \;=\; \sum_{k=1}^{N} \cosh(rQ)_{jk}\hat{a}_k^\dagger + \sinh(rQ)_{jk}\hat{a}_k. \tag{6.25}$$

Now we apply an annihilation operator on the jth site of the NMSV state, and the resulting output state is

$$
\begin{aligned}
\hat{a}_j|\psi_N\rangle \;&=\; \hat{a}_j\mathcal{S}(r)|0_10_2\ldots0_N\rangle = \mathcal{S}(r)\mathcal{S}(r)^\dagger\hat{a}_j\mathcal{S}(r)|0_10_2\ldots0_N\rangle \\
&=\; \mathcal{S}(r)\sum_{k=1}^{N}\big(\cosh(rQ)_{jk}\hat{a}_k - \sinh(rQ)_{jk}\hat{a}_k^\dagger\big)|0_10_2\ldots0_N\rangle \\
&=\; -\sum_{k=1}^{N}\sinh(rQ)_{jk}\,\mathcal{S}(r)\hat{a}_k^\dagger\mathcal{S}(r)^\dagger\,\mathcal{S}(r)|0_10_2\ldots0_N\rangle \\
&=\; -\sum_{k=1}^{N}\sinh(rQ)_{jk}\Big(\sum_{l=1}^{N}\cosh(rQ)_{kl}\hat{a}_l^\dagger + \sinh(rQ)_{kl}\hat{a}_l\Big)|\psi_N\rangle \\
&=\; -\sum_{k=1}^{N}\Big(\sinh(rQ)\cosh(rQ)_{jk}\hat{a}_k^\dagger + \sinh^2(rQ)_{jk}\hat{a}_k\Big)|\psi_N\rangle.
\end{aligned}
\tag{6.26}
$$

To get the second line, we use $\mathcal{S}(r)\mathcal{S}(r)^\dagger = I$ and Eq. (6.20) while in the third line, we use the fact that $\hat{a}_k|0_10_2\ldots0_N\rangle = 0$. The forth line is obtained by using Eq. (6.25). After a little manipulation, we rewrite Eq. (6.26) as

$$\sum_{k=1}^{N}\big(I + \sinh^2(rQ)\big)_{jk}\hat{a}_k|\psi_N\rangle = -\sum_{k=1}^{N}\sinh(rQ)\cosh(rQ)_{jk}\hat{a}_k^\dagger|\psi_N\rangle \tag{6.27}$$

$$\Rightarrow \sum_{k=1}^{N}\cosh^2(rQ)_{jk}\hat{a}_k|\psi_N\rangle = -\sum_{k=1}^{N}\big(\sinh(rQ)\cosh(rQ)\big)_{jk}\hat{a}_k^\dagger|\psi_N\rangle \tag{6.28}$$

$$\Rightarrow \hat{a}_j|\psi_N\rangle = -\sum_{k=1}^{N}\tanh(rQ)_{jk}\hat{a}_k^\dagger|\psi_N\rangle, \;\; \forall j. \tag{6.29}$$

Since the matrix, Q, is symmetric it is diagonalizable, and hence the hyperbolic relations also hold for it. Now Eq. (6.29) can be compared to a differential equation, given by

$$\frac{df}{dx} = -k(x)f \;\; \Rightarrow f = Ae^{-\int k(x)dx}. \tag{6.30}$$

By taking insight from the above solution, we forcefully write the solution of Eq. (6.29) as

$$|\psi_N\rangle = A\exp\Big(-\frac{1}{2}\sum_{jk=1}^{N}\tanh(rQ)_{jk}\hat{a}_j^\dagger\hat{a}_k^\dagger\Big)|0_10_2\ldots0_N\rangle, \tag{6.31}$$

where A is the normalization constant. Now we will check that the above form of $|\psi_N\rangle$ is indeed the solution of Eq. (6.29), by considering

$$\hat{a}_l|\psi_N\rangle = A\sum_{n}^{\infty}\frac{1}{n!}\hat{a}_l\Big(-\frac{1}{2}\sum_{jk=1}^{N}\tanh(rQ)_{jk}\hat{a}_j^\dagger\hat{a}_k^\dagger\Big)^n|0_10_2\ldots0_N\rangle, \tag{6.32}$$

and by observing

$$
\hat{a}_l\left(-\frac{1}{2}\sum_{jk=1}^{N}\tanh(rQ)_{jk}\hat{a}_j^\dagger\hat{a}_k^\dagger\right)^n = -n\sum_{m=1}^{N}\tanh(rQ)_{lm}\hat{a}_m^\dagger\left(-\frac{1}{2}\sum_{jk=1}^{N}\tanh(rQ)_{jk}\hat{a}_j^\dagger\hat{a}_k^\dagger\right)^{n-1}
$$
$$
+\left(-\frac{1}{2}\sum_{jk=1}^{N}\tanh(rQ)_{jk}\hat{a}_j^\dagger\hat{a}_k^\dagger\right)^n\hat{a}_l. \quad (6.33)
$$

By putting Eq. (6.33) in Eq. (6.32), we obtain

$$
\begin{aligned}
\hat{a}_l|\psi_N\rangle &= -A\sum_{n}^{\infty}\frac{1}{n!}n\sum_{m=1}^{N}\tanh(rQ)_{lm}\hat{a}_m^\dagger\left(-\frac{1}{2}\sum_{jk=1}^{N}\tanh(rQ)_{jk}\hat{a}_j^\dagger\hat{a}_k^\dagger\right)^{n-1}|0_10_2\ldots 0_N\rangle \\
&= -\sum_{m=1}^{N}\tanh(rQ)_{lm}\hat{a}_m^\dagger\left(A\sum_{n}^{\infty}\frac{1}{(n-1)!}\left(-\frac{1}{2}\sum_{jk=1}^{N}\tanh(rQ)_{jk}\hat{a}_j^\dagger\hat{a}_k^\dagger\right)^{n-1}\right) \\
&\qquad\qquad\qquad\qquad\qquad |0_10_2\ldots 0_N\rangle \\
&= -\sum_{m=1}^{N}\tanh(rQ)_{lm}\hat{a}_m^\dagger A\exp\left(-\frac{1}{2}\sum_{jk=1}^{N}\tanh(rQ)_{jk}\hat{a}_j^\dagger\hat{a}_k^\dagger\right)|0_10_2\ldots 0_N\rangle \\
&= -\sum_{k=1}^{N}\tanh(rQ)_{lk}\hat{a}_k^\dagger|\psi_N\rangle. \quad (6.34)
\end{aligned}
$$

6.1.2   Two-mode squeezed vacuum state

The two-mode squeezed vacuum state (TMSV) can be obtained by putting $N=2$ in Eq. (6.31), with

$$
Q = \begin{pmatrix} 0 & 1 \\ 1 & 0 \end{pmatrix}, \quad (6.35)
$$

and

$$
\tanh rQ = \begin{pmatrix} 0 & \tanh r \\ \tanh r & 0 \end{pmatrix}. \quad (6.36)
$$

The normalization constant $A=\frac{1}{\cosh r}$ and hence, the TMSV state, with r as the squeezing parameter, is given by

$$
\begin{aligned}
|\psi_2\rangle &= \frac{1}{\cosh r}e^{-\tanh r\hat{a}_1^\dagger\hat{a}_2^\dagger}|00\rangle \quad (6.37) \\
&= \frac{1}{\cosh r}\sum_{n=0}^{\infty}\frac{1}{n!}\left(-\tanh r\hat{a}_1^\dagger\hat{a}_2^\dagger\right)^n|00\rangle \\
&= \frac{1}{\cosh r}\sum_{n=0}^{\infty}(-\tanh r)^n|n\rangle|n\rangle, \quad (6.38)
\end{aligned}
$$

where $|n\rangle = \frac{(\hat{a}^\dagger)^n}{\sqrt{n}}|0\rangle$ is the occupation number state. Taking $|\psi_2\rangle$ as the initial state, the behavior of entanglement and non-Gaussianity, after adding or subtracting photons, have extensively been investigated [51–54] in last few years.

6.1.3 Four-mode squeezed vacuum state

Let us now consider the four mode squeezed vacuum state, (FMSV) which can be obtained by setting $N = 4$ in Eq. (6.31). The 4×4 matrix, Q, in this case, takes the form

$$Q = \frac{1}{2} \begin{pmatrix} 0 & 1 & 0 & 1 \\ 1 & 0 & 1 & 0 \\ 0 & 1 & 0 & 1 \\ 1 & 0 & 1 & 0 \end{pmatrix}, \tag{6.39}$$

and

$$\tanh(rQ) = \frac{1}{2} \tanh r \begin{pmatrix} 0 & 1 & 0 & 1 \\ 1 & 0 & 1 & 0 \\ 0 & 1 & 0 & 1 \\ 1 & 0 & 1 & 0 \end{pmatrix}, \tag{6.40}$$

with $A = \frac{1}{\cosh r}$. The FMSV state, then reads as [198, 204, 205]

$$|\psi_4\rangle = \frac{1}{\cosh r} \exp\Big(-\frac{1}{2} \tanh r \big(\hat{a}_1^\dagger + \hat{a}_3^\dagger\big)\big(\hat{a}_2^\dagger + \hat{a}_4^\dagger\big)\Big)|0000\rangle. \tag{6.41}$$

Expanding the exponential in Eq. (6.41), we have

$$|\psi_4\rangle = \frac{1}{\cosh r} \sum_{n=0}^\infty \Big(-\frac{1}{2}\tanh r\Big)^n \sum_{r_1,r_2=0}^n \sqrt{\binom{n}{r_1}\binom{n}{r_2}}|n-r_1\rangle|n-r_2\rangle|r_1\rangle|r_2\rangle. \tag{6.42}$$

Such an FMSV state can be prepared in the laboratory by using currently available technology [198]. In the next section, we will elaborate how one can prepare the FMSV state in the laboratory.

6.2 Preparation of FMSV state

To prepare [198] the FMSV state, we need two single mode squeezed vacuum (SMSV) states, with the same squeezing parameter r. Moreover, if for one mode, the variance of quadrature operator X_1 is squeezed to $\Delta X_1 = \frac{1}{2}e^{-r}$, then for the other one the opposite quadrature operator will be squeezed i.e., $\Delta X_2 = \frac{1}{2}e^{-r}$. The two SMSV states are given by

$$|r\rangle_1 = \exp\Big(\frac{r}{2}\big(\hat{a}_1^2 - \hat{a}_1^{\dagger 2}\big)\Big)|0\rangle = \frac{1}{\sqrt{\cosh r}}\exp\Big(-\tanh r\frac{\hat{a}_1^{\dagger 2}}{2}\Big)|0\rangle, \tag{6.43}$$

$$|-r\rangle_2 = \exp\Big(\frac{r}{2}\big(\hat{a}_2^{\dagger 2} - \hat{a}_2^2\big)\Big)|0\rangle = \frac{1}{\sqrt{\cosh r}}\exp\Big(\tanh r\frac{\hat{a}_2^{\dagger 2}}{2}\Big)|0\rangle. \tag{6.44}$$

These two SMSV states are sent through a $50:50$ beam spliter, $B_{12}(\frac{\pi}{4})$, as shown in Fig. 6.1, where the beam splitter [187, 188, 198] is given by

$$B_{12}(\theta) = e^{-\theta\big(\hat{a}_1^\dagger \hat{a}_2 - \hat{a}_1\hat{a}_2^\dagger\big)}. \tag{6.45}$$
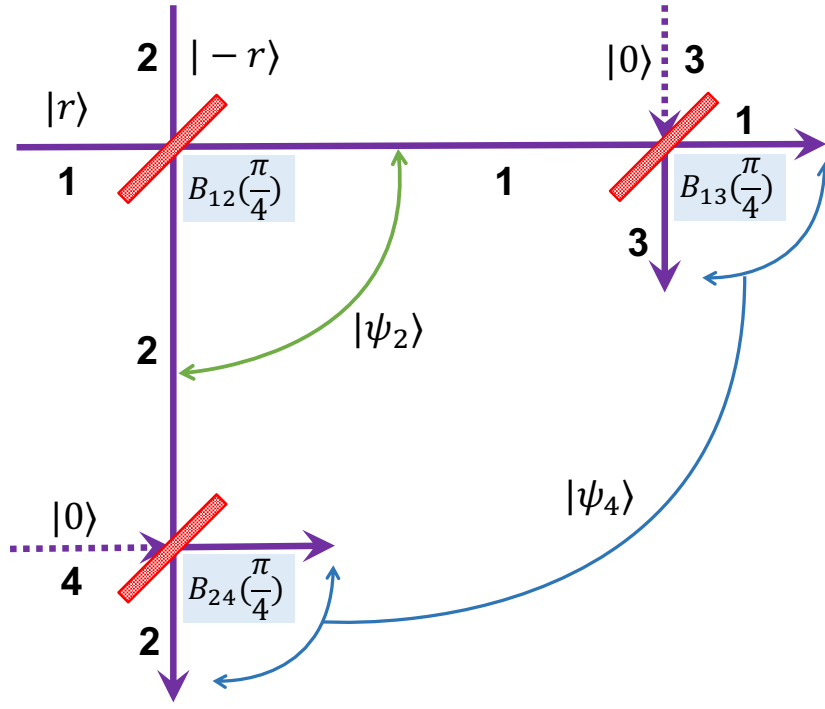
Figure 6.1:   Schematic description of the preparation of FMSV state in the laboratory. Here $|r\rangle$ and $|-r\rangle$ are two SMSV states with squeezing parameter r, squeezed different quadrature operators. After passing through the $50:50$ Beam splitter, it creats the TMSV state, $|\psi_2\rangle$, given in Eq. (6.37). Then the two modes of TMSV state pass through the another $50:50$ beam splitter along with the vacuums, resulting the FMSV state as in Eq. (6.41).

The output state then reads as

$$B_{12}\big(\tfrac{\pi}{4}\big)\,|r\rangle_1|-r\rangle_2 \;=\; B_{12}\big(\tfrac{\pi}{4}\big)\frac{1}{\cosh r}\exp\Big(\frac{1}{2}\tanh r\,(\hat{a}_2^{\dagger 2}-\hat{a}_1^{\dagger 2})\Big)B_{12}\big(\tfrac{\pi}{4}\big)^{\dagger}B_{12}\big(\tfrac{\pi}{4}\big)|00\rangle, \quad (6.46)$$

$$\;=\; \frac{1}{\cosh r}\exp\Big(B_{12}\big(\tfrac{\pi}{4}\big)\frac{1}{2}\tanh r\,(\hat{a}_2^{\dagger 2}-\hat{a}_1^{\dagger 2})B_{12}\big(-\tfrac{\pi}{4}\big)\Big)|00\rangle. \quad (6.47)$$

The term in the exponential can be written as

$$e^{-\hat{A}}\hat{B}e^{\hat{A}} \;=\; \hat{B}-[\hat{A},\hat{B}]+\frac{1}{2!}[\hat{A},[\hat{A},\hat{B}]]-\frac{1}{3!}[\hat{A},[\hat{A},[\hat{A},\hat{B}]]]+\cdots \quad (6.48)$$

$$\;=\; -\frac{1}{2}\tanh r\Big[(\hat{a}_2^{\dagger 2}-\hat{a}_1^{\dagger 2})+\pi\hat{a}_1^{\dagger}\hat{a}_2^{\dagger}-\frac{1}{2!}\frac{\pi^2}{4}(\hat{a}_2^{\dagger 2}-\hat{a}_1^{\dagger 2})-\frac{1}{3!}\frac{\pi^3}{4}\hat{a}_1^{\dagger}\hat{a}_2^{\dagger}+\frac{1}{4!}\frac{\pi^4}{4^2}(\hat{a}_2^{\dagger 2}-\hat{a}_1^{\dagger 2})$$

$$+\frac{1}{5!}\frac{\pi^5}{4^2}\hat{a}_1^{\dagger}\hat{a}_2^{\dagger}-\frac{1}{6!}\frac{\pi^6}{4^3}(\hat{a}_2^{\dagger 2}-\hat{a}_1^{\dagger 2})+\cdots\Big] \quad (6.49)$$

$$\;=\; -\frac{1}{2}\tanh r\Big[(\hat{a}_2^{\dagger 2}-\hat{a}_1^{\dagger 2})\underbrace{\Big\{1-\frac{1}{2!}\big(\tfrac{\pi}{2}\big)^2+\frac{1}{4!}\big(\tfrac{\pi}{4}\big)^4+\cdots\Big\}}_{\cos\left(\frac{\pi}{2}\right)=0}$$

$$+2\hat{a}_1^{\dagger}\hat{a}_2^{\dagger}\underbrace{\Big\{\big(\tfrac{\pi}{2}\big)-\frac{1}{3!}\big(\tfrac{\pi}{2}\big)^3+\frac{1}{5!}\big(\tfrac{\pi}{2}\big)^5\cdots\Big\}}_{\sin\left(\frac{\pi}{2}\right)=1} \quad (6.50)$$

$$\;=\; -\tanh r\,\hat{a}_1^{\dagger}\hat{a}_2^{\dagger}. \quad (6.51)$$

Here we put $\hat{A} = -\frac{\pi}{4}\big(\hat{a}_1^\dagger\hat{a}_2 - \hat{a}_1\hat{a}_2^\dagger\big)$, and $\hat{B} = \frac{1}{2}\tanh r\big(\hat{a}_2^{\dagger 2} - \hat{a}_1^{\dagger 2}\big)$. Putting Eq. (6.51) in Eq. (6.47), we obtain the TMSV, given in Eq. (6.37). The FMSV state can then be obtained when each part of the TMSV state along with two vacuum states are sent through two different $50:50$ beam spliters (see Fig. (6.1)), i.e.,

$$B_{13}\Big(\frac{\pi}{4}\Big)B_{24}\Big(\frac{\pi}{4}\Big)|\psi_2\rangle_{12}|00\rangle_{34} = \frac{1}{\cosh r}\exp\Big(-B_{13}\Big(\frac{\pi}{4}\Big)B_{24}\Big(\frac{\pi}{4}\Big)\tanh r\,\hat{a}_1^\dagger\hat{a}_2^\dagger B_{13}\Big(-\frac{\pi}{4}\Big)B_{24}\Big(-\frac{\pi}{4}\Big)\Big)|0000\rangle.$$
(6.52)

Once again the term in the exponential can be written as $e^{-\hat{A}}\hat{B}e^{\hat{A}}$, where

$$\hat{A} = \frac{\pi}{4}\big(\hat{a}_1^\dagger\hat{a}_3 - \hat{a}_1\hat{a}_3^\dagger + \hat{a}_2^\dagger\hat{a}_4 - \hat{a}_2\hat{a}_4^\dagger\big).$$
(6.53)

and $\hat{B} = \hat{a}_1^\dagger\hat{a}_2^\dagger$. Similarly the individual terms in the right hand side of Eq. (6.10) as

$$[\hat{A}, \hat{B}] = -\frac{\pi}{4}\big(\hat{a}_2^\dagger\hat{a}_3^\dagger + \hat{a}_1^\dagger\hat{a}_4^\dagger\big),$$
(6.54)

$$[\hat{A}, [\hat{A}, \hat{B}]] = -\frac{\pi^2}{2^3}\big(\hat{a}_1^\dagger\hat{a}_2^\dagger - \hat{a}_3^\dagger\hat{a}_4^\dagger\big),$$
(6.55)

$$[\hat{A}, [\hat{A}, [\hat{A}, \hat{B}]]] = \frac{\pi^3}{2^4}\big(\hat{a}_2^\dagger\hat{a}_3^\dagger + \hat{a}_1^\dagger\hat{a}_4^\dagger\big).$$
(6.56)

Putting the above equations in the exponential and using Eq. (6.10), we get

$$\begin{aligned}
e^{-\hat{A}}\hat{B}e^{\hat{A}} &= \tanh r\Big\{\hat{a}_1^\dagger\hat{a}_2^\dagger + \frac{\pi}{4}\big(\hat{a}_2^\dagger\hat{a}_3^\dagger + \hat{a}_1^\dagger\hat{a}_4^\dagger\big) - \frac{1}{2!}\frac{\pi^2}{2\cdot 2^2}\big(\hat{a}_1^\dagger\hat{a}_2^\dagger - \hat{a}_3^\dagger\hat{a}_4^\dagger\big) - \frac{1}{3!}\frac{\pi^3}{2\cdot 2^3}\big(\hat{a}_2^\dagger\hat{a}_3^\dagger + \hat{a}_1^\dagger\hat{a}_4^\dagger\big) \\
&\qquad + \frac{1}{4!}\frac{\pi^4}{2\cdot 2^4}\big(\hat{a}_1^\dagger\hat{a}_2^\dagger - \hat{a}_3^\dagger\hat{a}_4^\dagger\big) + \frac{1}{5!}\frac{\pi^5}{2\cdot 2^5}\big(\hat{a}_2^\dagger\hat{a}_3^\dagger + \hat{a}_1^\dagger\hat{a}_4^\dagger\big)\Big\} \qquad (6.57) \\
&= \tanh r\Big[\frac{1}{2}\big(\hat{a}_1^\dagger\hat{a}_2^\dagger + \hat{a}_3^\dagger\hat{a}_4^\dagger\big) + \frac{1}{2}\big(\hat{a}_1^\dagger\hat{a}_2^\dagger - \hat{a}_3^\dagger\hat{a}_4^\dagger\big)\Big\{1 - \frac{1}{2!}\Big(\frac{\pi}{2}\Big)^2 + \frac{1}{4!}\Big(\frac{\pi}{4}\Big)^4 + \cdots\Big\} \\
&\qquad + \frac{1}{2}\big(\hat{a}_2^\dagger\hat{a}_3^\dagger + \hat{a}_1^\dagger\hat{a}_4^\dagger\big)\Big\{\Big(\frac{\pi}{2}\Big) - \frac{1}{3!}\Big(\frac{\pi}{2}\Big)^3 + \frac{1}{5!}\Big(\frac{\pi}{2}\Big)^5\cdots\Big\}\Big] \qquad (6.58) \\
&= \frac{1}{2}\tanh r\big(\hat{a}_1^\dagger\hat{a}_2^\dagger + \hat{a}_3^\dagger\hat{a}_4^\dagger + \hat{a}_2^\dagger\hat{a}_3^\dagger + \hat{a}_1^\dagger\hat{a}_4^\dagger\big) \\
&= \frac{1}{2}\tanh r\big(\hat{a}_1^\dagger + \hat{a}_3^\dagger\big)\big(\hat{a}_2^\dagger + \hat{a}_4^\dagger\big). \qquad (6.59)
\end{aligned}$$

Substituting the expression in the exponential of Eq. (6.52), we obtain Eq. (6.41) of the FMSV state $|\psi_4\rangle$.

6.3 Photon-added and -subtracted FMSV state

In this section, we consider the FMSV state, $|\psi_4\rangle$, as an initial state and our aim is to find the characteristics of its entanglement after adding and subtracting a finite number of photons. For investigations, we use entanglement, according to the measures of entropy of entanglement and the logarithmic negativity, defined in Sec. 2.2.1 as measures of entanglement. Suppose m_i number of photons are added at each mode i, with $i = 1, 2, 3, 4$. Then the output four-mode (FM) state reads as

$$|\psi_{\{m_i\}}^{add}\rangle = \frac{1}{N^{add}}\sum_{n=0}^{\infty}\Big(-\frac{\tanh r}{2}\Big)^n\sum_{r_1, r_2=0}^{n}\sqrt{\binom{n}{r_1}\binom{n}{r_2}}\sqrt{\frac{(n-r_1+m_1)!}{(n-r_1)!}}\sqrt{\frac{(n-r_2+m_2)!}{(n-r_2)!}}$$

$$\sqrt{\frac{(r_1+m_3)!}{r_1!}}\sqrt{\frac{(r_2+m_4)!}{r_2!}} \times |n-r_1+m_1\rangle|n-r_2+m_2\rangle|r_1+m_3\rangle|r_2+m_4\rangle$$

$$\equiv \sum_{n=0}^{\infty}\sum_{r_1,r_2=0}^{n} p_{n,r_1,r_2}^{\{m_i\}}|n-r_1+m_1\rangle|n-r_2+m_2\rangle|r_1+m_3\rangle|r_2+m_4\rangle, \tag{6.60}$$

where N^{add} is the normalization constant. Similarly, after subtracting $\{m_i\}(i=1,2,3,4)$ number of photons from each mode of the FMSV state, the resulting state is given by

$$|\psi_{\{m_i\}}^{sub}\rangle = \frac{1}{N^{sub}}\sum_{n=M}^{\infty}\left(-\frac{\tanh r}{2}\right)^n\sum_{r_1=m_3}^{n-m_1}\sum_{r_2=m_4}^{n-m_2}\sqrt{\binom{n}{r_1}\binom{n}{r_2}}\sqrt{\frac{(n-r_1)!}{(n-r_1-m_1)!}}\sqrt{\frac{(n-r_2)!}{(n-r_2-m_2)!}}$$

$$\sqrt{\frac{r_1!}{(r_1-m_3)!}}\sqrt{\frac{r_2!}{(r_2-m_4)!}} \times |n-r_1-m_1\rangle|n-r_2-m_2\rangle|r_1-m_3\rangle|r_2-m_4\rangle$$

$$\equiv \sum_{n=M}^{\infty}\sum_{r_1=m_3}^{n-m_1}\sum_{r_2=m_4}^{n-m_2} q_{n,r_1,r_2}^{\{m_i\}}|n-r_1-m_1\rangle|n-r_2-m_2\rangle|r_1-m_3\rangle|r_2-m_4\rangle, \tag{6.61}$$

where N^{sub} is the normalization constant, and $M = \max\{m_1+m_3, m_2+m_4\}$. The above two equations will help us to obtain several single and two-mode reduced density matrices which are required to study the behavior of entanglement for a four-mode state in different bipartitions.

6.4 Comparison of entanglement enhancement between photon addition and subtraction

Our aim here is to investigate the effects on entanglement or QC of the FMSV state, when photons are added (subtracted) in (from) different modes. In particular, measures of entanglement as well as QC in a multipartite scenario, both in discrete and CV systems are limited [6, 39]. To characterize entanglement in CV system with multiple modes, one possibility is to compute von-Neumann entropy in different bipartition of modes. Another possibility is to study logarithmic negativity of two modes which can be obtained after discarding all the modes except two. In this section, we briefly discuss the local von Neumann entropy and the logarithmic negativity in CV systems. To study such behavior, we divide the modes into two different categories, viz.

(a) Player modes – the modes in which number of photons that we add (subtract) varies, and

(b) Spectator modes – the modes in which either no photon or fixed number of photons are added (subtracted) and hence plays a spectator role in the deGaussification process.

The comparison has been made between the situations, when the $m_i, i = 1, 2, \ldots$ photons are added in the player modes, and the scenario when the same number of photons are subtracted from the player modes. To execute such comparison, we introduce a quantity

$$\delta_{\mathcal{A}}^{E}(\{m_i\}) = E(\rho_{\mathcal{A}:\mathcal{B}}^{add\{m_i\}}) - E(\rho_{\mathcal{A}:\mathcal{B}}^{sub\{m_i\}}) \tag{6.62}$$

where $\mathcal{A}:\mathcal{B}$ is a bipartition with $\mathcal{A}\cap\mathcal{B}=\emptyset$. The positivity of $\delta^E(\{m_i\})$ implies that addition is better than subtraction from an entanglement perspective. It is clear that the behavior of $\delta_{\mathcal{A}}^E(\{m_i\})$ with $\{m_i\}$
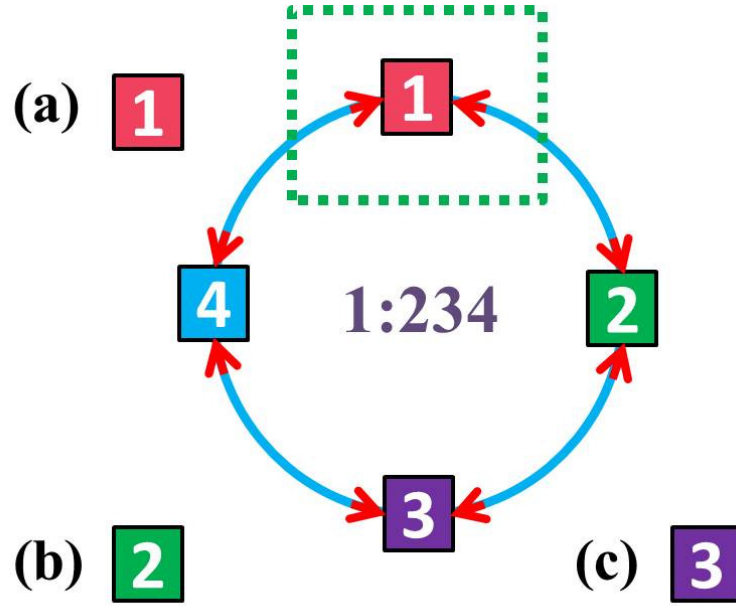
Figure 6.2: Schematic diagram of choices of player and spectator modes as well as partitions. If we fix the bipartition to be $1 : 234$ there are three nontrivial possibilities of choosing a single player in the photon-added and the subtracted FM state. There are the cases (a) - (c), and the number in the square mentioned for each case is the mode at which the photon is added/subtracted.

depends on the number of player and spectator modes as well as the bipartite splits.

6.4.1 Photon added and subtracted with one player mode

Let us first consider a situation in which one mode acts as a player while the rest are the spectator modes. We first restrict ourselves in the $1 : 234$ cut irrespective of the choice of the player mode. In this case, there exists three different possibilities of choosing a player mode which are as follows:

1. First mode as player and the rest as spectators,

2. Second mode as player and

3. third as player,

All of these possibilities are depicted in Fig. 6.2. From Eqs. (6.60) and (6.61), it is clear that fourth mode as a player is equivalent with case (b), and hence we exclude this case.

Single player mode in the smallest bipartition

Suppose that we add or subtract m_1 photons in the first mode without putting any number of photons in rest of the modes, as shown in Fig. 6.2(a). Here the first mode acts as a player. The reduced density matrices can be calculated from Eqs. (6.60) and (6.61), which read as

$$\rho_{1,m_1}^{add} = \frac{1}{N_1^{add}} \sum_{n=0}^{\infty} \frac{\tanh^{2n} r}{2^n} \sum_{r_1=0}^{n} \binom{n}{r_1} \frac{(n + m_1 - r_1)!}{(n - r_1)!} |n + m_1 - r_1\rangle\langle n + m_1 - r_1| \quad (6.63)$$

for photon addition, and

$$
\begin{aligned}
\rho_{1,m_1}^{sub} &= \frac{1}{N_1^{sub}} \sum_{n=m_1}^{\infty} \frac{\tanh^{2n}(r)}{2^n} \sum_{r_1=0}^{n-m_1} \binom{n}{r_1} \frac{(n-r_1)!}{(n-m_1-r_1)!} |n-m_1-r_1\rangle\langle n-m_1-r_1| \\
&= \frac{1}{N_1^{sub}} \sum_{n=0}^{\infty} \frac{\tanh^{2n} r}{2^n} \sum_{r_1=0}^{n} \frac{(m_1+r_1)!}{r_1!} \binom{n+m_1}{r_1+m_1} |r_1\rangle\langle r_1| \tag{6.64}
\end{aligned}
$$

for photon subtraction. We now analytically establish that entanglement, in the bipartition of the player and the spectator modes, increases with the number of photons added. But before going to this, we need to calculate the normalization constants N_1^{add} and N_1^{sub}.

$$
\begin{aligned}
N_1^{add} &= \sum_{n=0}^{\infty} \frac{\tanh^{2n} r}{2^n} \sum_{r_1=0}^{n} \binom{n}{r_1} \frac{(n+m_1-r_1)!}{(n-r_1)!} \\
&= \sum_{n=0}^{\infty} \frac{x^n}{2^n} \sum_{r_1=0}^{n} \binom{n}{r_1} \frac{(m_1+r_1)!}{r_1!} \tag{6.65}
\end{aligned}
$$

where we put $x = \tanh^2 r$, and the summation over r_1 can be written as

$$
\sum_{r=0}^{n} \binom{n}{r} \frac{(m+r)!}{r!} = (-1)^m \frac{d^m}{db^m} \left(\frac{1}{b} \left(a + \frac{1}{b} \right)^n \right) \Bigg|_{a=1,b=1}. \tag{6.66}
$$

The normalization constant finally reads as

$$
\begin{aligned}
N_1^{add} &= \sum_{n=0}^{\infty} (-1)^{m_1} \frac{d^{m_1}}{db^{m_1}} \left(\frac{1}{b} \frac{x^n}{2^n} \left(a + \frac{1}{b} \right)^n \right) \Bigg|_{a=1,b=1} \\
&= (-1)^{m_1} \frac{d^{m_1}}{db^{m_1}} \frac{1}{b} \frac{1}{1 - \frac{x}{2}\left(a + \frac{1}{b}\right)} \Bigg|_{a=1,b=1} \\
&= (-1)^{m_1-s} \frac{d^{m_1-s}}{db^{m_1-s}} \frac{\left(1 - a\frac{x}{2}\right)^s 1 \cdot 2 \cdots s}{\left(b - \frac{x}{2}(1+ab)\right)^{s+1}} \Bigg|_{a=1,b=1} \\
&= \frac{\left(1 - a\frac{x}{2}\right)^{m_1} m_1!}{\left(b - \frac{x}{2}(1+ab)\right)^{m_1+1}} \Bigg|_{a=1,b=1} = \frac{m_1!(2-x)^{m_1}}{2^{m_1}(1-x)^{m_1+1}}. \tag{6.67}
\end{aligned}
$$

Similarly, N_1^{sub} can be evaluated as

$$
\begin{aligned}
N_1^{sub} &= \sum_{n=m_1}^{\infty} \frac{x^n}{2^n} \sum_{r_1=m_1}^{n} \binom{n}{r_1} \frac{r_1!}{(r_1-m_1)!} \\
&= \sum_{n=m_1}^{\infty} \frac{x^n}{2^n} \frac{d^{m_1}}{db^{m_1}} (1+b)^n|_{b=1} = \frac{d^{m_1}}{db^{m_1}} \sum_{n=m_1}^{\infty} \frac{x^n}{2^n} (1+b)^n|_{b=1} \\
&= \frac{x^{m_1}}{2^{m_1-1}} \frac{d^{m_1}}{db^{m_1}} \frac{(1+b)^{m_1}}{2 - x(1+b)} \Bigg|_{b=1} = \frac{x^{m_1}}{2^{m_1}} \frac{2^{m_1} m_1!}{(1-x)^{m_1+1}} \tag{6.68}
\end{aligned}
$$

Proposition 1: *Entanglement increases with the addition of a single photon in a four-mode photon-added*

state, i.e.,

$$E(|\psi^{add}_{m_1+1}\rangle)_{1:234} \geq E(|\psi^{add}_{m_1}\rangle)_{1:234} \tag{6.69}$$

where $|\psi^{add}_{m_1+i}\rangle, i = 0, 1$ denotes the state in which $m_1 + i$ number of photons are added at the mode 1.

Proof: To evaluate entanglement in the $1 : 234$ bipartition, we have to study the single mode reduced density matrix, ρ^{add}_{1,m_1}, of the four-mode state $|\psi^{add}_{m_1}\rangle$. To prove $E(|\psi^{add}_{m_1+1}\rangle)_{1:234} \geq E(|\psi^{add}_{m_1}\rangle)_{1:234}$, it is equivalent to show $S(\rho^{add}_{1,m_1+1}) \geq S(\rho^{add}_{1,m_1})$. After inserting the normalization constant in Eq. (6.63), we get

$$\rho^{add}_{1,m_1} = 2^{m_1} \frac{(1-x)^{m_1+1}}{(2-x)^{m_1}} \sum_{r_1=0}^{\infty} f(r_1, x) \binom{m_1 + r_1}{m_1} |m_1 + r_1\rangle\langle m_1 + r_1| \tag{6.70}$$

$$= \sum_{r_1=0}^{\infty} g(x, m_1, r_1) |m_1 + r_1\rangle\langle m_1 + r_1| \tag{6.71}$$

and

$$f(r, x) = \sum_{n=r}^{\infty} \frac{x^n}{2^n} \binom{n}{r}, \tag{6.72}$$

and

$$g(x, m, r) = 2^m \frac{(1-x)^{m+1}}{(2-x)^m} f(r, x) \binom{m+r}{m}. \tag{6.73}$$

Therefore, entanglement in the player : spectator bipartition is given by

$$E(|\psi^{add}_{m_1}\rangle_{1:rest}) = S(\rho^{add}_{1,m_1}) = -\sum_{r_1=0}^{\infty} g(x, m_1, r_1) \log_2 g(x, m_1, r_1). \tag{6.74}$$

Now if we add one more photon to the state in Eq. (6.63), the entanglement is going to be

$$E(|\psi^{add}_{m_1+1}\rangle_{1:rest}) = -\sum_{r_1=0}^{\infty} g(x, m_1 + 1, r_1) \log_2 g(x, m_1 + 1, r_1). \tag{6.75}$$

Let us now evaluate $g(x, m_1 + 1, r_1)$ which simplifies as

$$\begin{aligned} g(x, m_1 + 1, r_1) &= 2^{m_1+1} \frac{(1-x)^{m_1+2}}{(2-x)^{m_1+1}} f(r_1, x) \binom{m_1 + r_1 + 1}{m_1 + 1} \\ &= 2^{m_1+1} \frac{(1-x)^{m_1+2}}{(2-x)^{m_1+1}} f(r_1, x) \left\{ \binom{m_1 + r_1}{m_1} + \binom{m_1 + r_1}{m_1 + 1} \right\} \\ &= \frac{2(1-x)}{(2-x)} g(x, m_1, r_1) + \frac{x}{2-x} g(x, m_1 + 1, r_1 - 1), \end{aligned} \tag{6.76}$$

by using Pascal's identity, and the recursion relation of $f(r, x)$, which is given by

$$\begin{aligned} f(r, x) &= \sum_{n=r}^{\infty} \frac{x^n}{2^n} \binom{n}{r} = \sum_{n=r}^{\infty} \frac{x^n}{2^n} \left(\binom{n-1}{r} + \binom{n-1}{r-1} \right) \\ &= \sum_{n=r+1}^{\infty} \frac{x^{n-1}}{2^{n-1}} \frac{x}{2} \binom{n-1}{r} + \sum_{n=r}^{\infty} \frac{x^{n-1}}{2^{n-1}} \frac{x}{2} \binom{n-1}{r-1} \end{aligned} \tag{6.77}$$
$$\tag{6.78}$$
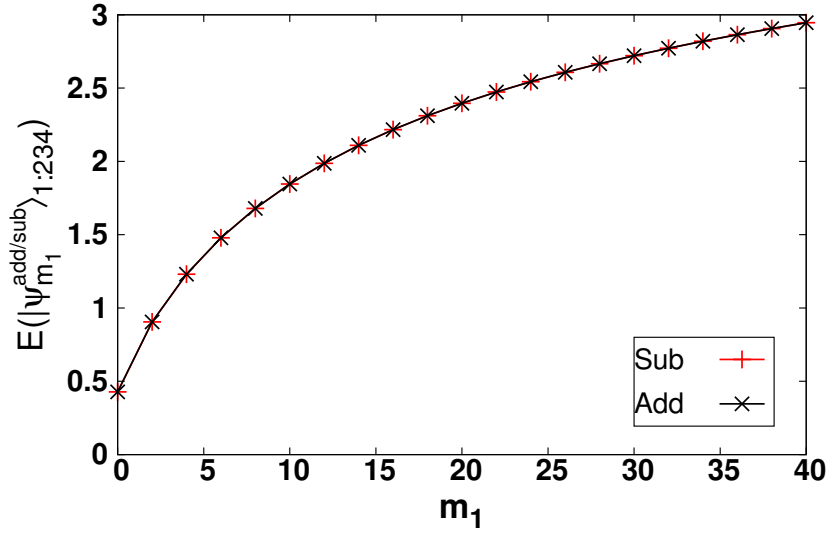
Figure 6.3: Behavior of $E(|\psi_{m_1}^{add}\rangle_{1:234})$ and $E(|\psi_{m_1}^{sub}\rangle_{1:234})$ vs. m_1. We add ($\times$) and subtract ($+$) upto 40 photons in (from) the first mode, and calculate entanglement in the $1:234$ bipartition, when no photons are added (subtracted) in (from) the spectator modes. As shown in the propositions, entanglement in both the cases increases monotonically with m_1 and they coincide. Here the entanglement is plotted in the unit of ebits while the abscissa is dimensionless.

$$= \sum_{n=r+1}^{\infty} \frac{x^n}{2^n} \frac{x}{2} \binom{n}{r+1} + \sum_{n=r}^{\infty} \frac{x^n}{2^n} \frac{x}{2} \binom{n}{r} \tag{6.79}$$

$$= \frac{x}{2} f(r+1, x) + \frac{x}{2} f(r, x) \tag{6.80}$$

$$\Rightarrow f(r, x) = \frac{x}{2-x} f(r-1, x). \tag{6.81}$$

Using the concavity of the function $h(x) = -x \log_2 x$, we get

$$h(g(x, m_1+1, r_1)) \geq \frac{2(1-x)}{(2-x)} h(g(x, m_1, r_1)) + \frac{x}{2-x} h(g(x, m_1+1, r_1-1)). \tag{6.82}$$

In the first line, we use the Pascal's identity, and in the third line, we substitute $n-1 \to n$, and $r-1 \to r$. Taking the sum over r_1 in both sides, we have

$$S(\rho_{1,m_1+1}^{add}) \geq \frac{2(1-x)}{(2-x)} S(\rho_{1,m_1}^{add}) + \frac{x}{2-x} S(\rho_{1,m_1+1}^{add}) \tag{6.83}$$

which immediately implies

$$S(\rho_{1,m_1+1}^{add}) \geq S(\rho_{1,m_1}^{add}). \tag{6.84}$$

Hence the proof. ∎

Similarly, one can also show that entanglement of the photon-subtracted state in the player : spectator split increases with number of photons subtracted from the state.

We are now going to analyze the effects on entanglement under addition and subtraction of same number of photons.

Proposition 2: *When a single mode acts as a player, entanglement between the player and the spectator*

modes of the photon-added state coincide with that of the photon-subtracted state.

Proof: To prove that the increase of entanglement in the multimode state is same for addition and subtraction, we consider the single mode reduced density matrix. The single site reduced density matrix of photon-subtracted state, after inserting N_1^{sub}, is given by

$$\rho_{1,m_1}^{sub} = (1-x)^{m_1+1} \sum_{r_1=0}^{\infty} \binom{m_1+r_1}{m_1} \underbrace{\sum_{n=r_1}^{\infty} \frac{x^n}{2^n} \binom{n+m_1}{r_1+m_1}}_{f_{sub}(r_1,m_1,x)} |r_1\rangle\langle r_1|. \tag{6.85}$$

Now $f_{sub}(r_1, m_1, x)$ can be evaluated by substituting $n - r_1 \to n$, $r_1 + m_1 \to m$ and $\frac{x}{2} \to v$,

$$\begin{aligned}
f_{sub}(r_1, m_1, x) &= \frac{x^{r_1}}{2^{r_1}} \sum_{n=0}^{\infty} v^n \binom{n+m}{m} = \frac{x^{r_1}}{2^{r_1}} \sum_{n=0}^{\infty} \frac{1}{m!} \frac{d^m}{dv^m} v^{n+m} \\
&= \frac{1}{m!} \frac{x^{r_1}}{2^{r_1}} \frac{d^m}{dv^m} \frac{v^m}{1-v} = \frac{x^{r_1}}{2^{r_1}} (1-v)^{-m-1} \\
&= \frac{x^{r_1} 2^{m_1+1}}{(2-x)^{m_1+r_1+1}}.
\end{aligned} \tag{6.86}$$

On the other hand, the reduced density matrix after adding same number of photons reads as

$$\rho_{1,m_1}^{add} = \sum_{r_1=0}^{\infty} 2^{m_1} \frac{(1-x)^{m_1+1}}{(2-x)^{m_1}} \frac{2}{2-x} \left(\frac{x}{2-x}\right)^{r_1} \binom{m_1+r_1}{m_1} |r_1+m_1\rangle\langle r_1+m_1|. \tag{6.87}$$

The above form has been obtained by substituting Eq. (6.77) of $f(r, x)$ in Eq. (6.70), which is

$$\begin{aligned}
f(r, x) &= \frac{x}{2-x} f(r-1, x) = \frac{x^r}{(2-x)^r} f(0, x), \\
&= \frac{x^r}{(2-x)^r} \sum_{n=0}^{\infty} \frac{x^n}{2^n} = \frac{x^r}{(2-x)^r} \frac{2}{(2-x)}
\end{aligned} \tag{6.88}$$

Comparing Eqs. (6.85) and (6.87), we have $S(\rho_{1,m_1}^{add}) = S(\rho_{1,m_1}^{sub})$. ∎

To visualize the above Propositions, we plot $S(\rho_{1,m_1}^{add/sub})$, with respect to m_1 by fixing the squeezing parameter $r = 0.4$ in Fig. 6.3. It clearly shows that the curve for photon addition merges with the curve of photon subtraction. Moreover, it shows that entanglement in that bipartition monotonically increases with the addition or subtraction of photons as shown in Proposition 1. Note here that although the results presented here are when the photons are added at the mode 1 and the bipartition is considered as player : spectator mode, the Propositions remain unaltered if another mode also acts as a player by keeping the similar bipartition.

Effects on entanglement due to change of player modes

We now consider the entanglement in the same bipartition as in the previous case, i.e., 1 : 234. However, the second or third mode now act as player and no photons are added in the rest of the modes. In the previous case, one block contained only the player mode while the other one contains all the spectator modes. In this case, one part of the partition contains one spectator mode while the other one consists of both the player and the rest of the spectator modes. In the previous case, we have already shown that
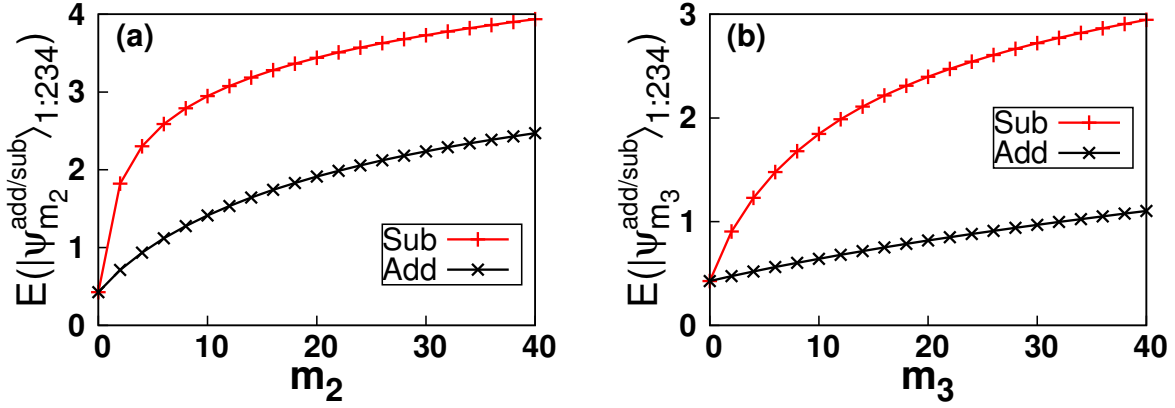
Figure 6.4: (a) Trends of $E(|\psi_{m_2}^{add}\rangle_{1:234})$ and $E(|\psi_{m_2}^{sub}\rangle_{1:234})$ with the number of photon-added (subtracted) in (from) the second mode. (b) Similar study has been carried out when the third mode acts as a player. Both the cases reveal that subtraction is better than addition. Ordinates are plotted in the unit of ebits while the abscissas are dimensionless.

the effects on entanglement due to addition and subtraction of photons are similar. We will now show whether such observation remains invariant even in this scenario.

Let us now take the four-mode squeezed vacuum state as input, and add (subtract) m_2 photons in (from) the second mode. As depicted in Fig. 6.4(a), we find that unlike the previous case, the photon-subtracted state possesses more entanglement in the $1:234$ bipartition than that of the photon-added state. The ordering remains unchanged if one takes the third mode as player and consider entanglement in the $1:234$ split (see Fig. 6.4(b)). Moreover, we observe that the amount of entanglement decreases in this scenario, compared to the case when the second mode acts as a player. Note here that if one takes the two-mode squeezed vacuum state as input, it was observed that the bipartite entanglement content of the photon-subtracted state is always lower than that of the photon-added state.

Bipartition with both player and spectator modes

We still restrict ourselves to the case of a single player. But we now move to the situations in which entanglement of a four-mode state is studied by considering a bipartition in which both sides of the split contain two modes, namely $12:34$ and $13:24$. The other split between modes, i.e., $14:23$, reflects a similar behavior, due to the symmetry of the four-mode state. In these two scenarios, photons are added or subtracted in the first mode, as shown in Fig. 6.5, and no photons are added or subtracted, in the other spectator modes.

To study entanglement of $|\psi_{m_1}^{add}\rangle$ ($|\psi_{m_1}^{sub}\rangle$) in the $12:34$ or $13:24$ bipartition, we require the two party reduced density matrices, ρ_{12,m_1}^{add}, ρ_{13,m_1}^{add}, ρ_{12,m_1}^{sub}, and ρ_{13,m_1}^{sub}. We have

$$
\begin{aligned}
\rho_{12,m_1}^{add} &= \frac{1}{N_{12}^{add}} \sum_{n,n'=0}^{\infty} \frac{x^{(n+n')/2}}{2^{n+n'}} \sum_{r_1,r_2=0}^{\min\{n,n'\}} \sqrt{\binom{n}{r_1}\binom{n}{r_2}} \sqrt{\binom{n'}{r_1}\binom{n'}{r_2}} \sqrt{\frac{(n+m_1-r_1)!}{(n-r_1)!}} \\
&\quad \times \sqrt{\frac{(n'+m_1-r_1)!}{(n'-r_1)!}} |n+m_1-r_1\rangle_1 |n-r_2\rangle_2 \langle n'+m_1-r_1|_1 \langle n'-r_2|_2,
\end{aligned}
$$
(6.89)
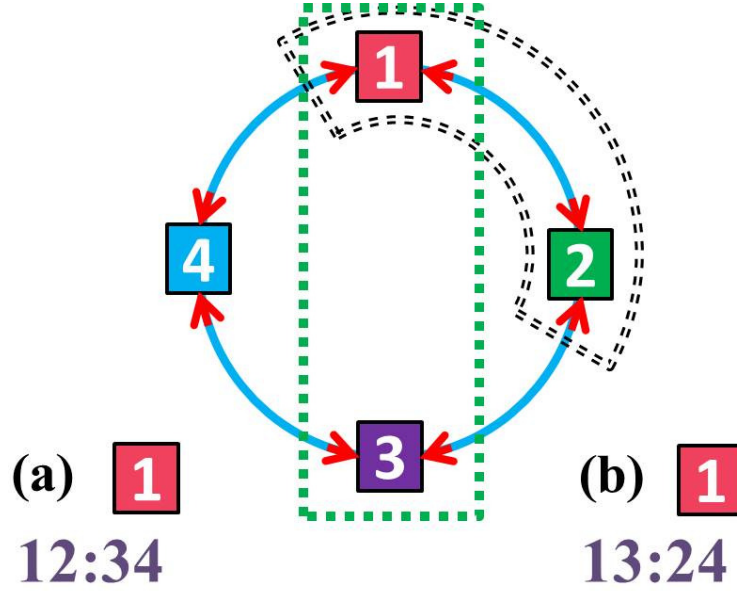
Figure 6.5: Schematic diagram of two different blocks, when a single mode, specifically the first mode, acts as a player.

and

$$
\begin{aligned}
\rho^{sub}_{12,m_1} = {} & \frac{1}{N^{sub}_{12}} \sum_{n,n'=m_1}^{\infty} \frac{x^{(n+n')/2}}{2^{n+n'}} \sum_{r_1=0}^{\min\{n,n'\}-m_1} \sum_{r_2=0}^{\min\{n,n'\}} \sqrt{\binom{n}{r_1}\binom{n}{r_2}} \sqrt{\binom{n'}{r_1}\binom{n'}{r_2}} \sqrt{\frac{(n-r_1)!}{(n-m_1-r_1)!}} \\
& \times \sqrt{\frac{(n'-r_1)!}{(n'-m_1-r_1)!}} |n-m_1-r_1\rangle_1 |n-r_2\rangle_2 \langle n'-m_1-r_1|_1 \langle n'-r_2|_2. \quad (6.90)
\end{aligned}
$$

Note that in the previous cases, where one partition contains only a single mode, we required single-site density matrices to calculate the entanglement, and they are always diagonal in the number basis. The same is not the case for two-site density matrices. Similarly, one can find out the reduced density matrices of ρ^{add}_{13,m_1} and ρ^{sub}_{13,m_1}. In both the scenarios, we observe that entanglement increases against the number of photons added, m_1 and same is true for subtraction of photons (see Fig. 6.6). Moreover, as observed in the previous case with the smallest partition consisting of the spectator mode, photon-subtracted state contains higher entanglement in the $12:34$ as well as $13:24$ partitions than that of the corresponding photon-added state. See Figs. 6.6(a) and 6.6(b).

We briefly mention here the method used to calculate $S(\rho^{add}_{12,m_1})$, and the other local entropies. The von Neumann entropy of ρ^{add}_{12,m_1} can be obtained if one can diagonalize the infinite dimensional matrix, given in Eq. (6.89). To calculate it, for fixed m_1, we have to truncate the summation upto a large value of n and n', say N for both, and calculate its trace, i.e., $\mathrm{tr}_N(\rho^{add}_{12,m_1})$, as well as von Neumann entropy, $S^N(\rho^{add}_{12,m_1})$. We then choose, $2N$ as maximum of n and n' and obtain the quantities. When the difference between $S^N(\rho^{add}_{12,m_1})$ and $S^{2N}(\rho^{add}_{12,m_1})$ is of the order of 10^{-6}, we take $S^N(\rho^{add}_{12,m_1})$ as the actual entropy. In Fig 6.7, for a fixed value of m_1, we plot $S^N(\rho^{add}_{12})$ and $\mathrm{tr}_N(\rho^{add}_{12})$ with the variation of N. With the increase of m_1, we observe that we require higher values of N. However, the figure shows both the quantities converge when $N \geq 10$, irrespective of the value of m_1. When we compute entropy or LN, we
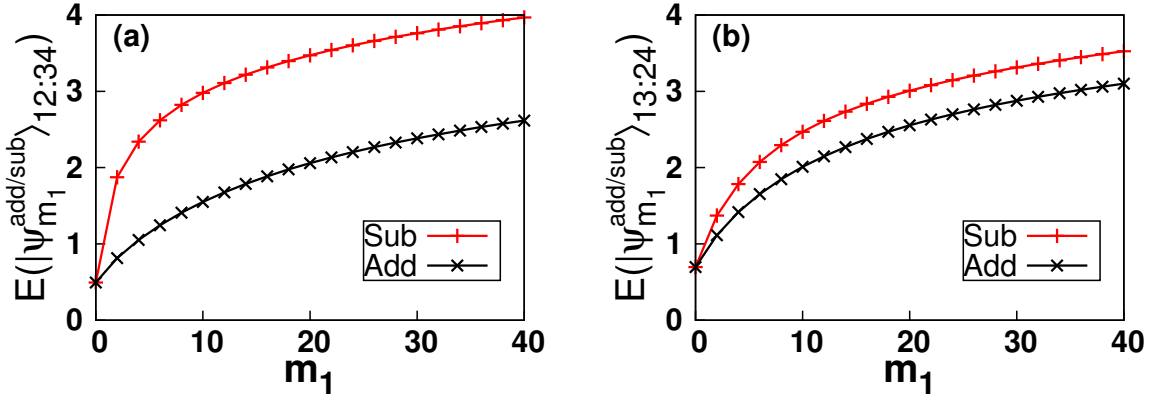
Figure 6.6: (Color online) Plots of entanglements of photon-added and -subtracted states in the $12:34$ (a) and $13:24$ (b) bipartitions with m_1. The ordinates are plotted in the unit of ebits while the abscissas are dimensionless.
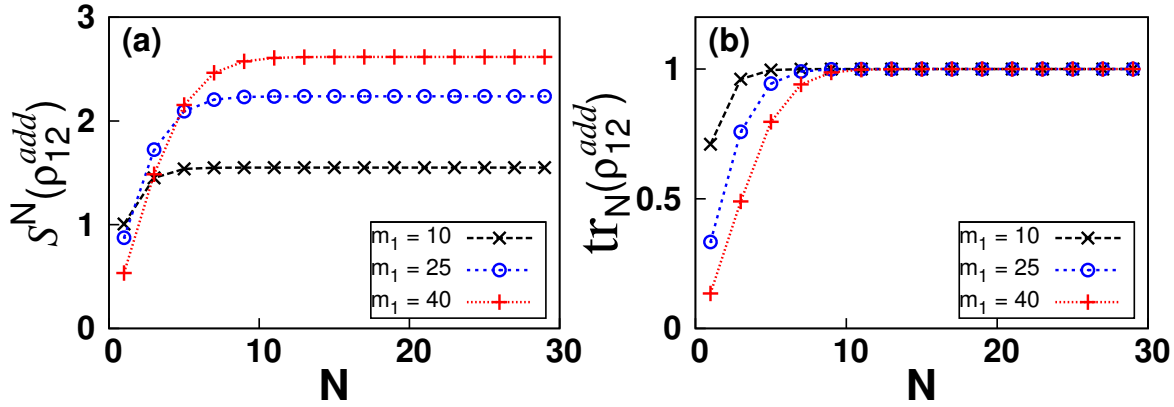
Figure 6.7: (Color online) Plot of convergence of von Neumann entropy, $\mathcal{S}^N(\rho^{add}_{12,m_1})$, in (a) and $\text{tr}_N(\rho^{add}_{12,m_1})$ in (b) against N which is the maximum value of n and n'. We choose three different values of m_1, viz. $m_1 = 10, 25, 40$. We find that for example, for $m_1 = 40$, trace goes to unity and the entropy (entanglement) converges for $N \geq 10$. Here the von-Neumann entropy is measured in the unit of bits and the trace and the abscissas are dimensionless.

always carry out a similar scaling analysis for choosing N.

6.4.2 Behavior of entanglement of photon-added and -subtracted states with two player modes

In this section, keeping the four-mode squeezed vacuum state as the input state, we increase the number of players from one to two modes, and hence the possibilities of choosing the player modes with nontrivial bipartition grows substantially. For a fixed bipartition, we investigate the nature of entanglement by changing the modes in which photons are added or subtracted. Upto now, we have shown that the entanglement content of the resulting state after subtracting photons is either equal or higher than that of the photon-added states. Let us now investigate whether such situation persist when two modes are players.
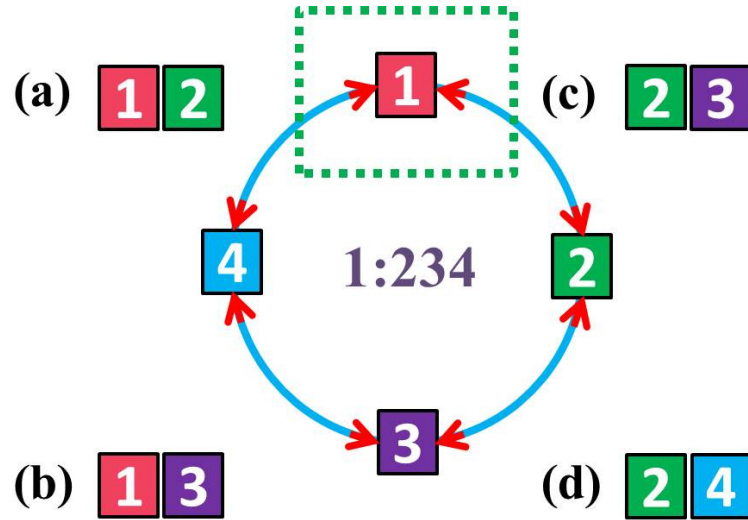
Figure 6.8: Schematic diagram of four non-trivial possibilities of choosing two modes as players in the 1 : 234 bipartition. Other choices can be shown as repetitions due to the symmetry of the FM state.

One part of the bipartite split contains a single mode

We begin by concentrating on the entanglement of the FM state after addition (subtraction) of photons in the 1 : 234 bipartition. In this scenario, there are four possibilities for adding and subtracting photons. As shown in Fig. 6.8, the modes that act as players are as follows:

(a) the first and the second mode,

(b) the first and the third mode,

(c) the second and the third mode, and

(d) the second and the fourth mode.

Other possibilities can be reduced to any one of the above four cases due to the symmetry in the four-mode squeezed state. Moreover, it can be shown that the entanglement pattern of cases (a) and (b) are qualitatively similar while cases (c) and (d) are analogous and hence the entanglement features will be studied in pairs.

Cases (a) and (b): We now consider the situation where either the first and the second modes act as players or the first and the third modes are players. We calculate the $\delta_1^E(m_1, m_i)$ $(i \neq 1)$, when no photons are added and subtracted from the spectator modes. We observe that there exists a region for which $\delta_1^E(m_1, m_i) > 0$, which is in contrast with the case when one mode was player in the preceding subsection (see Fig. 6.9(a)). As seen from the figure, for moderate values of m_1, the boundary between the positive and negative regions is almost a straight line and hence we can find the slope of the straight line which can help to study these cases quantitatively. We find that for high values of m_1, the slope of $\delta_1^E(m_1, m_3) = 0$ is approximately 0.28, which is small compared to the slope of $\delta_1^E(m_1, m_2) = 0$, which is 0.64 (see Fig. 6.9(d)). Moreover, we notice that max $[\delta_1^E(m_1, m_3)] = 0.2 < $ max $[\delta_1^E(m_1, m_2)] = 0.4$ while minimum value of $\delta_1^E(m_1, m_3)(= -2.0)$ is smaller than that of $\delta_1^E(m_1, m_2)(= -1.6)$, in the regions surveyed. Therefore, we can conclude that to create maximal entanglement in this scenario,
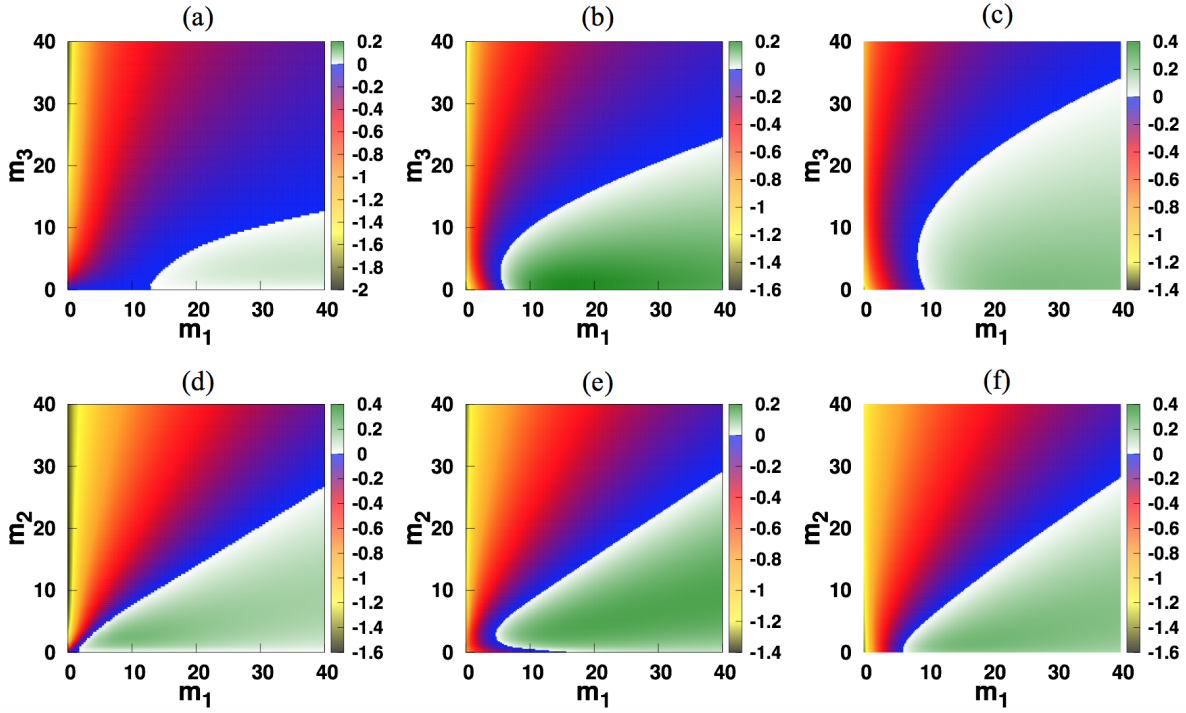
Figure 6.9: Top panel: Behavior of $\delta_1^E(m_1, m_3)$ against m_1 (horizontal axes) and m_3 (vertical axes) when the spectator modes are active, figure(a) both $m_2 = m_4 = 0$, figure (b) $m_2 = 5$, $m_4 = 0$ and in figure (c) $m_2 = m_4 = 5$. We see that by using fixed number of photons to the spectators modes, entanglement of photon added state can be enhanced much faster than the photon subtracted ones. Bottom panel: Similar behavior of $\delta_1^E(m_1, m_2)$ against m_1 (horizontal axes) and m_2 (vertical axes), when no photons are added in the spectator mode (figure (d)), only one spectator mode is active, $m_3 = 5$, $m_4 = 0$ in figure (e) and $m_3 = 0$, $m_4 = 5$ in figure (f). We find that the region where photon addition is better than the subtraction remains almost constant. All the axes are dimensionless, while entanglements are plotted in the unit of ebits.

photon addition is advantageous when one adds photons in the first and the second modes compared to the case of m_1 and m_3 being players (with $m_1 \gg m_i, i = 2, 3$).

In both the cases, spectator modes play an important role in the behavior of entanglement in the 1 : 234 bipartition. As depicted in Fig. 6.9 (b), entanglement in the photon-added state can be increased by adding photons in the spectator modes. For example, when $m_{2(4)} = 5$, $\delta_1^E(m_1, m_3)$ against m_1 and m_3 is depicted in Fig. 6.9(b) and for both $m_2 = m_4 = 5$ in Fig. 6.9(c) . Quantitative comparison can be made between Figs. 6.9 (c) and 6.9 (d). In particular, for $m_1 \gg m_3$, the region with $\delta_1^E(m_1, m_3) > 0$ when no photons are added (subtracted) in the spectator modes can be calculated. In this limit, we assume that the boundary is a straight line and hence the area is the area of a quadrilateral. Let us call the area as Δ_0. In this case, we calculate the area of the quadrilateral when $m_1 \geq 25$ and $m_1 \leq 40$, and we find $\Delta_0 \approx 160$. After adding (subtracting) 5 photons in the second or fourth modes, we find that the area, Δ_5, of the corresponding quadrilateral increases and $\Delta_5 \approx 253$. Moreover the area increases much more, as shown in Fig. 6.9 (c), when both the spectator modes are active, and in such a situation $\Delta_{5,5} \approx 425$. But the scenario is something different in the case of $\delta_1^E(m_1, m_2) > 0$, the area where photon addition produce much more entanglement than photon subtraction, is more or less invariant when the spectator modes are active, as shown in Figs. 6.9 (d), 6.9 (e) and 6.9 (f).
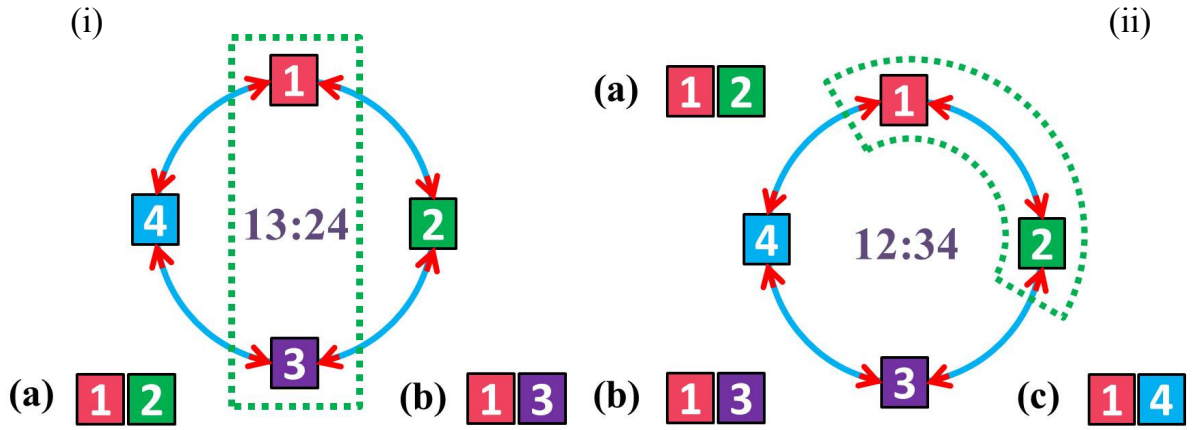
Figure 6.10: Distinct scenarios of the bipartition containing two modes and two player modes in the $13 : 24$ split (figure (i)) and $12 : 34$ (figure (ii)). For the $13 : 24$ bipartition there are two possibilities – (a) first and second as players, (b) first and third as players. In the $12 : 34$ split one can chose – (a) first and second as players, (b) first and third as players, and (c) first and forth as player.

Behavior of entanglement in the $1 : 234$ split for cases (c) and (d) are almost identical with the previous cases. The only difference is that entanglement of the subtracted state is always better than that of the added state when spectator modes are inactive. The picture changes, i.e. entanglement of the photon-added states starts increasing faster than the photon-subtracted states, like in the preceding cases, when fixed numbers of photons are added (subtracted) in the spectator mode(s).

Bipartition containing equal number of modes

We will now consider the case where, we still keep two modes as players but we now divide four-modes into two blocks consisting of two modes instead of one mode in the preceding discussion. In this case, the two nontrivial bipartitions are $12 : 34$ and $13 : 24$. Let us first concentrate on the bipartition $13 : 24$. In this case, the symmetry of the FMSV state after addition or subtraction of arbitrary number of photons in all the modes, given in Eqs. (6.60) and (6.61), ensures that there are only two nontrivial situations in the case of two player modes (see Fig. 6.10 (i)) . They are – (a) when the players are the first and the second modes, and (b) when first and third modes act as players. Cases (a) and (b) show similar entanglement behavior like previous cases, when one part of the bipartition contains a single mode, but the region where the photon addition is much more better than the subtraction changes it form in the plane of the player modes. Here we will briefly analyze this situations.

The reduced density matrix of the first and the third mode, for the photon-added state, is given by

$$
\begin{aligned}
\rho_{13,\{m_i\}}^{add} &= \text{tr}_{24}(|\psi_{\{m_i\}}^{add}\rangle\langle\psi_{\{m_i\}}^{add}|) \\
&= \sum_{n=0}^{\infty} \sum_{r_1=0}^{n} a_{n,r_1,q}|n + m_1 - r_1\rangle_1|m_3 + r_1\rangle_3\langle n + m_1 - q|_1\langle m_3 + q|_3, \quad (6.91)
\end{aligned}
$$
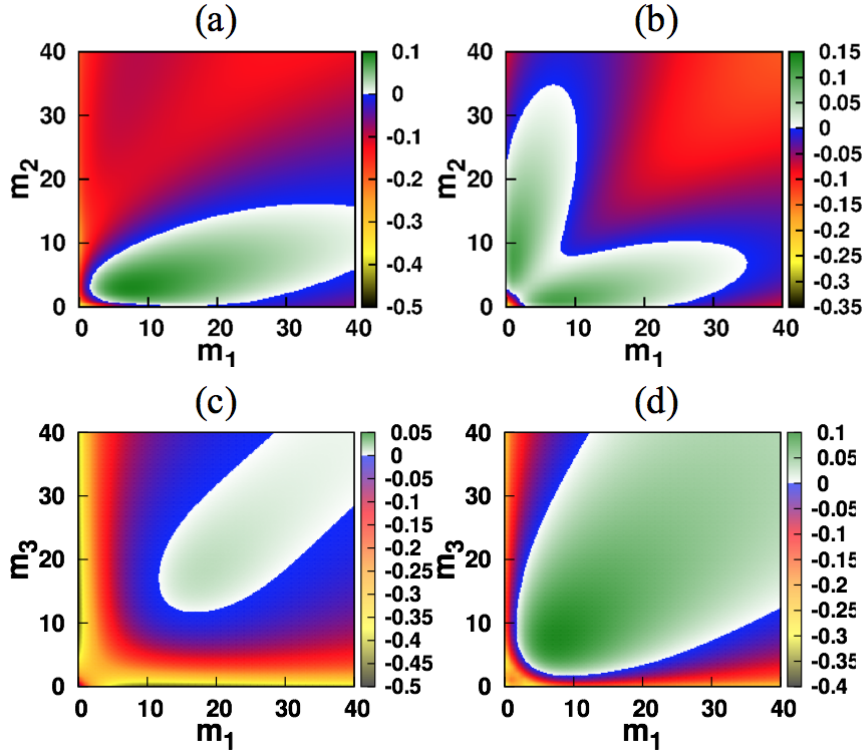
Figure 6.11: Role of spectator modes in δ_{13}^E in the plane of m_1, m_2 and m_1, m_3 when the player modes are active. In (a), $m_3 = 10$ and $m_4 = 0$, while in (b), $m_3 = m_4 = 5$. We see that spectator modes help to enhance entanglement in the photon-added state. In (c) no spectator mode is active, and a positive region emerges around the line $m_1 = m_3 > 14$, which can be enhanced more when one spectator mode is active, as shown in (d) where $m_2 = 4$. All the axes are dimensionless, while entanglements are plotted in the unit of ebits.

where we write

$$
a_{n,r_1,q} = \frac{1}{N_{13}^{add}} \frac{x^n}{2^n} \sum_{r_2=0}^{n} \left(\binom{n}{r_1}\binom{n}{q} \right)^{1/2} \binom{n}{r_2} \left(\frac{(n+m_1-r_1)!}{(n-r_1)!} \frac{(n+m_1-q)!}{(n-q)!} \frac{(m_3+r_1)!}{r_1!} \frac{(m_3+q)!}{(q)!} \right)^{1/2}
$$
$$
\frac{(n+m_2-r_2)!}{(n-r_2)!} \frac{(m_4+r_2)!}{r_2!}. \qquad (6.92)
$$

Similarly, one can also find the two party reduced density matrix, $\rho_{13,\{m_i\}}^{sub}$, for photon subtraction by tracing out the second and fourth modes in Eq. (6.61).

Case (a): If the first and second modes act as players, we find that subtraction is always better than addition for arbitrary values of m_1 and m_2. This case is similar to the case with a single mode being player and cases with second and third modes or second and fourth modes being players. To show once more that spectators play a fundamental role in interchanging the entanglement property for photon addition and subtraction, we elaborate the analysis in two scenarios – (1) when a fixed number of photons are added (subtracted) in a single spectator mode, a positive region emerges, which indicates that the quantum correlation in the $13 : 24$ bipartition is greater for photon addition than that for subtraction, as already seen before. An interesting point to note here is that a positive region appears for small values of m_2 and almost for all values of m_1. This is probably due to the fact that we add photons in the third mode which

belongs to the same block as the first mode. (2) When both the spectator modes are active, the positive region can be seen in both the axis due to symmetry present in the FM state, as depicted in Fig. 6.11(b). **Case** (b): When the first and third mode are chosen as player a small region emerges, where photon addition is better than the photon subtraction, in the plane of m_1 and m_3, in the vicinity of $m_1 = m_2$. The region exists for $m_{1(3)} > 14$, as shown in Fig. 6.11(c). This region increases as one make any one of the spectator modes active, and it increases much rapidly with the increase of number of photon added(subtracted) from the spectator mode, keep subtraction better than addition in the vicinity of $m_1 \approx 0$ and $m_3 \approx 0$, near about the axes. Fig 6.11(d) shows the emergence of this positive area for $m_2 = 4$.

Finally, we concentrate on a nontrivial partition, the $12 : 34$ cut (see Fig. 6.10(ii)). From the perspective of entanglement, this partition is unique. In this scenario, there are three ways to choose the players. We find that with and without participation of spectator modes, entanglement of photon subtraction always higher or equal to that of the photon addition which makes this situation exclusive from others.

6.5   Comparison of logarithmic negativity between two-mode and four-mode states

Upto now, we have considered an FMSV state as input and have compared the behavior of entanglement between photon-added and -subtracted states as well as entanglement of an output state in different bipartitions having different player and spectator modes. In this section, our aim is to make comparison between the output state obtained from the TMSV state after adding or subtracting photons and the two mode state obtained from the FMSV state. To perform such comparison, we discard two modes from the four-mode state and calculate the LN of the two mode reduced state, which we then compare with the LN of the photon-added (subtracted) state that is obtained from the TMSV state as the input [51–54]. In case of the TM state, the output state, after adding (subtracting) photons, still remains pure and hence LN can be calculated analytically [198]. However, for the FM case, the output state is mixed which is obtained by discarding two modes and we adopt the same mechanism as we have done to calculate von Neumann entropy of reduced density matrices, described in Sec. 6.4.1. In particular, we evaluate LN as well as trace for large $n = N$, and then by increasing N, we check whether trace goes to unity upto six decimal points. We truncate the system when trace has already converged to unity, upto six decimal points.

In the TMSV case, photons can be added to either of the modes or to both the modes. On the other hand, there are several scenarios for the four-mode states. If there is a single player, either one of the mode of the output state can act as player or none of the modes of the output state is the player. In case of two players, (i) two players can be the two modes of the output state, (ii) one mode of the output state can be a player, or (iii) the discarded modes can be the player modes.

Before considering the FMSV state, let us first consider the TMSV state as input. Note that the nature of LN qualitatively matches with the von Neumann entropy of the reduced density matrix. As shown in [51–54], when single mode acts as player, the LN for photon addition coincide with the subtraction, which is also the case for the von Neumann entropy. If both the modes act as players, photon addition is always beneficial for entanglement than the photon subtraction [51–54].

In case of a single player or two players in the FM state, if the output state contains the player mode(s), then the reduced two-mode state obtained from the photon-added state has higher LN than that of the
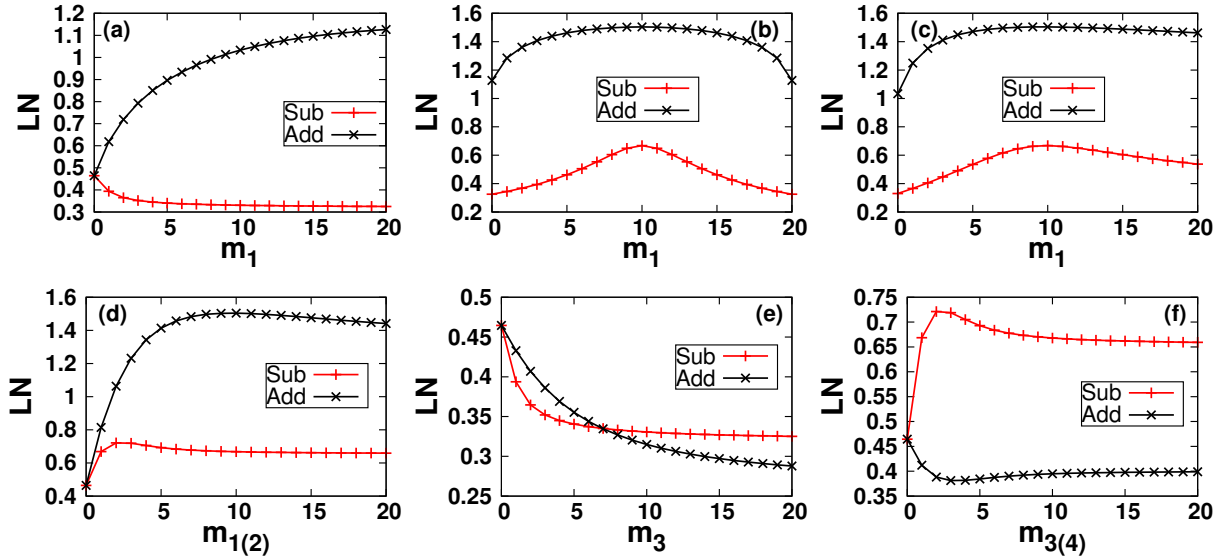
Figure 6.12:   LN between the first and second modes obtained from the FM output state. (a) First mode is player. (b) First and second modes are players with $m_1 + m_2 = 20$. (c) First mode is player while the second one is spectator with $m_2 = 10$. (d) First and second modes are players with $m_1 = m_2$. (e) Third mode as player, which has been traced out in this computation. (f) Third and Forth modes are player with $m_3 = m_4$. The ordinates are plotted in the unit of ebits while the abscissas are dimensionless.

photon-subtracted state. Hence, the behavior of LN of the output state from TM and FM state are identical. As we have shown, this is not the case if we consider the behavior of entanglement of pure four-mode output state in bipartitions. Fig. 6.12 depicts the behavior of LN of the two-mode reduced state from the four-mode output state when the two modes containing the output states, first mode as well as the second mode acts as player and the discarded modes of the two mode state are players. In Figs. 6.12(a)–(d), no photons are added (subtracted) in the spectator modes. We observe that when there is a single player e.g., the first mode of the reduced state, entanglement increases (decreases) monotonically, if photons are added (subtracted) (see Fig. 6.12(a)). However, such monotonicity with respect to the number of photons added (subtracted) is lost if photons are added (subtracted) in both the modes with total number of photons being fixed as shown in Fig. 6.12(b). A similar qualitative feature in entanglement is seen when the first mode acts as player while second mode is a spectator having fixed finite number of photons (see Fig. 6.12(c)) and equal number of photons added(subtracted) from both first and second mode (see Fig. 6.12(d)). We find that the bipartite entanglement reaches its maximum with respect to m_1, when equal number of photons are added (subtracted) in both the modes i.e. $m_1 = m_2$, in Fig 6.12(b) and $m_1 \approx m_2$ in Fig. 6.12(c). But this is not the case in Fig. 6.12(d), for photon addition the maximum entanglement is for $m_{1(2)} = 8$, and $m_{1(2)} = 3$ for subtraction.

Lastly, we consider the scenario, when we add and subtract photons in the discarded modes i.e., in the third and fourth modes, and we find LN between the first and the second modes, which are spectators. LN of the output state decreases if one of the discarded modes act as a player. For example, by taking third mode as player, we plot LN of the first and the second mode with m_3 in Fig. 6.12(e). Unlike previous cases, LN of the photon-subtracted state is higher than that of the added state when $m_3 \geq 9$ which can never be observed for the TM case. LN of the photon-subtracted state is more pronounced than that of the added one if both the discarded modes act as players. The same number of photons are

added (subtracted) in (from) both the spectator modes, i.e. $m_3 = m_4$, as shown in Fig. 6.12(f) in which $\text{LN}(\rho_{34}^{sub}) \geq \text{LN}(\rho_{34}^{add})$.
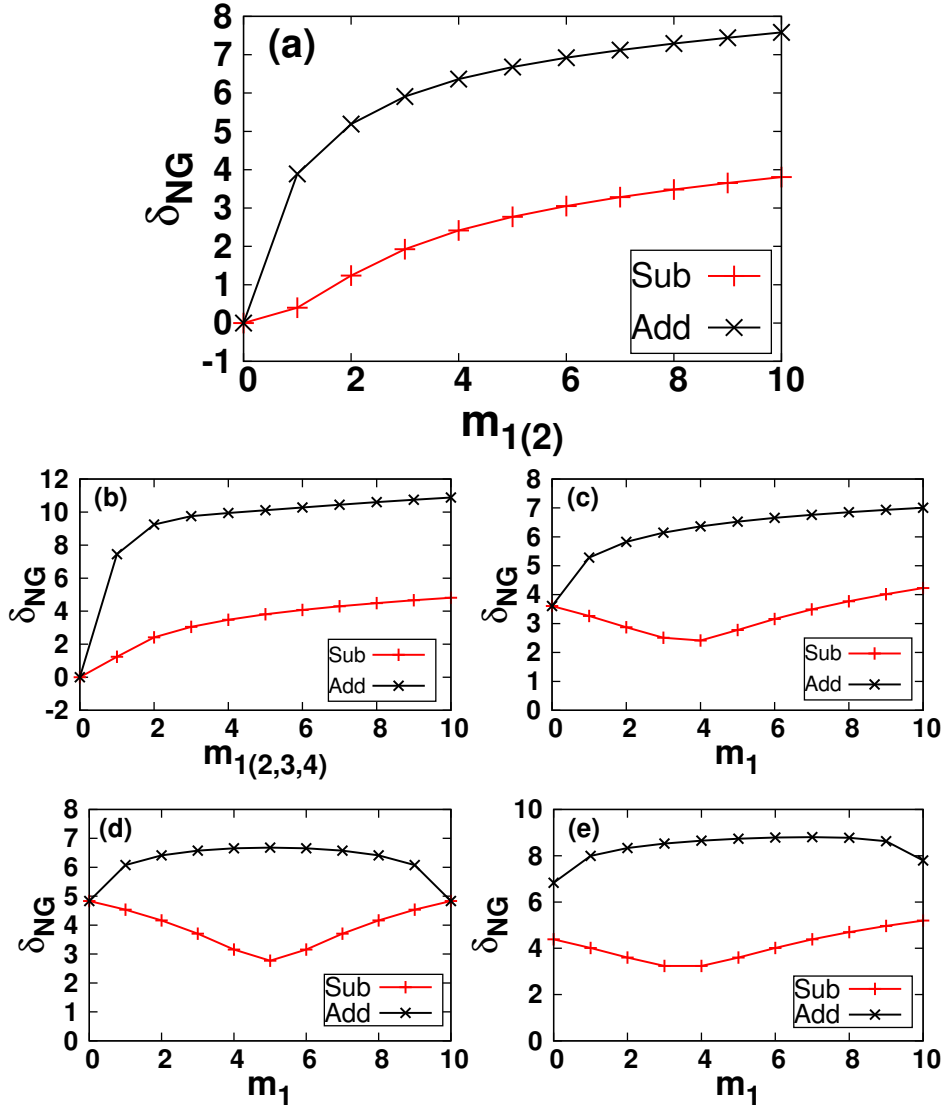
Figure 6.13: Behavior of non-Gaussianity measure, δ_{NG} against $m_i, i = 1, 2, 3, 4$. (a) First and second mode acts as players in which $m_1 = m_2$. (b) All the modes are players and equal number of photons are added (subtracted). (c) Only one mode is player and a fixed number of photons, $m_2 = 4$, are added (subtracted). (d) First and second modes are players with $m_1 + m_2 = 10$. Spectator modes are ineffective. (e) Spectator modes are active with $m_3 = 4$ and in player modes, $m_1 + m_2 = 10$. The ordinates are plotted in the unit of bits while the abscissas are dimensionless.

6.6 Measure of non-classicality in continuous variable systems

The negative value of the quasiprobability distribution, the Wigner function, [186] of a given state indicates the non-classical nature of the corresponding state while the positivity implies the opposite. On the other hand, it is known that the Wigner function of a Gaussian state is always positive [187,188]. Therefore, one can define a measure of non-Gaussianity or non-classicality by measuring the departure of a given state,

ρ, in a CV system from a Gaussian state. In terms of relative entropy distance, it is given by [206–208]

$$\delta_{NG}(\varrho) \quad = \quad S(\varrho||\varrho_G) = S(\varrho_G) - S(\varrho), \tag{6.93}$$

where $S(\eta||\sigma) = -\text{tr}(\eta \log_2 \sigma) - S(\eta)$, and ρ_G is a Gaussian state which has same covariance matrix and first moment as ρ. Here, $S(\sigma) = -\text{tr}(\sigma \log_2 \sigma)$ is the von Neumann entropy of σ.

For an N-mode continuous variable system ρ, with quadrature operators $\{\hat{q}_j, \hat{p}_j\}$, $j = 1, \ldots, N$, the covariance matrix σ is given by

$$\sigma_{jk} = \frac{1}{2} \langle \hat{\xi}_j \hat{\xi}_k + \hat{\xi}_k \hat{\xi}_j \rangle - \langle \hat{\xi}_j \rangle \langle \hat{\xi}_k \rangle, \tag{6.94}$$

where the expectation is computed with respect to the state ρ and

$$\hat{\xi} = (\hat{q}_1 \ \hat{p}_1 \ \hat{q}_2 \ \hat{p}_2 \ \cdots \ \hat{q}_N \ \hat{p}_N)^T. \tag{6.95}$$

The von Neumann entropy, $S(\varrho_G)$, of any Gaussian state can be calculated by using its covariance matrix, σ. For an N mode Gaussian state, ϱ_G, the von Neumann entropy is defined [36] as

$$S(\varrho_G) = \sum_{k=1}^{N} g(\nu_k), \tag{6.96}$$

where ν_k is the Williamson normal form [209] of the covariance matrix of the N-mode Gaussian state ϱ_G, and the function $g(x)$ is given by

$$g(x) = -\frac{x+1}{2} \log_2 \left(\frac{x+1}{2} \right) - \frac{x-1}{2} \log_2 \left(\frac{x-1}{2} \right). \tag{6.97}$$

As we have mentioned in the earlier section that the photon addition and subtraction is one of the ways to create a non-Gaussian state. Here, we quantify the departure of the photon-added (-subtracted) FMSV state from Gaussianity, as a function of added (subtracted) photons from the player modes. Since the photon-added (-subtracted) FM state is in a pure state, the second term of $\delta_{NG}(\rho)$, given in Eq. (6.93) vanishes. To calculate $\delta_{NG}(\rho)$, we have to find the covariance matrix of ρ_G, which is same as $\rho_{\{m_i\}}^{add/sub} = |\psi\rangle\langle\psi|_{\{m_i\}}^{add/sub}$. It is given by

$$\sigma_\varrho = \begin{pmatrix} \langle q_1^2 \rangle I & \langle q_1 q_2 \rangle \sigma_z & \langle q_1 q_3 \rangle I & \langle q_1 q_4 \rangle \sigma_z \\ \langle q_1 q_2 \rangle \sigma_z & \langle q_2^2 \rangle I & \langle q_2 q_3 \rangle \sigma_z & \langle q_2 q_4 \rangle I \\ \langle q_1 q_3 \rangle I & \langle q_2 q_3 \rangle \sigma_z & \langle q_3^2 \rangle I & \langle q_3 q_4 \rangle \sigma_z \\ \langle q_1 q_4 \rangle \sigma_z & \langle q_2 q_4 \rangle I & \langle q_3 q_4 \rangle \sigma_z & \langle q_4^2 \rangle I \end{pmatrix}, \tag{6.98}$$

where, $q_i = \hat{a}_i + \hat{a}_i^\dagger$, and the expectations are taken over the photon-added and -subtracted FM state, given in Eqs. (6.60) and (6.61) and

$$\langle q_1^2 \rangle^{add} \quad = \quad 1 + 2m_1 + 2 \sum_{n,r_1,r_2} (p_{n,r_1,r_2}^{\{m_i\}})^2 (n - r_1), \quad \langle q_2^2 \rangle^{add} = 1 + 2m_2 + 2 \sum_{n,r_1,r_2} (p_{n,r_1,r_2}^{\{m_i\}})^2 (n - r_2),$$

$$\langle q_3^2 \rangle^{add} \quad = \quad 1 + 2m_3 + 2 \sum_{n,r_1,r_2} (p_{n,r_1,r_2}^{\{m_i\}})^2 r_1, \qquad \langle q_4^2 \rangle^{add} = 1 + 2m_4 + 2 \sum_{n,r_1,r_2} (p_{n,r_1,r_2}^{\{m_i\}})^2 r_2,$$

$$\langle q_1 q_2 \rangle^{add} = 2 \sum_{n,r_1,r_2} p^{\{m_i\}}_{n,r_1,r_2} p^{\{m_i\}}_{n+1,r_1,r_2} \times \sqrt{(n+m_1-r_1+1)(n+m_2-r_2+1)},$$

$$\langle q_1 q_3 \rangle^{add} = 2 \sum_{n,r_2} \sum_{r_1=0}^{n-1} p^{\{m_i\}}_{n,r_1,r_2} p^{\{m_i\}}_{n,r_1+1,r_2} \sqrt{(n+m_1-r_1)(m_3+r_1+1)},$$

$$\langle q_1 q_4 \rangle^{add} = 2 \sum_{n,r_1,r_2} p^{\{m_i\}}_{n,r_1,r_2} p^{\{m_i\}}_{n+1,r_1,r_2+1} \times \sqrt{(n+m_1-r_1+1)(m_4+r_2+1)},$$

$$\langle q_2 q_3 \rangle^{add} = 2 \sum_{n,r_1,r_2} p^{\{m_i\}}_{n,r_1,r_2} p^{\{m_i\}}_{n+1,r_1+1,r_2} \times \sqrt{(n+m_2-r_2+1)(m_3+r_1+1)},$$

$$\langle q_2 q_4 \rangle^{add} = 2 \sum_{n,r_1} \sum_{r_2=0}^{n-1} p^{\{m_i\}}_{n,r_1,r_2} p^{\{m_i\}}_{n,r_1,r_2+1} \times \sqrt{(n+m_2-r_2)(m_4+r_2+1)},$$

$$\langle q_3 q_4 \rangle^{add} = 2 \sum_{n,r_1,r_2} p^{\{m_i\}}_{n,r_1,r_2} p^{\{m_i\}}_{n+1,r_1+1,r_2+1} \times \sqrt{(m_3+r_1+1)(m_4+r_2+1)},$$

where $\sum_{n,r_1,r_2}$ in the photon-added states, is the short form of $\sum_{n=0} \sum_{r_1=}^{n} \sum_{r_2=0}^{n}$. Further, for the photon-subtracted states,

$$\langle q_1^2 \rangle^{sub} = 1 - 2m_1 + 2 \sum_{n,r_1,r_2} (q^{\{m_i\}}_{n,r_1,r_2})^2 (n-r_1), \quad \langle q_2^2 \rangle^{sub} = 1 - 2m_2 + 2 \sum_{n,r_1,r_2} (q^{\{m_i\}}_{n,r_1,r_2})^2 (n-r_2),$$

$$\langle q_3^2 \rangle^{sub} = 1 - 2m_3 + 2 \sum_{n,r_1,r_2} (q^{\{m_i\}}_{n,r_1,r_2})^2 r_1, \qquad \langle q_4^2 \rangle^{sub} = 1 - 2m_4 + 2 \sum_{n,r_1,r_2} (q^{\{m_i\}}_{n,r_1,r_2})^2 r_2,$$

$$\langle q_1 q_2 \rangle^{sub} = 2 \sum_{n,r_1,r_2} q^{\{m_i\}}_{n,r_1,r_2} q^{\{m_i\}}_{n+1,r_1,r_2} \times \sqrt{(n-m_1-r_1+1)(n-m_2-r_2+1)},$$

$$\langle q_1 q_2 \rangle^{sub} = 2 \sum_{n,r_1,r_2} q^{\{m_i\}}_{n,r_1,r_2} q^{\{m_i\}}_{n+1,r_1,r_2} \times \sqrt{(n-m_1-r_1+1)(n-m_2-r_2+1)},$$

$$\langle q_1 q_3 \rangle^{sub} = 2 \sum_{n,r_2} \sum_{r_1=m_3}^{n-m_1-1} q^{\{m_i\}}_{n,r_1,r_2} p^{\{m_i\}}_{n,r_1+1,r_2} \times \sqrt{(n-m_1-r_1)(r_1-m_3+1)},$$

$$\langle q_1 q_4 \rangle^{sub} = 2 \sum_{n,r_1,r_2} q^{\{m_i\}}_{n,r_1,r_2} q^{\{m_i\}}_{n+1,r_1,r_2+1} \times \sqrt{(n-m_1-r_1+1)(r_2-m_4+1)},$$

$$\langle q_2 q_3 \rangle^{sub} = 2 \sum_{n,r_1,r_2} q^{\{m_i\}}_{n,r_1,r_2} q^{\{m_i\}}_{n+1,r_1+1,r_2} \times \sqrt{(n-m_2-r_2+1)(r_1-m_3+1)},$$

$$\langle q_2 q_4 \rangle^{sub} = 2 \sum_{n,r_1} \sum_{r_2=m_4}^{n-m_2-1} q^{\{m_i\}}_{n,r_1,r_2} q^{\{m_i\}}_{n,r_1,r_2+1} \times \sqrt{(n-m_2-r_2)(r_2-m_4+1)},$$

$$\langle q_3 q_4 \rangle^{sub} = 2 \sum_{n,r_1,r_2} q^{\{m_i\}}_{n,r_1,r_2} q^{\{m_i\}}_{n+1,r_1+1,r_2+1} \times \sqrt{(r_1-m_3+1)(r_2-m_4+1)},$$

where $\sum_{n,r_1,r_2}$, is the short form of $\sum_{n=M} \sum_{r_1=m_3}^{n-m_1} \sum_{r_2=m_4}^{n-m_2}$, and $M = \max\{m_1+m_3, m_2+m_4\}$. The $p^{\{m_i\}}_{n,r_1,r_2}$ and $q^{\{m_i\}}_{n,r_1,r_2}$ are given in Eqs. (6.60) and (6.61) respectively.

The Williamson normal form of Eq. (6.98) can be evaluated by using the prescription given in [210]. We numerically calculate the Williamson normal form of the matrix in Eq. (6.98) for both photon addition and subtraction and calculate the non-Gaussianity, which in this case reduces to $S(\rho^{add/sub}_{G,\{m_i\}})$.

In all the cases, photon addition leads to a rapid departure of Gaussianity than that of the photon subtraction. We also notice that if among four modes, photons are added only in two modes, then behavior of δ_{NG} obtained in the FM state and the TM state are qualitatively similar. It is clear from the behavior

of the non-Gaussianity measure that photon-subtracted state become slowly non-Gaussian as compared to the photon-added state and the behavior remains unchanged irrespective of the choices of the player and the spectator modes (see Fig. 6.13). The rich picture of the role of different modes, captured by entanglement, is not seen by the non-Gaussianity measure and hence indicates that there is possibly no direct connection between non-Gaussianity and entanglement content of the output state obtained after photon addition (subtraction) [51–54].

6.7 In Closing

In this chapter, we discuss the N-mode squeezed vacuum state, and find its form in terms of the Fock number basis for $N = 2$, TMSV state and for $N = 4$, FMSV state. We have also discussed the procedure to prepare the FMSV state in the laboratory by using linear optical devices. Photon addition and subtraction constitute useful methods to prepare non-Gaussian states. It has already been established that non-Gaussian states are useful in various quantum mechanical tasks ranging from entanglement distillation to quantum error correction. We have investigated the entanglement properties of the non-Gaussian states generated by adding or subtracting photons in Gaussian states. In case of two mode states, entanglement of photon-added states is known to be equal or higher than that of the photon-subtracted ones.

We have shown that this is not the case when one increases the number of modes. We found that for four-mode states, the trend of entanglement distribution in different bipartitions of the photon-added (-subtracted) states is much richer than that in the two-mode states. Specifically, we showed that there exists a scenario, in which multimode entanglement content of the photon-subtracted state is always higher than that of the corresponding photon-added one. The results remained unchanged even if one discarded two modes from the four-mode output state. Moreover, we showed that the picture that emerges from entanglement of the output state does not match with the behavior in the same states of distance-based non-Gaussianity measure. Upto now, it was known that among addition and subtraction, addition is more beneficial. But our work shows that photon subtraction can also be advantageous if we consider a state of a higher number of modes.

The main motivation to study such four-mode entangled state is to use this kind of states in communication protocols like, for example, the distributed dense coding with two senders and two receivers. We believe that by taking the four-mode squeezed vacuum state as the resource state quantum communication networks like the ones described in preceding chapters can be built by using continuous variable systems in near future, and our investigation on entanglement patterns of non-Gaussian multimode states is an small step towards that.

The results of this Chapter are based on the following paper:

1. *Subtraction better than addition: Entanglement in multimode squeezed vacuum post-interface with photons*, **Tamoghna Das**, R. Prabhu, Aditi Sen De, Ujjwal Sen, Phys. Rev. A **93**, 052313 (2016).

Chapter 7

Summary and Future Directions

In last few decades, it has been established that bipartite as well as multipartite quantum correlations (QC), in particular, entanglement plays a crucial role in many quantum technological tasks including quantum state transfer, classical information transmission, secure quantum key distribution, error correction, quantum computation etc. In particular, when the classical information transmission with the help of a shared entangled state (dense coding (DC)) is under consideration, we have noticed that for a single sender and a single receiver scenario, the capacity of dense coding is directly related to the entanglement of the shared bipartite pure quantum state. In other words, a pure bipartite state is useful for dense coding if and only if it is entangled. Such one-to-one correspondence between entanglement and capacities are missing for a shared bipartite mixed states as well as multipartite pure states. In this thesis, we mainly concentrate on multiport quantum communication scheme. There is no doubt that point-to-point communication has very limited commercial use and hence it is important to build a quantum communication network having advantages over classical protocols. Since it was seen that bipartite entangled states are useful for most of the communication protocols, sharing multipartite entangled states are believed to be advantageous in quantum information transfer. In recent times, a lot of interest has been created to characterize and quantify quantum correlations in a multiparty domain. However, a sheer connection between the capacity in the multiparty domain, especially multiport classical capacity of a quantum channel and the multiparty quantum correlation measures is still missing. There can be two prominent reasons for that – first, multipartite computable entanglement measures for arbitrary states is still not available although there are some entanglement measures for multipartite pure states which can be computed easily. Secondly the closed form of the multiparty classical/DC capacity for multiple senders to more than one receivers is not yet available in the literature. DC capacity is only known for multiple senders to a single receiver, and an upper bound is derived for the two receivers, when the receivers are in distant locations and can only allowed to perform local operations and classical communications (LOCC). In this thesis, we found a connection between the multiparty QC measures and the multiparty DC capacities of the shared state, when there are arbitrary numbers of senders and a single as well as two receivers.

Any information transfer protocol can not be executed in an isolated situation and hence some non-zero amount of environmental noise surely interact with the system, thereby possibly reducing the capability of the communication scheme. In case of DC, the noise can act either at the time of sharing of the quantum state among all the parties or can be present in the transmission channel, when the sender sends their

encoded part to the receiver(s). Finding the noisy multiparty DC capacity is, in general, very hard and there are only very few noise models for which the capacity is known for the single receiver case. And it was found that the DC capacity of the shared state decreases under this noisy scenario. In this thesis, we also addressed the effects of noise on the multiport classical capacities.

7.1 Summary of the Thesis

Before presenting the main results in this thesis, we briefly introduce some of the well known computable measures of multiparty entanglement and other QC, which can be broadly classified into two categories – distance-based and monogamy-based measures in Chapter 2. In the subsequent chapter, 3, we discuss the DC protocol for a shared state, involving both bipartite and multipartite states for both noiseless and noisy scenarios. The capacities of DC with multiple senders and a single receiver is derived. When the noise acts on the encoded part during transmission, the compact form of DC capacity for a covariant noise is also discussed. The main results obtained in this thesis is presented in chapters 4 to 6.

A connection between multiparty QC content and the multiparty DC capacity involving a single receiver for both noiseless and noisy scenario has been established in Chapter 4. In particular, we show that for the noiseless channel, if multipartite QC of an arbitrary multipartite state of arbitrary number of qubits is the same as that of the corresponding generalized Greenberger-Horne-Zeilinger state, then the multipartite dense coding capability of former is the same or better than that of the generalized Greenberger-Horne-Zeilinger state. The result is generic in a sense that the above relation holds for the multiparty QC measures defined from two different perspectives, the geometric entanglement and the monogamy-based QC measures. Interestingly, it was also shown that in a noisy channel scenario, for both uncorrelated and correlated noise models, the relative abilities of the quantum channels to transfer classical information can get inverted by administering a sufficient amount of noise. When the shared state is an arbitrary multipartite mixed state, we also establish a link between the classical capacity for the noiseless case and multipartite quantum correlation measures, in particular, the discord monogamy score.

In Chapter 5, we consider a case of classical information transfer between arbitrary number of senders and two receivers, situated in two distant locations so that they are only allowed to perform LOCC operations. The exact DC capacity in this case is not yet known even for the noiseless case, only the upper bound was derived which was shown to saturate for the Greenberger-Horne-Zeilinger state. We discuss these results in details in this chapter. We then derived an upper bound on the LOCC-DC capacity in presence of noise in the transmission channel which is further tightened for the covariant noisy channel. We explicitly evaluated the upper bounds on the noisy LOCC-DC capacity for amplitude damping, phase damping, and Pauli channels, when a four-qubit GHZ state is shared between two senders and two receivers. We also established a relation between the genuine multipartite entanglement and the upper bound on the capacity of distributed dense coding or LOCC-DC, of shared four-qubit quantum state, both in the noiseless and in the noisy scenarios.

Upto now, we discussed all the results obtained in finite-dimensional Hilbert spaces. However, one of the important physical systems in which quantum communication schemes can be realized is the class of continous variable systems. In chapter 6, we investigated the entanglement patterns of non-Gaussian photon added and subtracted four mode squeezed vacuum states, in several bipartitions and the same for the two-mode reduced density matrix obtained from the four-mode state. Note that non-Gaussian states

are shown to be essential for certain quantum information tasks and photon addition-subtraction to a gaussian state is an useful method to create a non-Gaussian state in the laboratory with currently available technology. We have analytically proved that the entanglement increases monotonically, with the addition and subtraction of photons. Unlike, two-mode squeezed states under photon-addition and subtraction, we found that the photon-subtracted state in this four-mode case can give us higher entanglement than the photon added state.

7.2 Future Directions

We witnessed the fact that by using a shared maximally entangled state, the sender can send classical information to the receiver upto the doubled of its classical limit. In the DC protocol as shown in section 3.1.1, we have seen that when the shared state is maximally entangled, the DC protocol is deterministic in nature, i.e., the messages that the senders want to send can be encoded to the mutually orthogonal states which can be perfectly discriminated by global measurements. Moreover, we noticed that such deterministic nature does not exists, thereby becoming a probabilistic scheme, when the shared entanglement is slightly deviated from its maximal value. At this point, the question that one can ask is the following: Is it possible to design a quantum communication protocol which can deterministically transfer classical information, beyond the classical value with the help of a shared state which is not maximally entangled in a single copy level? In particular, we want to address the following query: Suppose Alice and Bob share an arbitrary pure quantum state $|\psi_{AB}\rangle \in \mathcal{H}^A \otimes \mathcal{H}^B$, in the finite dimensional Hilbert spaces of dimensions d_A and d_B respectively. Depending on the messages that Alice wants to send, she can choose the unitary operators $\{U_A^x\}$, such that

$$\langle \psi_{AB}|(U_A^{y\dagger} \otimes I_B)(U_A^x \otimes I_B)|\psi_{AB}\rangle = \delta_{xy}, \tag{7.1}$$

i.e., the encoded states, $|\psi_{AB}^x\rangle = U_A^x \otimes I_B|\psi_{AB}\rangle$, are always mutually orthogonal. Here, we assume that $|\psi_{AB}\rangle$ is not maximally entangled, i.e., all of its Schmidt coefficients (see Eq. (2.10)) are not equal. Now the task is to find out the maximal numbers of $\{U_A^x\}$, such that the above equation holds for all $|\psi_{AB}\rangle$. Suppose that the maximal number of such unitary operators is $N_{\max}^\psi$, we will then say that the deterministic dense coding is possible if and only if $N_{\max}^\psi > d_A$, where d_A is the classical limit of the information transfer. This DC protocol is also different from the DC protocol discussed in Chapter 3, since it can be achieved in a single-copy level, rather than of considering an asymptotic way of transferring classical bits in a probabilistic manner. Here, Alice encodes the classical information by acting unitary operators on her parts in such a way that upon receiving the entire system, Bob can always distinguish the output states without any error i.e., deterministically by performing global measurements. Such protocol for a single sender and a single receiver was introduced in Ref. [126], and coined the name deterministic dense coding (DDC) which has hence been extensively studied [127–130] for a single sender and a single receiver. Since the protocol is at the single-copy level, it is also important from an experimental point of view. For a proposal of experiment, one can also look in Ref. [211].

The capacity of DDC, can be quantified as $\log_2(N_{\max}^\psi)$, which is clearly $\leq C(|\psi_{AB}\rangle)$, the DC capacity defined in Sec. 3.10. For an unentangled state, the DDC capacity reduces to the classical limit, while the maximally entangled states saturate the upper bound, coinciding with the DC capacity. However, it was observed [126] that unlike the DC capacity, there is no one to one connection of DDC with entanglement
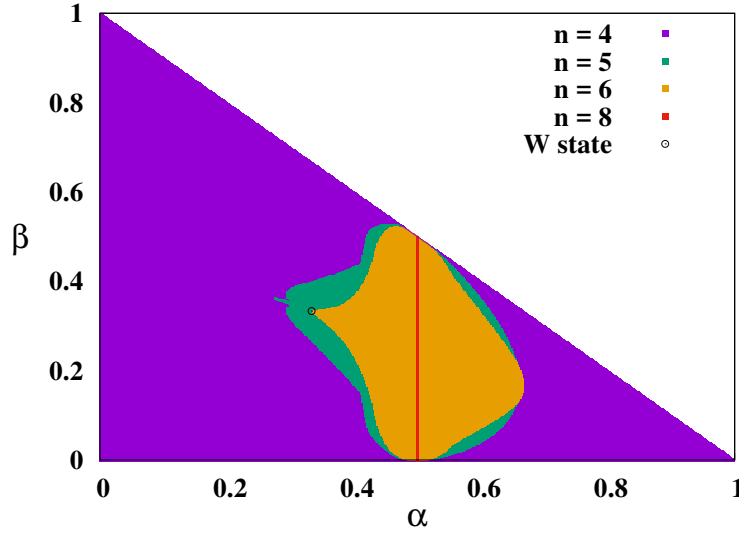
Figure 7.1: Map of maximal number of unitaries N_{max}^{gW} for gW states, given in Eq. (7.3), shared between two senders S_1, S_2 and a single receiver R, with respect to their parameters α and β. All quantities are dimensionless.

content of a shared state. In particular, it was proven that the entire family of bipartite pure states with $d_A = d_B = 2$, except the maximally entangled state, the Bell states given in Sec. 3.1.1 [126], is useless for DDC. Such no-go theorem is no more true if one goes beyond qubit system, e.g., for a state, $|\psi_{AB}\rangle \in \mathbb{C}^3 \otimes \mathbb{C}^3$, the Hilbert space of dimension 3 over the complex field.

However, without going to the higher dimensional system, one can also try to find out whether DDC is possible even in the qubit system, by increasing the numbers of senders and receivers. Let us consider a $(M + 1)$-party pure state $|\psi_{S_1 S_2 ... S_M R}\rangle$ which is shared between the M senders, $S_1, S_2, ..., S_M$, and a single receiver, R. The set for arbitrary local unitary matrices, $\{U_{S_k}^x\}$, is performed by each sender, S_k. Our task is to find out the maximal number of unitaries of the form $\{\bigotimes_k U_{S_k}^x\}$ such that the set of output states $\{\bigotimes_k U_{S_k}^x \otimes \mathbb{I}_R |\psi_{S_1 S_2 ... S_M R}\rangle\}$ that has been sent to the receiver is mutually orthogonal to each other. In other words, we need to find $\{U_{S_k}^x\}$, satisfying

$$\langle \psi_{S_1 S_2 ... S_M R}| \big(\bigotimes_k U_{S_k}^y \otimes \mathbb{I}_R\big)^\dagger \big(\bigotimes_{k'} U_{S_{k'}}^x \otimes \mathbb{I}_R\big) |\psi_{S_1 S_2 ... S_N R}\rangle = \delta_{xy}. \tag{7.2}$$

To obtain the capacity of DDC in this multi-senders scenario, one requires to find out the maximal number of such local unitaries, N_{max}^ψ.

In Ref. [61], we address this question of building a DDC network between several senders and a single receiver. Interestingly, we have found that DDC is possible if a three-qubit pure state is shared between two senders and a single receiver. The set of three-qubit pure states can be divided into two disjoint sets of states [213], according to their transformability under stochastic local operations and classical communication (SLOCC), – the GHZ [56] and the W classes [131]. We show that the DDC scheme can also capture this difference. In particular, we have analytically found that the DDC protocol with quantum advantage is *not* possible when the shared state is a generalized GHZ state except when it is a GHZ state for which DDC and DC attain the maximum capacities. We show that such no-go theorem for DDC with the generalized GHZ states also holds for more than two senders and a single receiver. On the other hand,

by numerical simulations, we have found that the DDC scheme can be executed by using the generalized W states, given by

$$|gW_{S_1 S_2 R}\rangle = \sqrt{\alpha}|001\rangle + \sqrt{\beta}|010\rangle + \sqrt{1-\alpha-\beta}|100\rangle, \qquad (7.3)$$

beyond the classical limit, which is clearly depicted in Fig. 7.1. In the same figure, we map numerically-obtained values of N_{max}^{gW} with the parameters of the gW state, α and β, which clearly depicts the quantum advantage of DDC. We also perform a comparison between the states from the GHZ- and the W-classes according to their usefulness in DDC. In case of a single sender and a single receiver, it was found that for two-qudit states, the maximal number of unitary operators can not be $d^2 - 1$ [212]. For more than one senders, when a $(M+1)$-party state is shared between M senders and a single receiver, each having dimension d, we also observe that the maximal number of unitaries cannot reach $d^{M+1} - 1$. We have explicitly verified for $d = 2$ and for $M = 2$ and 3 [61].

In the case of a single receiver, the question also remains unsolved for the DDC protocol with mixed states, i.e. whether such DDC scheme with quantum advantage exists for arbitrary mixed states. Towards developing a deterministic quantum communication network, it is still an open question whether one can design a DDC protocol having quantum advantage with the arbitrary number of receivers, when all the receivers are in distant locations. Even, for the case of two distant receivers, the distributed DDC turns out to be more complicated. In case of two receivers, to address the question of DDC with arbitrary pure states, one requires to consider optimization over unitary encodings and at the same time, one has to design a LOCC protocol to distinguish the orthogonal states produced by the senders as discussed in Sec. 5.3.2 for the probabilistic dense coding protocol. Such questions are interesting and require careful analysis. Our aim is to overcome these shortcomings in building quantum communication network in near future.

Bibliography

[1] C. H. Bennett and G. Brassard, in Proceedings of the International Conference on Computers, Systems and Signal Processing, Bangalore, India (IEEE, NY, 1984).

[2] A. Ekert, Phys. Rev. Lett. **67**, 661 (1991).

[3] N. Gisin, G. Ribordy, W. Tittel, and H. Zbinden, Rev. Mod. Phys. **74**, 145 (2002).

[4] C. H. Bennett, and S. J. Wiesner, Phys. Rev. Lett. **69**, 2881 (1992).

[5] C. H. Bennett, G. Brassard, C. Crépeau, R. Jozsa, A. Peres, and W. K. Wootters, Phys. Rev. Lett. **70**, 1895 (1993).

[6] R. Horodecki, P. Horodecki, M. Horodecki, and K. Horodecki, Rev. Mod. Phys. **81**, 865 (2009).

[7] A. R. Calderbank and P. W. Shor, Phys. Rev. A **54**, 1098 (1996).

[8] A. M. Steane, Phys. Rev. Lett. **77**, 793 (1996).

[9] H. J. Briegel, D. Browne, W. Dür, R. Raussendorf, and M. van den Nest, Nat. Phys. **5**, 19 (2009).

[10] M. Lewenstein, A. Sanpera, V. Ahufinger, B. Damski, A. Sen(De), and U. Sen, Adv. Phys. **56**, 243 (2006).

[11] L. Amico, R. Fazio, A. Osterloh, and V. Vedral, Rev. Mod. Phys. **80**, 517 (2008).

[12] A. S. Holevo, Probl. Pereda. Inf. **9**, 3 (1973).

[13] B. Schumacher and M. D. Westmoreland, Phys. Rev. A **56**, 131 (1997).

[14] A. S. Holevo, IEEE Trans. Inf. Theory **44**, 269 (1998).

[15] T. Hiroshima, J. Phys. A: Math. Gen. **34**, 6907 (2001).

[16] S. Bose, M.B. Plenio, and V. Vedral, J. Mod. Opt. **47**, 291 (2000).

[17] G. Bowen, Phys. Rev. A **63**, 022302 (2001).

[18] M. Horodecki, P. Horodecki, R. Horodecki, D. Leung, and B. Terhal, Quantum Inf. and Comput. **1**, 70 (2001).

[19] X. S. Liu, G.L. Long, D. M. Tong, and F. Li, Phys. Rev. A **65**, 022304 (2002).

[20] M. Ziman and V. Bužek, Phys. Rev. A **67**, 042321 (2003).

[21] D. Bruß, G. M. D'Ariano, M. Lewenstein, C. Macchiavello, A. Sen(De), and U. Sen, Phys. Rev. Lett. **93**, 210501 (2004).

[22] D. Bruß, M. Lewenstein, A. Sen(De), U. Sen, G. M. D'Ariano, and C. Macchiavello, Int. J. Quant. Inf. **4**, 415 (2006).

[23] Z. Shadman, H. Kampermann, C. Macchiavello, and D. Bruß, New J. Phys. **12**, 073042 (2010).

[24] Z. Shadman, H. Kampermann, C. Macchiavello, and D. Bruß, Phys. Rev. A **84**, 042309 (2011).

[25] Z. Shadman, H. Kampermann, C. Macchiavello, and D. Bruß, Phys. Rev. A **85**, 052306 (2012).

[26] Z. Shadman, H. Kampermann, C. Macchiavello, and D. Bruß, Quantum Measure. Quantum Metrol. **1**, 21 (2013).

[27] A. Shimony, Ann. N.Y. Acad. Sci. **755**, 675 (1995).

[28] A. Sen(De) and U. Sen, Phys. Rev. A **81**, 012308 (2010).

[29] A. Sen(De) and U. Sen, arXiv:1002.1253 [quant-ph].

[30] V. Coffman, J. Kundu, and W. K. Wootters, Phys. Rev. A **61**, 052306 (2000).

[31] R. Prabhu, A.K. Pati, A. Sen(De), and U. Sen, Phys. Rev. A **85**, 040102(R) (2012).

[32] K. Mattle, H. Weinfurter, P. G. Kwiat, and A. Zeilinger, Phys. Rev. Lett. **76**, 4676 (1996).

[33] D. Leibfried, R. Blatt, C. Monroe, and D. Wineland, Rev. Mod. Phys. **75**, 281 (2003).

[34] L. M. K. Vandersypen and I. L Chuang, Rev. Mod. Phys. **76**, 1037 (2005).

[35] H. Weinfurter, Europhys. Lett. **25**, 559 (1994).

[36] A. S. Holevo, M. Sohma, and O. Hirota, Phys. Rev. A **59**, 1820 (1999).

[37] S. L. Braunstein, and H. J. Kimble, Phys. Rev. A **61**, 042302 (2000).

[38] J. Eisert, and M. B. Plenio, Int. J. Quant. Inf. **1**, 479 (2003).

[39] S. L. Braunstein, and P. van Loock, Rev. Mod. Phys. **77**, 513 (2005).

[40] F. Dell'Anno, S. De Siena, and F. Illuminati, Phys. Rep. **428**, 53 (2006).

[41] P. Kok, W. J. Munro, K. Nemoto, T. C. Ralph, J. P. Dowling, and G. J. Milburn, Rev. Mod. Phys. **79**, 135 (2007).

[42] J. Eisert, S. Scheel, and M. B. Plenio, Phys. Rev. Lett. **89**, 137903 (2002).

[43] G. Giedke and J. I. Cirac, Phys. Rev. A **66**, 032316 (2002).

[44] M. Ohliger, K. Kieling, and J. Eisert, Phys. Rev. A **82**, 042336 (2010).

[45] M. Ohliger and J. Eisert, Phys. Rev. A **85**, 062318 (2012).

[46] F. Dell'Anno, S. De Siena, L. Albano, and F. Illuminati, Phys. Rev. A **76**, 022301 (2007).

[47] F. Dell'Anno, S. De Siena, and F. Illuminati, Phys. Rev. A **81**, 012333 (2010).

[48] S. Lloyd and S. L. Braunstein, Phys. Rev. Lett. **82**, 1784 (1999).

[49] G. S. Agarwal and K. Tara, Phys. Rev. A **43**, 492 (1991).

[50] A. Zavatta, A. Viciani, and M. Bellini, Science **306**, 660 (2004).

[51] T. Opatrný, G. Kurizki, D. -G. Welsch, Phys.Rev. A **61**, 032302 (2000).

[52] S. Olivares, M. G. A. Paris, R. Bonifacio, Phys. Rev. A **67**, 032314 (2003).

[53] S. Y. Lee, S. W. Ji, H. J. Kim, and H. Nha, Phys. Rev. A **84**, 012302 (2011).

[54] C. Navarrete-Benlloch, R. García-Patrón, J. H. Shapiro, and N. J. Cerf, Phys. Rev. A, **86**, 012328 (2012).

[55] T. Das, R. Prabhu, A. Sen(De), U. Sen, Phys. Rev. A **90**, 022319 (2014).

[56] D. M. Greenberger, M. A. Horne, and A. Zeilinger, in Bell's Theorem, Quantum Theory, and Conceptions of the Universe, ed. M. Kafatos (Kluwer Academic, Dordrecht, The Netherlands, 1989).

[57] T. Das, R. Prabhu, A. Sen(De), U. Sen, Phys. Rev. A **92**, 052330 (2015).

[58] T. Das, R. Prabhu, A. Sen(De), U. Sen, Phys. Rev. A **93**, 052313 (2016).

[59] C. Macchiavello and G.M. Palma, Phys. Rev. A **65**, 050301(R) (2002).

[60] S. L. Braunstein and H. J. Kimble, Phys. Rev. Lett. **80**, 869 (1998).

[61] S. Roy, T. Chanda, T. Das, A. Sen (De), and U. Sen, arXiv:1707.02449.

[62] A. Einstein, B. Podolsky, and N. Rosen, Phys. Rev. **47**, 777 (1935).

[63] J. S. Bell, Physics **1**, 195 (1965).

[64] J. F. Clauser, M. A. Horne, A. Shimony, and R. A. Holt Phys. Rev. Lett. **23**, 880 (1969).

[65] A. Kitaev, Ann. Phys. (NY) **303**, 2 (2003).

[66] M. Żukowski, A. Zeilinger, M.A. Horne, and H. Weinfurter, Acta Phys. Pol. A **93**, 187 (1998).

[67] M. Hillery, V. Bužek, and A. Berthiaume, Phys. Rev. A **59**, 1829 (1999).

[68] R. Cleve, D. Gottesman, and H.-K. Lo, Phys. Rev. Lett. **83**, 648 (1999).

[69] A. Karlsson, M. Koashi, and N. Imoto, Phys. Rev. A **59**, 162 (1999).

[70] K. Chen and H.-K. Lo, Quantum Inf. Comput. **7**, 689 (2007).

[71] K. Mattle, H. Weinfurter, P. G. Kwiat, and A. Zeilinger, Phys. Rev. Lett. **76**, 4656 (1996).

[72] W.-B. Gao, C.-Y. Lu, X.-C. Yao, P. Xu, O. Gühne, A. Goebel, Y.-A. Chen, C.-Z. Peng, Z.-B. Chen, and J.-W. Pan, Nat. Phys. **6**, 331 (2010).

[73] J-W Pan, Z-B Chen, C.-Y. Lu, H. Weinfurter, A. Zeilinger, and M. Żukowski, Rev. Mod. Phys. **84**, 777 (2012).

[74] T. E. Northup and R. Blatt, Nat. Photonics **8**, 356 (2014).

[75] M. Mirhosseini, O. S. Magaña-Loaiza, M. N. O'Sullivan, B. Rodenburg, M. Malik, M. P. J. Lavery, M. J. Padgett, D. J. Gauthier, R. W. Boyd, New J. Phys. **17**, 033033 (2015).

[76] M. Krenn, J. Handsteiner, M. Fink, R. Fickler, R. Ursin, M. Malik, A. Zeilinger, PNAS **113**, 13648 (2016).

[77] X.-L. Wang, L.-K. Chen, W. Li, H.-L. Huang, C. Liu, C. Chen, Y.-H. Luo, Z.-E. Su, D. Wu, Z.-D. Li, H. Lu, Y. Hu, X. Jiang, C.-Z. Peng, L. Li, N.-L. Liu, Y.-A. Chen, C.-Y. Lu, and J.-W. Pan, Phys. Rev. Lett. **117**, 210502 (2016).

[78] D. Bouwmeester, J-W Pan, K. Mattle, M. Eibl, H. Weinfurter ,and A. Zeilinger, Nature **390**, 575 (1997).

[79] D. Boschi, S. Branca, F. De Martini, L. Hardy, and S. Popescu, Phys. Rev. Lett. **80**, 1121 (1998).

[80] D. Leibfried, R. Blatt, C. Monroe, and D. Wineland, Rev. Mod. Phys. **75**, 281 (2003).

[81] D. Leibfried, E. Knill, S. Seidelin, J. Britton, R. B. Blakestad, J. Chiaverini, D. B. Hume, W. M. Itano1, J. D. Jost, C. Langer, R. Ozeri, R. Reichle, and D. J. Wineland, Nature **438**, 639 (2005).

[82] H. Hafner, C. F. Roose, and R. Blatt, Phys. Rep. **469**, 155 (2008).

[83] K. Singer, U. Poschinger, M. Murphy, P. Ivanov, F. Ziesel, T. Calarco, and F. Schmidt-Kaler, Rev. Mod. Phys. **82**, 2609 (2010).

[84] L.-M. Duan, and C. Monroe, Rev. Mod. Phys. **82**, 1209 (2010).

[85] T. Monz, P. Schindler, J. T. Barreiro, M. Chwalla, D. Nigg, W. A. Coish, M. Harlander, W. Hansel, M. Hennrich, and R. Blatt, Phys. Rev. Lett. **106**, 130506 (2011).

[86] J. T. Barreiro, J.-D. Bancal, P. Schindler, D. Nigg, M. Hennrich, T. Monz, N. Gisin, and R. Blatt, Nat. Phys. **9**, 559 (2013).

[87] T. Schaetz, M. D. Barrett, D. Leibfried, J. Chiaverini, J. Britton, W. M. Itano, J. D. Jost, C. Langer, and D. J. Wineland, Phys. Rev. Lett. **93**, 040505 (2004).

[88] X. Fang, X. Zhu, M. Feng, X. Mao, and F. Du, Phys. Rev. A **61**, 022307 (2000).

[89] W. Daxiu, Y. Xiaodong, L. Jun, S. Xianping, Z. Xizhi, and L. Maili, Chinese Science Bulletin **49**, 423 (2004).

[90] L. M. K. Vandersypen and I. L Chuang, Rev. Mod. Phys. **76**, 1037 (2005).

[91] C. Negrevergne, T. S. Mahesh, C. A. Ryan, M. Ditty, F. Cyr-Racine, W. Power, N. Boulant, T. Havel, D.G. Cory, and R. Laflamme, Phys. Rev. Lett. **96**, 170501 (2006).

[92] I. Oliveira, R. Sarthour Jr. T. Bonagamba, E. Azevedo, J. C. C. Freita, *NMR Quantum Information Processing*, (Elsevier Science, 2007), and references therein.

[93] M. Baur, A. Fedorov, L. Steffen, S. Filipp, M. P. da Silva, and A. Wallraff, Phys. Rev. Lett. **108**, 040502 (2012).

[94] R. Barends, J. Kelly, A. Megrant, A. Veitia, D. Sank, E. Jeffrey, T. C. White, J. Mutus, A. G. Fowler, B. Campbell, Y. Chen, Z. Chen, B. Chiaro, A. Dunsworth, C. Neill, P. OMalley, P. Roushan, A. Vainsencher, J. Wenner, A. N. Korotkov, A. N. Cleland, and J. M. Martinis, Nature **508**, 500 (2014).

[95] C.-P. Yang, Q.-P. Su, S.-B. Zheng, and F. Nori, New J. Phys. **18**, 013025 (2016).

[96] J. Lee, M. S. Kim, Y. J. Park, and S. Lee, J. Mod. Opt. **47**, 2151 (2000).

[97] G. Vidal and R.F. Werner, Phys. Rev. A **65**, 032314 (2002).

[98] M. B. Plenio, Phys. Rev. Lett. **95**, 090503 (2005).

[99] A. Peres, Phys. Rev. Lett. **77**, 1413 (1996).

[100] M. Horodecki, P. Horodecki, and R. Horodecki, Phys. Lett. A **223**, 1 (1996).

[101] C. H. Bennett, D. P. DiVincenzo, J. Smolin, and W. K. Wootters, Phys. Rev. A **54**, 3824 (1996).

[102] C. H. Bennett, G. Brassard, S. Popescu, B. Schumacher, J. A. Smolin, and W. K. Wootters Phys. Rev. Lett. **76**, 722 (1996); Erratum Phys. Rev. Lett. **78**, 2031 (1997).

[103] S. Hill and W. K. Wootters, Phys. Rev. Lett. **78**, 5022 (1997).

[104] W. K. Wootters, Phys. Rev. Lett. **80**, 2245 (1998).

[105] E. Knill and R. Laflamme Phys. Rev. Lett. **81**, 5672 (1998).

[106] A. Datta, A. Shaji and C. M. Caves Phys. Rev. Lett. **100**, 050502 (2008).

[107] C. H. Bennett, D. P. DiVincenzo, C. A. Fuchs, T. Mor, E. Rains, P. W. Shor, J. A. Smolin and W. K. Wootters Phys. Rev. A **59** 1070 (1999)

[108] M. Horodecki, A. Sen(De), U. Sen, and K. Horodecki, Phys. Rev. Lett. **90**, 047902 (2003).

[109] K. Modi, A. Brodutch, H. Cable, T. Paterek and V. Vedral, Rev. Mod. Phys. **84** 1655 (2012).

[110] A. Bera, T. Das, D. Sadhukhan, S. S. Roy, A. Sen(De) and U. Sen, arXiv:1703.10542.

[111] W. H. Zurek, Ann. Phys. Lpz. **9**, 855 (2000).

[112] H. Ollivier and W. H. Zurek Phys. Rev. Lett. **88**, 017901 (2001).

[113] L. Henderson and V. Vedral J. Phys. A: Math. Gen. **34**, 6899 (2001).

[114] J. Oppenheim, M. Horodecki, P. Horodecki, and R. Horodecki Phys. Rev. Lett. **89**, 180402 (2002).

[115] M. Horodecki, K. Horodecki, P. Horodecki, R. Horodecki, J. Oppenheim, A. Sen(De), and U. Sen Phys. Rev. Lett. **90**, 100402 (2003).

[116] M. Horodecki, P. Horodecki, R. Horodecki, J. Oppenheim, A. Sen(De), U. Sen, and B. Synak-Radtke, Phys. Rev. A **71**, 062307 (2005).

[117] B. Dakić, V. Vedral, and Č. Brukner, Phys. Rev. Lett. **105**, 190502 (2010).

[118] K. Modi, T. Paterek, W. Son, V. Vedral and M Williamson, Phys. Rev. Lett. **104**, 080501 (2010).

[119] C. C. Rulli and M. S. Sarandy, Phys. Rev. A **84**, 042109 (2011).

[120] C. H. Bennett, H. J. Bernstein, S. Popescu, and B. Schumacher, Phys. Rev. A **53**, 2046 (1996)

[121] T. J. Osborne and F. Verstraete, Phys. Rev. Lett. **96**, 220503 (2006).

[122] M. Koashi, and A. Winter Phys. Rev. A **69**, 022309 (2004).

[123] P. Badziag, M. Horodecki, A. Sen(De), and U. Sen, Phys. Rev. Lett. **91**, 117901 (2003).

[124] M. Horodecki, J. Oppenheim, A. Sen(De), and U. Sen, Phys. Rev. Lett. **93**, 170503 (2004).

[125] J. Preskill Lecture notes on Quantum Information and Computation http://www.theory.caltech.edu/ people/preskill/ph229/

[126] S. Mozes, J. Oppenheim, and B. Reznik, Phys. Rev. A **71**, 012311 (2005).

[127] S. Wu, S. M. Cohen, Y. Sun, and R. B. Griffiths, Phys. Rev. A **73**, 042311 (2006).

[128] P. Bourdon, E. Gerjuoy, J. McDonald, and H. Williams, Phys. Rev. A **77**, 022305 (2008).

[129] M. Beran and S. Cohen, Phys. Rev. A **79**, 032307 (2009).

[130] C.-W. Tsai and T. Hwang, Opt. Comm. **283**, 4397 (2010).

[131] A. Zeilinger, M. A. Horne, and D. M. Greenberger, in Proceedings of Squeezed States and Quantum Uncertainty, edited by D. Han, Y. S. Kim, and W. W. Zachary, NASA Conf. Publ. 3135, 73 (1992).

[132] V. Vedral, M. B. Plenio, M. A. Rippin, and P. L. Knight, Phys. Rev. Lett. **78**, 2275 (1997).

[133] V. Vedral and M. B. Plenio, Phys. Rev. A **57**, 1619 (1998).

[134] M. Horodecki, P. Horodecki, and R. Horodecki, Phys. Rev. Lett. **84**, 2014 (2000).

[135] M. A. Nielsen and I. L. Chuang, *Quantum Computation and Quantum Information* (Cambridge University Press, Cambridge, 2000).

[136] A. Peres, *Quantum Theory: Concepts and Methods* (Kluwer, Dordrecht, 1993 , pp. 131-133).

[137] K. Życzkowski, P. Horodecki, A. Sanpera, and M. Lewenstein, Phys. Rev. A **58**, 883 (1998).

[138] P. Horodecki, Phys. Lett. A **232**, 333 (1997).

[139] M. Horodecki, P. Horodecki, and R. Horodecki, Phys. Rev. Lett. **80**, 5239 (1998).

[140] S. Luo and S. Fu, Phys. Rev. Lett. **106**, 120401 (2011).

[141] T. M. Cover, J. A. Thomas, Elements of Information Theory (John Wiley and Sons, New Jersey, 2006).

[142] B. Groisman, S. Popescu, and A. Winter, Phys. Rev. A **72**, 032317 (2005).

[143] N. J. Cerf, and C. Adami, Phys. Rev. Lett. **79**, 5194 (1997).

[144] Y. Huang New J. Phys. **16**, 033027 (2014).

[145] T. Chanda, T. Das, D. Sadhukhan, A. K. Pal, A. Sen(De), and U. Sen Phys. Rev. A **92**, 062301 (2015).

[146] J. M. Raimond, M. Brune, and S. Haroche, Rev. Mod. Phys. **73**, 565 (2001).

[147] D. Leibfried, R. Blatt, C. Monroe, and D. Wineland Rev. Mod. Phys. **75**, 281 (2003).

[148] M. B. Plenio and V. Vedral, J. Phys. A **34**, 6997 (2001).

[149] K. Modi, T. Paterek, W. Son, V. Vedral, and M. Williamson, Phys. Rev. Lett. **104**, 080501 (2010).

[150] R. Prabhu, A.K. Pati, A. Sen(De), and U. Sen, Phys. Rev. A **85**, 040102(R) (2012).

[151] R. Prabhu, A.K. Pati, A. Sen(De), and U. Sen, Phys. Rev. A **86** 052337 (2012).

[152] M. N. Bera, R. Prabhu, A. Sen(De), and U. Sen, Phys. Rev. A **86**, 012319 (2012).

[153] H. S. Dhar, A. K. Pal, D. Rakshit, A. Sen(De), and U. Sen, Lectures on General Quantum Correlations and their Applications (Springer International Publishing, pp 23–64, 2017).

[154] A. Kumar, R. Prabhu, A. Sen (De), and U. Sen, Phys. Rev. A, **91**, 012341 (2015).

[155] J. Anandan and Y. Aharonov, Phys. Rev. Lett. **65**, 1697 (1990).

[156] Y-K. Bai, Y-F. Xu, and Z. D. Wang, Phys. Rev. Lett. **113**, 100503 (2014).

[157] T. R. de Oliveira, M. F. Cornelio, and F. F. Fanchini, Phys. Rev. A **89**, 034303 (2014).

[158] Y-C. Ou and H. Fan, Phys. Rev. A **75**, 062308 (2007).

[159] H. He and G. Vidal, Phys. Rev. A **91**, 012339 (2015).

[160] A. Kumar, Phys. Lett. A **380**, 3044 (2016).

[161] Y-K. Bai, N. Zhang, M-Y. Ye, and Z. D. Wang, Phys. Rev. A **88**, 012123 (2013).

[162] H. C. Braga, C. C. Rulli, T. R. deOliveira, and M. S. Sarandy, Phys. Rev. A **86**, 062106 (2012).

[163] S-Y. Liu, Y-R. Zhang, L-M. Zhao, W-L. Yang, and H. Fan, Ann. Phys. **348**, 256 (2014).

[164] B. Toner and F. Verstraete, arXiv:quant- ph/0611001.

[165] B. Toner, Proc. R. Soc. A **465**, 59 (2009).

[166] M. Seevinck, Quant. Inf. Proces. **9**, 273 (2010).

[167] M. D. Reid, Phys. Rev. A **88**, 062108 (2013).

[168] A. Milne, S. Jevtic, D. Jennings, H. Wiseman, and T. Rudolph, New J. Phys. **17**, 019501 (2015).

[169] R. Ramanathan, A. Soeda, P. Kurzynski, and D. Kaszlikowski, Phys. Rev. Lett. **109**, 050404 (2012).

[170] P. Kurzynski, A. Cabello, and D. Kaszlikowski, Phys. Rev. Lett. **112**, 100401 (2014).

[171] G. L. Giorgi, Phys. Rev. A **84**, 054301 (2011).

[172] X. Li, Q. Pan, J. Jing, J. Zhang, C. Xie, and K. Peng, Phys. Rev. Lett. **88**, 047904 (2002).

[173] J. Jing, J. Zhang, Y. Yan, F. Zhao, C. Xie, and K. Peng, Phys. Rev. Lett. **90**, 167903 (2003).

[174] B. Schumacher Phys. Rev. A. **51**, 2738 (1995).

[175] M. Horodecki and M. Piani J. Phys. A: Math. Theor. **45**, 105306 (2012).

[176] K. Kraus, General state changes in quantum theory, Ann. Phys. **64**, 311, (1971).

[177] N. J. Cerf, Phys. Rev. Lett. **84**, 4497 (2000).

[178] D. I. Fivel, Phys. Rev. Lett. **74**, 835 (1995).

[179] M.A. Cirone, A. Delgado, D.G. Fischer, M. Freyberger, H. Mack, and M. Mussinger, Quant. Inf. Proc. **1**, 303 (2002).

[180] N. D. Mermin, Phys. Rev. Lett. **65**, 1838 (1990).

[181] M. Ardehali, Phys. Rev. A **46**, 5375 (1992).

[182] A.V. Belinskii and D.N. Klyshko, Phys. Usp. **36**, 653 (1993).

[183] R. Bhatia, *Matrix Analysis* (Springer-verlag, New York, 1997).

[184] P. Hayden, D. Leung, P.W. Shor, and A. Winter, Commun. Math. Phys. **250**, 371 (2004).

[185] B. Schumacher, M. Westmoreland, and W. K. Wootters, Phys. Rev. Lett. **76**, 3452 (1996).

[186] E. Wigner, Phys. Rev. **40**, 749 (1932).

[187] C. Gerry (Author) and P. Knight, *Introductory Quantum Optics* (Cambridge University Press, 2004).

[188] M. O. Scully and M. S. Zubairy, *Quantum Optics* (Cambridge University Press, 1997).

[189] A. R. Usha Devi, R. Prabhu, and M. S. Uma, Eur. Phys. J. D **40**, 133 (2006).

[190] M. Dakna, L. Knöll, and D. -G. Welsch, Eur. Phys. J. D **3**, 295 (1998).

[191] V. Parigi, A. Zavatta, M. S. Kim, and M. Bellini, Science **317**, 1890 (2007).

[192] A. Ourjoumtsev, A. Dantan, R. Tualle-Brouri, and P. Grangier Phys. Rev. Lett. **98**, 030502 (2007).

[193] M. D. Levenson and R.M. Shelby, J. of Mod. Opt. **34**, 775 (1987).

[194] M. Reck, A. Zeilinger, H. J. Bernstein, and P. Bertani, Phys. Rev. Lett. **73**, 58 (1994).

[195] H.Y. Fan, X.T. Liang, and J.H. Chen, Mod. Phys. Lett. B **16**, 861 (2002).

[196] H. Fan and J. Ouyang, Mod. Phys. Lett. B **17**, 1293 (2003).

[197] U. L. Andersen, J. S. Neergaard-Nielsen, P. van Loock , and A. Furusawa, Nat. Phys. **11**, 713 (2015)

[198] A. Kitagawa, M. Takeoka, M. Sasaki, A. Chefles, Phys. Rev. A. **73**, 042310 (2006).

[199] P. van Loock, C. Weedbrook, and M. Gu, Phys. Rev. A **76**, 032321 (2007).

[200] M. Yukawa, R. Ukai, P. van Loock, and A. Furusawa, Phys. Rev. A **78**, 012301 (2008).

[201] L. Y. Hu and H. Y. Fan, Int. J. Theor. Phys. **47**, 1058 (2008).

[202] P. van Loock, Fortschr. Phys. **50**, 1177 (2002) and references thereto.

[203] S. Armstrong, J.-F. Morizur, J. Janousek, B. Hage, N. Treps, P. K. Lam and H.-A. Bachor, Nat. Comm. **3**, 1026 (2012), and references therein.

[204] X. Ma and W. Rhodes, Phys. Rev. A **41**, 4625 (1990).

[205] L. Hu and H. Fan, Europhys. Lett. **85**, 60001 (2009).

[206] M. G. Genoni, M. G. A. Paris, and K. Banaszek, Phys. Rev. A. **78**, 060303(R) (2008).

[207] M. G. Genoni, and M. G. A. Paris, Phys. Rev. A. **82**, 052341 (2010).

[208] P. Marian and T. A. Marian, Phys. Rev. A **88**, 012322 (2013).

[209] J. Williamson. Am. J. of Math. **58**, 141 (1936).

[210] M. M. Wolf, Phys. Rev. Lett. **100**, 070505 (2008).

[211] Q.-M. Song, B.-L. Fang, and L. Ye, Opt. Comm. **284**, 510 (2011).

[212] Z. Ji, Y. Feng, R. Duan, and M. Ying, Phys. Rev. A **73**, 034307 (2006).

[213] W. Dür, G. Vidal, and J. I. Cirac, Phys. Rev. A **62**, 062314 (2000).